Fine tuning Rh^{II} complexes with tethered, axial coordination: structural studies and application to diazo-mediated cyclopropanation reactions

A Dissertation Presented for the
Doctor of Philosophy
Degree
The University of Tennessee, Knoxville

Derek Cressy
May 2021

ACKNOWLEDGEMENTS

To begin, I would like to thank Dr. Ampofo Darko for accepting me as one of his first graduate students. I am most grateful for his guidance and instruction throughout my graduate career. His openness to research ideas established an atmosphere of cooperativity. His willingness to aid in developing an idea made it feel like collaboration and inspired independent ideas. I would also like to thank my committee members, Dr. Brian Long, Dr. Michael Best, and Dr. Joe Bozell. The time and energy they have put forth towards my education have been invaluable. I am thankful for them pushing me to keep improving.

Another instrumental part of this journey was the Darko group members. Each group member has had an influence on my graduate career. A special thank you to Dr. Brad Anderson for showing me the power of trituration and many other useful chemical tricks. I would also like to single out Will Sheffield, Anthony Abshire, and Cris Zavala. They have been indispensable as study partners and sounding boards during this time. Even beyond all the chemistry help, your support and friendship have been just as beneficial.

None of this would have been possible without the support of my family. I don't believe that anything I would put in words here would even begin to describe what a blessing and help they been in this endeavor, but I would be remiss if I did not at least make an effort. To begin, I am forever grateful for my wife Sarah, and the understanding and patience she has shown me since we began this adventure. She knew that graduate school was part of my plans and yet she still decided to marry me, "enrolling" herself in graduate school as well. I want to thank her for tolerating and enduring the long nights, limited weekends, and having to change plans on a moment's notice. I am always amazed that I have not reached the end of her patience with my constant tardiness and forgetfulness. It is my goal to continue to show my appreciation for all that you have done well after graduate school.

I would not be where I am today had it not been for the years of work put forth by my parents. Many life lessons were learned growing up, even if it seemed like nothing was sticking, and have been invaluable during my time in graduate school. I am grateful for you easing many worries by being a constant support. In addition to my parents, I would like to thank my in-laws who have helped me and my wife through this time. Your support has also made the game of life more enjoyable, and easier than it would have

been otherwise. I appreciate the understanding and patience you have shown me when I was working during some of the holidays.

Finally, I would like to thank the members of Laurel Church of Christ for all the support my wife and I have received from them. The friendships that we have are so important to us and have been a source of much strength as we have progressed through graduate school. Your many prayers and continued support have been an integral part of my graduate school career.

ABSTRACT

The cyclopropane moiety is an attractive synthetic target due to its application in pharmaceuticals and medicinal research. One effective synthetic strategy involves the formation of metal carbenoid species from diazo reagents. The carbenoid then reacts with an olefin substrate to generate the cyclopropane ring. Of the metal complexes that can facilitate this reaction, dirhodium(II) paddlewheel complexes are arguably the most prevalent catalysts. This is because modification of the bridging ligands enables control to be exerted over the catalyst's chemoselectivity and enantioselectivity. Exploiting the axial site as a control element is often overlooked as strongly coordinated Lewis bases inhibit catalysis. Despite this, Lewis base additives have been observed to increase enantioinduction in cyclopropanation reactions and axial coordination has been suggested as a possible explanation. However, leveraging axial coordination as a control element remains a problem due to the difficulty of controlling the coordination of exogenous ligand.

The goal of my research is the development of heteroleptic dirhodium(II) paddlewheel complexes with tethered thioether ligands that are capable of axial coordination. Tethering of the Lewis base anchors the thioether proximal to the axial site to provide control over axial coordination. Solid and solution-state characterization indicated that axial coordination was present as part of a rapid equilibrium. The electrochemical analysis demonstrated the ability of different thioethers to modulate the electrophilicity of the complex. These complexes were then tested as catalysts in the cyclopropanation of olefins and diazo reagents. It was shown that the novel complexes were better suited for more reactive diazo reagents and afforded higher yields than control catalysts.

Table of Contents

List of Tables

List of Schemes

List of Figures

List of Abbreviations

acac – acetoacetate

Bi – bismuth

cod – 1,5-cyclooctadiene

Cy – cyclopropyl

de – diastereomeric excess

dr – diastereomeric ratio

ee – enantiomeric excess

Fc – ferrocene

Fc^+ – ferrocenium

hr – hour

HOMO – highest occupied orbital

HPLC – high performance liquid chromatography

LUMO – lowest unoccupied orbital

mg – miligram

mL – milliliter

Ms – mesityl

ND – not determined

NR – no reaction

OAc – acetate

OTf – triflate

Ph – phenyl

$P(OPh)_3$ – triphenyl phosphite

Rh – rhodium

Rh_2(biTSP)$_2$ – dirhodium(II) bis-1,3-[N,N'-di(4-tert-butyl-benzene-sulfonyl)-(2*S*,2'*S*),(5*R*,5'*R*_-5,5'-prolinate]benzene

Rh_2(*S*-BTPCP)$_4$ – dirhodium(II) tetrakis-(*S*)-(1-(4-bromophenyl)-2,2-diphenylcyclopropanecarboxylate

Rh_2(*S*-IBAZ)$_4$ – dirhodium(II) (2-methyl-1-propyl (*S*)-2-oxaazetidine-4-carboxylate)

Rh_2(*S*-PTAD)$_4$ – dirhodium(II) tetrakis[(*R*)-(-)-(1-adamantyl)-(N-phthalimido)acetato]

Rh_2(*S*-PTTL)$_4$ – dirhodium(II) tetrakis[N-phthaloyl-(*S*)-tertleucinate]

Rh_2(*S*-PTTL)$_3$TPA – dirhodium(II) tris[*N*-phthaloyl-(*S*)-tert-leucinate] triphenylacetate

Rh_2(*S*-DOSP)$_4$ – dirhodium(II) tetrakis[1-[[4-dodecylphenyl]sulfonyl]-prolinate]

Rh_2(*S*-MCPIM)$_4$ – dirhodium(II) tetrakis{methyl 1-[3′(*S*)-phenyl-2′(*S*)cyclopropanecarbonyl]-2-oxo-imidazolidine-4(*S*)-carboxylate

Rh_2(*S*-MEOX)$_4$ – dirhodium(II) tetrakis[methyl 2-oxo-oxazolidine-4(*S*)-carboxylate]

Rh_2(*S*-MEPY)$_4$ – dirhodium(II)tetrakis[methyl 2-pyrrolidone-5(*S*)-carboxylate]

Rh_2(*S*-NNTL)$_4$ – dirhodium(II) tetrakis[N-naphthalimide-(*S*)-tertleucinate]

Rh_2(*S*-TBSP)$_4$ – dirhodium(II) tetrakis[1-[(4-tert-butylphenyl)sulfonyl]-(2*S*)-pyrrolidinecarboxylate]

Rh_2(*S*-TCPTAD)$_4$ – dirhodium(II) tetrakis[2-(adamantan-2-yl)-2-(4,5,6,7-tetrachloro-1,3-dioxoisoindolin-2-yl)acetate]

Rh_2(*S*-TCPTTL)$_4$ – dirhodium(II) tetrakis[*N*-tetrachlorophthaloyl-(*S*)-*tert*-leucinate]

Rh_2(*p*-Ph-TPCP)$_4$ – dirhodium(II) tetrakis-(*S*)-(1-(4-phenyl)-2,2-diphenylcyclopropanecarboxylate

Rh_2(TPA)$_4$ – dirhodium(II) tetrakistriphenylacetate

rt – room temperature

SC-XRD – single crystal x-ray diffraction spectroscopy

^{t}Bu – tert butyl

TEA – triethylamine

TFA – trifluoroacetic acid

Ts – tosyl

TsCl – tosyl chloride

Chapter 1 - Introduction

1.1 Cyclopropanation Mediated by Diazo-Derived Carbenoids

The cyclopropane moiety has continued to play a prominent role in the development of pharmaceuticals.[1, 2] The cyclopropane's ability to confer desired physiological properties, such as increased hydrophilicity, or impart a rigid conformation makes it a powerful tool for drug design.[3, 4] From 2012-2018, the Federal Drug Administration approved 18 new drugs that contain a cyclopropane ring, which represents 8.5% of all approved drugs during that period.[3] Isolation of natural products that demonstrate potential therapeutic value further drives the desire for methods of synthesizing cyclopropane rings.[5-7] The most prevalent methods for cyclopropanation can be divided into six major categories (Figure 1.1). Each of these methods has been applied in the synthesis of medicinally relevant molecules or natural products.[8-10] Many of these require the formation of a divalent carbon species known as a carbene. Investigation of the reaction of free carbenes with olefins showed that a mixture of *cis* and *trans* cyclopropane rings was generated in small quantities, in addition to a range of hydrocarbon side products. These results led to carbenes being described as "the most indiscriminate reagent in organic chemistry".[11]

Despite this moniker, continued research led to the discovery that combining diazo compounds with certain transition metals generated stabilized carbenes. These metal-stabilized complexes were termed carbenoids. Many transition metals can form isolable carbenoid complexes or reactive carbenoid intermediates that facilitate the cyclopropanation of olefins. The generic mechanism for the cyclopropanation of olefins with diazo compounds is similar for each metal (Scheme 1.1). The initial step is the electrophilic attack of a diazo reagent by the metal center. The metal center then aids in the extrusion of dinitrogen to generate an electrophilic carbenoid species (Scheme 1.1, A). The reactive carbenoid undergoes a nucleophilic attack by the olefin substrate (Scheme 1.1, B). A common transition state for cyclopropane formation is via transition state C (Scheme 1.1, C), where the cyclopropane is formed in a concerted, yet asynchronous, step. Although this transition state is very common, it is not observed for all metals.[12-16] The formation of the cyclopropane then results in the regeneration of the

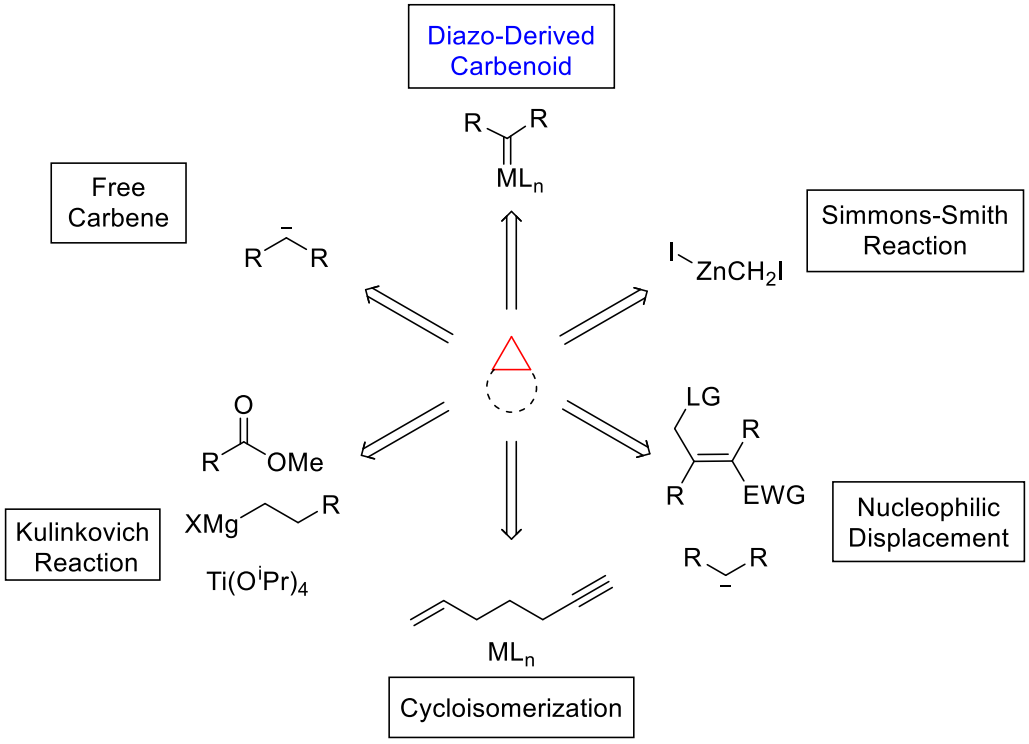

Figure 1.1 Different methods commonly employed for cyclopropanation of olefin substrates

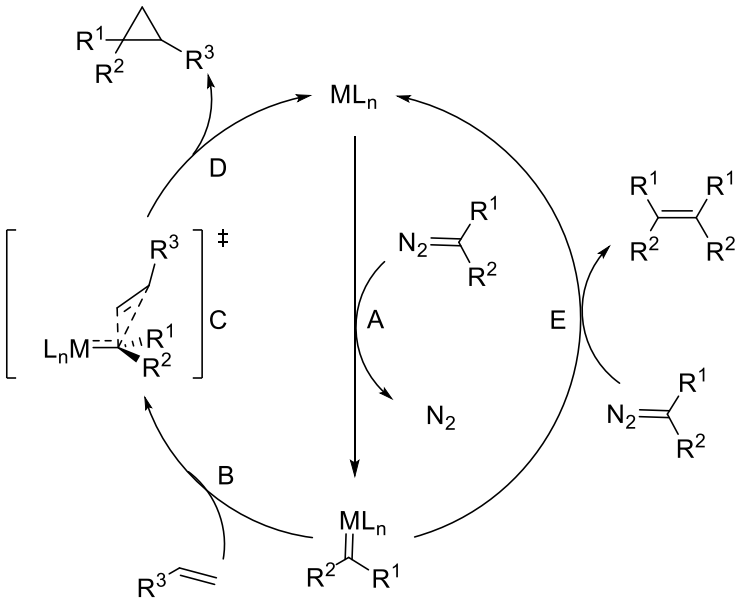

Scheme 1.1 General mechanism for cyclopropanation of olefin substrates with metal carbenoids derived from diazo compounds

catalyst (Scheme 1.1, D). An alternative unproductive pathway is often observed when the carbenoid is intercepted by another equivalent of the diazo reagent, resulting in a homocoupled dimer product (Scheme 1.1, E).

The metal carbenoid is not limited to cyclopropanation reactions, however, and can participate in a myriad of reactions. These reactions include X-H (X= C, O, N, Si, S) insertion, ylide formation, and cyclopropenation.[17, 18] The wide applicability inherently brings about the complication of rendering reactions chemoselective. This is especially true during total synthesis when multiple reactive functional groups are present. One method of controlling the chemoselectivity involves protecting groups. This is an effective strategy but increases the number of synthetic steps. A more desirable method of controlling chemoselectivity is by modulating the catalyst's reactivity. There are examples where the chemoselectivity of the reaction is dependent on the identity of the ligands stabilizing the metal of the catalyst. Development of methods to tune the electronic nature of the metal, and thereby affect the carbene, should allow further improvements to chemoselectivity.

Another aspect of chemoselectivity is favoring cyclopropanation over the undesired homocoupled dimer. Different methods have been developed to avoid the formation of the homocoupled dimer. One such method is the addition of an excess of the olefin substrate. The increased concentration of olefin substrate allows for the preferential trapping of the carbenoid by the olefin, rather than another molecule of the diazo reagent. Although this method has been effective, it is not without limitations. Cyclopropanation is often conducted in the early steps of the synthesis with readily available olefins. This way, complex olefins that required time and resources to make are not wasted. The early installation of the cyclopropane ring also introduces the reactive cyclopropane intermediate that must now be compatible with any future reactions. Development of catalysts that enable the use of equimolar amounts of olefin and diazo reagent would allow the installation of cyclopropane rings later in syntheses, resulting in new synthetic design strategies. Another method of minimizing the formation of the homocoupled dimer involves the slow addition of the diazo reagent, often over 12 hours or more. This minimizes the concentration of the diazo reagent and facilitates the carbenoid being intercepted by the olefin. Despite being effective, it is desirable to eliminate, or at least mitigate, the formation of the unwanted side product through the choice of catalyst.

The choice of diazo reagent is another way of controlling the carbenoid intermediate, and thereby chemoselectivity. Diazo compounds substituted with an electron withdrawing group (EWG) are classified as acceptor diazo compounds (Figure 1.2). Esters are a common EWG and have been the benchmark for diazo decomposition reactions. The EWG stabilizes the diazo through resonance and enables easier handling as compared to diazomethane. This resonance also makes electrophilic attack by the metal difficult, which is why acceptor/acceptor diazo reagents are not as reactive (Figure 1.2, a). Conversely, electron donating groups (EDGs) make the diazo carbon more susceptible to electrophilic attack, which facilitates the coordination of the carbon to the metal. The opposite reactivity trend is observed regarding the carbenoid, as EWGs make the carbenoid even more electrophilic (Figure 1.2, b). Because the acceptor and acceptor/acceptor diazo reagents lead to more reactive carbenoids, the homocoupled dimer product is commonly observed. The increased reactivity of these carbenoids was also associated with a decrease in the diastereoselectivity. For this reason, "balanced" donor/acceptor diazo compounds were developed where the EDG attenuates the reactivity of the carbenoid.[19, 20] Although the donor/acceptor diazo reagents mitigate the formation of the homocoupled dimer, they do not prevent the side reaction in all instances.[21] Using the diazo reagent to control the reactivity of the carbenoid limits the reaction scope, as only select diazo reagents may be employed. Instead, it is preferable that the carbenoid's reactivity be controlled by the catalyst, allowing for the use of a wider range of diazo reagents.

The most common metals applied to the cyclopropanation of olefins from diazo mediated carbenoids are those in Group 9 and Group 11. As such, they will be the focus of this overview. Due to the wide application of cyclopropanation reactions, many recent reviews have been compiled that include sections on carbenoid mediated cyclopropanation.[10, 22-26] Especially helpful is the annual review of the chemistry of the transition metal to carbon double and triple bond, which began in 1997.[27-29] For each of the nonradioactive Group 9 and 11 transition metals, an outline of the seminal works regarding cyclopropanation will be provided, followed by recent applications. As discussed previously, it is common practice to use different techniques to limit the formation of the homocoupled dimer product. Therefore, in the course of this review, it should be understood that one or more of these techniques were employed unless otherwise stated.

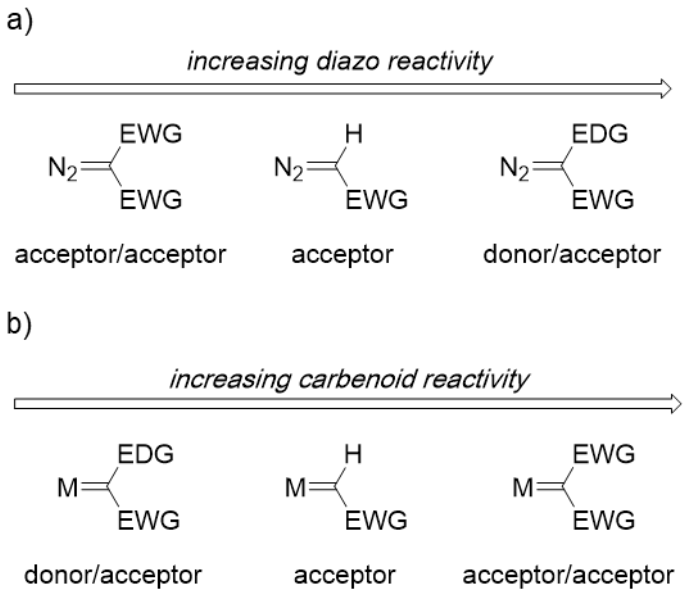

Figure 1.2 Different classifications and reactivity trends of a) diazo reagents and b) the corresponding metal carbenoids

1.1.1 Copper

Copper has become ubiquitous in the discussion of diazo mediated carbenoid cyclopropanation due to early examples involving Cu bronze and $Cu(SO_4)_2$ (Figure 1.3).[30] Good yields were obtained and improved upon by introducing ligands that increased the solubility of the complex. Both Cu(I) and Cu(II) complexes have been applied as catalysts, but it was demonstrated that Cu(II) complexes are reduced to Cu(I) by diazo reagents. This reduction process was corroborated by the application of other reducing agents.[31] Regardless of which catalyst was implemented, only a slight preference was observed for the *trans* isomer.

Nozaki and co-workers were able to achieve the asymmetric cyclopropanation of styrene and ethyl diazoacetate (EDA) by incorporating a chiral salicylaldimine ligand to afford a *trans*:*cis* ratio of 2.3:1 and an ee of 6% for each isomer.[32] The asymmetric product was attributed to the *in-situ* generation of a Cu/salicylaldimine complex. Based on the stoichiometry of ligand to Cu salt, it was believed that the active catalyst had a ligand:Cu ratio of 1:1. Although only modest enantioselectivity was observed, this reaction was the first example of asymmetric catalysis mediated by a metal carbenoid. Not only did this experiment bring about the development of Cu catalysis, it also set in motion the investigation of other metals for asymmetric catalysis.

The work by Aratani and co-workers provided an improvement to the enantioselectivity achieved by Nozaki through a tridentate salicylaldimine derived ligand (Figure 1.4).[33] Through methodical analysis of structure-activity relationships in the enantioselective synthesis of chrysanthamic acid derivatives, trends were established for salicylic acid derived ligands. It was determined that diastereoselectivity was primarily dictated by the choice of diazo reagent. Minimal diastereoselectivity was observed with EDA. As the steric demands of the ester's alkoxy group increased, a preference for the *trans* diastereomer was observed. The best *trans*:*cis* ratio was obtained with an adamantyl (Ad) group. An increase in enantioselectivity for the *trans* isomer was also observed as the size of the ester's alkoxy group was increased. Further salicylaldimine derivatives were synthesized with variations of the aryl group and different substituents at the chiral center (Figure 1.5).[34] A clear increase in enantioselectivity of the chrysanthamic esters was observed with the addition of substituents on the aryl ring. More sterically demanding substituents further increased enantioselectivity. The effect of aryl

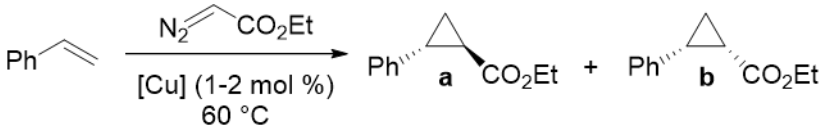

Catalyst	Yield %	**a**/**b**
Cu bronze	53	1.9:1
$Cu(acac)_2$	71	2.6:1
$Cu(OTf)_2$	97	1.9:1
$CuCl \cdot P(OPh)_3$[a]	84	2.5:1

[a]Reaction conducted at rt

Figure 1.3 Cyclopropanation of styrene and EDA with select Cu complexes

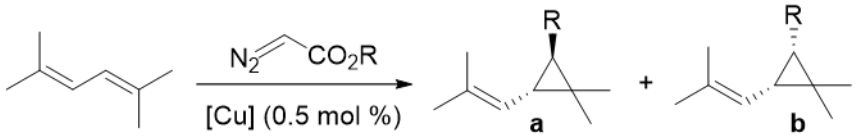

R	Yield (%)	**a**/**b**	ee **a** (%)	ee **b** (%)
Et	54	51:49	68	62
^{t}Bu	74	75:25	75	46
Ad	82	84:16	85	46

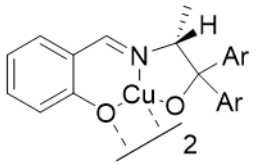

Ar = (2-OOct)(5-^{t}Bu)Ph

Figure 1.4 Increased diastereoselectivity as a result of more sterically demanding alkoxy groups on diazo esters

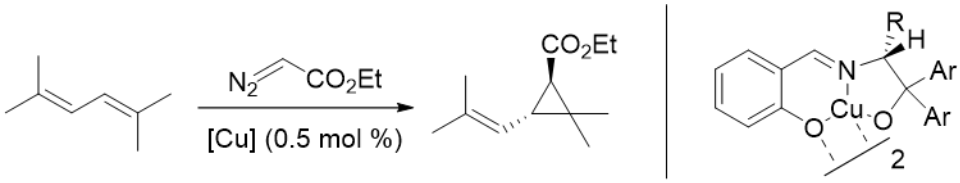

R	Ar	ee (%)
Me	Ph	5
Me	(2-OBu)Ph	50
Me	(2-OBu)(5-^{t}Bu)Ph	60
Me	(2-OOct)(5-^{t}Bu)Ph	70

R	Ar	ee (%)
Bn	Ph	9
^{i}Pr	Ph	10
^{t}Bu	Ph	19

Values are estimations based on graphical representation in ref 34

Figure 1.5 Influence of Cu salicylaldimine catalysts on enantioselectivity in the cyclopropanation of chrysanthamic acid derivative

substituents was more pronounced than that observed upon varying the substituent at the chiral center. The highest ee was obtained when the bulky aryl substituents were combined with the methyl group at the chiral center. This combinatorial effect was essential for the high enantioselectivity (Figure 1.5). The methodology developed was applied to the synthesis of cilastatin, which inhibits the metabolism of the antibacterial imipenem.[35]

As research progressed in the field, other classes of ligands demonstrated superior yields and stereoselectivities when compared to these salicylaldimine complexes. Many different ligand scaffolds have been investigated since the initial discovery by Nozaki. Of these, the most common ligand scaffolds are semicorrins, bis(oxazolines), and other nitrogenous chelating agents such as bipyridines.

1.1.1.1 Cyclopropanation with Semicorrin Cu(I) Complexes

After the discovery of salicylaldimine complexes, Pfaltz and co-workers developed Cu catalysts incorporating chiral semicorrin ligands.[36] Good yields were obtained with each of the catalysts, with a slight preference for the *trans* isomer (Table 1.1, entries 1-3). As was observed with the salicylaldimine catalysts, reactions of diazo esters with sterically demanding alkoxy groups resulted in a more diastereoselective reaction compared to less sterically demanding esters (Table 1.1, entry 3-5). Both the *trans* and *cis* isomer had higher ee (~10%) than the salicylaldimine catalysts. However, the scope of the olefin substrate was limited to activated olefins such as styrene and dienes. High stereoselectivity (82:18 *trans*:*cis*, 92% ee for each isomer) was maintained with the nonactivated alkene 1-heptene, but only with a modest yield (~30%).

1.1.1.2 Cyclopropanation with Bis(oxazoline) Cu(I) Complexes

One of the most noteworthy ligands used in conjunction with Cu cyclopropanation is the bis(oxazoline) ligand, also known as BOX ligand (Figure 1.6). Catalysis with BOX complexes has been the subject of multiple reviews that cover cyclopropanation of olefins with metal carbenoids generated from diazo reagents.[37, 38] BOX compounds are reminiscent of the semicorrin ligand. Both are five-membered heterocycles containing a nitrogen atom. However, BOX ligands also contain an oxygen in the heterocyclic ring.

Table 1.1 Cyclopropanation of styrene and acceptor diazo reagents with Cu(I) semicorrin complexes

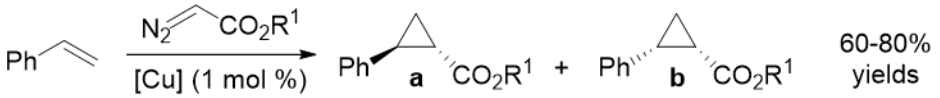

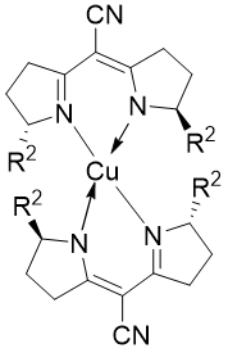

1 $R^2 = CO_2Me$
2 $R^2 = CH_2OSi(Me)_2{}^tBu$
3 $R^2 = CMe_2OH$

Entry	R^1	Catalyst	***a*/b**	ee **a**	ee **b**
1	Et	**1**	74:26	23	19
2	Et	**2**	75:25	59	45
3	Et	**3**	73:27	85	68
4	^{t}Bu	**3**	81:19	93	92
5	*l*-ment	**3**	85:15	91	90

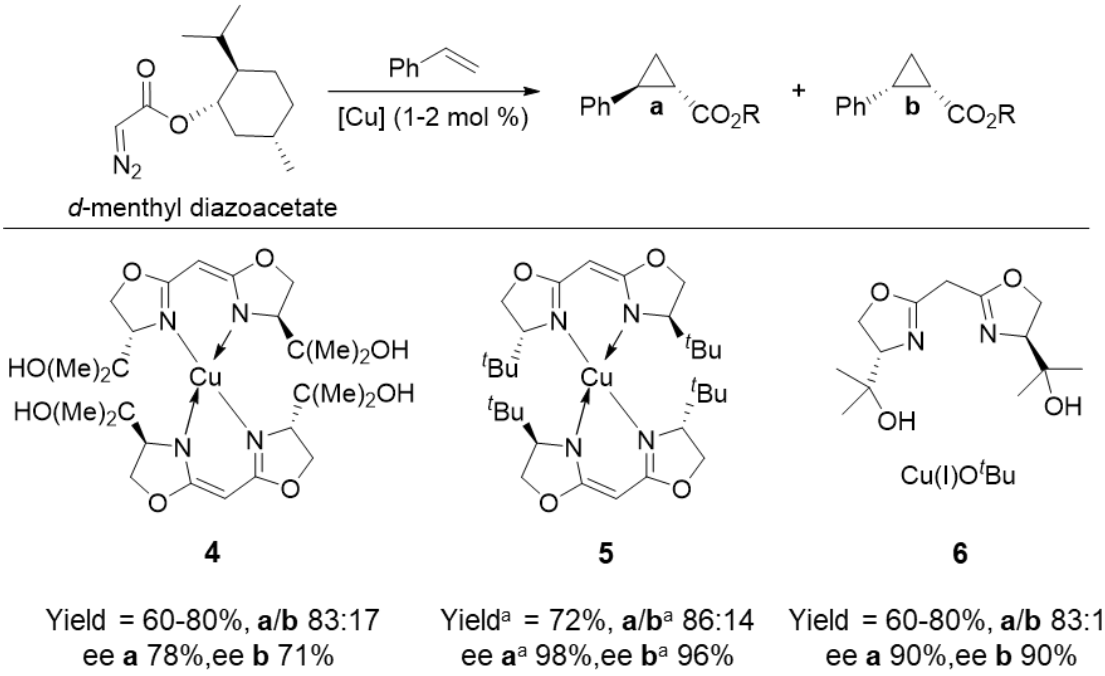

Figure 1.6 Cyclopropanation of styrene and *d*-menthyl diazoacetate with Cu BOX complexes

For this reason, chiral moieties that were applied to the Cu semicorrin complexes were also incorporated into Cu BOX complexes (Figure 1.6).[39, 40] The isolated Cu BOX complex **4** afforded yields and diastereoselectivities comparable to semicorrin ligands. However, an improvement in the enantioselectivity was observed with complex **5**, upon varying the oxazoline substituent. It was also demonstrated that the active Cu complex could be generated *in situ* by combining a Cu salt and an equimolar amount of ligand. This was evidenced by the similar yields, diastereoselectivity, and enantioselectivity observed when comparing an isolated complex to one generated in situ (Figure 1.6, compare **4** and **6**).

The BOX ligand **7** (Figure 1.7) was then examined with the more reactive diazo reagent EDA. Even though the yield and diastereoselectivity were similar compared to the analogous semicorrin complex, the enantioselectivity of the BOX complex was much lower. Even so, further ligand development demonstrated that the oxazoline substituents influenced enantioselectivity. It was demonstrated that the more sterically demanding ^{t}Bu group was among the best for enantioselectivity, though no change was observed in diastereoselectivity (Figure 1.7, compare **7**-**10**).[41] Variation of substituents on the bridging carbon also influenced the diastereoselectivity of the reaction (Figure 1.7, compare **9**, **11-12**). However, no trend could be established to guide further ligand development. The introduction of substituents onto the carbon linker led to improvements in diastereoselectivity in some cases, but the major influence of diastereoselectivity is primarily dictated by the choice of diazo ester. Additional ligand development investigated using heteroatoms to bridge the two oxazolines rather than carbon. The inclusion of heteroatoms as the bridging atom also afforded high yields and enantioselectivity of the desired cyclopropanes. Yet this was not a drastic improvement upon that obtained with carbon as the bridging atom (Figure 1.7, compare **9** to **13**-**14**).

Asymmetric induction for both semicorrin and BOX catalysts stems from the C_2 symmetry of the complex where the Cu and the heterocyclic rings are considered planar.[42] A quadrant system about the Cu can then be generated by two intersecting planes. One plane includes the ligand and Cu metal. The second plane includes the Cu metal and is orthogonal to the first plane (Figure 1.8, a). The substituents on the oxazoline rings occupy two quadrants (quadrants 1 and 4), leaving two open quadrants (quadrants 2 and 3). The decomposition of the diazo reagent generates a carbenoid, which occupies the plane orthogonal to the plane of the ligand. It was determined that the carbon of the ester was not in conjugation with the carbene carbon. This then means that the alkoxy group of the

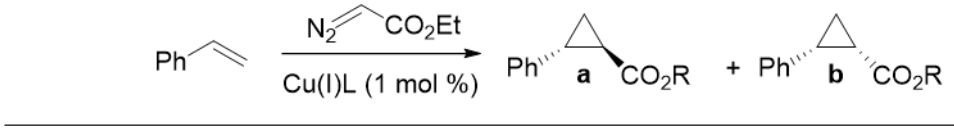

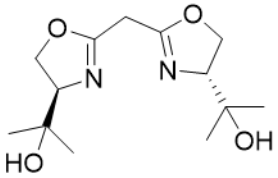

7
Yield = 88%
a/**b** 75:25
ee **a** 48%
ee **b** 36%

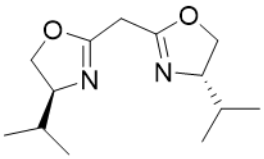

8
Yield = 72%
a/**b** 71:29
ee **a** 46%
ee **b** 31%

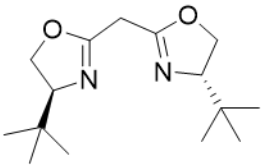

9
Yield = 80%
a/**b** 77:23
ee trans 98%
ee *cis* 93%

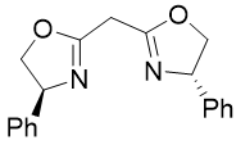

10
Yield = 81%
a/**b** 70:30
ee **a** 60%
ee **b** 52%

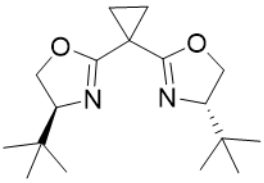

11
Yield = 85%
a/**b** 84:16
ee **a** >99%
ee **b** >99%

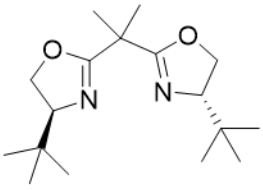

12
Yield[a] = NR
a/**b** 73:27
ee **a** 99%
ee **b** 97%

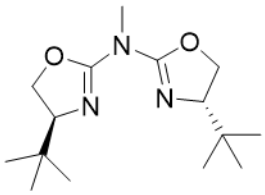

13
Yield[b] = 82%
a/**b** 73:27
ee **a** 92%
ee **b** 84%

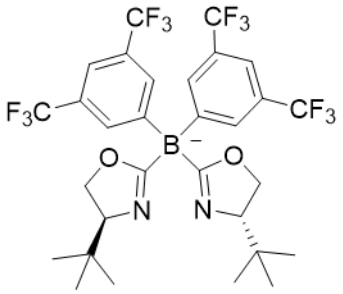

14
Yield = 89%
a/**b** 68:32
ee **a** 77%
ee **b** 68%

[a] Diazo reagent was methyl diazoacetate [b] 0.1 mol % catalyst loading

Figure 1.7 Effect of the backbone of the BOX ligand on catalytic activity

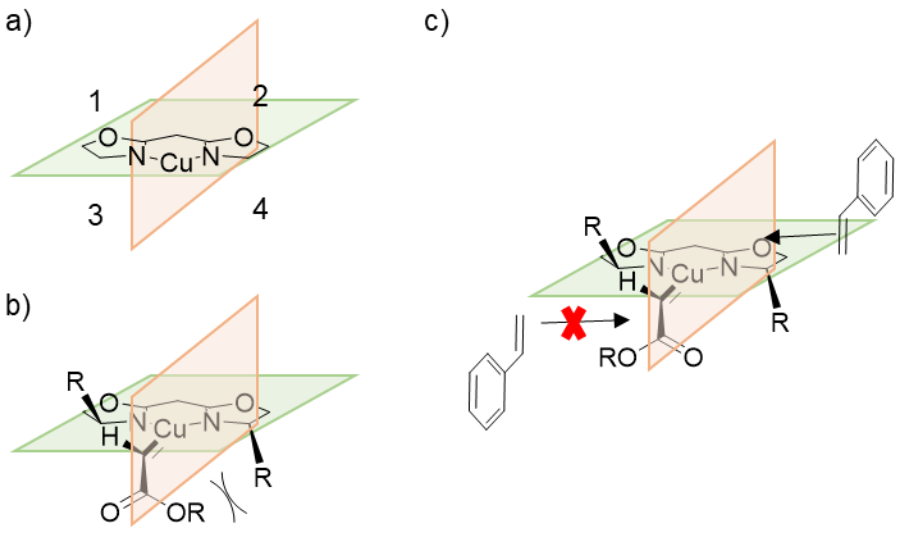

Figure 1.8 The a) different quadrants of Cu(I) complexes b) orientation of the carbenoid and chiral ligands and c) the approach of the olefin substrate

ester occupies either quadrant 3 or 4. Steric repulsion between the ester and chiral substituent is expected should the ester group be in quadrant 4 (Figure 1.8, b). This results in the preferred orientation where the alkoxy group of the ester occupies quadrant 3 (Figure 1.8, c). Experimental results support this model, as sterically demanding diazo esters afforded higher diastereoselectivity. The ester occupying quadrant 3 and the oxazoline substituents blocking quadrants 1 and 4 leave only one vector for the substrate to approach. Although the quadrant method provides a qualitative explanation of selectivity, it has minimal application towards predicting absolute configuration without experimental testing. More recent advancements towards stereochemical prediction have been made through computational analysis. By fitting data from a pool of experimental data, Aguado-Ullate and co-workers were able to accurately predict the stereochemical outcome in the cyclopropanation of styrene with EDA.[43]

Further ligand development led to the synthesis of tris(oxazoline) ligands which incorporate side arm substituents which can coordinate to the metal in a tripodal fashion. Side arm substituents are any group or functionality that is not the same as the original oxazoline group. Inclusion of side arm ligands is intended to increase the stereoselectivity of a reaction by acting as directing groups or blocking groups, thereby limiting the number of approach vectors for the olefin substrate. The side arm group could also possibly be a method of tuning the electronics of the metal center, making it more, or less, electrophilic.

Comparable yields and diastereoselectivity were obtained with Cu tris(oxazoline) and Cu BOX complexes; however, higher enantioselectivity was observed with Cu tris(oxazoline) complexes.[44] The tris(oxazoline) Cu complexes developed by Tang and co-workers facilitated the cyclopropanation of styrene with donor/acceptor diazo reagents in high yields and enantioselectivity, which was previously not observed with Cu catalysts.[45] Although the specifics are not certain, it is clear that the addition of the extra oxazoline moiety did increase the yield and enantioselectivity (Figure 1.9, **15**). It should be noted that only the yields of the *trans* isomer were reported, so the lower yields of **16** and **17** may be a result of low diastereoselectivity.

1.1.1.2 Cyclopropanation with Bipyridyl and Diamine Cu(I) Complexes

Bipyridine ligands have been employed to stabilize many metal centers and have been applied as catalysts in an array of reactions. Unsurprisingly, they were also applied

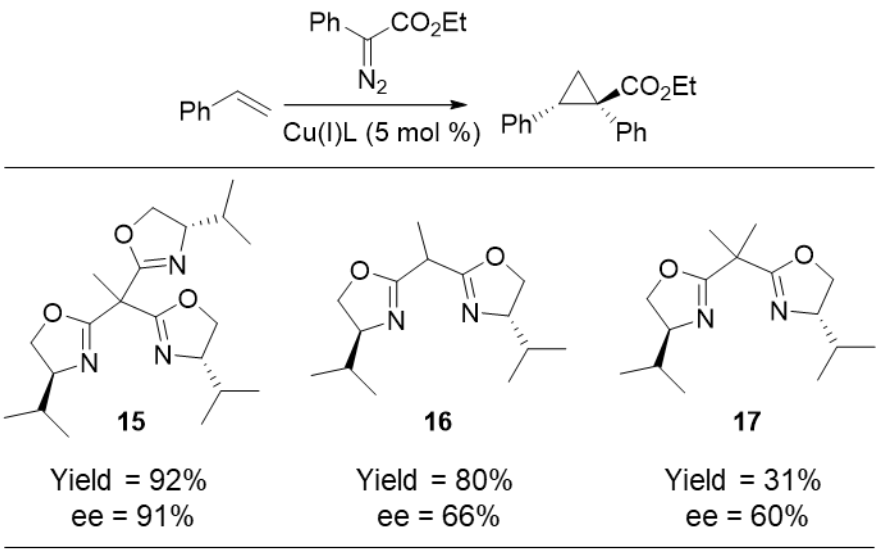

Figure 1.9 Effect of side arm substituents of Cu(I) BOX complexes

to cyclopropanation (Figure 1.10). The resemblance of bipyridine to BOX and semicorrin ligands made them logical candidates to promote the asymmetric cyclopropanation of olefins through the incorporation of chiral carbons at the 6 positions of the pyridine rings.[41] Based on the success of the semicorrin complex, initial tests were conducted using a similar chiral substituent seen in compound **18**. Incorporation of more sterically demanding substituents resulted in an increase in enantioinduction (Figure 1.10, **18**- **20**).[46] The increased steric bulk also seemed to result in an increase in the diastereomeric ratio. Further ligand development involved the incorporation of rings attached to the pyridine rings as a means of locking the chiral substituents near the Cu metal. This led to results similar to those observed with straight chains (Figure 1.10, **21-22**). As before, more sterically demanding substituents were more enantioselective (Figure 1.10, **23**-**24**).

Like BOX ligands, bipyridine ligands with various linkers were investigated.[47, 48] The addition of the *gem*-dimethyl did afford a more enantioenriched product. Unlike the BOX complexes, however, incorporation of bridging *gem*-dimethyl groups did not drastically improve enantioselectivity (Figure 1.10, compare **25** and **26**). Even the yield, reported as a range, did not best previous bipyridyl catalysts. Expansion of the bridging group resulted in lower stereoselectivity due to the chiral groups not being in proximity to the metal center (Figure 1.10, **25**-**28**).

The quadrant system developed for BOX complexes, as a means of explaining the observed stereochemical outcome, can also be applied to bipyridyl complexes. As can be seen, bipyridyl complexes are efficient catalysts for cyclopropanation of olefins. Diastereoselectivity seems to be lower with bipyridine complexes compared to Cu BOX complexes. This trend is highlighted with complexes **23** and **24** where ^{t}Bu diazoacetate, which typically results in high diastereoselectivity, afforded comparable diastereoselectivity when EDA was employed.[49] Despite this, the Cu pyridine complexes resulted in yields and enantioselectivity that are consistent with Cu BOX complexes.

1.1.1.4 Recent Developments in Cyclopropanation with Cu(I) Complexes

The applicability of copper catalysts continues to be observed. Many catalysts have been tested in the classic cyclopropanation of styrene and EDA to provide insight into its catalytic ability. However, the possibility still remains that a catalyst that performed poorly in this standard reaction may excel in a different cyclopropanation reaction. One

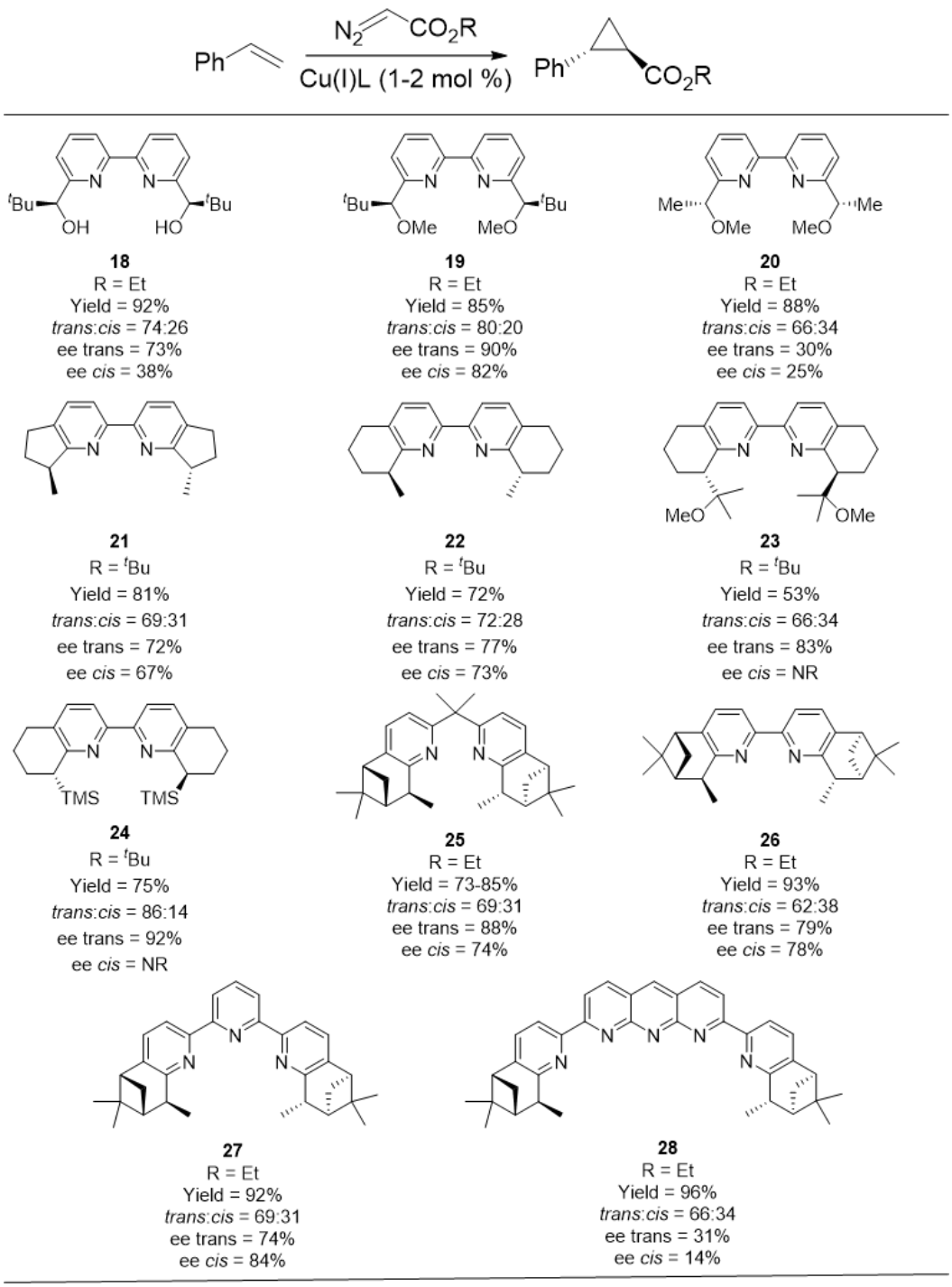

Figure 1.10 Cyclopropanation with select Cu(I) bipyridyl complexes

method for developing these reactions has been through the screening of a wide array of BOX ligands to find a complex that affords good stereoselectivity and at least moderate yields. Further catalyst screenings determine if favorable side arm effects can be used to increase the stereoselectivity. This methodology has been applied successfully in several instances for the cyclopropanation of multiply substituted olefins, a notoriously difficult substrate for cyclopropanation by metal carbenoids (Figure 1.11).[50-52] Activated alkenes such as styrene derivatives afforded good yields and stereoselectivities while nonactivated alkenes did not produce the desired cyclopropane product in a diastereoselective manner. Both *trans* and *cis* olefins yielded the desired cyclopropanes in good yields and high stereoselectivity. Extension of the alkyl chain resulted in lower yields, especially with the *cis* isomer. Further conjugation of the π system also resulted in a highly stereoselective and high yielding reaction. Another recent example followed a similar protocol in developing the cyclopropanation of a styryl derivative. Cyclopropanation of 1,2-*cis* disubstituted olefins using acceptor/acceptor diazo agents was also realized. Each disubstituted olefin afforded high stereoselectivity and modest to excellent yields depending on olefin substitution.[52, 53] Another interesting example of using catalyst screening methods involves the cyclopropanation of disubstituted alkenylboranes to afford borylcyclopropanes.[54] It should be noted, however, that an increase in catalyst loading (up to 5 mol %) was required to facilitate these reactions.

The continued utility of Cu complexes is realized through their application in recent syntheses of natural products and biologically relevant molecules. One synthetic application is taking advantage of the cyclopropane ring as a synthetic handle for further transformations. This strategy is made possible by the reactivity of cyclopropanes due to ring strain.[55] Both Ichikawa and Watanabe implemented this approach for the enantioselective syntheses of exigurin and (+)-exiguamide (Figure 1.12).[56, 57] The Cu(II) salicylaldimine complex facilitated the reaction with a lower catalyst loading than CuOTf, although elevated temperatures (80 °C) were required to drive the reaction forward. Under these conditions, the Cu salicylaldimine complex resulted in a higher yield of the desired cyclopropane. Sawada and co-workers also employed a cyclopropane as a synthetic handle for the synthesis of (+)-colletoic acid. The asymmetric cyclopropanation occurred with high enantioselectivity (91 % ee, >99% ee after recrystallization).

Another synthetic application of Cu catalysis is the synthesis of the cyclopropane as part of the final product. A recent example was the synthesis of the natural product

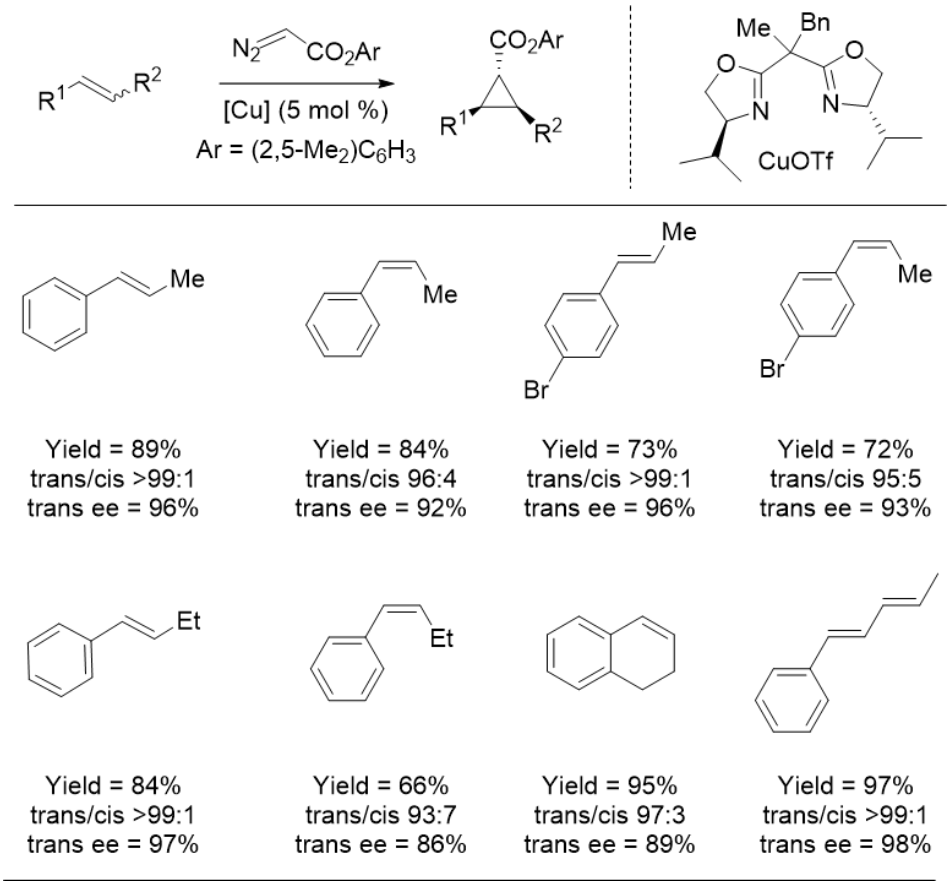

Figure 1.11 Cyclopropanation of internal olefins with a Cu(I) BOX complex

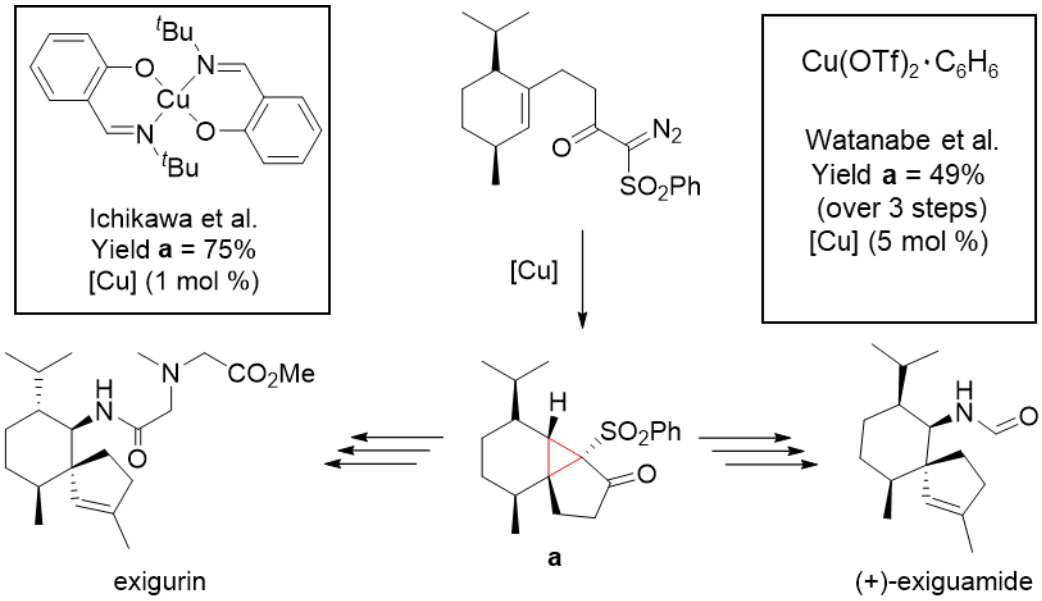

Figure 1.12 Total syntheses of exigurin and (+)-exiguamide using cyclopropanation with Cu(I) catalysts as a key step

(+)-salivileucalin B (Figure 1.13, a), which demonstrated cytotoxicity for different cancer lines.[58, 59] Exposure of the diazo compound to Cu hexafluoroacetoacetate (hfacac) resulted in the installation of the cyclopropane ring via intramolecular cyclopropanation of the aryl ring. It should be noted a high catalyst loading (10 mol %) was required for this intramolecular transformation. The requirement for high catalyst loading was also observed for the synthesis of the E ring of the core to the polycyclic natural product Andilesin C, which required 25 mol % of achiral $Cu(acac)_2$ (Figure 1.13,b).[60] Although this portion of the molecule has been accomplished, work towards a total synthesis is ongoing.

Intermolecular cyclopropanation reactions with Cu complexes continue to be an efficient method of establishing chiral centers. Unlike the intramolecular examples, chiral Cu complexes play a more prominent role in achieving the desired asymmetric product. Two recent examples involve BOX ligands **29** and **30**, derived from D-glucosamine (Figure 1.14, a and b). The cyclopropanation of methyl indole led preferentially to the *exo* cyclopropane product with good enantioselectivity. This expands upon already established methodology for the synthesis of many alkaloid compounds via inter or intramolecular cyclopropanation of indole derivatives.[61] From this cyclopropane intermediate, (-)-desoxyeseroline could be accessed in five steps (Figure 1.14, a).[62] Cyclopropanation of 1-heptene and EDA using **30** establishes the stereocenters of the cyclopropane ring of (+)-grenadamide (Figure 1.14, b).[63] The ester was then used as a functional handle for the addition of the rest of the molecule. Cyclopropanation of an olefin via a Cu BOX carbenoid species was also implemented towards the synthesis of the core of cryptotrione. This reaction gave high yields (95%) and good dr (>10:1) for the desired product (Figure 1.14, c).[64]

1.1.2 Silver

While Ag has been known to decompose diazo reagents and form Ag carbenoids, its application towards cyclopropanation has been limited. This is believed to be due to the competition between carbenoid formation and a Wolff rearrangement.[65] The rearrangement results from Ag acting as a Lewis acid to facilitate the formation of a ketene, rather than a carbenoid. In an attempt to synthesize Ag(I) carbenoids, Dias and co-workers developed Ag(I) scorpionate complexes (Figure 1.15, a). Subjecting complex **31** to dimethyl diazomalonate resulted in the coordination of the diazo reagent without diazo

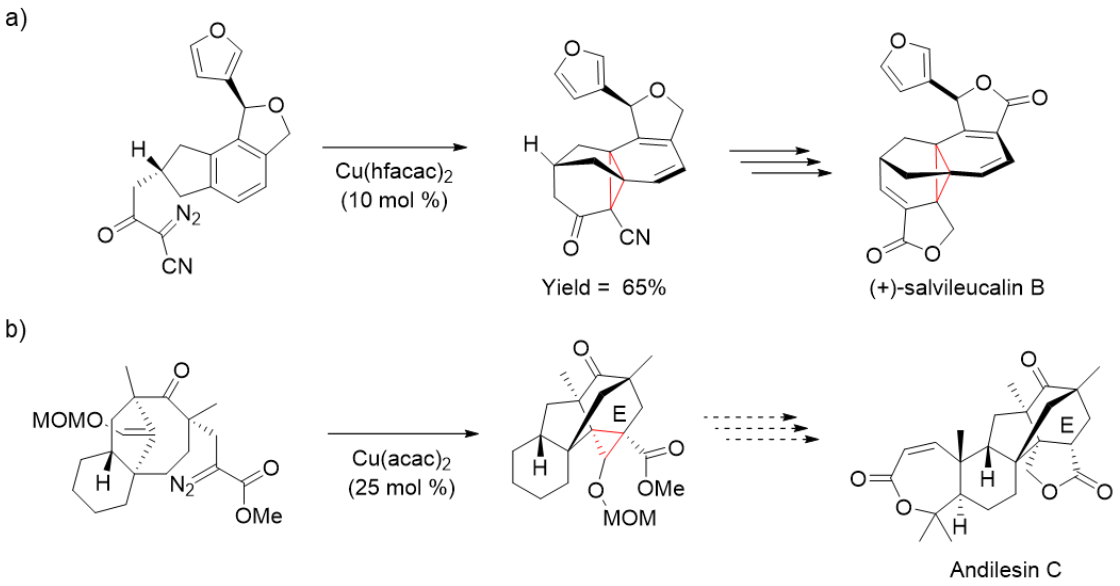

Figure 1.13 Total syntheses employing Cu(I) catalysts to install asymmetric cyclopropane ring

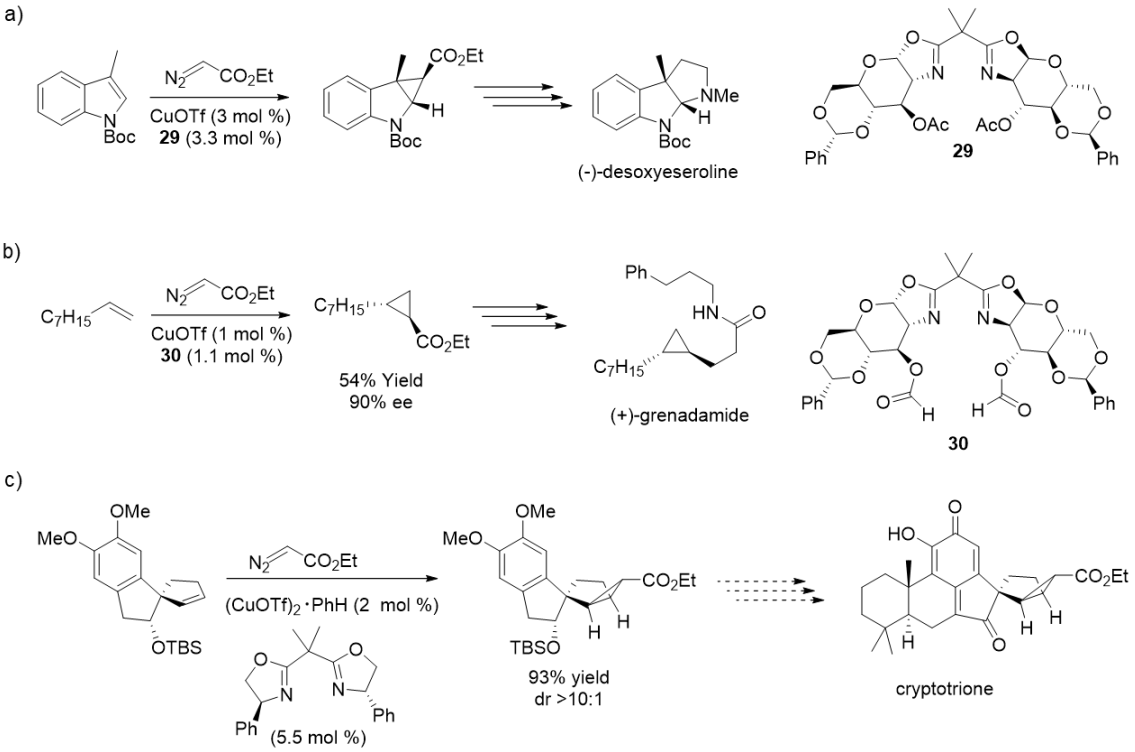

Figure 1.14 Total syntheses using Cu(I) catalysts to install the desired cyclopropane

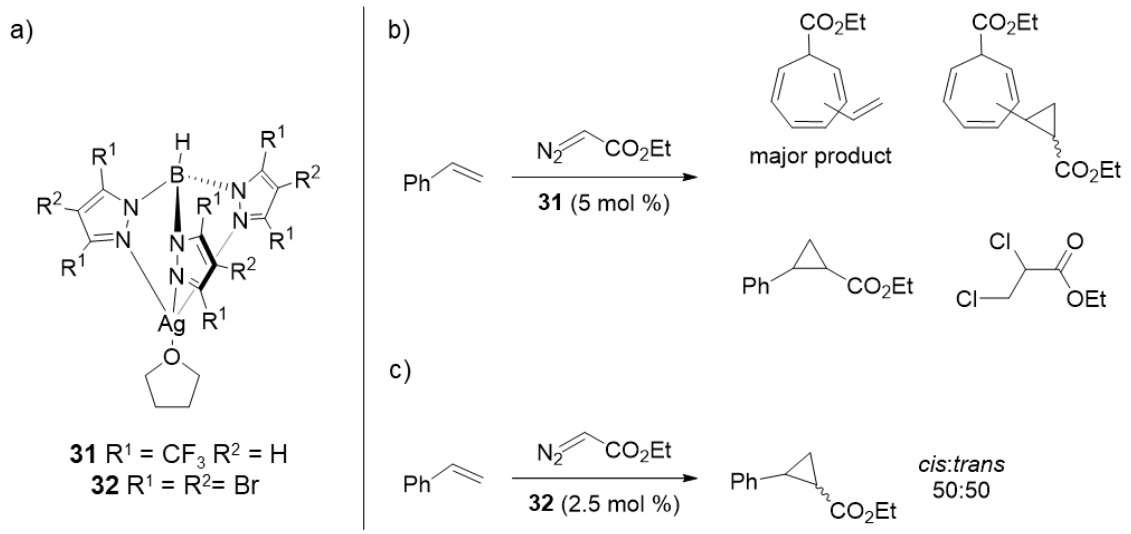

Figure 1.15 Example of a) Ag(I) scorpionate complexes and b) application as catalysts in cyclopropanation of styrene and EDA

decomposition.[66] Attempts were made to synthesize the analogous complex with EDA, but no stable complex could be isolated. Rather, gas evolution was observed, indicating the diazo reagent was being decomposed. Applying the scorpionate complex as a catalyst for the cyclopropanation of styrene and EDA resulted in a complex mixture of products (Figure 1.15, b). The mixture of products included cycloheptatrienes, resulting from a Buchner reaction, as the major product. However, a mixture of cyclopropane products was also observed. The brominated scorpionate Ag(I) complex **32** facilitated the same reaction to afford the cyclopropane product as a 1:1 mixture of the *cis* and *trans* isomers.[67] In each of these cases, the overall yield was not reported but did set the precedent for Ag(I) carbenoid mediated cyclopropanation.

Davies and co-workers demonstrated that cyclopropanation of styrene and donor/acceptor diazo reagents could be facilitated by simple Ag(I) salts (Figure 1.16).[68] A wide range of Ag(I) salts were examined and It was noted that the anion affected the yield of the reaction. Anions with strong electron withdrawing groups resulted in lower yields. Of these silver salts, $AgSbF_6$ was compared to $Rh_2(OAc)_4$ and demonstrated higher chemoselectivity, regioselectivity, and diastereoselectivity. Despite these advantages, the Ag salts were not enantioselective. This was not unexpected because no chiral ligands were investigated.

1.1.2.1 Recent Developments for Cyclopropanation of Olefins by Ag(I) Carbenoids

Not many recent reports have been made on homogeneous Ag(I) catalysts. One example from 2019 by Wang and co-workers demonstrated chemoselective cyclopropanation of indoles with vinyl diazoacetates. The application of simple Ag(I) salts as catalysts resulted in cyclopropanation of the olefin, rather than alkylation. Further optimization of the reaction showed that $AgNTf_2$ afforded the highest yield of the salts tested. A substrate scope was then conducted showing a high tolerance for the incorporation of aryl substituents on both the indole substrate and aryl vinyl diazo reagents (Figure 1.17, **33**-**35**,**38**).[69] Addition of bulkier substituents on the aryl ring of the indole did not inhibit the reaction or decrease the diastereomeric ratio. Variation of the protecting group (PG) resulted in only moderate to good yields, indicating the importance of the

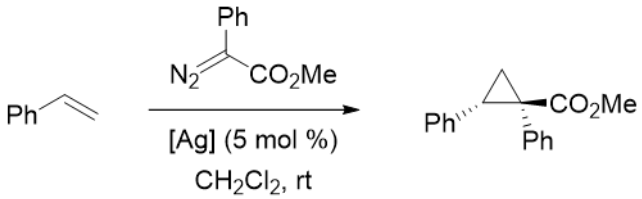

Catalyst	*Yield %*	Catalyst	*Yield %*
$AgSbF_6$	91	$AgNO_3$	67
$AgBF_4$	85	AgO_2CCF_3	64
$AgCO_2Ph$	75	AgOAc	29
$AgNTf_2$	70	Ag_2SO_4	NR

Figure 1.16 Cyclopropanation of styrene and methyl phenyldiazoacetate with Ag(I) salts

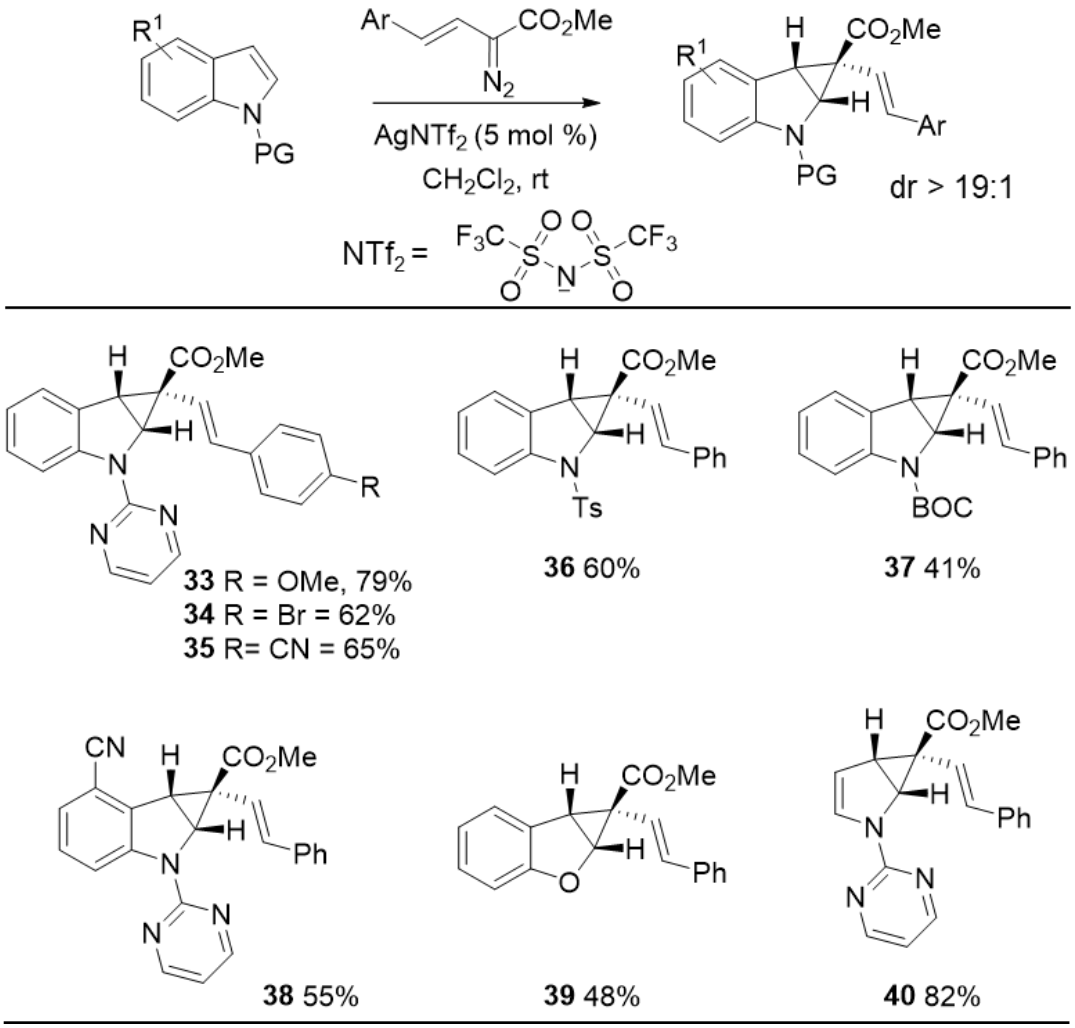

Figure 1.17 Cyclopropanation of N-protected indole with $AgNTf_2$

2-pyrimidinyl PG (Figure 1.17, **33**,**36**-**37**). This could have been the result of the additional N atoms further activating the olefin, which promoted cyclopropanation. Successful cyclopropanation was further observed with protected pyrroles, in addition to benzofuran **39**. Introduction of the more electronegative oxygen atom did result in lower yields but maintained the same dr (>19:1) as observed with indole (Figure 1.17, **39**-**40**). It is worth noting that good to great yields were obtained even without employing techniques to limit the formation of the homocoupled diazo product.

1.1.3 Gold

One of the last metals to demonstrate the ability to generate carbenoids from diazo compounds, gold has begun to see an increase in research. In 2005, Fructos and co-workers observed that an Au(I) N-heterocyclic carbene (NHC) complex facilitated the cyclopropanation of styrene and EDA (Figure 1.18, a).[70] The Au(I) species was generated *in situ* with the addition of a halogen scavenger such as sodium tetrakis(3,5-bis(trifluoromethyl)phenyl)borate (NaBArF). Halogen removal also generated an open metal binding site for coordination of the diazo reagent. As such, halogen scavengers have become a staple in the application of Au NHC complexes for the decomposition of diazo compounds. The Au(I) catalysts were able to facilitate the cyclopropanation of styrene and EDA but a formal sp^2 C–H insertion was the major product. Cyclooctene was also tested and resulted in a high yield (99%) of the cyclopropane. In this case, no other products were detected (Figure 1.18, b). The diastereoselectivity was not reported for these reactions, nor was enantioselectivity reported. Despite no asymmetric induction being observed, these reactions provided the foundation for future ligand development.

1.1.3.1 Cyclopropanation with Au(I) Phosphine Complexes

Based on the ability of the NHC ligand to facilitate cyclopropanation, electronically similar phosphines were also investigated as ligands. The antimony hexafluoride salts of the Au(I) phosphine complexes were applied as catalysts for the cyclopropanation of styrene and EDA, resulting in no reaction. However, a donor/acceptor diazo reagent resulted in formation of the cyclopropane product in high yield, exclusively as the *trans* isomer (Figure 1.19, a).[71] Unlike with NHC catalysts, no insertion products were observed.

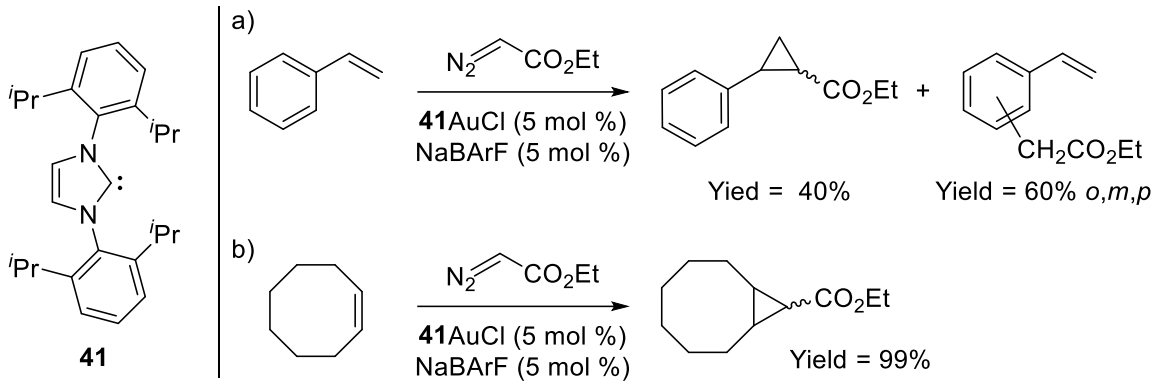

Figure 1.18 **C**yclopropanation of olefins via an Au(I) NHC complex

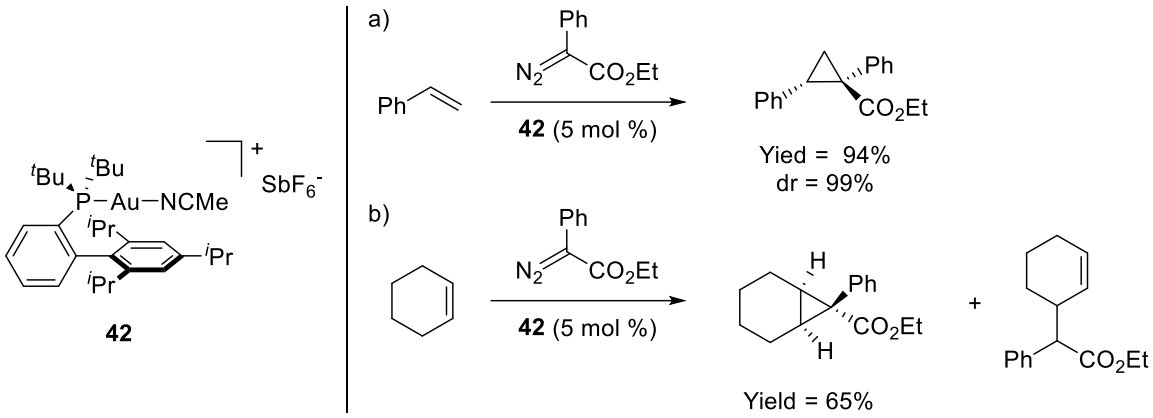

Figure 1.19 Cyclopropanation of olefins with an Au(I) phosphine complex

Cyclohexene was tested as a substrate and resulted in the formation of the cyclopropane product. Even though only a single diastereomer was observed, it was accompanied by trace amounts of the C–H insertion product (Figure 1.19, b).

1.1.3.2 Recent Developments for Cyclopropanation of Olefins by Au(I) Carbenoids

Phosphine ligands found further application by facilitating asymmetric cyclopropanation when a bidentate spirocyclic phosphine ligand was complexed to the Au metal (Figure 1.20, a). The more elaborate diazo reagent, diazooxindole, underwent cyclopropanation with 1,2-disubstituted olefins to afford spirocyclopropyloxindoles. Both the *cis* and *trans* olefins readily underwent cyclopropanation. It was noted that cyclopropanation of *cis* olefins could be accomplished by generating the Au(I) catalyst *in situ* (Figure 1.20, b).[72] Conversely, the same study indicated cyclopropanation of *trans* olefins required addition of the isolated Au(I) catalyst. Each of the 12 *trans* olefin substrates afforded highly diastereoselective (>20:1 dr) and enantioselective (ee ≥ 88%) products. A variety of *trans* olefins were also tested and gave similar results to that observed with *cis* olefins but afforded the opposite diastereomer. It should be noted that the formation of the *cis* cyclopropane required generation of the Au(I) complex *in situ*. Conversely, the *trans* cyclopropane was formed by the addition of the isolated Au(I) complex. The phosphine ligand **43** was also incorporated into an Au(I) catalyst that proved efficient for the cyclopropanation of 1,1-disubstituted olefins containing fluorinated substituents (Figure 1.20, c).[73]

Another class of chiral Au(I) catalyst was developed by incorporating monodentate phosphoramidite ligands (Figure 1.21). These catalysts were shown to be active with donor/acceptor diazo reagents to afford the cyclopropanation of enamides, providing access to complex N-heterocyclic compounds.[74] The active catalyst was once again generated *in situ* by the introduction of a halogen scavenger. The desired cyclopropane product was obtained in good yields but remained lower than many other cyclopropanation reactions. This could be a result of the rapid addition of the diazo reagent which could result in a higher concentration of diazo compound, resulting in the formation of the homocoupled product. Of the three catalysts tested, the Au(I) catalyst with ligand **44** afforded the highest yield. Despite only achieving modest to good yields, only a single

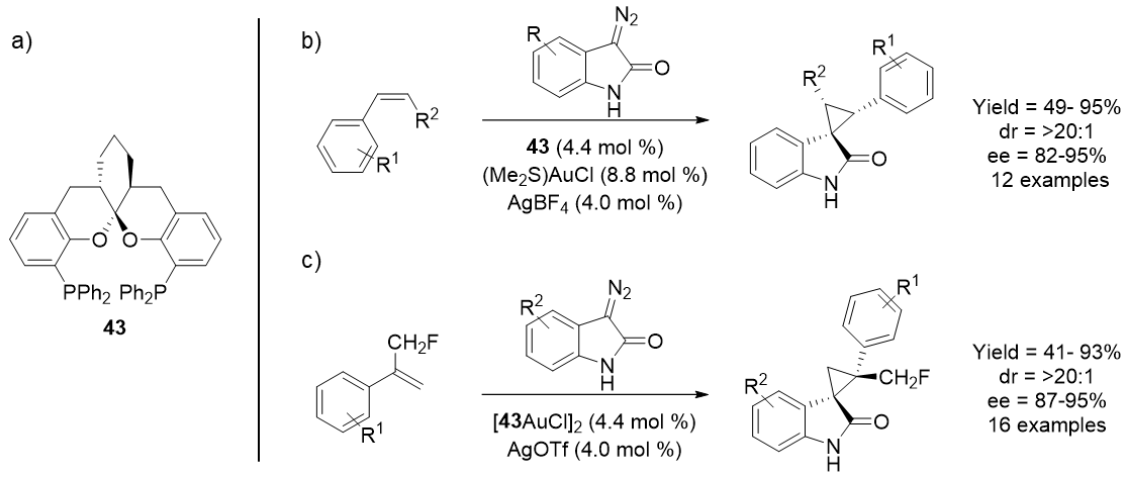

Figure 1.20 Asymmetric Cyclopropanation of olefins with Au(I) bisphosphine complexes

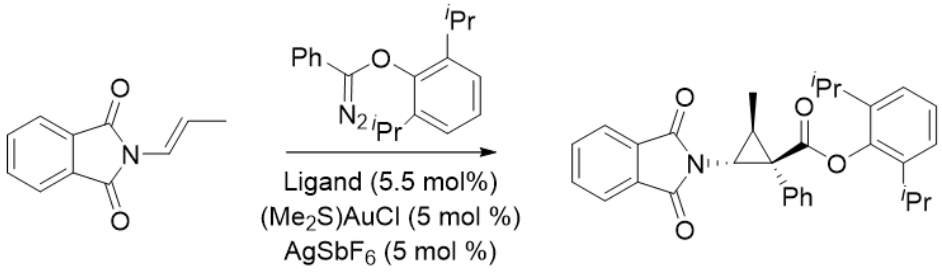

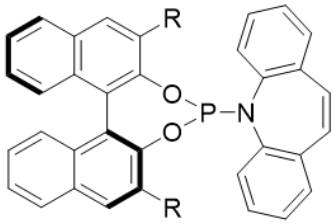

44 R = 3,5-$(CF_3)_2C_6H_3$

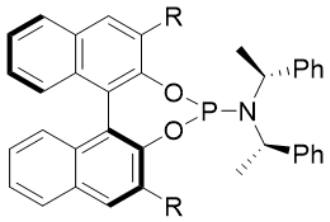

45 R = H
46 R = 3,5-$(CF_3)_2C_6H_3$

Ligand	*Yield (%)*	ee (%)
44	66	98
45	47	40
46	52	81

Figure 1.21 Asymmetric cyclopropanation of enamides with chiral Au(I) phosphoramidite complexes

diastereomer of the cyclopropane product was observed with each of the catalysts. Again, the Au(I) catalyst with ligand 44 was the lead catalyst, achieving the highest enantioselectivity. It appeared that bulky aryl substituents played a large part in facilitating higher enantioselectivities.

Quite recently, Peréz et. al. demonstrated that ethylene could be cyclopropanated with EDA in 62% yield by an Au(I) NHC complex (Figure 1.22).[75] The reaction was conducted with the catalyst and diazo compound dissolved in dichloromethane (DCM) under an ethylene atmosphere. It was noted that a silver salt halogen scavenger was required to facilitate reactivity. The product distribution seemed to be controlled by the choice of silver salt. In each case, only small amounts of the homocoupled diazo product were observed.

1.1.4 Rhodium

The most prevalent Rh complex for cyclopropanation of olefins is the dirhodium(II) paddlewheel (Rh^{II}) complex.[76] The most common Rh^{II} complex is dirhodium(II) tetrakisacetate ($Rh_2(OAc)_4$), which consists of four bridging ligands and two axial sites (Figure 1.23). The axial site is the catalytically active site with only one of the Rh atoms generating a carbenoid per turnover.[77] Work by Teyssié and co-workers demonstrated the potential of Rh^{II} carboxylate complexes as catalysts for the cyclopropanation of olefins with diazo reagents.[78] Variation of the electron donating ability of the bridging ligand enabled chemospecific intramolecular reactions (Figure 1.24).[79] The benchmark $Rh_2(OAc)_4$ gave nearly 1:1 product distribution between the cyclopropanation product and the C-H insertion product. The more electron poor catalyst dirhodium(II) tetrakisperfluorobutyrate ($Rh_2(pfb)_4$) afforded the formal C–H insertion product as a single product. Conversely, the electron rich Rh^{II} complex dirhodium(II) tetrakiscarprolactamate ($Rh_2(cap)_4$) was selective for cyclopropanation to afford the fused bicyclic compound.[79] This indicated that modification of the bridging ligand heavily influenced the electronics of the metal, and thereby modulated the carbenoid reactivity during the intramolecular reaction.

A small degree of diastereocontrol was exhibited with achiral Rh^{II} complexes during intermolecular cyclopropanation (Figure 1.25).[80] It can be seen the electron rich Rh^{II} complex dirhodium(II) tetrakisacetamidate ($Rh_2(acam)_4$) resulted in a modest

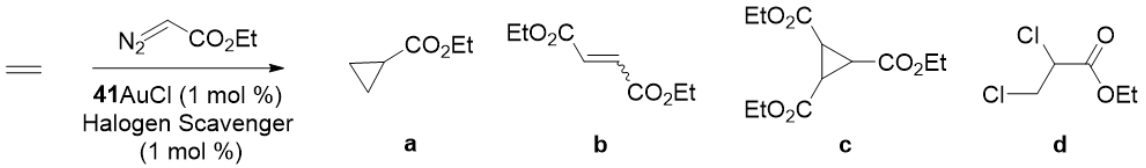

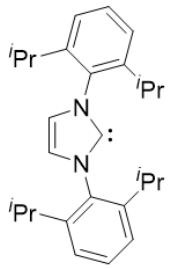

41

Halogen Scavenger	*% **a***	*% **b***	*% **c***	*% d*	*% EDA*
None	0	4	0	0	40
AgOTf	2	2	9	ND	80
$AgSbF_6$	25	0	ND	>70	ND
NaBArF	62	2	ND	ND	36

Figure 1.22 Cyclopropanation of ethylene and EDA with an Au(I) NHC complex

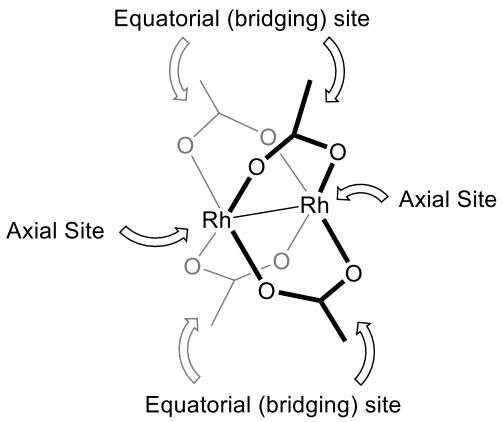

Figure 1.23 The Rh^{II} $Rh_2(OAc)_4$ with the bridging site and axial site labeled

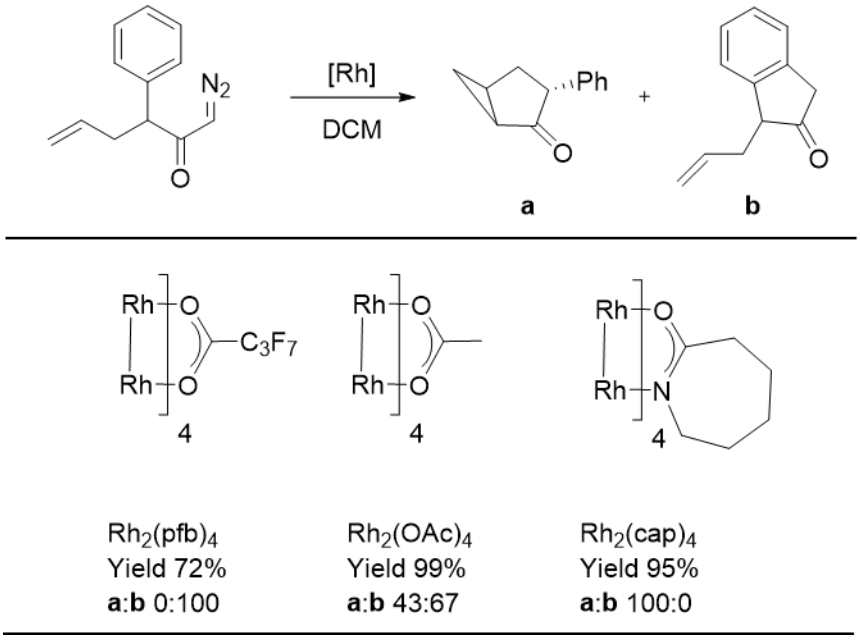

Figure 1.24 Chemoselectivity of electron rich and electron poor Rh^{II} catalysts

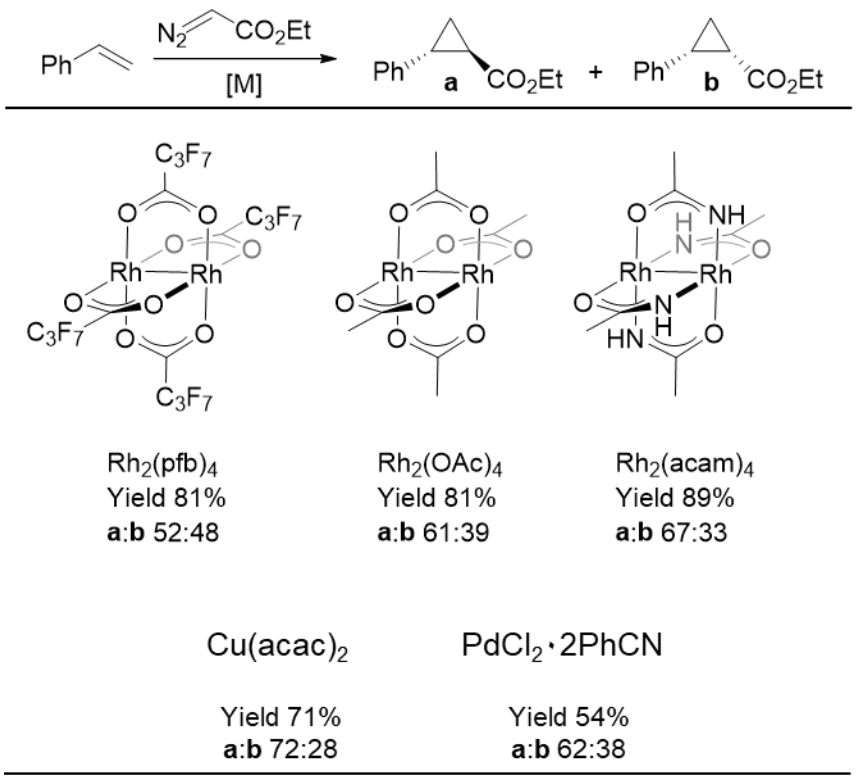

Figure 1.25 Diastereoselectivity of electron rich and electron poor achiral Rh^{II} catalysts and other common catalysts

increase in selectivity for the *trans* product. The yields achieved with Rh^{II} complexes were higher than other common metal catalysts, despite being less diastereoselective.[30] This indicated the Rh^{II} complexes were more reactive, which could enable lower catalyst loading.

Unlike many other catalysts, Rh^{II} complexes contain a bimetallic core. The second Rh does not interact directly with the carbene but does influence the electronics of the Rh bound to the carbene. This interaction is best understood when considered with a 3 center/ 4 electron (3c/4e) model. The simplest example of a 3c/4e system is H_3^- and can be represented by two resonance structures (Figure 1.26, a). A classic 2 center/ 2 electron (2c/2e) bond is present between two hydrogen atoms (H_b and H_c). The third hydrogen atom (H_a) forms a dative bond by donating into the antibonding orbital of H_b and H_c. This donation can lead to the formation of a 2c/2e bond between H_a and H_b, leaving H_c to form a dative bond. However, calculations indicate that this molecule is better represented as an average, with H_b forming two weaker bonds with both H_a and H_c. When applied to the Rh^{II} carbenoid species, the three centers are the two Rh atoms and the carbene carbon (Figure 1.26, b). The first resonance structure shows the Rh–Rh as the 2c/2e bond, and the carbene forms a dative bond by donating into the Rh–Rh antibonding orbital. The second resonance structure involves the formal oxidation of one Rh and the reduction of the distal Rh. As in the case of H_3^-, calculations indicated that Rh was bound to both the carbene carbon and Rh and is believed to be the major contributor.[81] The presence of two Rh(II) centers is further supported by experimentation. Analysis of an isolated Rh^{II} carbenoid species demonstrated the oxidation state of the Rh metals does not occur.[82]

The current understanding of the catalytic cycle is shown in Scheme 1.2 with an overlay of the pertinent orbitals.[13, 81, 83] Initiation of the process arises from the coordination of the diazo reagent to the electrophilic Rh metal at the axial site of the Rh^{II} complex (Scheme 1.2, **a**). After this coordination, the π backbonding from the π* of the Rh^{II} complex promotes the loss of dinitrogen (Scheme 1.2, **b**), the rate-limiting step, resulting in the carbenoid species (Scheme 1.2, **c**). This species is most accurately modeled as a 3c/4e system describe above. Stabilization of the electrophilic carbenoid arises from electron donation from the Rh metal via π backbonding. A stepwise pathway (Scheme 1.2, **d** and **e**) is supported by experimental and computational kinetic isotope effect experiments.[13] However, this process occurs so rapidly it has been classified as an asynchronous concerted process. The process begins when the electrophilic carbenoid

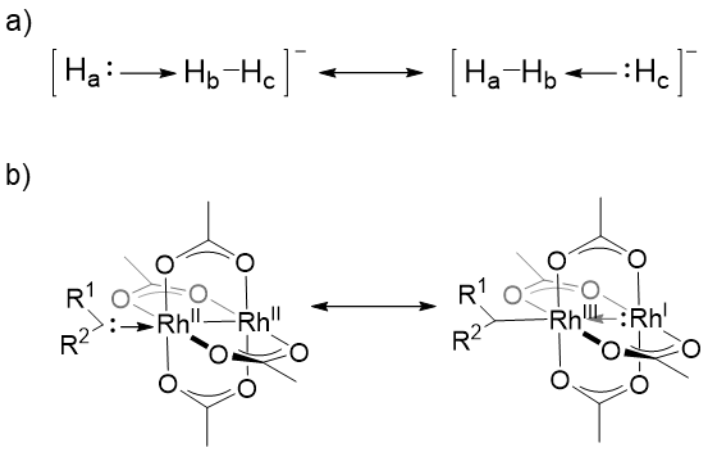

Figure 1.26 Resonance forms of the 3c/4e systems of a) H_3^- and a b) Rh^{II} carbenoid

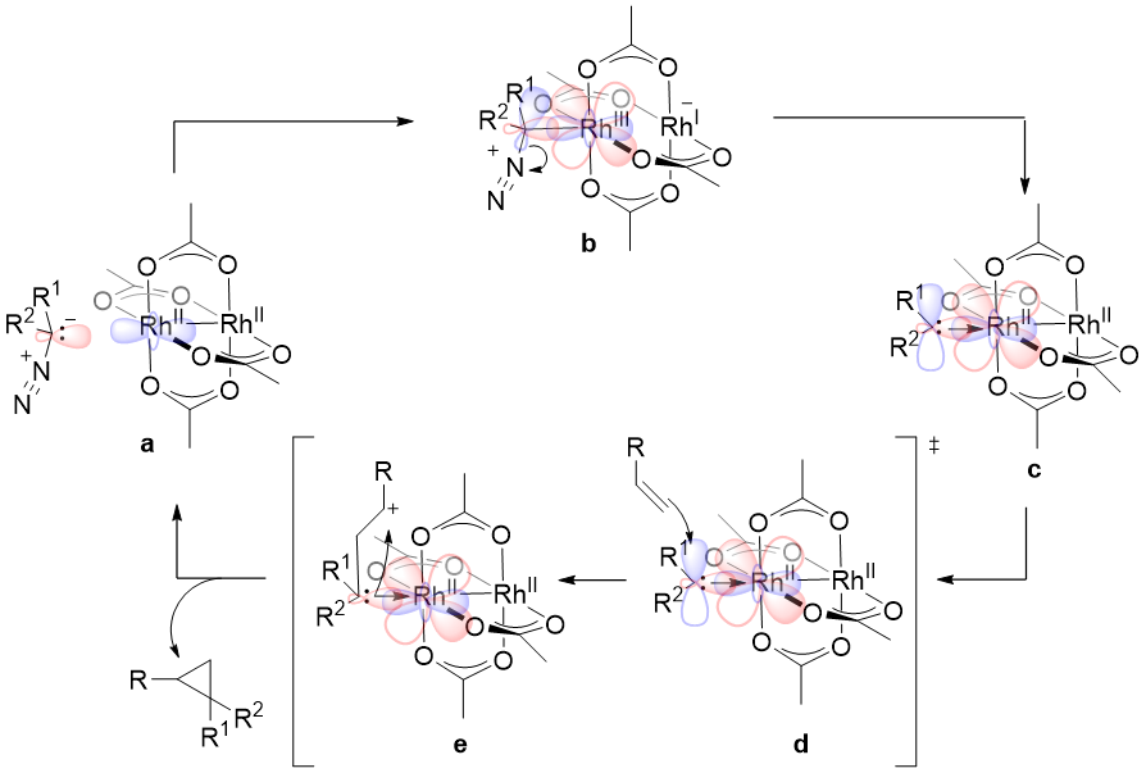

Scheme 1.2 Catalytic cycle of cyclopropanation of styrene with a diazo compound by a Rh^{II} complex a) coordination of diazo b) backbonding by Rh facilitates extrusion of nitrogen c) the reactive carbenoid d) nucleophilic attack by the olefin e) and final ring closure

is then attacked (Scheme 1.2, **d**) by the olefin substrate in an end-on fashion. The σ portion of the 3e/4c then completes the cyclopropanation (Scheme 1.2, **e**) and regenerates the catalyst, completing the catalytic cycle.

Over time, a large library of Rh^{II} complexes was generated with different bridging ligands leading to improved diastereoselectivity, in a highly enantioselective fashion.[84] Of the many Rh^{II} complexes, those based on carboxamidiate, carboxylate, and N-protected amino acids have proven most successful and widely applied.

1.1.4.1 Rh^{II} Complexes Derived from Carboxamidates

Chiral Rh^{II} carboxamidate complexes were first realized by Doyle and co-workers with the synthesis of dirhodium(II)tetrakis[methyl 2-pyrrolidone-5(*S*)-carboxylate] (Rh_2(*S*-MEPY)$_4$) **47**, based on a chiral pyrrolidinone ligand (Table 1.2).[85] Further ligands were developed based on oxazolidinone, imidazolidinone, and azetidinone moieties.[86] Both the *R* and *S* enantiomer of many carboxamidate catalysts have been synthesized, but the *S* enantiomer is the most prevalent due to the availability of the corresponding amino acid starting material.

Applying these complexes in the benchmark intermolecular cyclopropanation of styrene and EDA showed that the azetidinate complex was the most reactive carboxamidate complex (Table 1.2, entry 2). However, the carboxamidate catalysts tested resulted in lower yields than the carboxylate $Rh_2(OAc)_4$. It was noticed that carboxamidates tended to favor the *cis* cyclopropane rather than the thermodynamically favored *trans* cyclopropane, although not by a large margin (Table 1.2, entries 1-4).[87] Controlling diastereoselectivity was challenging even with esters containing large alkoxy groups, which worked with other metals. However, these large alkoxy groups did facilitate an increase in enantioselectivity, most notably of the *cis* isomer (Table 1.2, entries 5-7). Despite providing access to the *cis* enantiomer, these reactions were not as high yielding as more easily synthesized catalysts.

Conversely, carboxamidate Rh^{II} complexes were shown to be highly effective in intramolecular asymmetric cyclopropanation reactions. Compared to a common Cu BOX complex, the enantioselectivity observed with the carboxamidates was significantly higher (Table 1.3, compare entry 1 to others).[88] It was noted that high enantioselectivity was

Table 1.2 Cyclopropanation of styrene and EDA with various Rh^{II} complexes

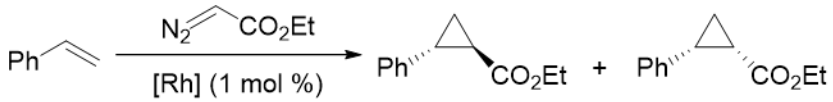

Entry	Catalyst	R	*Yield (%)*	**a**/**b**	*ee* ***b*** *(%)*
1	Rh_2(*S*-MEPY)$_4$	Et	59	56:44	33
2	Rh_2(*S*-IBAZ)$_4$	Et	62	36:64	68
3	Rh_2(*S*-PHOX)$_4$	Et	41	34:66	57
4	$Rh_2(OAc)_4$	Et	93	62:38	ND
5	Rh_2(*S*-MEPY)$_4$	*l*-menthyl	34	52:48	80
6	Rh_2(*S*-IBAZ)$_4$	*l*-menthyl	56	38:62	88
7	Rh_2(*S*-PHOX)$_4$	*l*-menthyl	19	27:73	72
8	$Rh_2(OAc)_4$	*l*-menthyl	82	68:32	ND

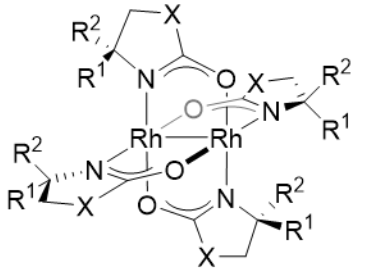

pyrrolidinate

47 (X = CH_2 R^1 = CO_2Me R^2 = H) : Rh_2(*S*-MEPY)$_4$

48 (X = CH_2 R^1 = H R^2 = Ph) : Rh_2(*S*-PHOX)$_4$

oxazolidinate

49 (X = O R^1 = CO_2Me R^2 = H) : Rh_2(*S*-MEOX)$_4$

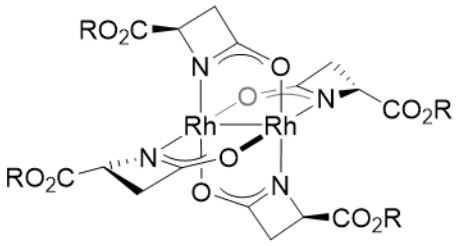

azetidinate

50 R= $(CH_3)_2CHCH_2$ Rh_2(*S*-IBAZ)$_4$

Table 1.3 Selected examples of intramolecular cyclopropanation with Rh^{II} carboxamidate catalysts compared to a Cu(I) Box catalyst

Entry	Catalyst	R^1	R^2	R^3	*Yield %*	ee
1	$Cu(MeCN)_4PF_6$/**12**	Me	Me	H	80	13
2	Rh_2(*S*-MEPY)$_4$	Me	Me	H	82	98
3	Rh_2(*R*-MEPY)$_4$	Me	Me	H	83	98
4	Rh_2(4*S*,2'*S*,3'*S*-MCPIM)$_4$	H	H	Me	70	80
5	Rh_2(4*S*,2'*R*,3'*R*-MCPIM)$_4$	H	H	Me	65	52
6	Rh_2(*S*-MEPY)$_4$	H	C_6H_5	H	45	≥94
7	Rh_2(*S*-MEPY)$_4$	C_6H_5	H	H	59	65

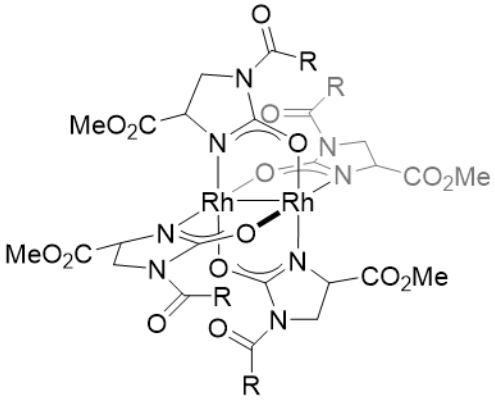

imidizolinate

R =

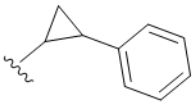

51 Rh_2(MCPIM)$_4$

achieved when either enantiomer of the carboxamidate ligand was incorporated as the bridging ligand (Table 1.3, entries 2-3). This was in contrast to a separate study where a clear drop in enantioselectivity was observed when comparing two Rh^{II} complexes containing two diastereomers as the bridging ligands (Table 1.3, entries 4-5).[89] The *cis* isomer of the olefin resulted in higher enantioselectivity, compared to the *trans* isomer (Table 1.3, entry 6-7).[90]

The formation of asymmetric products is made possible because the chiral group of the bridging ligands protrude over the axial site. In the case of Rh_2(*S*-MEPY)$_4$ (Figure 1.27, a) the chiral methyl esters are protruding over the axial site.[91] By defining a plane that is perpendicular to the Rh–Rh bond, the ligands can be defined as protruding over either the α or the β face (Figure 1.27, b). The methyl esters of Rh_2(*S*-MEPY)$_4$ are arranged in an α, α, β, β orientation such that a "wall" is generated on one side of the axial site (Figure 1.27, c). This "wall" blocks one face of the carbenoid from nucleophilic attack by the olefin substrate resulting in an enantioselective reaction. Common small acceptor diazo reagents, such as EDA, will have little to no preference for the ester orientation which results in mixtures that are essentially racemic. As the alkoxy group of the diazo reagent becomes larger, such as ^{t}Bu or menthyl diazoester, the ester interacts with the chiral ligand sphere resulting in higher enantioselectivity.

The effect is heightened when intramolecular reactions are conducted. Intramolecular cyclopropanations are often used to facilitate the formation of lactones and can be rationalized through the formation of a chair-like intermediate (Figure 1.27, d). The folding of the chair happens opposite of the chiral wall due to increased steric interactions between the wall and decomposed diazo compound. Further influence of the catalyst can be seen with a preference for terminal alkenes. Internal substitution of the olefin results in a higher energy intermediate due to the substituent (R^1 Figure 1.27, d) oriented directly into the paddlewheel structure.

1.1.4.2 Rh^{II} Complexes Derived from Prolinates

Prolinate complexes were first discovered by McKervey and co-workers and were demonstrated to efficiently decompose diazo reagents.[92] When applied to classic acceptor diazo compounds, their selectivity was lower than that observed with carboxamidates.[93] The combination of reactive diazo reagent and reactive Rh^{II}

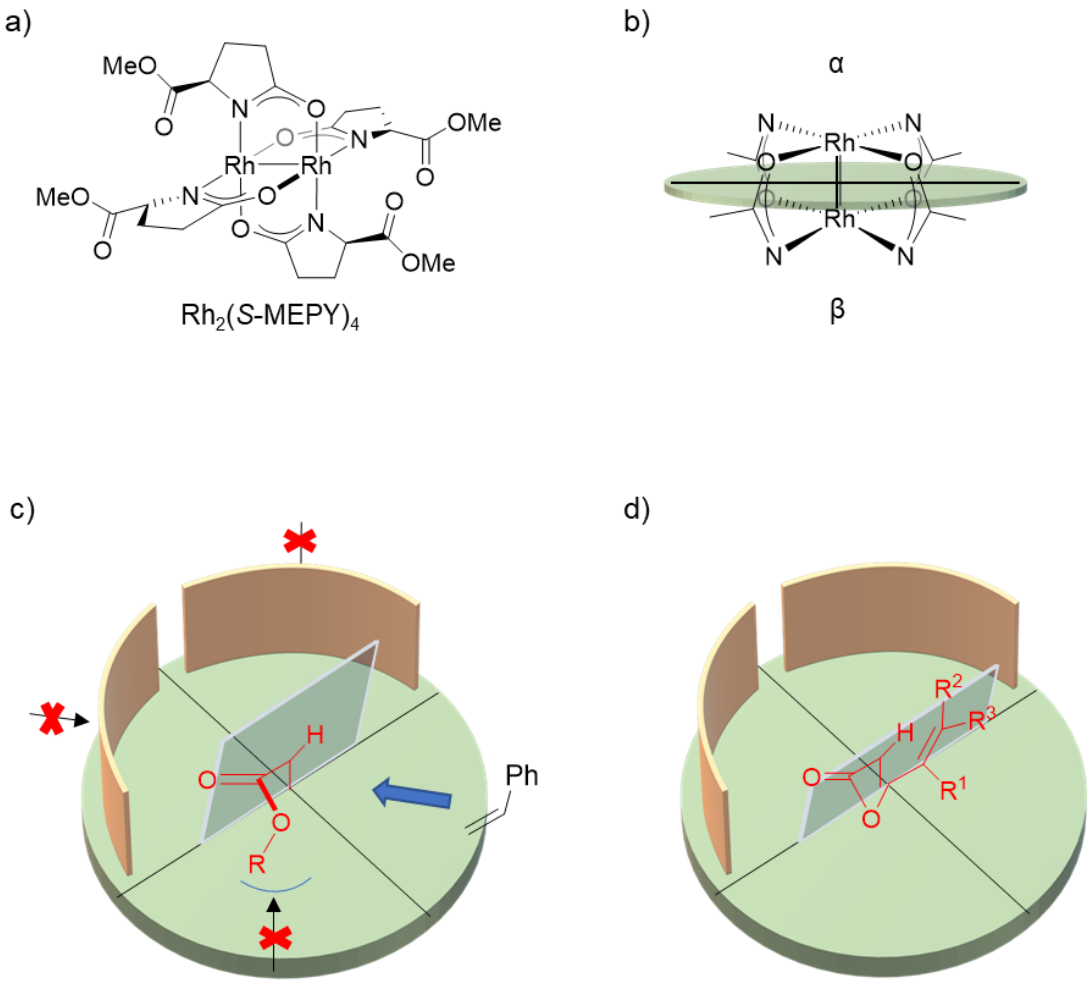

Figure 1.27 a.) Carboxamidate Rh_2(*S*-MEPY)$_4$ b.) Designation of α and β faces based on a plane perpendicular to the Rh–Rh bond c.) Substrate approach dictated by chiral groups on bridging ligands d.) Folding of intramolecular reactions leads to higher stereoselectivity

carboxylate complexes generated a very reactive carbenoid species, which diminished selectivity. The prolinate catalysts gained notoriety with the development of donor/acceptor diazo reagents. The donor moiety stabilized the diazo reagent and required more reactive Rh^{II} carboxylate complexes to facilitate diazo decomposition.[20]

As a means of facilitating the formation of enantiopure cyclopropanes, a series of chiral Rh^{II} prolinate complexes were applied as catalysts, many of which resulted in high enantioinduction (Figure 1.28).[94] Substitution of the aryl sulfonyl did not have a large influence on enantioinduction (Figure 1.28, **52a**-**e**). A more profound effect was observed when changing the solvent to pentane (Figure 1.28, **52b** and **52c** in parentheses). Acyclic aryl sulfonates were examined but led to a drastic decrease in selectivity, indicating the importance of the prolinate ring (Figure 1.28, **53a-b**). Further investigation of the importance of the ring structure was examined with the picolinate and azetidecarboxylate derivatives, **52f** and **52g** respectively. Each of these catalysts afforded the same ee of 81%, indicating that the five-membered prolinate seems to be preferred but not required. The enantioselectivity of the reaction could be improved further (up to 98% e.e) by reducing the reaction temperature (-78 °C) but could only be accomplished with **52c** due to solubility. No direct comparison of the yields of **52c** at 25 °C and -78 °C were given. However, lower yields were obtained with **52c** at -78 °C when compared to reactions run at 25 °C with **52b**.

Rh^{II} prolinate complexes demonstrated further utility when reacted with another donor/acceptor diazo compound wherein the vinyl group was replaced with an aryl ring.[95] Cyclopropanation of styrene and methyl phenyldiazoacetate afforded high yields and stereoselectivity that matched vinyldiazoacetate. Again, high diastereoselectivities were obtained with the Rh^{II} prolinate complexes Rh_2(*S*-TBSP)$_4$ (**52b**) and Rh_2(*S*-DOSP)$_4$ (**52c**). Solvent again played a role as pentane resulted in more stereoselective reactions than those conducted in DCM. In addition to improving the stereochemical outcome of reactions, the donor/acceptor diazo compounds also facilitated more chemoselective reactions with Rh^{II} prolinate catalysts.[93]

Asymmetric induction once again relies on the orientation of the chiral groups of the bridging ligand protruding over the axial site. It has generally been accepted that the ligands of Rh^{II} prolinate complexes, such as Rh_2(*S*-DOSP)$_4$ (Figure 1.29, a), adopt an α, β, α, β orientation.[96] The high level of enantioinduction is believed to occur because the protruding chiral groups minimize the possible approach vectors of the olefin substrate

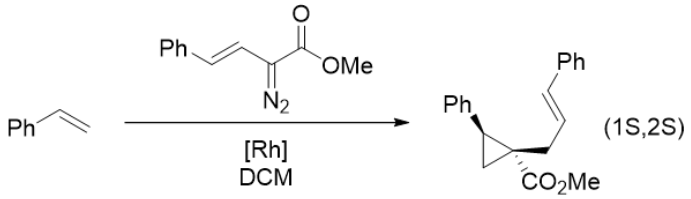

[Rh]	Ar	n	R	ee (%)
52a	Ph	2	-	74
52b	4-(^{t}Bu)C_6H_4	2	-	74 (90[a])
52c	4-($C_{12}H_{25}$)C_6H_4	2	-	79 (92[a])
52d	4-(NO_2)C_6H_4	2	-	83
52e	4-(OMe)C_6H_4	2	-	76
52f	4-(^{t}Bu)C_6H_4	1	-	81[a]
52g	4-(^{t}Bu)C_6H_4	3	-	81[a]
53a	4-(Me)C_6H_4	-	^{i}Pr	30
53b	4-(^{t}Bu)C_6H_4	-	CH_2Ph	6

[a]Pentane used as solvent

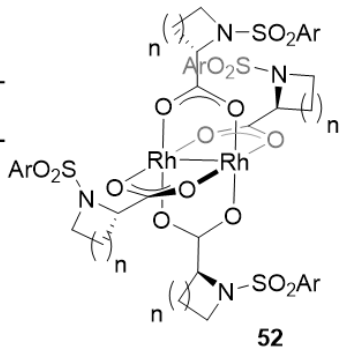

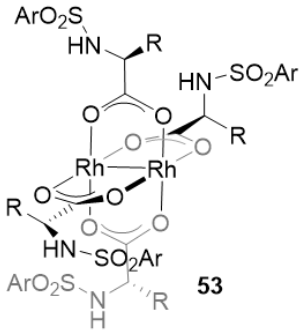

Figure 1.28 Cyclopropanation of styrene and vinyl diazoacetates by Rh^{II} prolinate complexes

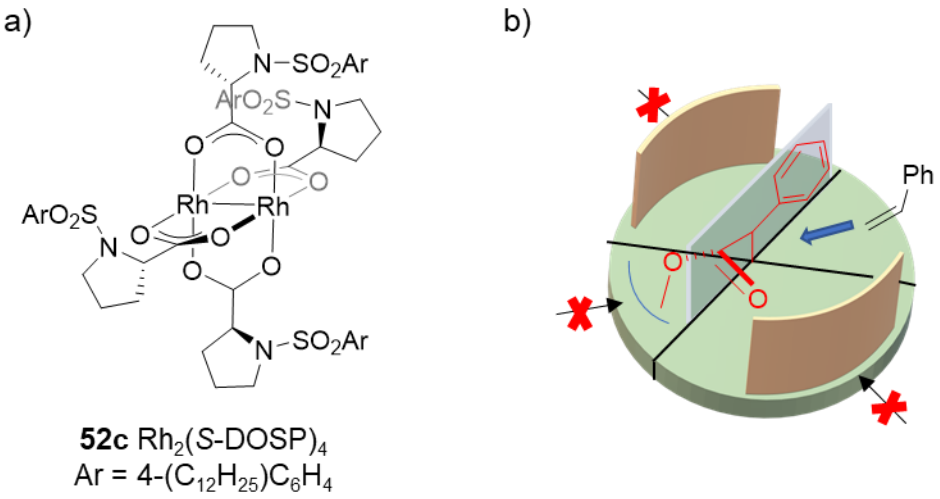

52c Rh_2(*S*-DOSP)$_4$
Ar = 4-($C_{12}H_{25}$)C_6H_4

Figure 1.29 Rh^{II} carboxylate catalyst Rh_2(*S*-DOSP)$_4$ and b) the proposed orientation of protruding bridging ligands responsible for enantioselectivity

(Figure 1.29, b). In conjunction with the ligands, the alkoxy group of the carbenoid blocks another angle of approach by the olefin substrate (Figure 1.29, b). The ester is positioned in this quadrant due to the steric requirements of the phenyl ring.[20, 97] Furthermore, the bulk of the phenyl ring of the donor/acceptor carbenoid further restricts the approach of the olefin substrate.[98]

Diastereoselectivity was predicted to rely on the approach of the olefin substrate, which is dictated by the steric requirement of the olefin substrate. The olefin substrate attacks in an end-on fashion which results in the bulkiest substituent being oriented away from both the ester carbonyl and the plane of the Rh metal.[13] Highly substituted olefins result in poorer yields than terminal olefin substrates, which agrees with an end-on approach of the substrate.

1.1.4.3 Rh^{II} Complexes Derived from N-protected Amino Acids

Another class of Rh^{II} carboxylate complex was originally developed by Hashimoto and co-workers based on phthalimide protected amino acids. The first of these complexes were derived from alanine, valine, and phenyl alanine.[99] Davies and co-workers developed similar catalysts that retained the phthalimide group and replaced the amino acid group with an adamantyl (Ad) group (Figure 1.30).[100] These complexes have seen larger applications in the realm of C-H insertion reactions, but have also been applied to cyclopropanation.[101] In the standard cyclopropanation reaction of styrene and methyl phenyldiazoacetate, the phthalimide catalyst Rh_2(*S*-PTAD)$_4$ (**54a**) gave comparable yields to Rh_2(*R*-DOSP)$_4$ (87 and 85%, respectively) but in much lower ee (21% and 88% respectively).[102] Despite this unfavorable result, the Rh^{II} phthalimide catalyst Rh_2(*S*-PTAD)$_4$ proved to be effective when donor/acceptor diazo reagents lacked a methyl ester as the acceptor group (Figure 1.30). Each report showcased a range of different olefin substrates that resulted in high yields of the cyclopropane product in highly diastereoselective enantioselective transformations.[103-106] In each instance, the donor/acceptor diazo reagent contained an aryl donating group which is believed to play a role in the high stereoselectivity.

The scope of diazo compounds was further expanded for this class of Rh^{II} catalyst by Charette and co-workers in the cyclopropanation of styrene with acceptor/acceptor

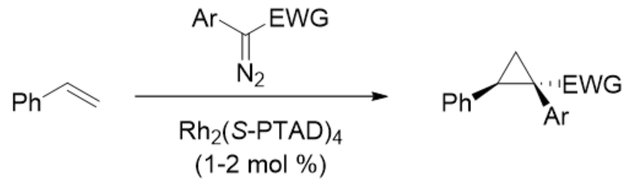

EWG	*Yield (%)*	*dr*	ee (%)
CN	up to 90	up to >30:1	up to 90
CF_3	up to 80	>30:1	up to 95
COR	up to 95	up to >30:1	up to 98

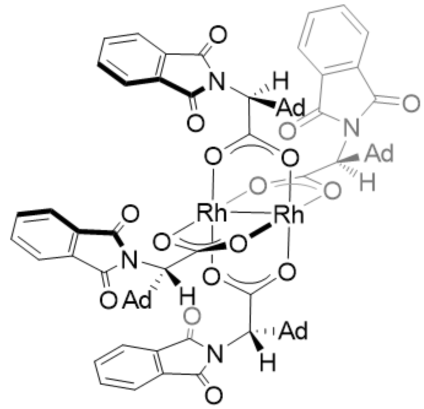

54a Rh_2(*S*-PTAD)$_4$

Figure 1.30 Cyclopropanation of styrene with donor/acceptor diazo reagents with non-ester EWGs by Rh_2(*S*-PTAD)$_4$

diazo reagents. A comparison of different Rh^{II} phthalimide catalysts resulted in moderate to good yields without high stereoselectivity (Figure 1.31).[107] Even so, a trend was observed that more sterically demanding R groups resulted in higher diastereoselectivity (Figure 1.31, **54b**-**d**). This trend was not observed for enantioselectivity. Decoration of the aryl ring of the phthalimide group with halogens resulted in higher yields and great stereoselectivity (Figure 1.31, **54e**-**h**). It was stated that binding interactions between the halogens and the π cloud of the aryl ring of the phthalimides made a more rigid chiral pocket. This increased rigidity was cited as the cause of increased stereoselectivity.[107] Other acceptor/acceptor diazo reagents were examined and overall good selectivity, both dr and ee, was observed with each diazo reagent. Yet it was noted that the presence of an aryl ketone was required to facilitate high selectivity, while the identity of the second EWG was not as critical. Substitution of the aryl ketone resulted in a decrease in yield but maintained high stereoselectivity.

Although a rationale for the high selectivity has been developed for this new class of Rh^{II} catalyst, it is still being modified. When Hashimoto incorporated alanine or phenyl alanine as the ligand precursors, the final Rh^{II} complex adopted the α, α, β, β orientation like that observed with the carboxamidates synthesized by Doyle. However, incorporation of sterically demanding groups such as the ^{t}Bu group of Rh_2(*S*-PTTL)$_4$ (Figure 1.32, a), afforded Rh^{II} complexes where phthalimide portion of the ligands were oriented in an α, α, α, α manner (Figure 1.32, b).[108] This orientation generates two unequivocal axial sites. A "chiral crown" is formed by the phthalimide groups above one axial site, due to enantiopure bridging ligands. The second axial site was thought to be catalytically inactive because the ^{t}Bu groups appeared to block the axial site. Based on the crystal structure, the distance between each protruding phthalimide group in the "chiral crown" alternates between long and short, which aids in stereoselectivity (Figure 1.32, c). The model for selectivity put forth by Fox arises from the protruding groups of the bridging ligands blocking two approaches of the substrate while the ester blocks a third. With these vectors blocked, a single approach is possible (Figure 1.32, d).[96] This model for stereoselectivity was further supported by experimental results where Rh_2(*S*-PTAD)$_4$ resulted in higher enantioselectivity during cyclopropanation compared to Rh_2(*S*-PTTL)$_4$. The reason for the increased enantioselectivity was believed to arise from the bulkier Ad group more effectively blocking the second axial site. This model found further support when a

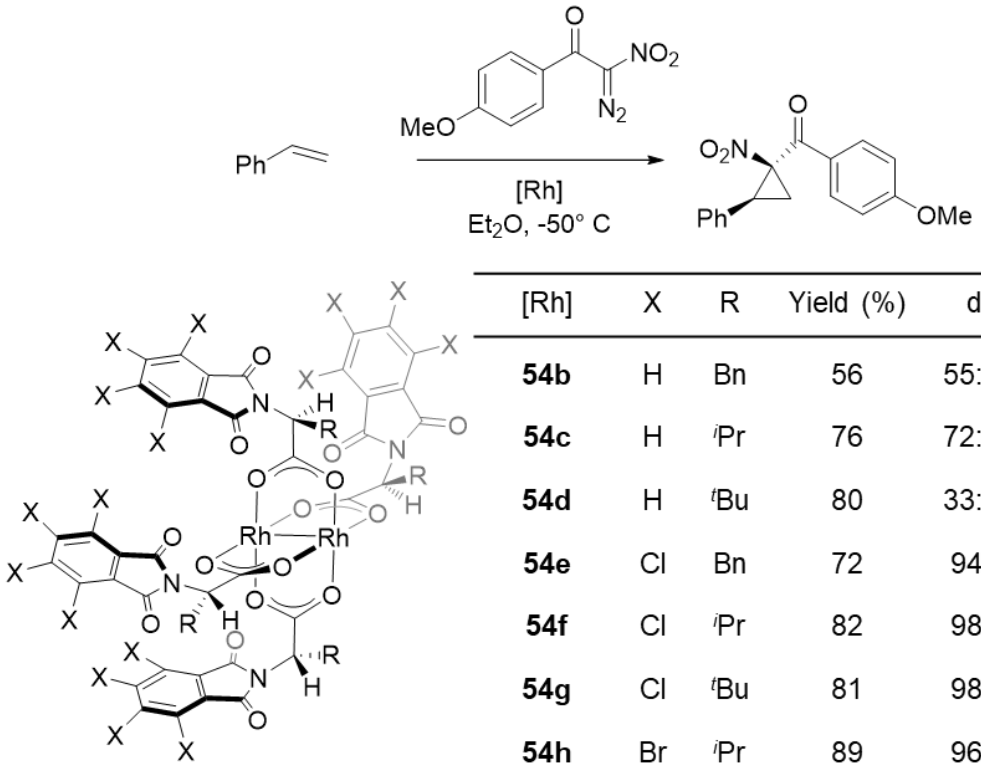

[Rh]	X	R	Yield (%)	dr	ee (%)
54b	H	Bn	56	55:45	43
54c	H	*i*Pr	76	72:28	16
54d	H	*t*Bu	80	33:67	2
54e	Cl	Bn	72	94:6	91
54f	Cl	*i*Pr	82	98:2	91
54g	Cl	*t*Bu	81	98:2	93
54h	Br	*i*Pr	89	96:4	80

Figure 1.31 Cyclopropanation of styrene with acceptor/acceptor diazo reagents by phthalimide Rh^{II} complexes

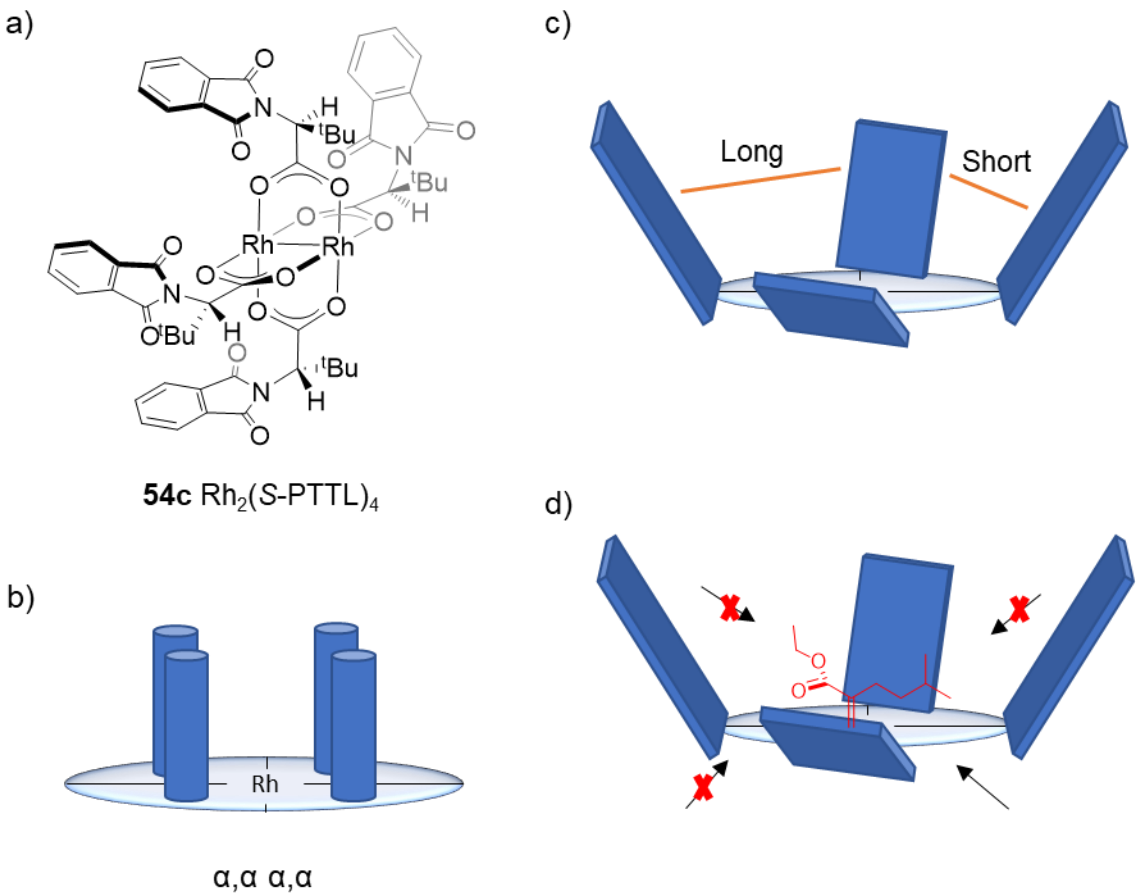

Figure 1.32 Rationalization of stereoselectivity of Rh^{II} phthalimide complexes based on ligand orientation

carbenoid species of Rh_2(*S*-PTTL)$_4$ was crystallized and the α, α, α, α orientation was observed .[96]

The crystallization of Rh_2(*S*-PTAD)$_4$ raised questions about the accepted method of enantioinduction. The chiral crown was still present but solvent was bound to the axial sites.[108] This showed axial coordination at the "blocked" axial was indeed possible even with sterically bulky Ad groups. To this point, the mode of enantioinduction was predicated on solid-state structures rather than solution-based analysis. Solution-based data was obtained by Charette and co-workers by analyzing Rh_2(*S*-PTTL)$_4$ by two-dimensional ^{1}H NMR.[107] This analysis showed that the PTTL ligands underwent a dynamic process that resulted in the rotation of at least one ligand. It was not determined if more than one ligand had undergone rotation. It is possible that the catalyst adopted an α, β, α, β orientation or possibly an α, α, α, β orientation.

The possibility of the α, α, α, β orientation affording high enantioinduction was observed by Fox and co-workers through the synthesis of a heteroleptic carboxylate Rh^{II} complex **55** (Figure 1.33).[109] Replacement of a chiral ligand with an achiral ligand resulted in a pseudo α, α, α, β orientation, where each phthalimide group surrounds the same axial site. A comparison of the reactivity of the heteroleptic complex with the homoleptic variant (Figure 1.33) showed that the heteroleptic complex **55** gave the desired cyclopropane in higher yields and enantioselectivity than the homoleptic complex **54c**. This trend was observed with several different substrates. These combined results raised the question as to which orientation catalytically active Rh^{II} phthalimide catalysts adopt in solution. Furthermore, it demonstrated that a symmetrical axial site is not required for enantioinduction

1.1.4.4 Recent Developments for Cyclopropanation of Olefins by Rh^{II} Carbenoids

The extension of intermolecular cyclopropanation reactions with carboxamidate ligands was accomplished by Charette and co-workers with a phosphonate/cyano acceptor/acceptor diazo reagent (Figure 1.34).[110] When this reaction was attempted with Rh^{II} prolinate and phthalimide complexes, high asymmetric induction was not observed. In contrast, the carboxamidate catalyst Rh_2(*S*-IBAZ)$_4$ afforded high yields, diastereoselectivity, and enantioselectivity. The substitution of the phosphonate group with the isosteric ^{t}Bu ester also resulted in high yields and selectivity. Even more

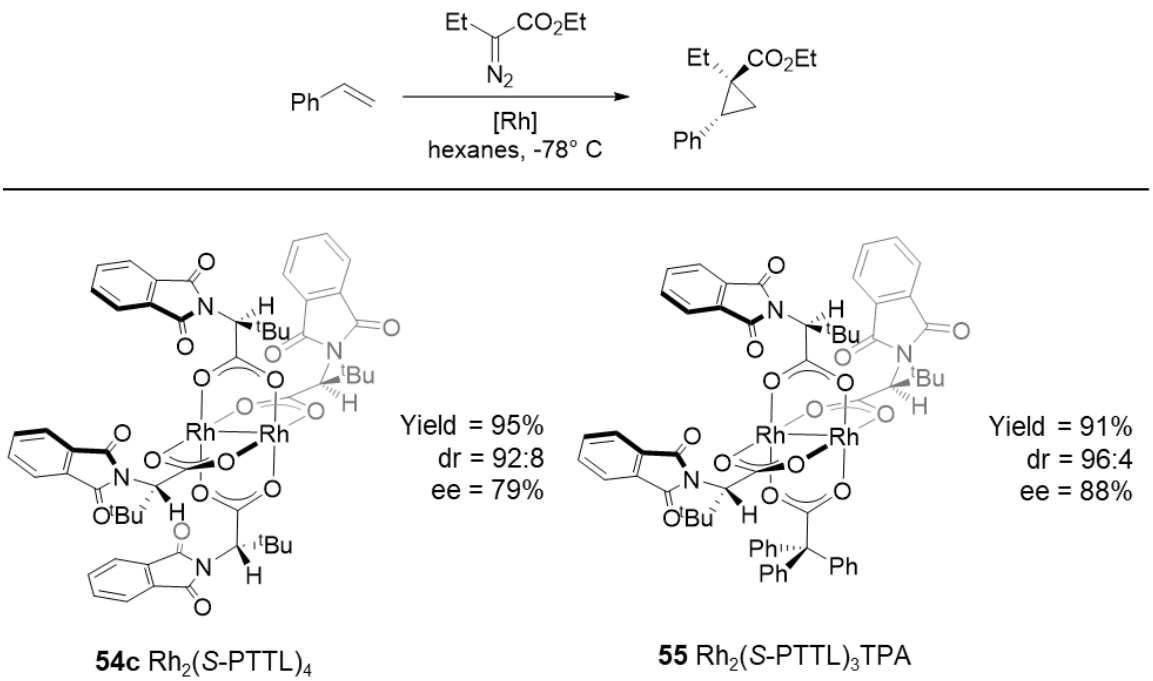

Figure 1.33 Comparison of homoleptic and heteroleptic Rh^{II} catalysts with different ligand orientations

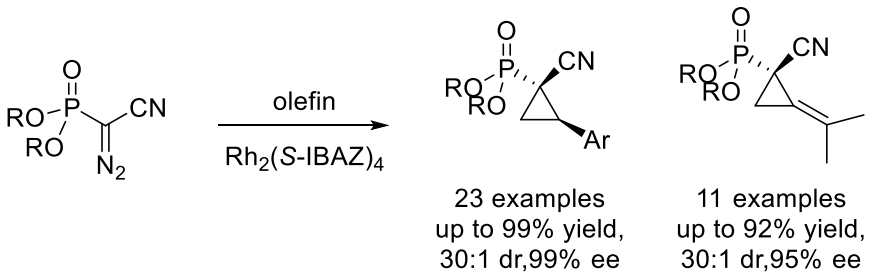

Figure 1.34 Cyclopropanation of olefins with acceptor/acceptor diazo reagents by a Rh^{II} carboxamidate complex

impressive was the cyclopropanation of allene derivatives to afford the alkylidenecyclopropane, due to the low nucleophilic nature of allenes.

A new class of Rh^{II} carboxylate catalyst emerged as the Davies group developed triarylcyclopropanecarboxylates as effective cyclopropanation catalysts (Figure 1.35, a). The introduction of more steric bulk was achieved through the incorporation of cyclopropane rings decorated with aryl groups. Interestingly, the key synthetic step in ligand synthesis included asymmetric cyclopropanation of an olefin by a Rh^{II} catalyst. The Rh^{II} triarylcyclopropanecarboxylate complexes adopted the same α, β, α, β orientation proposed for Rh_2(*S*-DOSP)$_4$ (Figure 1.35, b) with the cyclopropane rings contributing to a more rigid structure for Rh_2(*S*-BTPCP)$_4$ than the alkyl chains of Rh_2(*S*-DOSP)$_4$.[111] The rigid ligands generated a chiral box surrounding the axial site (Figure 1.35, c), reminiscent of that proposed for Rh_2(*S*-PTAD)$_4$, but maintained two equivalent axial sites.

Initial investigation into reactivity for the cyclopropanation of styrene with methyl styryldiazoacetate afforded higher yields and enantioselectivity compared to Rh_2(*S*-DOSP)$_4$ (Table 1.4, entry 1 vs 3). The ligand conformation leads to reactivity similar to phthalimide catalysts where diazo esters besides methyl diazo esters were cyclopropanated in high yields and stereoselectivity (Table 1.4, entries 1 and 2 vs 3 and 4). Another distinguishing feature of the triarylcyclopropanecarboxylate catalysts is their ability to be used at very low (.001 mol%) catalyst loading while still maintaining high yields without a decrease in enantioselectivity (Table 1.4, entry 5).[112] An in-depth kinetic study demonstrated that Rh^{II} triarylcyclopropanecarboxylate complexes decomposed diazo reagents slower than prolinate and phthalimide catalysts, but often resulted in an increase in ee. The high stereoselectivity and low catalyst requirements have caused this new class of Rh^{II} to be incorporated into catalyst screenings. The applicability of this new class of catalyst was demonstrated with the formal synthesis of the commercial antiviral Beclabuvir. This had previously been reported and utilized Rh_2(*S*-DOSP)$_4$ for the cyclopropanation step. Substitution of Rh_2(*S*-DOSP)$_4$ with Rh_2(R-*p*-PhTPCP)$_4$ improved the enantioselectivity and with 1/200th of the catalyst required.

Progress in method development was made in the cyclopropanation of heterocyclic compounds. Davies and co-workers examined the cyclopropanation of pyrroles and donor/acceptor diazo reagents with Rh^{II} carboxylate catalysts and found that Rh_2(*S*-DOSP)$_4$ resulted in the highly enantioenriched doubly cyclopropanated product.

a)

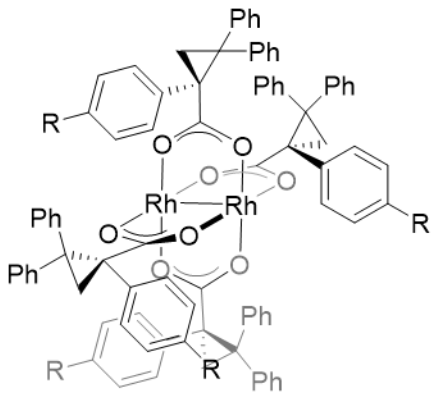

56a R = Br Rh_2(*R*-BTPCP)$_4$
56b R = Ph Rh_2(*R*-*p*-PhTPCP)$_4$

b)

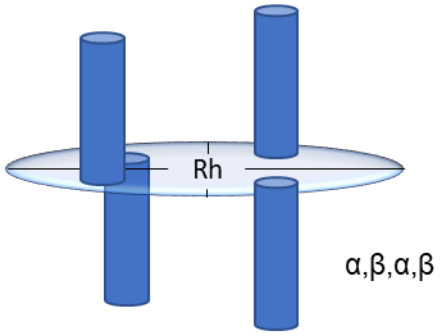

c)

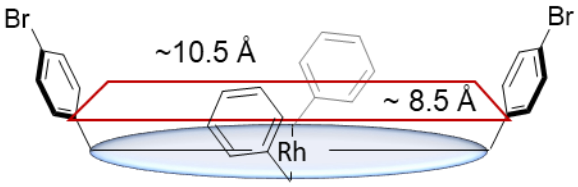

Figure 1.35 a) Rh^{II} triarylcyclopropanecarboxylate complex b) α, β, α, β orientation of ligands c) The chiral box generated resembling Rh^{II} phthalimide complexes

Table 1.4 Cyclopropanation of styrene and styryldiazoacetates by Rh^{II} triarylcyclopropanearboxylates

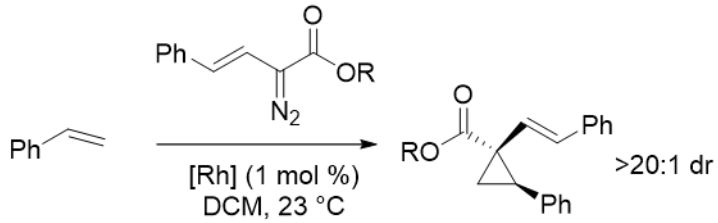

Entry	[Rh]	R^1	Yield (%)	ee (%)
1	Rh_2(*R*-BTPCP)$_4$	Me	86	91
2	Rh_2(*R*-BTPCP)$_4$	^{t}Bu	87	95
3	Rh_2(*R*-DOSP)$_4$	Me	80	81
4	Rh_2(*R*-DOSP)$_4$	^{t}Bu	80	16
5[a]	Rh_2(*R*-BTPCP)$_4$	Me	46	92
6[a]	Rh_2(*R*-DOSP)$_4$	Me	38	81

[a] 0.001 mol % [Rh]

However, the singly cyclopropanated pyrrole was not realized until later when the Rh_2(*R*-*p*-PhTPCP)$_4$ was applied as a catalyst and proceeded in a highly enantioselective manner (Figure 1.36, a).[113] In conjunction with pyrrole, cyclopropanation of furans and donor/acceptor diazo reagents with Rh_2(*S*-TCPTTL)$_4$ led to the singly cyclopropanated product because of the EWG substituent of the furan (Figure 1.36, b). This product was further modified to generate derivatives of paraconic acids, which have demonstrated a range of pharmacological and biological activity.[114]

The electrophilic nature of the Rh^{II} carbenoid often led to low yields with electron deficient olefins, due to the decreased nucleophilicity of the olefin. This made incorporating electron withdrawing groups onto cyclopropanes difficult. Despite this trend, cyclopropanation of electron deficient olefins was realized. One such class of substrate includes the electron withdrawing acrylate derivatives that underwent cyclopropanation with donor/acceptor diazo reagents (Figure 1.37).[115] Incorporation of both aryl and styryl diazoacetates afforded the ester cyclopropane with high stereoselectivity in 22 cases.

Rather than use electron deficient olefins, Reissig and co-workers introduced electron withdrawing groups as part of the diazo reagent. These fluorinated species were of particular interest in biological studies (Figure 1.38).[116] High yields were obtained, which is not surprising as activated olefins generally result in high yields. No enantioselectivity was achieved because only achiral catalysts were examined. A slight preference for one diastereomer was observed and was dependent on the diazo reagent. The major diastereomer was only identified in one example and was identified as the *trans* isomer.

Charette and co-workers were able to incorporate fluorine with fluorinated olefins using Rh_2(*S*-BTPCP)$_4$ (Figure 1.39).[117] High yields required the presence of an aryl substituent to enhance the nucleophilicity of the olefin (Figure 1.39, compare **57** to **58**-**59**). Even so, moderate yields of ester and bromo substituted olefins were obtained with great diastereoselectivity and good enantioselectivity. Electronic perturbations of the aryl ring of the donor/acceptor diazo reagents were well tolerated and provided good to excellent yields (Figure 1.39, compare **60**-**62**). The reaction of donor/acceptor diazo reagents was overall more diastereoselective and enantioselective. In the case of the *p*-NO_2 aryl diazo reagent, a larger scale (2g diazo reagent) was accomplished and maintained its stereoselectivity with an improved yield of 95%. Applying the same catalyst, the Charette

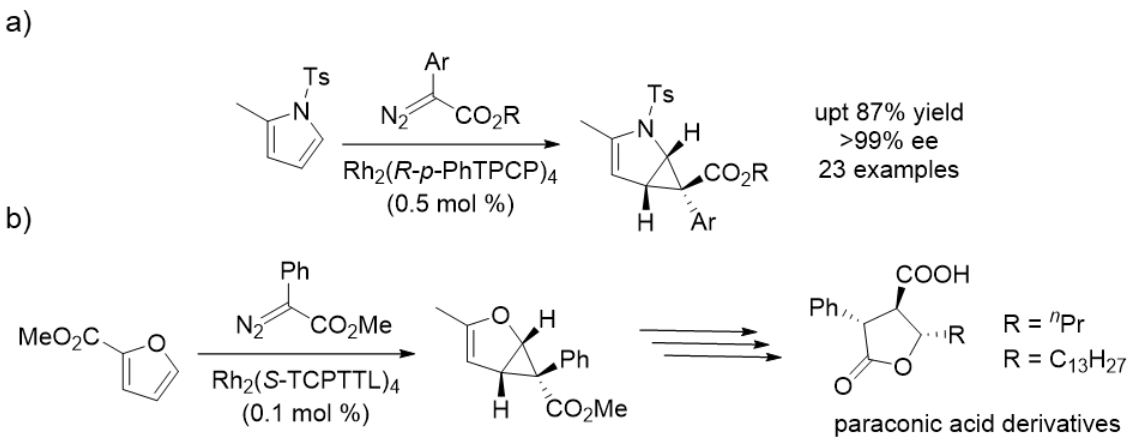

Figure 1.36 Cyclopropanation of aromatic heterocycles by Rh^{II} complexes

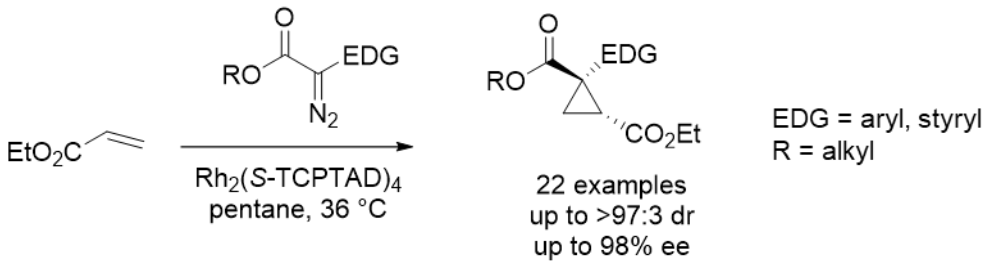

Figure 1.37 Incorporation of electron withdrawing groups onto cyclopropanes

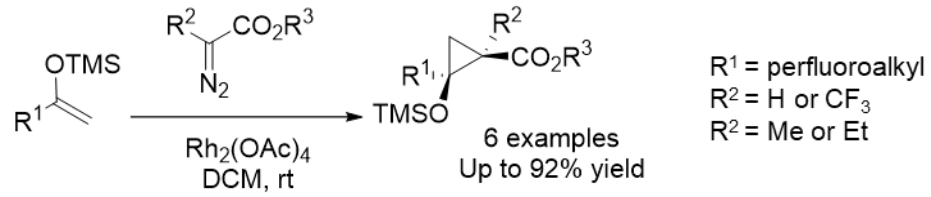

Figure 1.38 Incorporation of fluorine with fluorinated diazo reagents

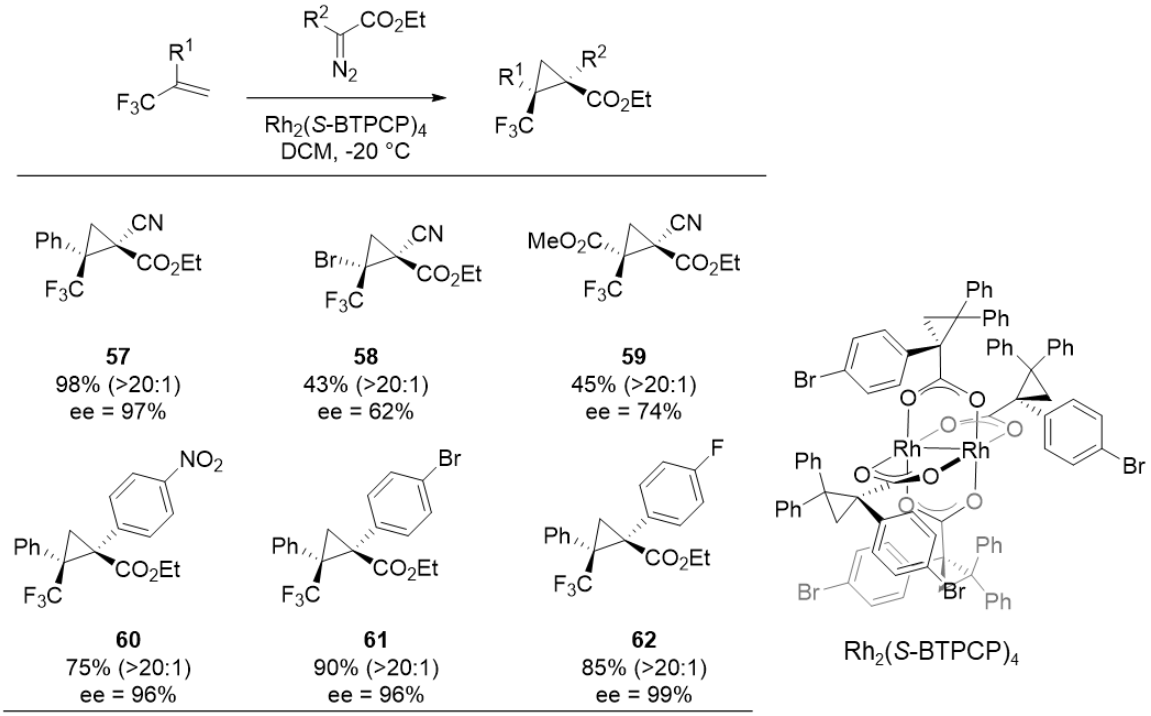

Figure 1.39 Select substrate scope of the cyclopropanation of α-CF_3 styrene substrates by Rh_2(*S*-BTPCP)$_4$

group was able to synthesize mono-(halo)-methyl cyclopropanes, again achieving high diastereoselectivity and enantioselectivity.[118] It was then demonstrated that the cyclopropane products could be functionalized further, resulting in biologically relevant molecules.

Cyclopropanation of vinyl fluorides was accomplished with acceptor/acceptor diazo reagents. Interestingly, Rh^{II} complexes afforded the desired halogenated product while other common catalyst metals, such as Cu, resulted in no detectable product.[119] Further investigation included the cyclopropanation of vinyl fluorides with allylic esters using donor/acceptor diazo reagents.[120] Additionally, the possibility of asymmetric cyclopropanation was investigated by employing chiral Rh^{II} catalysts rather than the achiral catalysts used previously. Prolinate catalysts were examined but were not as selective as phthalimide catalyst Rh_2(*S*-TCPTTL)$_4$ (**54f**). Examination of the reaction scope demonstrated that the reaction did not tolerate electronic perturbations well (Figure 1.40). Both strong electron withdrawing groups and donating groups resulted in no reaction or trace amounts of product (Figure 1.40, **63**-**65**). However, smaller perturbations by inductively withdrawing groups were more successful (Figure 1.40, **66**-**70**). The yields were variable, but high diastereoselectivity and enantioselectivity were observed in most examples.

Installation of cyclopropane rings has found wide application in the synthesis of biologically relevant molecules, with Rh^{II} complexes often being the catalyst of choice. This can be seen by two recent synthesis of (-)-cycloclavine by the Wipf and Dong groups (Figure 1.41).[121, 122] Each group employed chiral Rh^{II} catalysts to facilitate the asymmetric cyclopropanation of an olefin to establish the final cyclopropane ring. Wipf and co-workers installed the cyclopropane ring early in the synthesis. Alternatively, the synthetic route by Dong employed a late-stage cyclopropanation strategy, installing the cyclopropane ring at the end. Dong's synthesis provided an overall higher yield and required more steps, although each route provided the enantiomerically pure product. High diastereoselectivity was also observed in the synthesis of (−)-dendroside C Aglycon (Figure 1.42).[123] The cyclopropanation resulted in the common *syn* addition of the carbenoid, which set the bridgehead chiral centers. The stereochemistry of the alcohol substituent of the cyclopropane ring was also established in this step.

The enantioselective total synthesis of piperaborenine B was realized by Fox and co-workers through the synthesis of a bicyclobutane intermediate, which was then

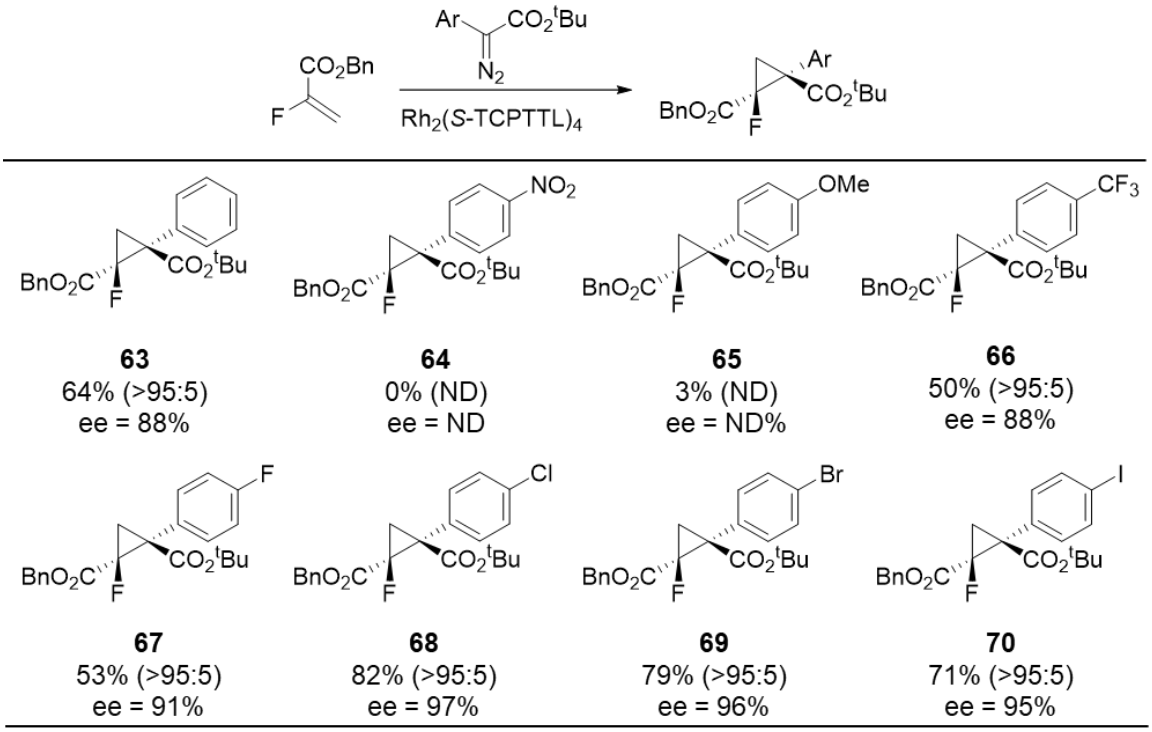

Figure 1.40 Select substrate scope of the cyclopropanation of vinyl fluoride substrates by Rh_2(*S*-TCPTTL)$_4$

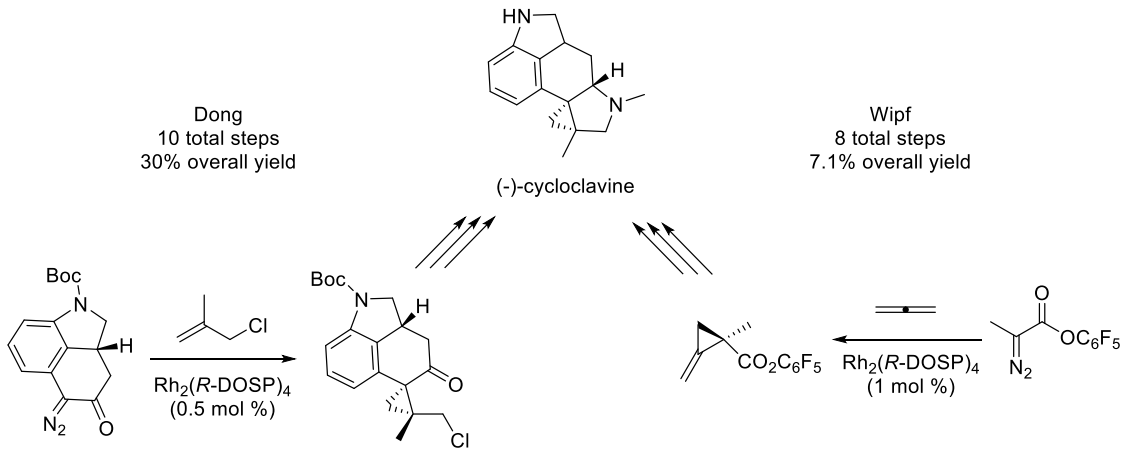

Figure 1.41 Independent total synthesis of (-)-cycloclavine relying on Rh^{II} catalyst for formation of cyclopropane ring

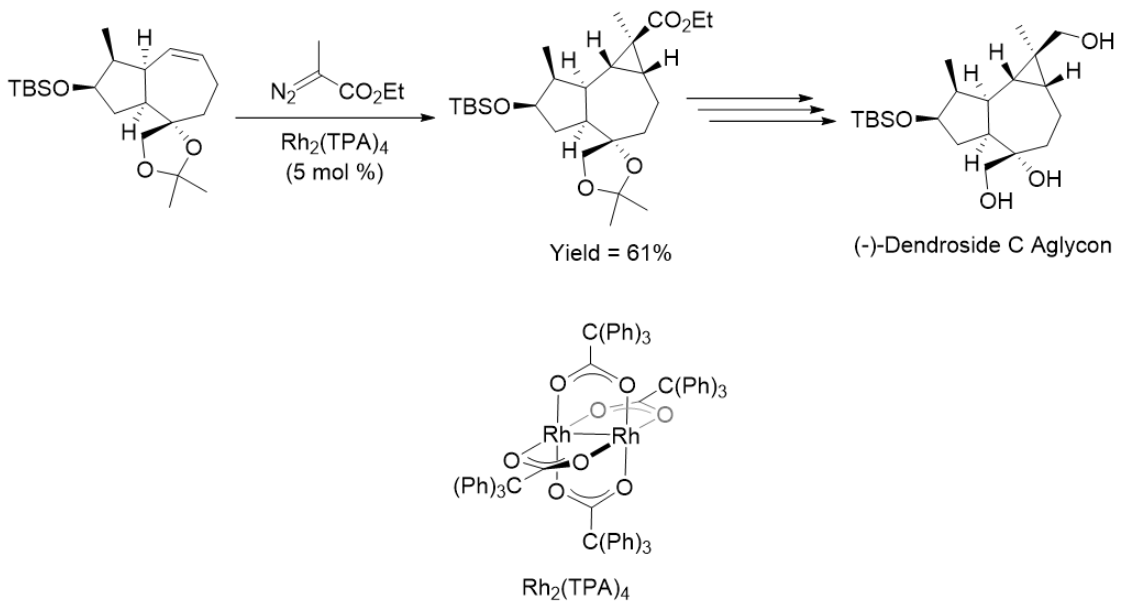

Figure 1.42 Generation of cyclopropane ring in total synthesis of (-)-dendroside C aglycon

expanded to the cyclobutane by nucleophilic attack (Figure 1.43).[124] Previous work towards the bicyclobutane **71** demonstrated that a maximum of 88% ee could be obtained using a variety of Rh^{II} catalysts. Interestingly, the heteroleptic catalyst **72** developed by Fox and co-workers afforded the desired bicyclobutane ring in 92% ee. The stereochemistry set in this step established three of the four stereocenters of the final molecule. This provided another example where a complex with inequivalent axial sites resulted in a higher ee than the symmetrical parent complex.

Another synthetic strategy involves the application of the donor/acceptor diazo reagent styryldiazoacetate in an effective cascade sequence involving cyclopropanation of the olefin, followed by a Cope rearrangement.[125, 126] This well-established sequence continues to see application towards the synthesis of natural products and biologically relevant molecules.[127] The formal synthesis of the enantiopure (-)-englerin A was realized with this strategy using the achiral catalyst dirhodium(II) tetrakisoctanoate ($Rh_2(OOct)_4$) (Figure 1.44, a).[128] Two diastereomers were generated in high yield (90%) and were separable by column chromatography, so further stereochemical optimization was foregone. The same cascade was applied to the synthesis of terpene natural products. Single diastereomers could be synthesized selectively based on whether Rh_2(*R*-PTAD)$_4$ or Rh_2(*S*-PTAD)$_4$ was chosen as the catalyst. This selectivity enabled the asymmetric synthesis of the natural product (+)-barekoxide (Figure 1.44, b).[129] The high stereoselectivity achieved by this cascade is a result of both the high selectivity of the Rh^{II} catalysts and preferred transition state of the Cope rearrangement when a cyclopropane is present.[127] An impressive display of stereoselectivity that can be achieved with this strategy was the installation of 10 stereocenters in one reaction, two of which are quaternary carbons. In conjunction, four new rings are generated in the cyclopropanation/ Cope rearrangement/ Diels-Alder cascade (Figure 1.44, c).[130] The cyclopropanation occurs twice and is followed by a selective Cope rearrangement, which facilitates the Diels-Alder reaction to afford the final product.

1.1.5 Cobalt

One of the first examples of Co carbenoids for cyclopropanation reactions involved Co complexes of camphor derivatives. The oxime derivative facilitated the cyclopropanation of styrene and EDA and was high yielding (Figure 1.45).[131] In addition,

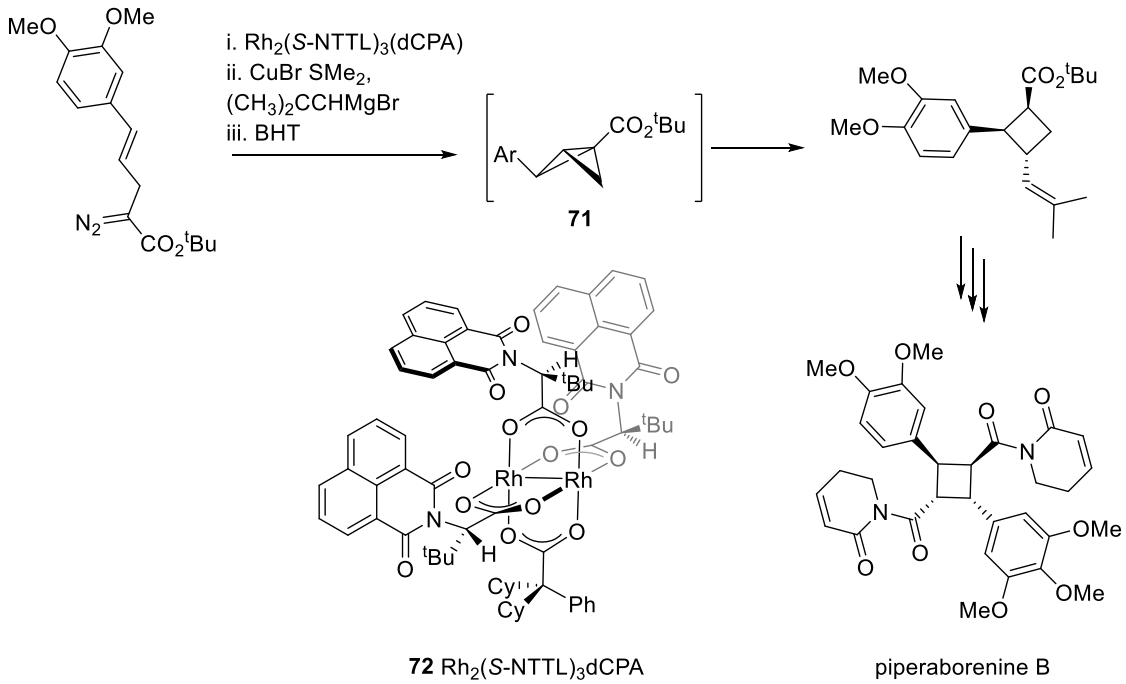

Figure 1.43 Total synthesis of piperaborenine B that relies on a heteroleptic Rh^{II} catalyst

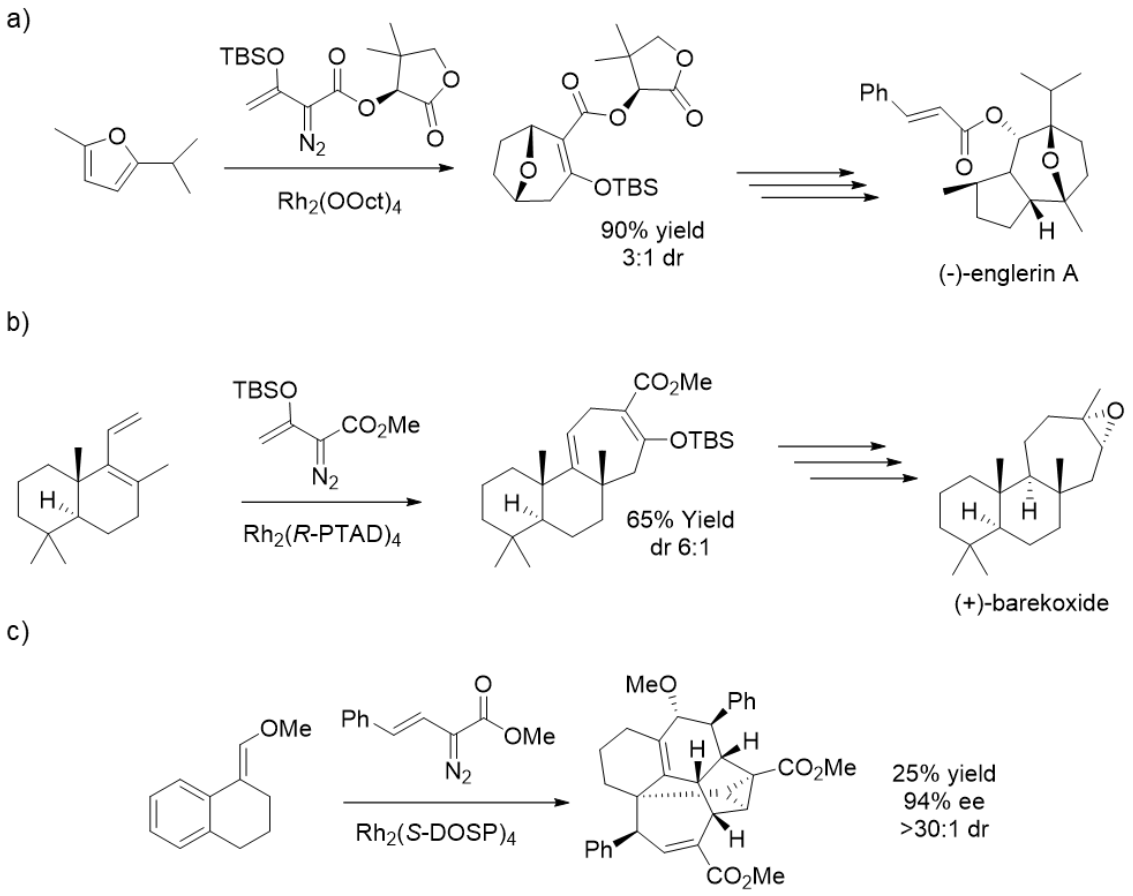

Figure 1.44 Recent examples of the cyclopropanation/Cope rearrangement cascade

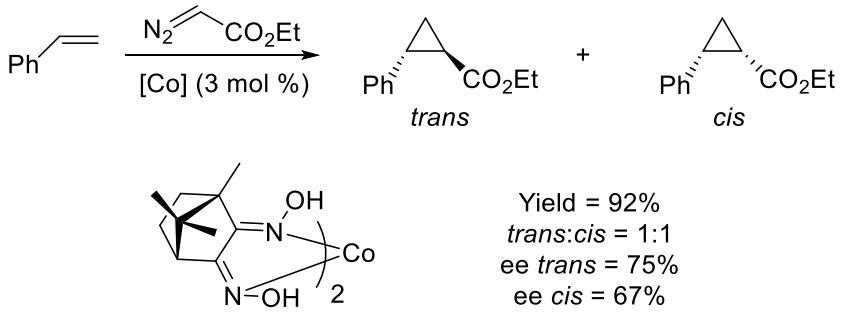

Figure 1.45 Early example of cyclopropanation of styrene by a Co catalyst

good enantioselectivity for both the *trans* and *cis* isomers was observed. However, the *trans* and *cis* isomers were typically found to be present in equal amounts. Similar results were obtained with 1,1-disubstituted olefins when at least one substituent was an aryl ring. Electron deficient olefins resulted in low yields. Best results were obtained when reactions were conducted in neat substrate, but dilution in select organic solvents could be tolerated to a point (olefin concentration of ~ 3M).

1.1.5.1 Cyclopropanation with Co(II) and Co(III) Salen Complexes

Salen compounds were applied to generate Co(II) complexes that were tested as cyclopropanation catalysts.[132, 133] Application of chiral Co(II) salen complexes as catalysts for the cyclopropanation of styrene and ^{t}Bu diazo acetate resulted in good yield and enantioselectivity of the *trans* cyclopropane (Figure 1.46). Increased yields and reaction rates were achieved by the addition of N-methyl imidazole (NMI), while also enhancing the ee of the favored *trans* isomer. Through systematic modification of the salen ligand, Ikeno and co-workers determined that incorporating sterically demanding substituents on the diamino backbone resulted in increased enantioselectivity (Figure 1.46, **75**-**77**).[133] Control of the *trans*:*cis* ratio was influenced by the group at the terminal α-keto position. The acetyl group showed an increased selectivity for the *trans* isomer while esters afforded the highest *trans*:*cis* ratio (Figure 1.46, compare **75**, **78**-**79**). The combination of these findings led to the synthesis of **79** which afforded the highest yield (99%) and was most selective (91:9 *trans*:*cis*, 96% ee *trans*). Salen complexes with a Co(III) metal center were also investigated and afforded similar results to the optimized Co(II) complex, but did not require an additive. Additionally, a lower catalyst loading (1 mol %) was found sufficient and indicated the Co(III) is more reactive than the Co(II).

Further development led to salen complexes that incorporated axial chirality in addition to the chiral centers of the diamine backbone (Figure 1.47). These catalysts provided the same high yield and enantioselectivity observed with the previous series of catalysts (Figure 1.46) but preferentially formed the *cis* isomer rather than the *trans* isomer. The choice of enantiomer was made possible by changing the chiral center of the diamine backbone (Figure 1.47, compare **81** and **82**).[134] Although the enantioselectivity and *cis*:*trans* ratio are high, there was a drastic decrease in yield when the *S* enantiomer

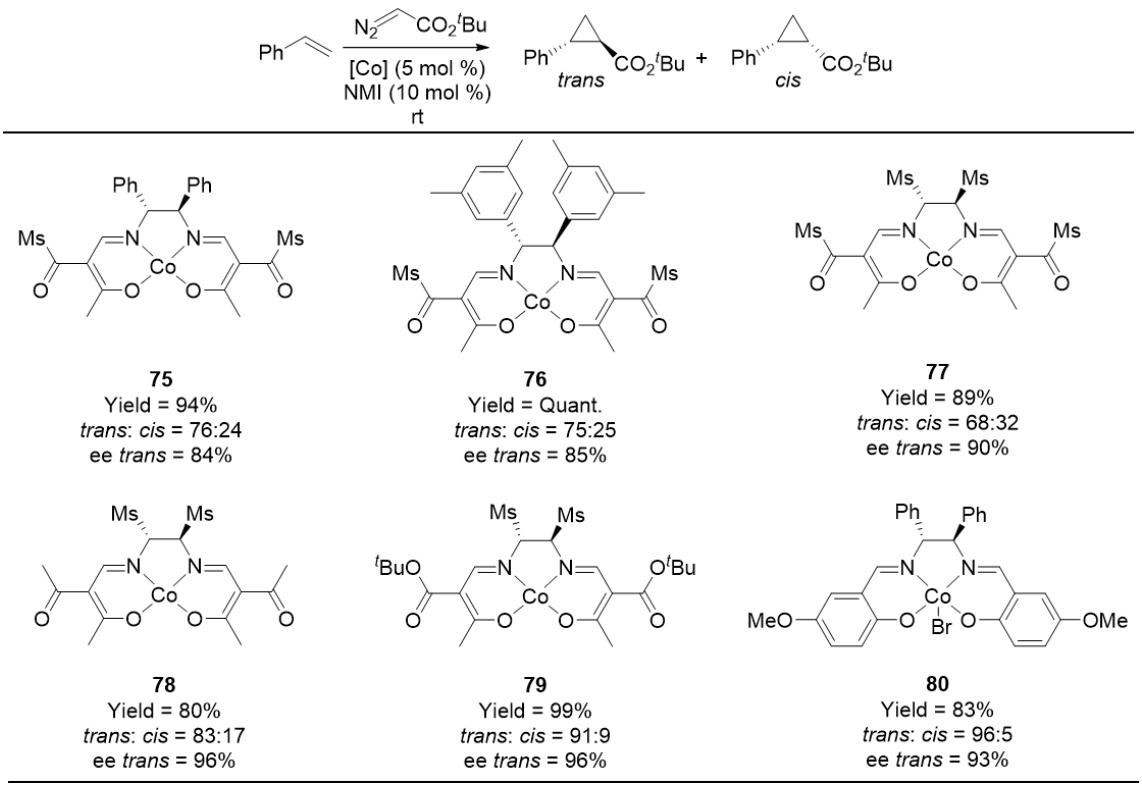

Figure 1.46 Cyclopropanation of styrene with Co(II) salen complexes

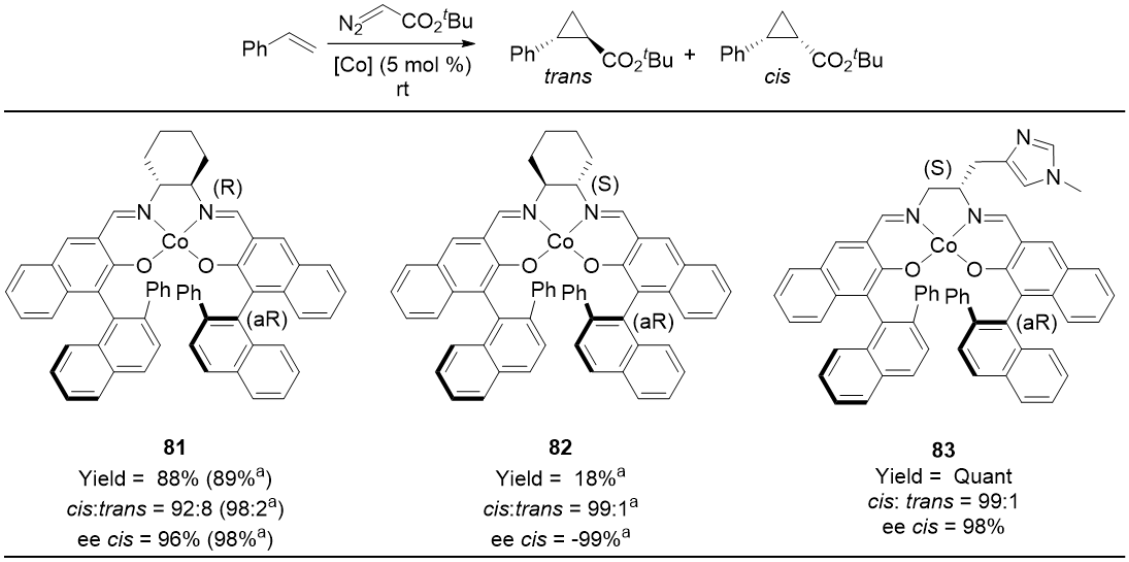

[a] Reaction run with 10 mol % NMI additive

Figure 1.47 Cyclopropanation of styrene and ^{t}Bu diazoacetate with Co(II) salen complexes with axial chirality

was used. These catalysts afforded high yields and enantioselectivities without an additive. However, introduction of a tethered imidazole group (Figure 1.47, **83**) resulted in a quantitative yield without a reduction in diastereo or enantioselectivity. It was believed that axial coordination of the tethered imidazole was responsible for the increased yield.[135]

Based on the experimental results that have been obtained, a model was proposed that rationalizes the high selectivity of Co(II) salen complexes (Figure 1.48).[136] It was believed that enantioselectivity was dictated by the chiral groups on the diamine backbone. This was based on the observation that switching the chirality of the diamine ring resulted in opposite enantiomers. This also indicated that the olefin approaches along the Co–N bond. The difference in the *cis*:*trans* ratio was then rationalized by the orientation of the alkoxy group of the ester. With the aryl group of complex **81** present, the alkoxy group is directed forward, which would promote olefin attack with the aryl, or bulkiest substituent, on the opposite side (Figure 1.48, a). After clearing the diamine backbone, it was then suggested that the olefin underwent a rotation. This rotation resulted in the observed diastereoselectivity and enantioselectivity. Conversely, when the salen ligand has a methyl substituent **84**, the alkoxy group was able to be directed backward. The olefin now approaches with the aryl group oriented to the now less sterically congested side (Figure 1.48, b). A rotation of the olefin was again proposed to afford the observed product.

1.1.5.2 Cyclopropanation with Co(II) Porphyrin Derivatives

Porphyrins are a class of macrocycle and comprise four pyrrole units that form a pocket capable of binding many different metals (Figure 1.49). Changing the linker between the heterocycles affords different porphyrin derivatives. One such derivative is the corrin ring (Figure 1.49), which is most notably found in naturally occurring vitamin B_{12}. Vitamin B_{12} participates in a range of biological processes, often as a coenzyme.[137] A coenzyme is a non-protein compound that is required for an enzyme to be catalytically active. Because vitamin B_{12} was the active site in an array of reactions as a coenzyme, the organometallic complex was investigated as an independent catalyst. It was believed the presence of chiral centers in proximity to the metal center could facilitate asymmetric induction. When derivatives of vitamin B_{12} were applied to the cyclopropanation of styrene

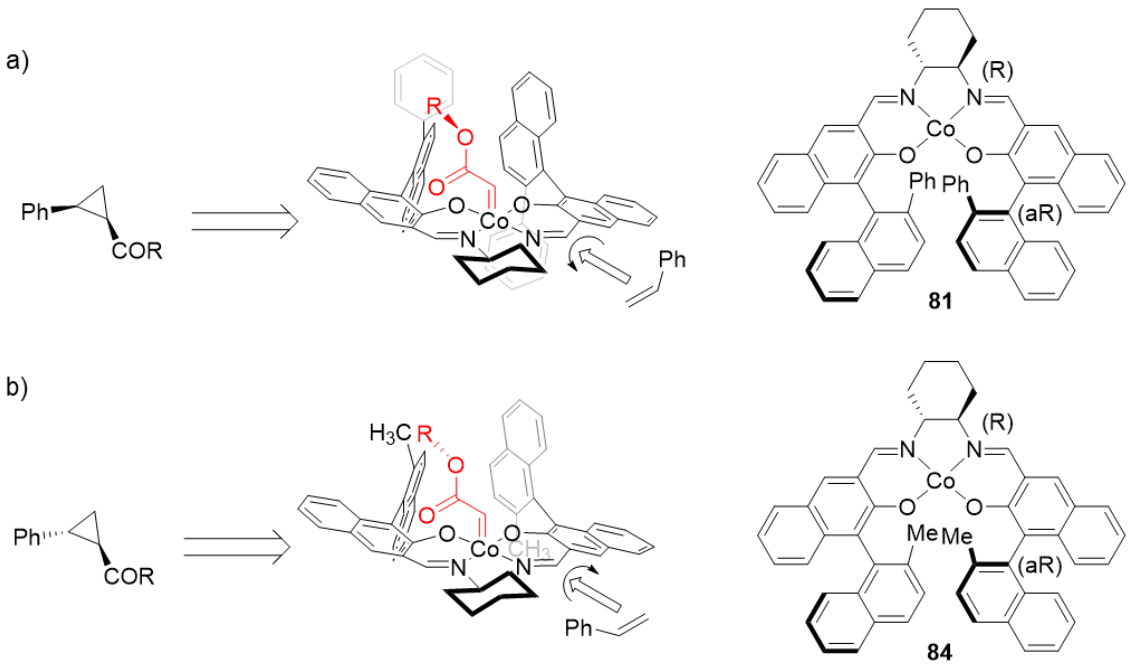

Figure 1.48 Rationalization for formation of the a) *cis* isomer over the b) *trans* isomer and high enantioselectivity of Co(II) salen complexes

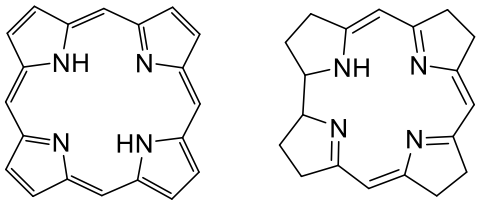

porphyrin corrin

Figure 1.49 Structures of porphyrin and corrin macrocycles

with EDA, it was found that the cyclopropane product was generated in high yields (Figure 1.50).[138] The cyano derivative with a formal Co(I) center resulted in only moderate yields. The chiral centers did result in the *cis* isomer being favored, but not by a large margin. Likewise, slight enantioselectivity was observed, but was close to racemic. Another defining feature of these reactions was the absence of the homocoupled dimer product. No techniques, such as excess olefin or slow addition of diazo, were required to prevent the formation of the homocoupled dimer product. These examples demonstrated that Co corrin complexes were capable catalysts for the cyclopropanation of olefins, but the chiral centers were not positioned to induce highly enantioenriched products.

Building off the success of vitamin B_{12} derivatives, Co(II) porphyrin catalysts were developed by Zhang and co-workers (Figure 1.51).[139, 140] The tetraphenyl Co(II) porphyrin **87** proved to be an effective catalyst for the formation of the cyclopropane product, even showing moderate diastereoselectivity. Incorporation of chiral groups at two of the meso positions (R, Figure 1.51) resulted in enantioinduction without any increase in the diastereomeric ratio (Figure 1.51, **85**-**86**). It was noted that the presence of the methoxy ether resulted in the highest enantioselectivity of the major *trans* isomer. Improvements to diastereoselectivity were obtained by implementing a rigid cyclopropane ring but only modest enantioselectivity was observed (Figure 1.51, **88**). To mimic vitamin B_{12} derivatives, which were more enantioselective, 4-dimethylaminopyridine (DMAP) was added to generate a pentacoordinate Co metal. The additive resulted in a decrease in yield but nearly doubled the ee of three different catalysts (Figure 1.51, results in parentheses). Examination of different additives and solvents revealed that a *trans* influence was present. It was hypothesized that the coordination of the additive resulted in the rigidification of the complex, resulting in a more structured chiral pocket.[141] Introduction of another chiral center through the use of an aziridine ligand did not result in improved enantioselectivity (Figure 1.51, **89**). Rather, a decrease in enantioselectivity was observed.

Further catalyst development involved modification of the achiral aryl groups and probing different chiral groups (Figure 1.52).[142] Insight into the electronic effect of the achiral aryl groups was gained by the addition of methoxy substituents (Figure 1.52, **90a**-**92a**), while the introduction of ^{t}Bu groups (Figure 1.52, **90b**-**92b**) were incorporated to investigate steric influence. The methoxy groups led to an increase in the *cis*:*trans* ratio in each instance with concomitant lowering of the yield, as compared to **87**. A less

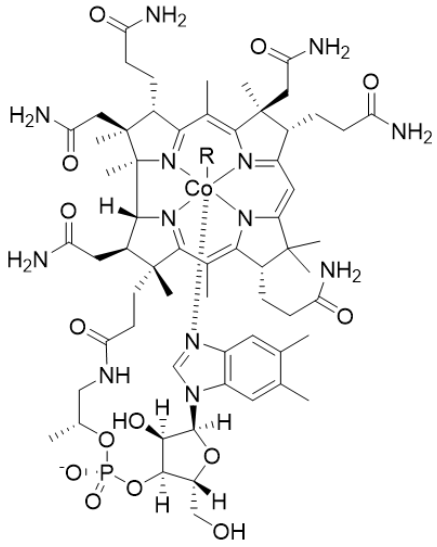

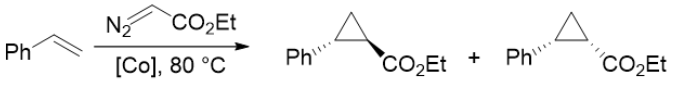

R	*Yield %*	*cis:trans*	ee *cis*(*trans*)
CN	34	56:44	47(29)
Me	86	61:39	62(52)
5'-deoxyadenosyl	82	61:39	61(51)
HO·HCl	98	61:39	64(54)

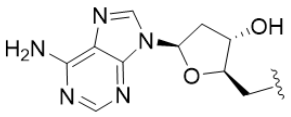

= 5'-deoxyadenosyl

Figure 1.50 Vitamin B_{12} derivatives used as cyclopropanation catalysts

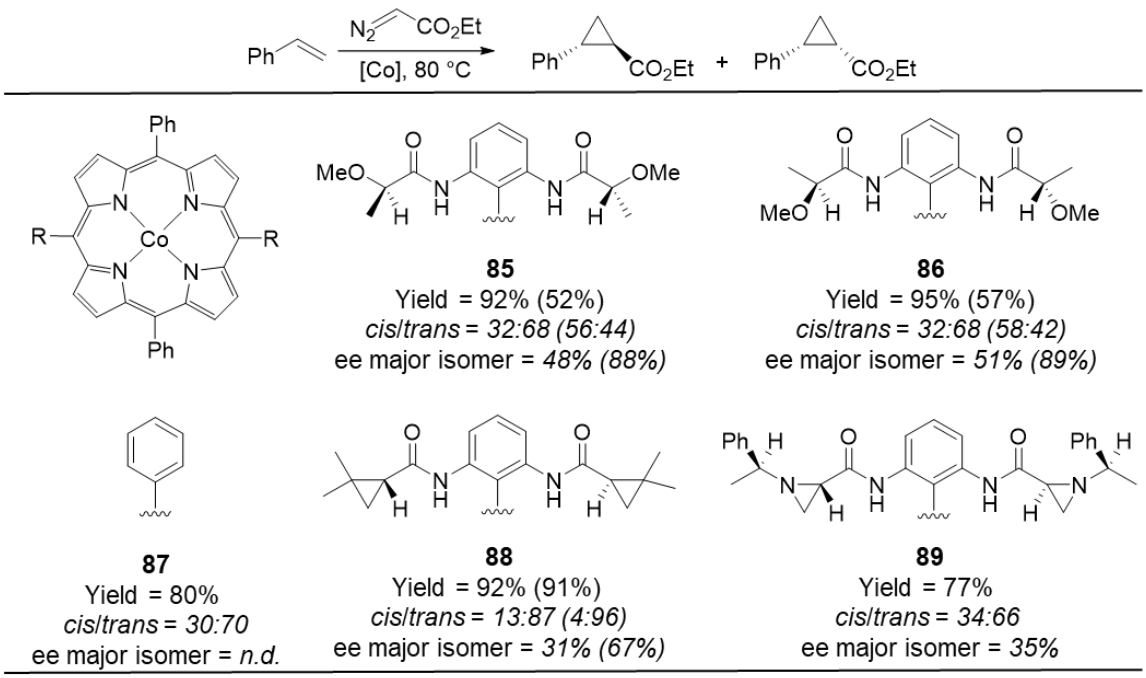

Values in parenthesis results with 0.5 equivalents of DMAP as additive

Figure 1.51 Cyclopropanation of styrene by Co(II) porphyrin complexes

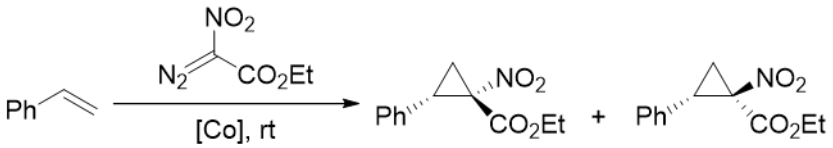

Catalyst	*Yield %*	*cis:trans*	% ee *cis*
87	15	58:42	ND
90a	69	81:19	47
90b	20	67:33	33
91a	99	91:9	58
91b	99	91:9	81
92a	< 5	85:15	ND
92b	31	66:34	-23

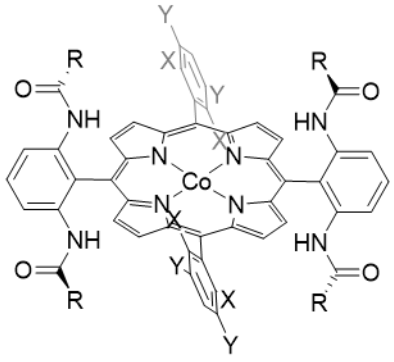

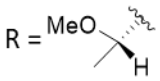

90a X = OMe Y = H
90b X = H Y = ^{t}Bu

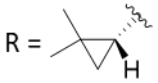

91a X = OMe Y = H
91b X = H Y = ^{t}Bu

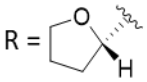

92a X = OMe Y = H
92b X = H Y = ^{t}Bu

Figure 1.52 Investigation of the influence of the achiral aryl groups of porphyrin Co(II) complexes

substantial increase in *cis*:*trans* ratio was observed with the introduction of the ^{t}Bu groups, indicating that electronics had a larger influence on selectivity. When *p*-toluenesulfonyl diazo reagents were applied, high diastereoselectivity was observed for each catalyst.[143] No additive was included in these reactions and high selectivity was still maintained.

The Zhang group then investigated the influence of the position of the chiral group. A bridging ligand with axial chirality positioned the chiral groups above the active site rather than on the side (Figure 1.53).[144] This was done as a means of generating a chiral pocket around the metal center. Different carbon lengths between the bridging binaphthyl group and the amides were investigated to modify the distance between the chiral group and the metal center. When no methylene units were incorporated, no reaction was observed (Figure 1.53, **93a**). Lengthening the chain resulted in high yields of the desired cyclopropane product. However, a decrease in ee was observed as the linker was extended (Figure 1.53, **93b** and **93c**). This indicated that a linker is needed to allow room for carbenoid formation, but distancing of the chiral moiety prevented chiral induction.

In each of the previously discussed examples of Co(II) porphyrin catalysis, no techniques were employed to minimize the formation of the homocoupled dimer product. Yet it was observed that cyclopropanation of diazo compounds with Co(II) porphyrin complexes does not generate appreciable amounts of the homocoupled dimer products. This is believed to result from the Co(II) porphyrin complexes proceeding through a slightly different mechanism, compared to other metals. Although Co(II) porphyrin complexes proceed through a carbenoid intermediate, it should be noted that the carbenoid has two different binding modes. One binding mode involves the participation of the porphyrin ligand to generate a “bridged carbene” (Scheme 1.3).[41] Alternatively, the carbene can bind solely to the Co metal center generating a “terminal carbene” (Scheme 1.3). The terminal carbene results in the formal oxidation of the Co resulting in a free radical localized on the carbene carbon. The radical then reacts with the styrene substrate leading to a metalloradical complex. Termination of the radical results in the formation of the cyclopropane product and reduction of the Co(III) center. The formation of the radical intermediate was also demonstrated experimentally for salen Co(II) complexes.[145]

Direct research into why the catalysts with bridging chiral groups are stereoselective is limited, but it can be rationalized based on comparison to analogous Fe porphyrins.[146] It is believed that diastereoselectivity is dictated by the lower portion of the bridging ligand. Preferential positioning of the diazo reagent leads to the high

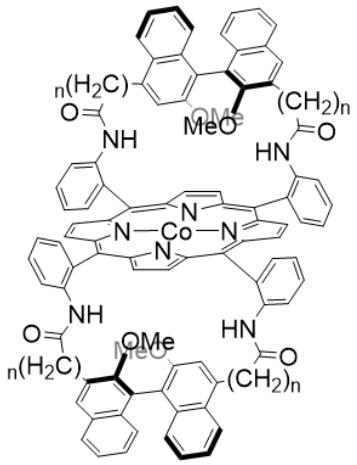

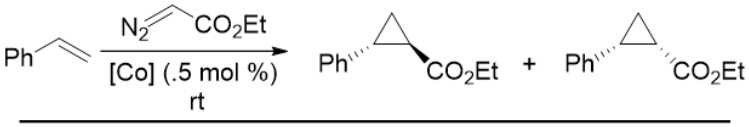

Catalyst	n	*Yield* %	*cis:trans*	% ee *cis*(*trans*)
93a	0	NR	ND	ND
93b	1	93	18:82	66 (31)
93c	2	89	16:84	50 (26)

Figure 1.53 Cyclopropanation by Co(II) porphyrin catalysts with bridging chiral ligands

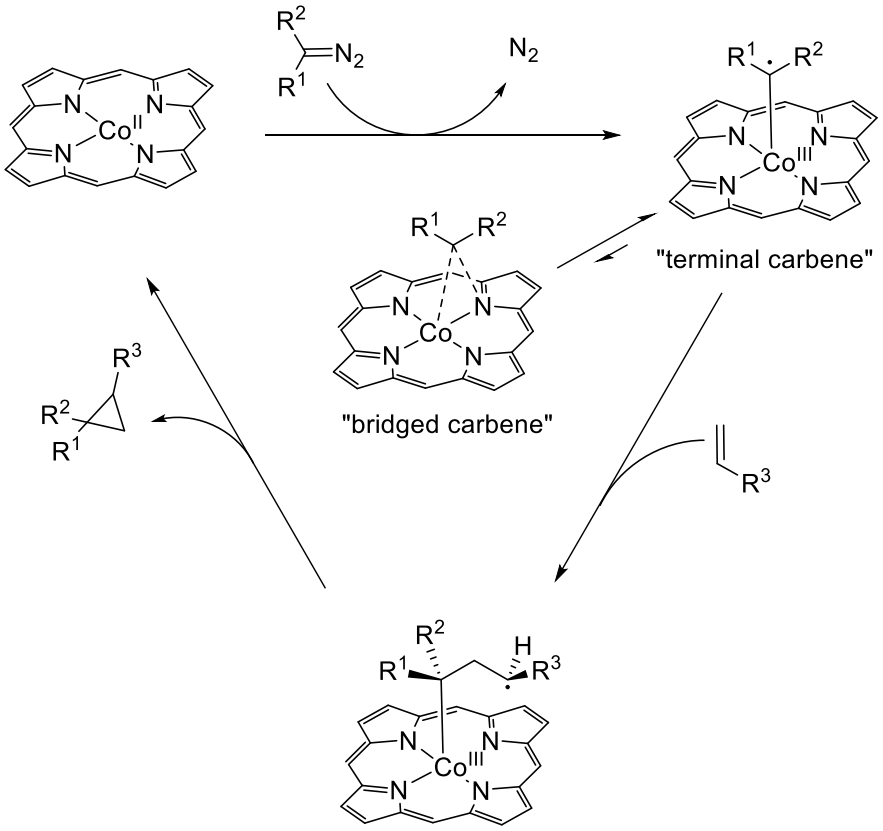

Scheme 1.3 Radical mechanism for cyclopropanation with the Co(II) porphyrin complexes

diastereoselectivity (Figure 1.54). The upper portion of the bridging ligand, in combination with the steric requirements of the substrate, then dictates the absolute configuration of the final product. The selectivity of Co(II) porphyrin complexes without a bridging ligand was postulated to arise from H-bonding. This is based on the increased enantioselectivity observed when the chiral group contained oxygen as a H-bond acceptor, which would lock the ligand into a specific conformation (Figure 1.55, a). High enantioselectivity was also observed when the chiral group was locked in place using a cyclopropane ring. When the oxygen H-bond acceptor was replaced by nitrogen, the enantioselectivity was drastically reduced.[147] Another H-bond between the N–H bond of the amide and the carbonyl oxygen of the diazo reagent is believed to influence reactivity of these complexes (Figure 1.55, b). This bonding interaction stabilizes the radical intermediate and is cited as the reason for the porphyrin complex's exceptional reactivity. This same interaction has been invoked as a possible explanation for the increased diastereoselectivity.

1.1.5.3 Recent Advances in Cyclopropanation with Co(II) Complexes

In 2014, a Co(II) salen catalyst was developed for the cyclopropanation of disubstituted olefins. Different 1,1-disubstituted olefins were examined and proceeded with high enantioselectivity (Figure 1.56). The *trans* isomer was the favored diastereomer in each case investigated. The usefulness of this methodology was showcased in the synthesis of the dual inhibitor of serotonin and norepinephrine reuptake, (+)-synosutine.[148] Further application of Co(II) salen complexes was found for the cyclopropanation of electron deficient heterocycles, resulting in dearomatization (Figure 1.57).[149] The Co(II) salen complexes favored the formation of the *cis* isomer, rather than the *trans* observed with similar salen complexes, and gave enantiomeric ratios (er) up to 95%. Further examples investigating the scope of the reaction gave moderate to great yields (45-91%). Each substrate afforded the *cis* product as the major isomer and most ers were above 90:10.

Zhang and co-workers expanded the number of Co(II) porphyrin catalysts by incorporating different substituents on the cyclopropane ring (Figure 1.58, a). This introduced another chiral center in an effort to improve enantioinduction. These catalysts were then screened with various acceptor/acceptor diazo reagents (Figure 1.58, b). The optimal catalyst was based on which catalyst afforded the best combination of yield,

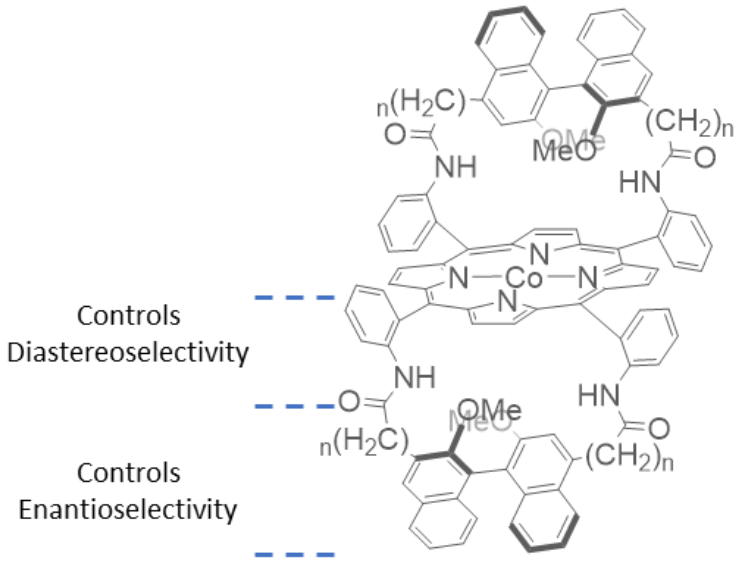

Figure 1.54 Source of diastereoselectivity and enantioselectivity with bridged porphyrin Co complexes based on analogous Fe porphyrin complexes

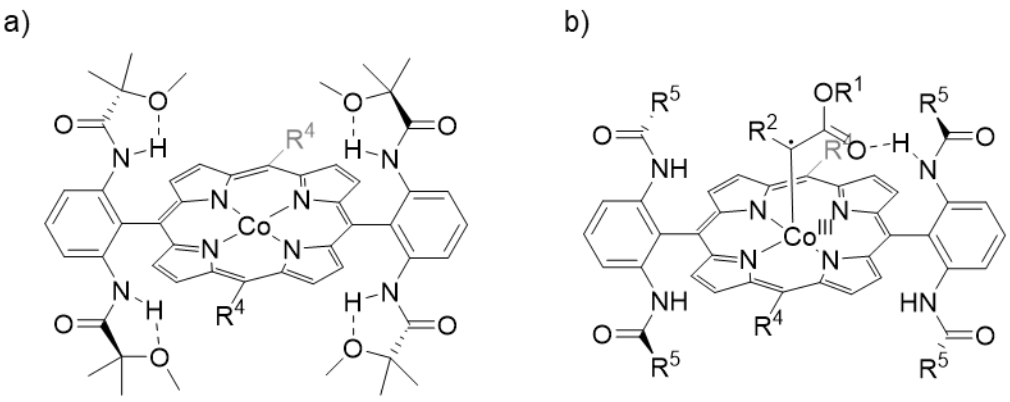

Figure 1.55 H-bonding interactions that facilitate asymmetric induction of Co(II) porphyrin catalysts

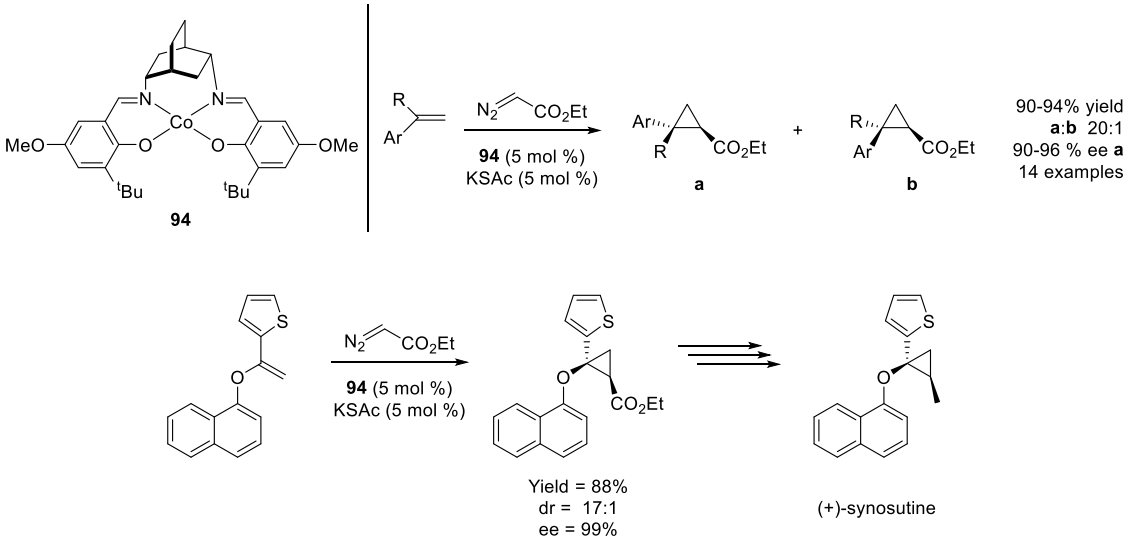

Figure 1.56 Cyclopropanation of 1,1-disubstituted olefins with Co(II) salen catalyst and application towards total synthesis

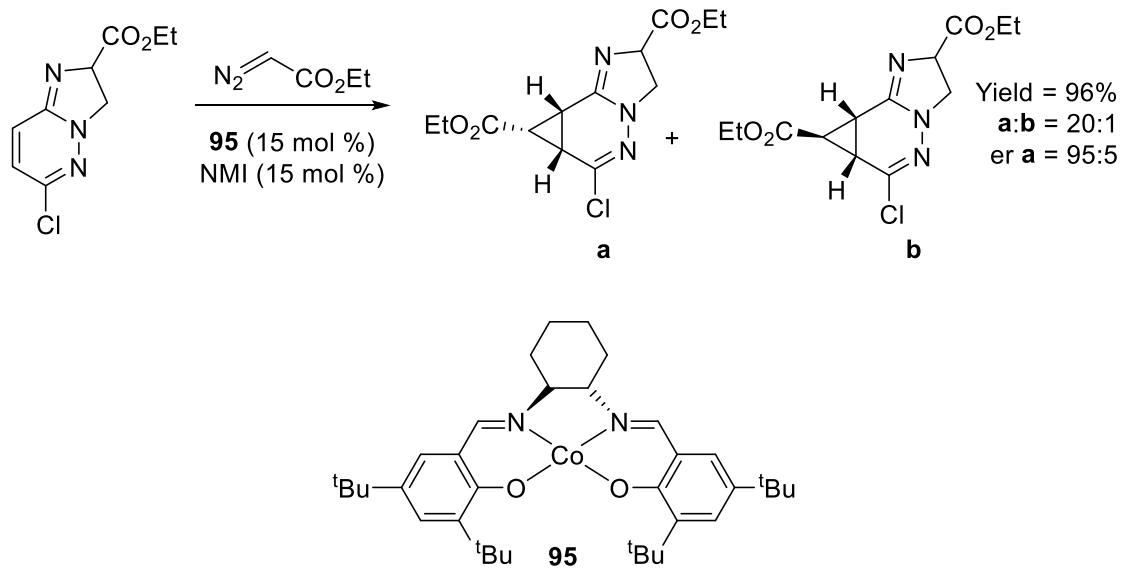

Figure 1.57 Cyclopropanation of heteroaromatic olefins with Co(II) salen complexes

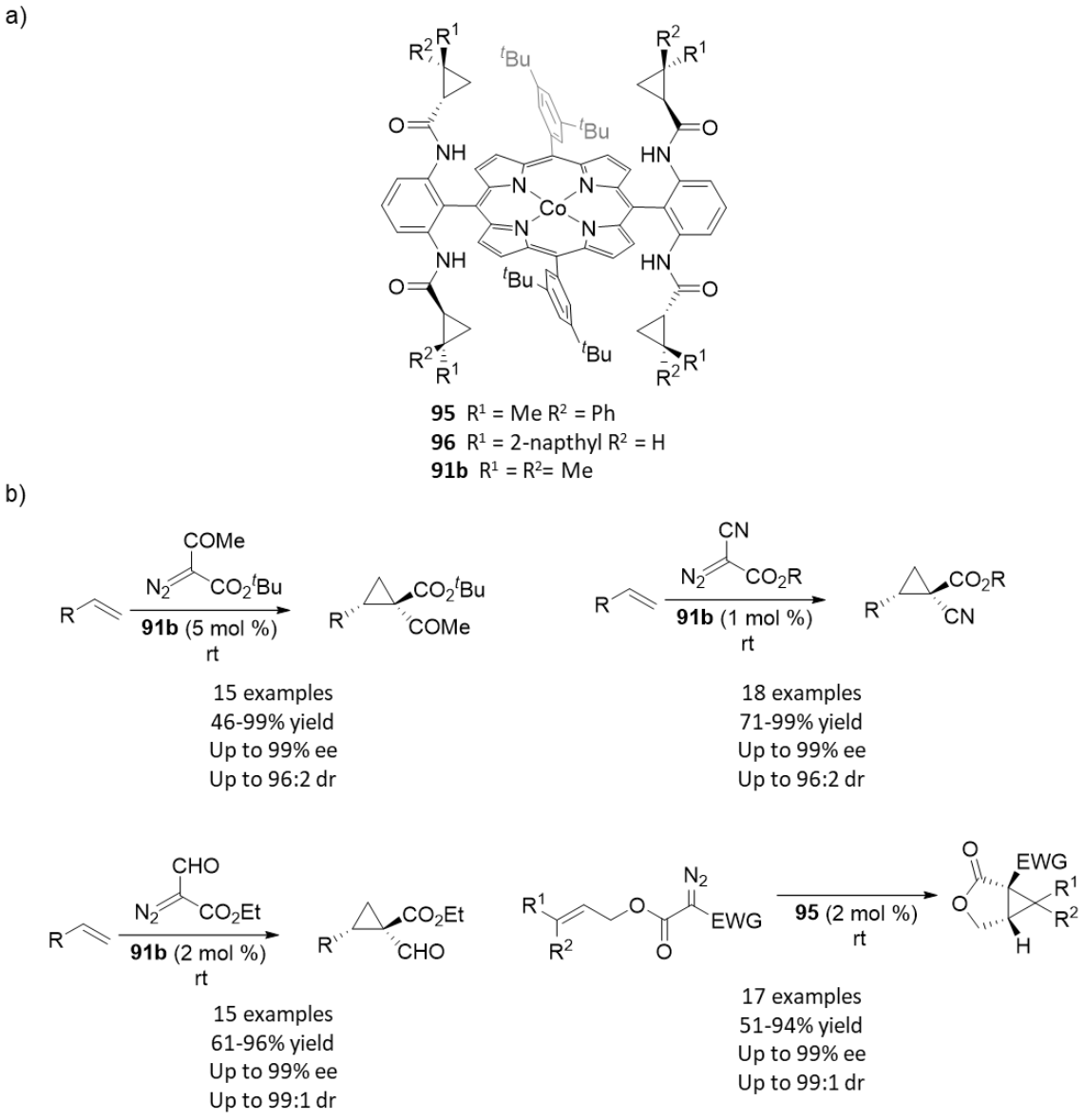

Figure 1.58 Recent examples of a) Co(II) porphyrin complexes and b) their application in asymmetric cyclopropanation

diastereoselectivity, and enantioselectivity. When these parameters were considered the most suitable catalyst was often the dimethyl cyclopropane substituent (**91b**). High diastereoselectivity and enantioselectivity were observed with aryl olefins and even electron deficient acrylates.[150, 151] Another large step was made in the cyclopropanation of olefins with diazo reagents containing an aldehyde acceptor group.[152] This is the first example of incorporating an aldehyde in such a manner. It was also demonstrated that this class of catalyst was capable of intramolecular reactions in addition to intermolecular reactions.[153] Again, a range of different acceptor functionalities were used in conjunction with the ester.

A new series of Co porphyrin catalysts was developed wherein the chiral pocket was replaced with a cage extending directly over the Co metal (Figure 1.59).[154] The bridging ligand does not prevent catalytic activity. Rather, the cage complexes **97** and **98** resulted in an increased yield and enantioselectivity compared to the established complex **91b**. The cage appeared to be instrumental for obtaining high ees as the pocket of complex **99** did not have high ees. The diastereoselectivity of these catalysts was very high, with the *trans* isomer predominating for each catalyst

Application of cyclopropanes synthesized by Co(II) porphyrin complexes was realized in pharmacological structure-activity relationship (SAR) experiments. The olefin 2-vinylpyridine was effectively cyclopropanated as a means of achieving the desired enantiomer (97% ee) of the potential agonist (Figure 1.60).[155] Previous methods for synthesizing similar cyclopropanes with other metals suffer due to coordination of the pyridine moiety, yet a good yield (69%) was achieved.

1.1.6 Iridium

1.1.6.1 Cyclopropanation with Ir(III) Salen Complexes

Early investigations demonstrated that Ir could decompose diazomethane to afford dinitrogen, ethylene, and other side products. This was corroborated later in the formation of Ir carbenoid complexes that were studied via crystallography.[156] The application of Ir towards cyclopropanation was observed more recently than the other metals that have been discussed. In 2016, Ir salen complexes were applied by Katsuki and co-workers for the cyclopropanation of styrene with diazo reagents (Figure 1.61).[157] The initial

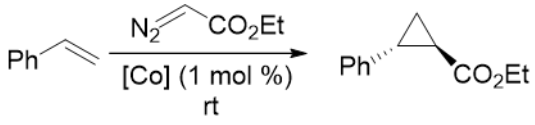

Catalyst	*Yield %*	*cis:trans*	% ee *trans*
91b	67	*10:90*	34
97	93	5:95	96
98	84	5:95	88
99	*73*	*5:95*	14

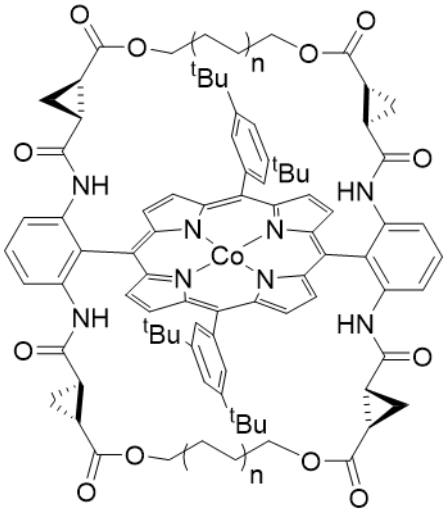

97 n = 1, **98** n =2
Cage

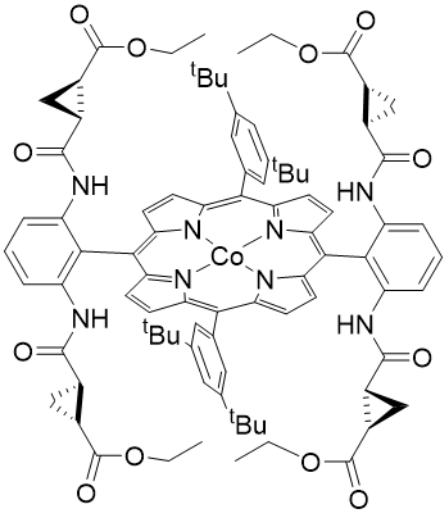

99
Pocket

Figure 1.59 Bridged Co(II) porphyrin catalysts for cyclopropanation of styrene

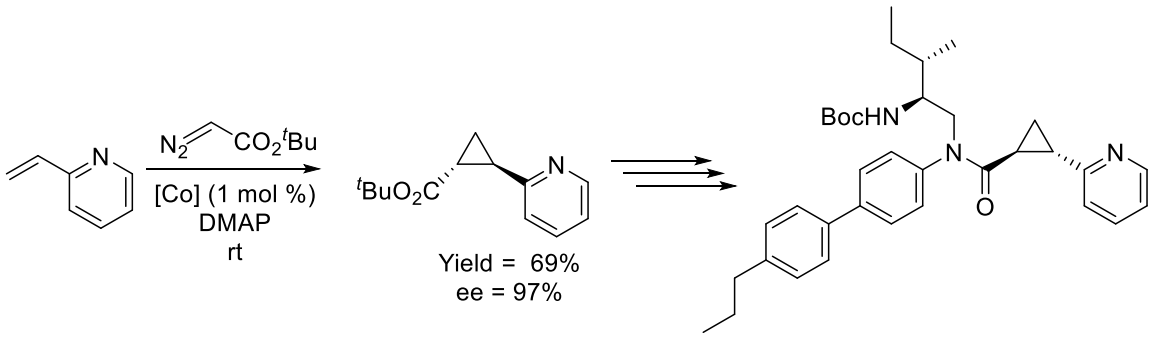

Figure 1.60 Application of cyclopropane generated by Co(II) porphyrin catalysts for SAR studies

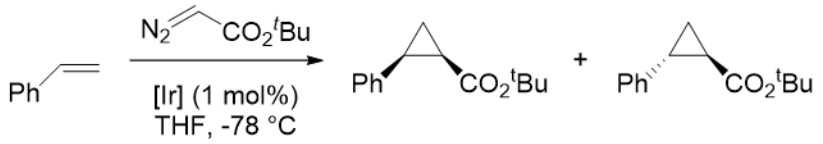

[Ir]	Yield (%)	*cis.trans*	ee (%) *trans*	ee (%) *cis*
100	99	>99:1	>99	ND
101	44	41:59	63	60
102	99	>99:1	98	ND
103	43	58:42	-37	70

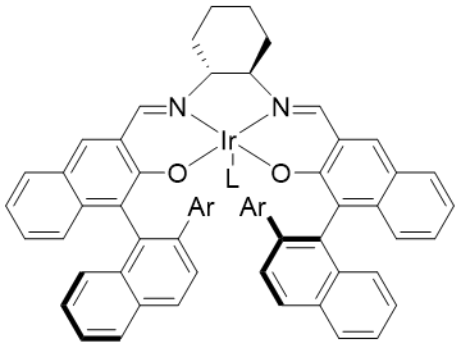

100 L = *p*-$CH_3C_6H_4$ Ar = Ph
101 L = *p*-$CH_3C_6H_4$ Ar = H
102 L = C_6H_5 Ar = Ph

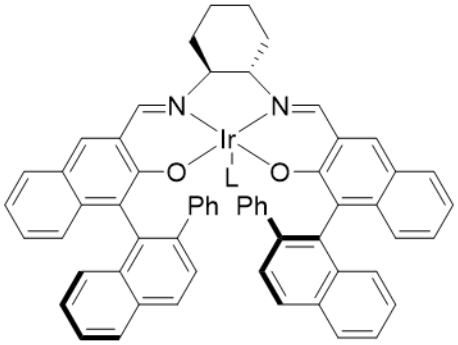

103 L = *p*-$CH_3C_6H_4$ Ar = Ph

Figure 1.61 Cyclopropanation of styrene with Ir(III) salen complexes

investigation of the cyclopropanation of styrene with ^{t}Bu diazoacetate with an Ir(III) salen complex afforded the *cis* isomer as the major product (>99:1 *cis*:*trans*) and achieved high enantioselectivities (>90% ee) when low temperatures were maintained.[158] High enantioselectivity was also observed when EDA was the diazo reagent. The Ph substituent on the naphthyl ring of complex **100** was believed to be responsible for high diastereoselectivity and enantioselectivity. Replacing the Ph group with a hydrogen atom affords complex **101** and resulted in a less stereoselective reaction. This was accompanied by a decrease in yield. Complex **103**, the diastereomer of complex **100**, demonstrated a preference for the opposite enantiomer of the *trans* isomer. Interestingly, the yield and diastereoselectivity were much lower. No major change in reactivity was observed when the apical ligand was changed to another aryl hydrocarbon (Figure 1.61, compare **100** and **102**). It is worth noting that these results are similar to a Co(II) complex that incorporated a similar salen ligand (See Figure 1.47). Having established the complex as an efficient catalyst, the scope of olefins was expanded to cyclic and substituted olefins. The introduction of multiple substituents on the olefin led to a decrease in the yield and selectivity with 1,1-disubstituted olefins and only trace amounts with 1,2-disubstiuted olefins.

The Ir(III) salen catalyst **101** was also applied by the Katsuki group in the synthesis of natural cyclopropane fatty acids.[159] Cyclopropane fatty acids are a class of compounds that have been observed in many natural products and have demonstrated antibacterial and antifungal activity.[160] The Katsumi group was able to apply their Ir salen catalyst to generate the cyclopropane in good yields (Figure 1.62). More impressive than the yield was the high enantioselectivity (98% ee) for the desired *cis* isomer.

1.1.6.2 Recent Advances in Cyclopropanation with Ir(III) Complexes

Iridium porphyrin complexes were also shown to be effective catalysts for the cyclopropanation of olefins. The reactivity of each complex was heavily reliant on the coordinating ability of the apical ligands.[161] High diastereoselectivity for the *trans* product was observed but was not enantioselective. The use of porphyrin complexes had been made enantioselective by using natural and modified enzymes as catalysts. Just as vitamin B_{12} is a coenzyme, porphyrin complexes with various metal centers have been installed as coenzymes as a means of facilitating abiological reactions.[162] In this process,

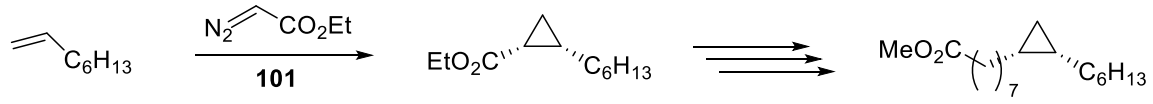

Figure 1.62 Asymmetric cyclopropanation of olefins with EDA by an Ir salen complex

researchers harnessed the high selectivity of enzymes for the synthesis of commodity chemicals, rather than biologically relevant compounds. One such example from Key and co-workers incorporated Ir into the porphyrin ring of mutated enzymes.[163] When the mutated enzymes were applied as a catalyst for the cyclopropanation of styrene with EDA, the enzymes were highly diastereoselective for the *cis* isomer (Table 1.5, entries 1-2). Furthermore, both enantiomers could be synthesized selectively with high fidelity (98% ee) based on which mutant enzyme catalyst was employed. This is contrasted by applying the free Ir(Me)-PIX coenzyme, which preferentially showed a slight preference for the *trans* isomer and was not enantioselective (Table 1.5, entry 3). Substituted aryl olefins and functionalized olefins afforded good to high yields while aliphatic olefins, terminal or internal, were low yielding. Applying the same mutant enzymes to different olefin substrates was not successful. Rather, new mutant enzymes were synthesized to match different olefin substrates to maintain the high diastereoselectivity and enantioselectivity.

1.2 Research Motivation

It is evident that cyclopropanation continues to be the focus of research, as evidenced by the new applications. Examples of each metal facilitating cyclopropanation with high yields and in a highly stereoselective manner are known. It should be noted that the success of each metal is highly dependent on the ligand and diazo reagent. Each set of catalysts has its own set of strengths and weaknesses. Copper complexes are often inexpensive and ligand scaffolds that afford high enantioselectivity are easily accessible. On the other hand, Cu catalysts often require the use of acceptor diazo reagents. This limits the diversity of compounds that can be synthesized. Further synthetic limitations can result from the propensity of olefins to coordinate Cu, resulting in catalyst inhibition.[164]

Ag complexes have been applied towards cyclopropanation, but the yields are often lower due to side reactions. Furthermore, these reactions are often not asymmetric due to the lack of chiral Ag catalysts. Au complexes afforded enantioselective cyclopropane products but often suffered from low yields due to the formation of undesired side products. Cobalt complexes are promising candidates for *cis*-selective cyclopropanation, rather than the more common *trans* isomer, and are generated in an

Table 1.5 Protein structure of Fe-CYP119 (Image obtained from PDB 1107) and the Ir coenzyme used to replace the Fe coenzyme as a catalyst for cyclopropanation

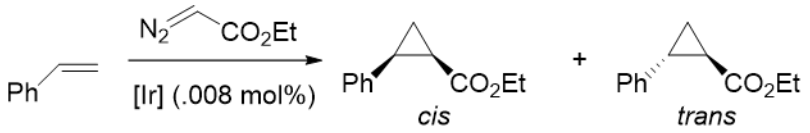

Entry	[Ir] Parent Mutant	Additional Mutations	Yield (%)	*cis:trans*	ee (%) *cis*
1	Ir(Me)-CYP119 (+)	L155W	80	90:1	98
2	Ir(Me)-CYP119 (-)	V254L	74	73:1	-98
3	Free Ir(Me)-PIX	-	N	1:4	0

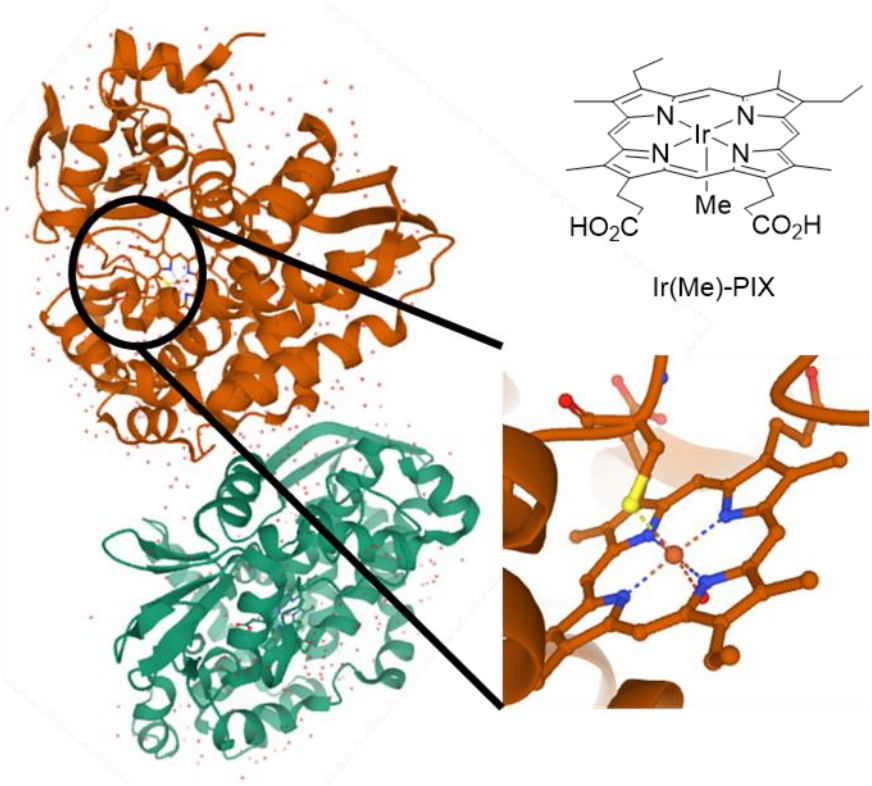

enantioselective manner. Furthermore, the natural abundance of Co makes it desirable as a means of limiting costs. The generation of a radical intermediate may limit functional group tolerance and would, therefore, benefit from catalysts that can also generate the *cis* isomer via the traditional metal carbenoid.

Of the metals applied in this reaction, it can be argued Rh^{II} catalysts are the most popular. The judicious choice of bridging ligand provides impressive control over both the electronic nature and steric environment around the catalytically active axial site. This control has enabled the use of a wider range of diazo reagents, which facilitates the introduction of a wider range of functionality. Although Rh is an expensive noble metal, the high activity of Rh^{II} allows for low catalyst loading, even with more complex olefin substrates. The stability of the Rh^{II} complex has also enabled the catalyst to be recycled or incorporated into flow reactors.[165] These recycling conditions also help lower the amount of Rh required.

Much of the development of Rh^{II} complexes has been achieved by using bridging ligands as the control element. This is often in the form of a homoleptic Rh^{II} complex where each bridging ligand is the same. Most research has been dedicated, as can be seen in section 1.1.4, to the introduction of chiral ligands for asymmetric induction. Additionally, the ligands are often carboxylate type ligands which results in minimal change to the Rh metal centers. This causes each catalyst to have similar reactivity with regards to chemoselectivity. As Rh^{II} catalysts can facilitate a wide array of reactions, a means of controlling chemoselectivity is required. A semblance of chemoselectivity can be achieved through sterically bulky bridging ligands. These sterically cumbersome ligands dictate that the least sterically hindered reactive functional group on a substrate will react first. However, this limits the applicability of these catalysts as chemoselectivity is determined by the substrate.

Chemoselectivity, with regards to preventing the undesired homocoupling of the diazo reagent, has also been controlled to a certain extent. An excess of olefin is one method but is less viable when using hard to synthesize late-stage olefin substrate. This often mandates cyclopropanation occurring early in synthesis strategies or sacrificing large quantities of late stage materials. High olefin concentrations are often coupled with the slow addition of diazo reagent, thereby minimizing amount of diazo reagent present. The slow addition requires more equipment, but most importantly, requires more time. One, or a combination, of these techniques has been employed in all but a few examples

provided in this chapter. It is desirable that chemoselectivity be controlled by the catalyst, which can be accomplished through modifying the electronics of the Rh metal, and thereby the carbenoid.

We hypothesized that electronic control of the carbenoid could be achieved by axial coordination. Coordination of one axial site by a LB should result in electronic communication through the Rh–Rh bond, thereby modulating the Rh^{II} carbenoid species at the other axial site. By controlling the donating strength of the LB, the electronics of the catalyst, and subsequently the carbenoid, could be finely tuned. A less electrophilic carbenoid is expected by selecting a more electron donating LB. Conversely, weaker LB donors could be employed to facilitate a more electrophilic carbenoid. This tuning is then expected to result in control of chemoselectivity, such as favoring cyclopropanation over the formation of the homocoupled dimer of the diazo reagent. This would be similar to the control of chemoselectivity observed by changing the bridging ligands (see section 1.1.4).

Our overarching research goal is the synthesis of heteroleptic complexes of the formula Rh_2A_3B, where A and B are different bridging ligands. Ligand A would be common ligands from proven chiral catalysts such as Rh_2(*S*-PTAD)$_4$ or Rh_2(*S*-MEOX)$_4$, while ligand B would contain a tethered LB. The combination of the two ligands is predicted to combine the benefits of the proven chiral ligands and the predicted chemoselectivity from axial coordination. This combination is expected to allow highly enantioselective transformations of complex substrates in a directed manner. Controlling chemoselectivity through axial coordination of the catalyst would eliminate, or mitigate, the need for protecting groups.

Axial coordination of exogenous Lewis bases (LBs) resulted in increased enantioselectivity of cyclopropanation reactions with other metals (see section 1.1.5). Examples in the literature show contradictory results upon the addition of LBs to cyclopropanation reactions using Rh^{II} catalysts. In some instances, a decrease in enantioselectivity and yield is observed. In other examples the yield remained unchanged but was more enantioselective. These studies bring into question the role of axial coordination and its effect on enantioselectivity. The synthesis of the proposed Rh^{II} complexes would also provide for a more direct study of axial coordination with regards to enantioselectivity. Through this understanding, it may be possible to harness the benefits of axial coordination, while avoiding the disadvantages.

Before synthesizing the chiral Rh^{II} described above, we first sought to synthesize

a series of novel heteroleptic Rh^{II} complexes with achiral acetate groups (Ligand A) and a ligand with a tethered LB (Ligand B). These complexes would allow us to validate the hypothesis that axial coordination can be used to tune the Rh^{II} carbenoid. Chapter two focuses on developing the synthesis of these novel complexes and their characterization. Different spectroscopic techniques were conducted to ascertain if axial coordination was present. Electrochemical experiments were also conducted to determine if electronic information could be transmitted through the Rh–Rh bond. Chapter three outlines the application and evaluation of the complexes as catalysts in the cyclopropanation of olefins with different diazo reagents. Chapter four provides all the relevant experimental procedures. Finally, all the corresponding NMR spectra and crystallographic information are in the appendices.

Chapter 2 -

Synthesis and Characterization of Thioether Functionalized Oxazolidinonate Rh^{II} Complexes

Portions of this chapter were adapted from the publication by Brad Anderson, Derek Cressy, Jay Patel, Caleb Harris, Glen Yapp, John Berry, and Ampofo Darko in the peered reviewed article:

Anderson, B. G.; Cressy, D.; Patel, J. J.; Harris, C. F.; Yap, G. P. A.; Berry, J. F.; Darko, A., Synthesis and Catalytic Properties of Dirhodium Paddlewheel Complexes with Tethered, Axially Coordinating Thioether Ligands. *Inorganic Chemistry* **2019,** *58* (3), 1728-1732

Dr. Brad Anderson, assisted by Jay Patel, was responsible for synthesis, characterization, catalytic screening of the carboxylate derived catalyst, and writing the manuscript. Derek Cressy was responsible for the synthesis, characterization, catalytic screening involving the oxazolidinone derived catalyst, and UV-Vis, along with aiding in manuscript preparation. Dr. Glenn Yapp was responsible for solving the crystal structure for the oxazolidinone derived complex. Dr. Caleb Harris was responsible for CV analysis. Prof. John Berry and Prof. Ampofo Darko both advised the work.

Portions of this chapter were also adapted from a manuscript by Derek Cressy, Cris Zavala, Anthony Abshire, Will Sheffield and Ampofo Darko, which is currently published as a preprint:

Cressy, D.; Zavala, C.; Abshire, A.; Sheffield, W.; Darko, A., Tuning Rh(II)-Catalyzed Cyclopropanation with Tethered Thioether Ligands. *Dalton Trans*. **2020**. DOI 10.1039/D0DT03019H

Derek Cressy was responsible for the synthesis, characterization, x-ray structure elucidation, catalyst screening, UV-Vis, electrochemical analysis, and manuscript preparation. Cris Zavala was responsible for catalytic testing and aided in manuscript preparation. Anthony Abshire was responsible for all calculations, while Will Sheffield aided in characterization and manuscript preparation. Prof. Ampofo Darko advised the work.

2.1 Abstract

Rh^{II} complexes have seen extensive use as catalysts for the decomposition of diazo compounds to generate reactive carbenoid species. The reactivity of the Rh^{II} complexes has traditionally been controlled through the bridging ligands, while investigations of using the axial site as a control element have been limited. A series of Rh^{II} complexes equipped with an oxazolidinone bridging ligand containing a tethered thioether have been synthesized. The tethered thioether was designed to coordinate to the axial site as a means of tuning the reactivity of the carbenoid species. Oxazolidinone ligands were synthesized via modified or established procedures from different amino acid starting materials. Different methods for exchanging the oxazolidinone ligand for an acetate of $Rh_2(OAc)_4$ were investigated. It was determined the use of a Soxhlet and microwave method provided the desired complexes in suitable yields for further testing. Select spectral and electrochemical studies were then conducted to investigate the properties of these catalysts and identify axial coordination of the tethered thioether.

2.2 Introduction

2.2.1 Synthetic Methods for Rh^{II} Complexes

The first synthesis of a Rh^{II} complex was that of $Rh_2(OAc)_4$ (Figure 2.1, a). Upon refluxing $RhCl_3$ trihydrate in glacial acetic acid, the Rh(III) was reduced to Rh(II), generating $Rh_2(OAc)_4$.[166] Conversely, an oxidative pathway had been developed for the synthesis of Rh^{II} formamidate complexes starting from a Rh(I) species (Figure 2.1, b). These complexes typically only contained two bridging ligands. The remaining equatorial sites were occupied by solvent molecules and resulted in a cationic complex.[167, 168] The most common method of Rh^{II} complex synthesis relies on the substitution of the acetate ligands of $Rh_2(OAc)_4$ (Figure 2.1, c).[76] Although the acetate groups are kinetically inert at room temperature, heating $Rh_2(OAc)_4$ in the presence of a different carboxylate ligand facilitates ligand exchange. This exchange could be promoted by the addition of a base. Exchange of carboxamidate ligands proved more difficult and required the ligand to be melted, followed by the addition of $Rh_2(OAc)_4$.[169]

A leading technique for synthesizing Rh^{II} complexes, with either carboxylate or

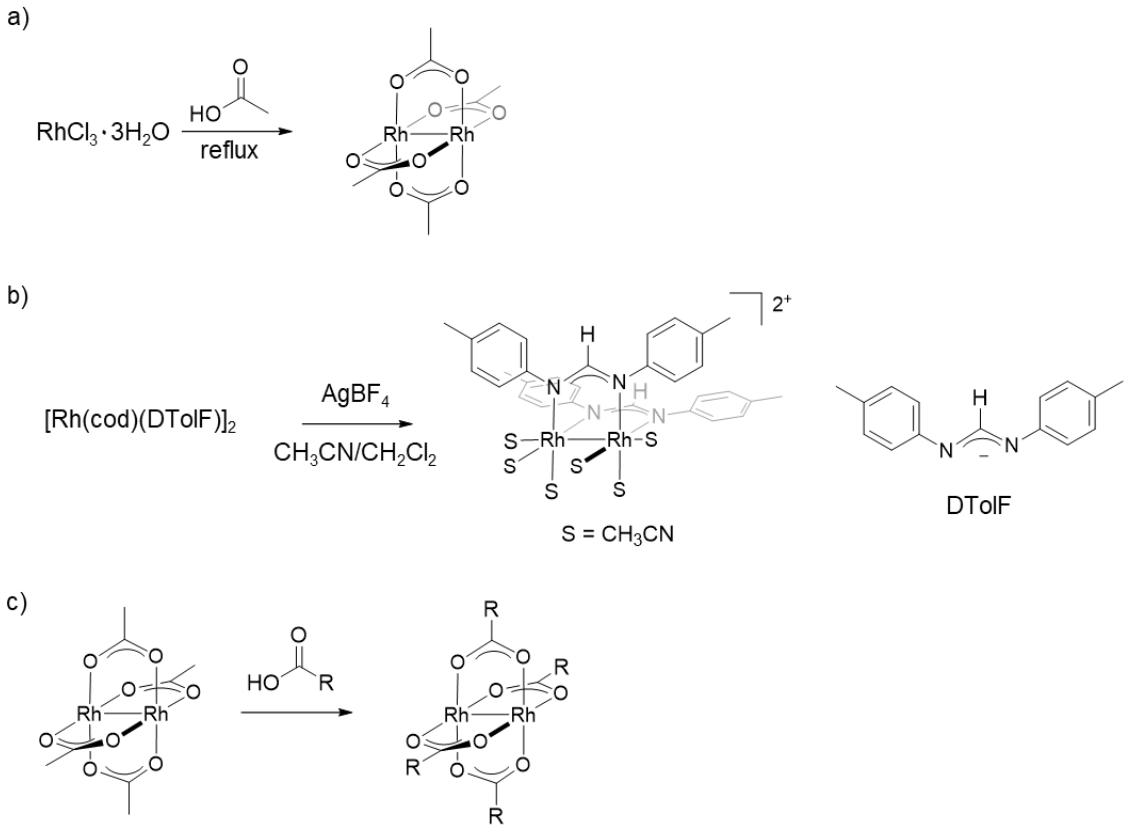

Figure 2.1 Examples of the synthesis of Rh^{II} complexes from a) Rh(III) b) Rh(I) and c) Rh(II).

carboxamidate ligands, involves manipulation of the equilibrium of the ligand exchange reaction. This is accomplished with the unconventional application of a Soxhlet apparatus. Traditionally, the thimble of a Soxhlet apparatus would be charged with a reagent that is moderately soluble in the reaction solvent. This facilitates the slow addition of the reagent and minimizes the amount of solvent required (Figure 2.2, left). When utilizing a Soxhlet apparatus for the synthesis of Rh^{II} complexes, the reaction flask is charged with $Rh_2(OAc)_4$, the new ligand, and a non-coordinating solvent (Figure 2.2, right). As the reaction progresses, acetic acid is generated after being displaced by the new ligand. Chlorobenzene (PhCl) is typically chosen as a solvent because it is a non-coordinating solvent which forms an azeotrope with acetic acid. This azeotrope then travels up the Soxhlet and is neutralized after condensing into the thimble charged with sodium carbonate. The removal of the acetic acid from the reaction mixture, in conjunction with an excess of the desired ligand, facilitates the complete substitution of bridging acetate ligands.

In addition to $Rh_2(OAc)_4$, several other Rh^{II} derivatives, such as dirhodium(II) tetrakistetratrifluoroacetate ($Rh_2(TFA)_4$) and dirhodium(II) tetrakiscarbonate ($Rh_2(CO_3)_4$), have found use as starting materials for ligand exchange.[84, 170] In the case of $Rh_2(TFA)_4$, the inductively withdrawing fluorine atoms cause the TFA group to be a better leaving group than acetate. The increased lability of the ligand allows for ligand exchange at room temperature.

2.1.2 Mechanism of Ligand Exchange

Despite the wide application of the ligand exchange of $Rh_2(OAc)_4$, questions about the exact mechanism remain. It is believed that the initial step is the coordination of the new ligand to the axial site (Figure 2.3, Intermediate II). This is predicated on the ease with which $Rh_2(OAc)_4$ forms adducts with Lewis bases at the axial site.[171, 172] The association of the ligand at the axial site is then believed to facilitate the displacement of the acetate ligand. Support for this mechanism was observed by NMR in the synthesis of Rh^{II} complexes with orthometallated phosphines, although the more electrophilic Rh^{II} precursor $Rh_2(TFA)_4$ was used.[173] The associative mechanism may not be the only pathway, as a dissociative pathway is also plausible (Figure 2.3, Intermediates IV and V).

Different binding modes have been discovered through the synthesis of Rh^{II}

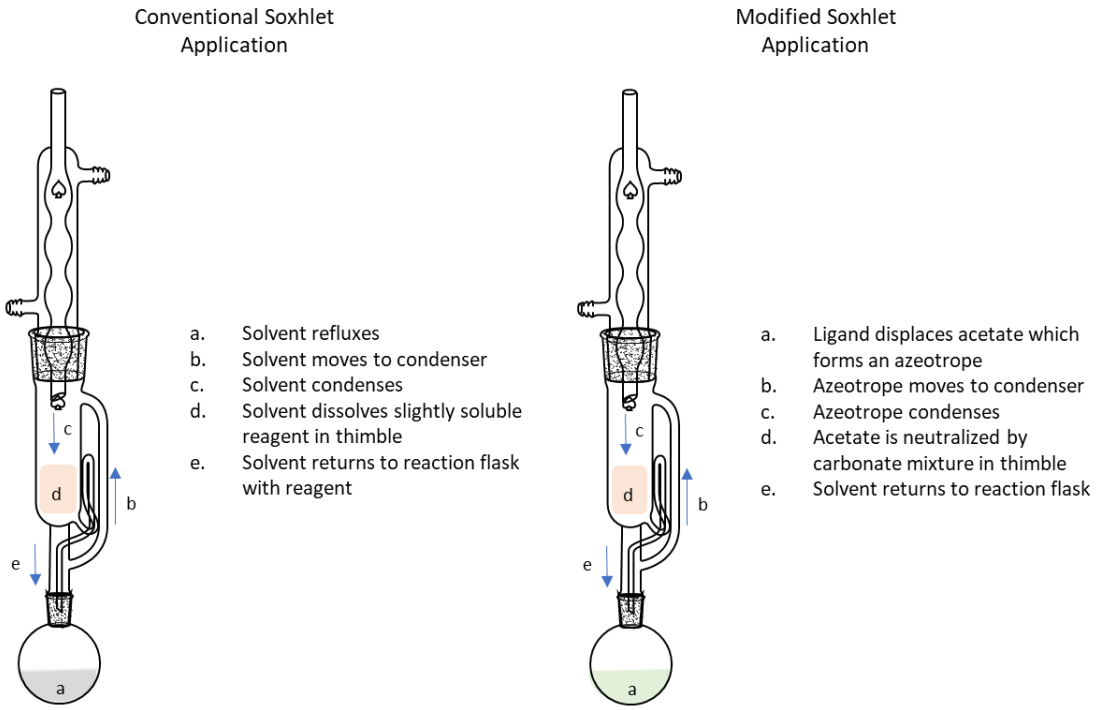

Figure 2.2 Application of a Soxhlet apparatus via the conventional method (left) and modified method (right) for ligand exchange of Rh^{II} complexes

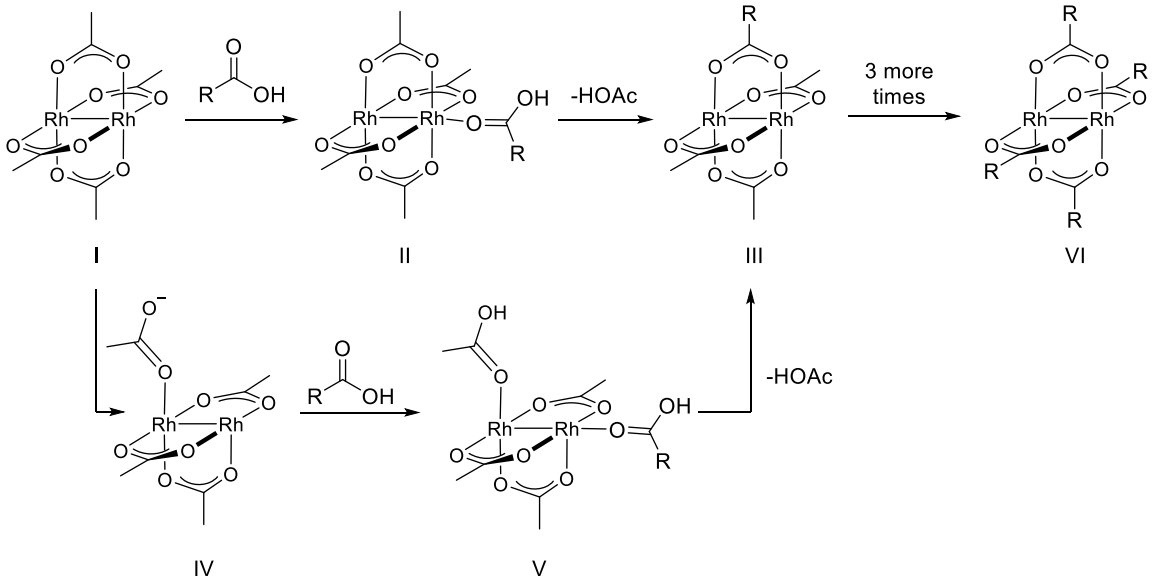

Figure 2.3 Proposed mechanism for ligand exchange of $Rh_2(OAc)_4$ involving axial coordination

complexes. These complexes provide further insight into possible intermediates during ligand exchange. This includes Rh^{II} complexes where an acetate group, or another ligand, is bound both axially and equatorially (Figure 2.4, a).[174] During the synthesis of orthometallated phosphines, it was possible to track the transition from an axial-equatorial bound ligand to an equatorial-equatorial bridging ligand. Furthermore, Rh^{II} complexes have been observed where the new bridging ligand binds to two equatorial sites but does not bridge both Rh metal centers (Figure 2.4, b).[175] In most instances, these binding modes are observed when strongly coordinating bridging ligands are employed.

Regardless of the ligand exchange pathway, it has been demonstrated that carboxamidate ligands exchange in sequential order. Each of the *mono*, *bis*, *tris*, and *tetra*-substituted complexes were identified and tracked via HPLC.[176] The displacement of acetates becomes harder as more substitutions occur. Despite these accepted steps, it remains ambiguous whether an associative or dissociative mechanism governs the reaction.

2.1.3 Isomers of Rh^{II} Complexes

Substitution of the bridging ligand will generate a mixture of substitution products regardless of equivalent or inequivalent donating atoms, such as carboxylates and carboxamidates respectively. A more complex mixture is generated when the donating atoms are inequivalent, due to the presence of different isomers. This is well illustrated by considering carboxamidate bridging ligands with both oxygen and nitrogen as donating atoms (Figure 2.5, a). These isomers are classified by the number of each nitrogen and oxygen atom surrounding a single Rh atom. Each of these isomers have been synthesized, and it was determined the thermodynamically favored isomer was the *cis*-(2,2) isomer.[170, 171]

The formation of *bis*-substituted complexes gives rise to an even more complex mixture of isomers.[170, 171] This can again be illustrated with carboxamidate ligands. If both nitrogen atoms are bound to the same Rh atom, the isomer is said to be in the *anti*-configuration. Conversely, it is labeled *syn* when both N atoms are bound to the same Rh (Figure 2.5, b). Additional isomers arise in the case of the *cis*-*anti* configuration due to rotational isomerism. Consider a *mono*-substituted Rh^{II} complex with the carboxamidate pointed down (Figure 2.5, c). Another ligand can then be added, either on the left or the

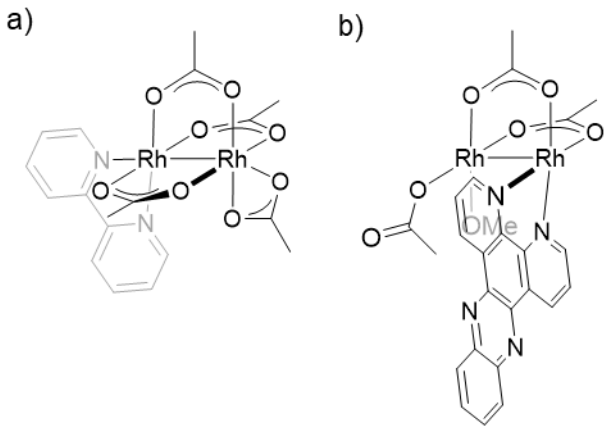

Figure 2.4 Rh^{II} complexes exhibiting a) axial/equatorial and b) non-bridging equatorial binding modes

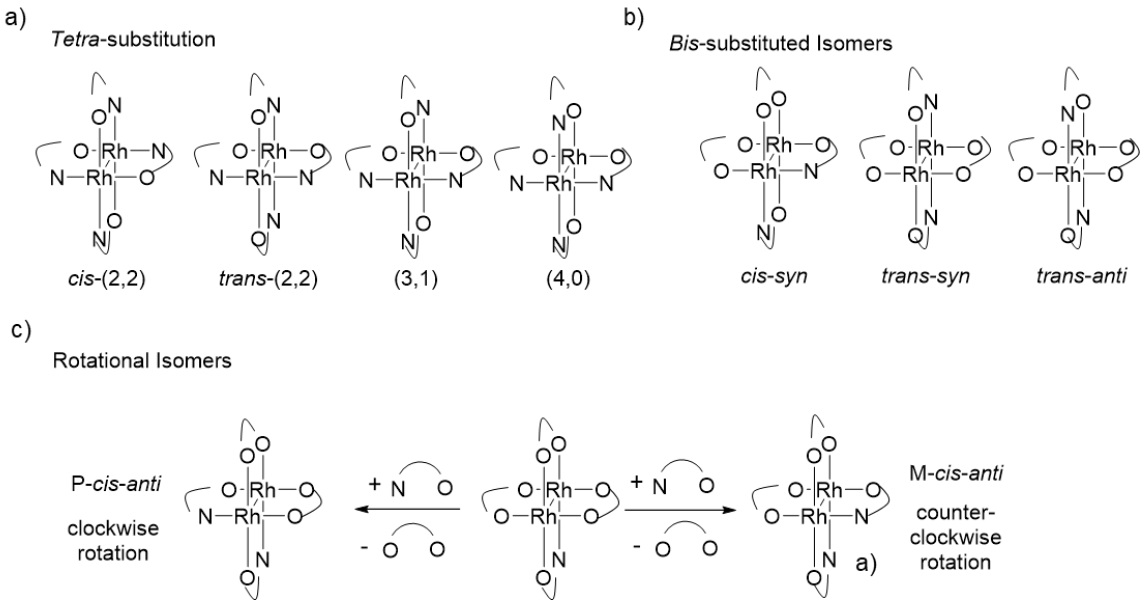

Figure 2.5 Possible isomers from substitution with non-equivalent donor atoms.

right side. These two isomers can be differentiated by imagining the rotation of the ligand going downward, so that it aligns with the second ligand. Rotation in the clockwise direction indicates the P-*cis*-*anti* isomer while counterclockwise rotation indicates the M-*cis*-*anti* isomer.

2.1.4 Synthesis of Heteroleptic Rh^{II} Complexes

Heteroleptic complexes have been synthesized but are not as prevalent as homoleptic catalysts. One technique for synthesizing heteroleptic complexes involves the synthesis of a mixture of complexes with the formula $Rh_2(OAc)_n(TFA)_{4-n}$, starting from $Rh_2(OAc)_4$. These heteroleptic complexes then became the starting material for another ligand exchange reaction. The electron withdrawing TFA ligand is preferentially displaced over the acetate ligands, which enables a degree of control over the number of ligand substitutions (Figure 2.6, a). This method was employed by Lou and co-workers to synthesize many of the isomers discussed previously using a urea-based bridging ligand.[170] This process affords higher reported yields of the desired catalyst but still relies on the formation and separation of a statistical mixture. It also adds steps to the synthesis.

Heteroleptic complexes where one bridging ligand is not an acetate ligand have also been realized. This method involves the synthesis of a homoleptic complex to introduce the first desired ligand (Figure 2.6, b). This homoleptic complex becomes the starting material in another ligand exchange reaction with the second ligand of interest. This method was investigated by the Fox group to generate a heteroleptic catalyst.[109] A moderate yield of the *mono*-substituted product was obtained but required long reaction times. Unlike ligand displacement with $Rh_2(OAc)_4$, the PTTL ligand does not azeotrope with the solvent and is not removed from the reaction mixture. It is plausible that this aided in the formation of the heteroleptic product, because the equilibrium is not being shifted forward by removal of the original ligand.

Yet another method of synthesizing heteroleptic complexes is the addition of multiple ligands to a solution of $Rh_2(OAc)_4$ (Figure 2.6, c). Controlling the substitution of the final product is difficult. The only influence over the substitution comes from dictating the relative concentration of each of the ligands. Even when ligand concentration is controlled, the product mixture is more heavily influenced by the ease of which each ligand

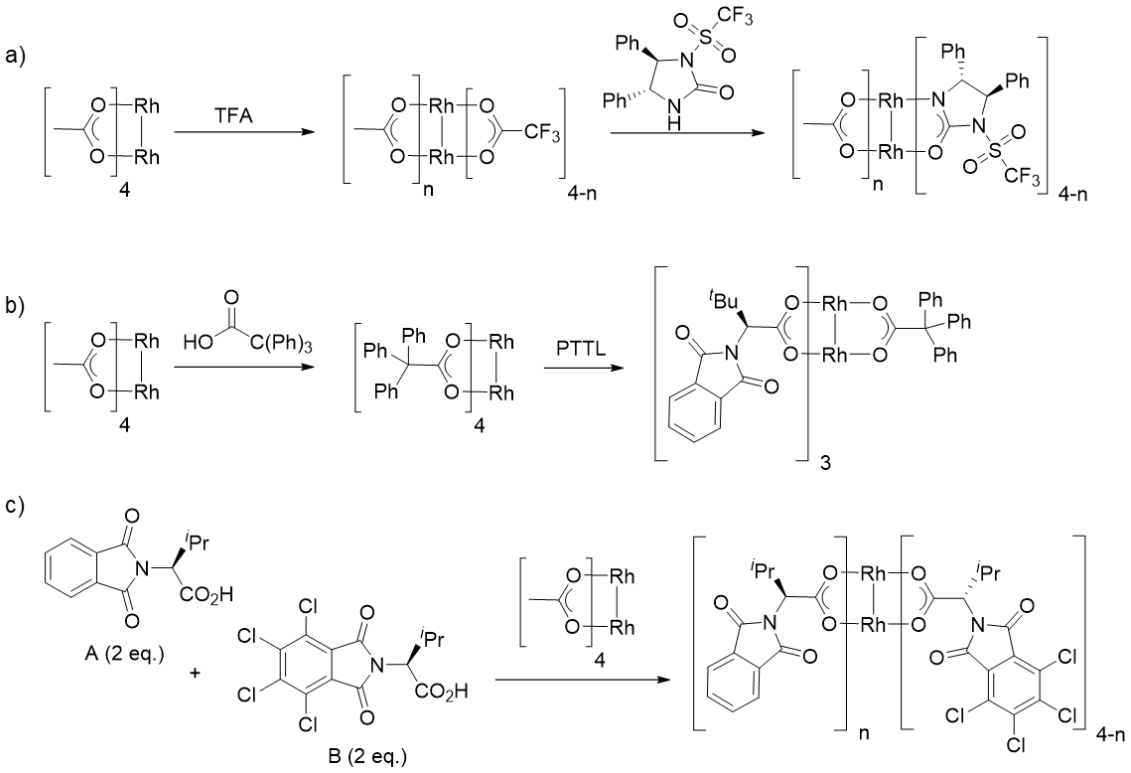

Figure 2.6 Different methods used to synthesize heteroleptic Rh^{II} complexes

displaces the acetates of $Rh_2(OAc)_4$. This methodology was employed by Charette and co-workers for the synthesis of heteroleptic Rh^{II} complexes of the type $Rh_2(A)_2(B)_2$.[177] Two equivalents (based on $Rh_2(OAc)_4$) of both ligand A and B were added to refluxing $Rh_2(OAc)_4$ in PhCl, and resulted in a mixture of products. This method proved effective because the polarity difference between each complex was sufficient to allow for the separation of the complex mixture of products. The same methodology was also shown to work with other known N-protected amino acid ligands.

2.3 Catalyst Design

Investigation of the axial site as a means of catalyst control required a catalyst where axial coordination would not require the addition of exogenous LB. To this end, we believed tethering the LB to a bridging ligand would be the most effective method. Both Bera and Ball had previously synthesized heteroleptic Rh^{II} complexes with tethered groups that coordinated to the axial site.[178, 179] The bridging donor atoms do not dissociate readily and, therefore, keep the LB proximal to the axial site, even if the LB dissociates. This chelate effect will increase the local concentration of the LB at the axial site without the need for high concentrations of exogenous LBs. Taking inspiration from these complexes we began designing ligands that could eventually be incorporated onto already established, successful, chiral Rh^{II} catalysts. When synthesizing the novel complexes, *mono*-substitution was desired (Figure 2.7, left). The formation of the *mono*-substituted product would result in the formation of a single isomer, rather than a complex mixture. Additionally, a *mono*-substituted product would only result a single axial site being blocked. This would leave the remaining axial site open for catalysis.

The primary concern when considering which bridging ligand to employ was the promotion of axial coordination. It was believed that this could be achieved by a rigid back bone, which would anchor the LB near the axial site. The incorporation of a ring system was believed to be an effective method of incorporating a rigid ligand. A variety of cyclic carboxamidates have been incorporated as bridging ligands, unlike cyclic carboxylates. As such, carboxamidates were predicted to be the most suitable for incorporating cyclic bridging ligands (Figure 2.7, right).

Two of the most prominent cyclic carboxamidate ligands were based on pyrrole

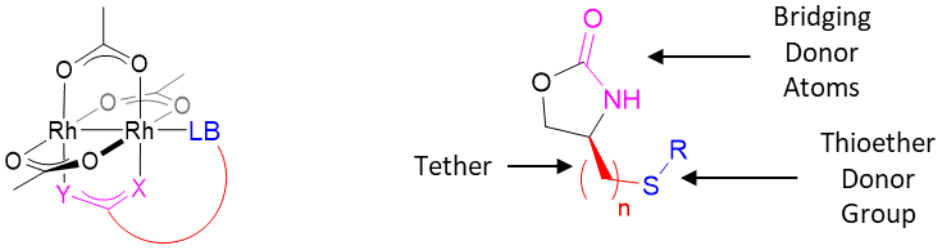

Figure 2.7 General catalyst design (left) and target oxazolidinone ligands (right) with the bridging donor atoms (pink), tether (red), and LB donor (blue).

and oxazolidinone ligands. The electron donation from the nitrogen of these ligands resulted in less electrophilic Rh^{II} complexes. As a result, the Rh^{II} complex may decompose diazo reagents so slowly that reaction times are too long to be practical. This would be compounded by additional electron donation from the axially coordinated Lewis base. Oxazolidinates were predicted to mitigate this issue regarding the electrophilicity of the Rh^{II} complex. The oxazolidinone moiety is less basic than the similar pyrrolidinone, due to the inductively withdrawing oxygen, and is expected to increase the electrophilicity of the Rh^{II} complex.

Consideration was then given to the identity of the LB donor group. Nitrogen-based ligands, such as amines and nitrogen heterocycles, came to mind as good candidates and have been examined as solvent as well as additives. However, these often resulted in decreased reaction rates due to their strong binding to the axial site, but also resulted in increased stereoselectivity.[180] Phosphines are another common Lewis base for modulating a metal center and were investigated as exogenous ligands but were shown to decrease the reaction rate.[181] Conversely, weaker LB donors such as esters were incorporated as additives and resulted in enantioselectivity being increased without a drop in yield.[182] Based on these observation, weaker donors were considered. Thioethers were identified as good candidates and had already demonstrated the ability to coordinate readily to Rh^{II} complexes.[183, 184] The stereoelectronic effects of thioethers have been studied and observed to follow similar electronic trends as phosphines. However, they appear to be more heavily influenced by steric hindrance.[185-187] Incorporation of aryl thioethers provides a means of investigating electronic tunability of the thioether donor while alkyl thioethers will probe steric effects.

In addition to the ligand back bone, the question of the tether length was also considered. A tether length of two methylene units was predicted to be most stable, as it would form a six-member ring upon axial coordination of the thioether. Alternatively, a one methylene unit linker would afford a five-membered ring, which would also be predicted to be stable. The combination of these two features was anticipated to ensure proximity of the thioether to the axial site and thereby ensure axial coordination.

2.4 Ligand Synthesis

The first ligand synthesized was the oxazolidinone **107**. This was accomplished

from the readily available amino acid L-methionine, via a previously established procedure (Scheme 2.1).[188] The synthetic pathway was predicted to leave the chiral center undisturbed, which would limit the number of Rh^{II} complex isomers after ligand exchange. Esterification of L-methionine **104** was followed by carbamate formation to afford compound **105**. Reduction of **105** generated alcohol **106** which was then cyclized to afford the desired ligand **107**. By starting from **104**, the thioether functionality was already present in addition to having established a tether of two methylene units.

Seeking to examine a range of thioether derivatives, an alternative synthetic route was explored. The route was based on an established procedure and developed to afford a series of ligands derived from aspartic acid **108** (Scheme 2.2).[189] Again, esterification and carbamate formation yielded compound **109**, which was then reduced to diol **110**. Cyclization of **110** generated the oxazolidinone **111**. Compound **111** was then tosylated to provide compound **112**. Nucleophilic substitution of **112** provided access to a variety of thioethers **113**-**116**, depending on the thiol selected. This alternate route afforded ligands with the same two methylene unit tether, as seen in molecule **107**. It also provided the common intermediate **112** for generating different thioether derivatives.

A single crystal of **112**, suitable for SC-XRD, was grown from slow evaporation of DCM (Figure 2.8). The asymmetric unit comprised three molecules of compound **112** with the hydrogens of the amides participating in H-bonding. It appeared that the chiral center remained unchanged; however, this was not confirmed for the bulk sample.

The thioetherfication step was initially accomplished through an established procedure that required 10 equivalents of the thiol. As more expensive thiols were required for examining electronic influence on the Rh^{II} complexes, it was desirable to reduce the amount of thiol required. During thioetherfication reactions, a white precipitate was generated and was presumed to be *p*-toluenesulfonic acid from the displaced tosyl group (Table 2.1). This indicated that the reaction was being driven forward by Le Chatlier's principle through both the high concentration of thiol and precipitation of one of the products. It was believed the precipitation of the tosylate would be a sufficient driving force for the reaction and eliminate the need for excess thiol reagent. This hypothesis was tested by reacting 1.5 equivalents of the thiol with compound **112** and resulted in a 74% yield, which was comparable to the 78% yield obtained with 10 equivalents (Table 2.1, entries 1-2). This was expanded to another thiol derivative and an increase in yield was

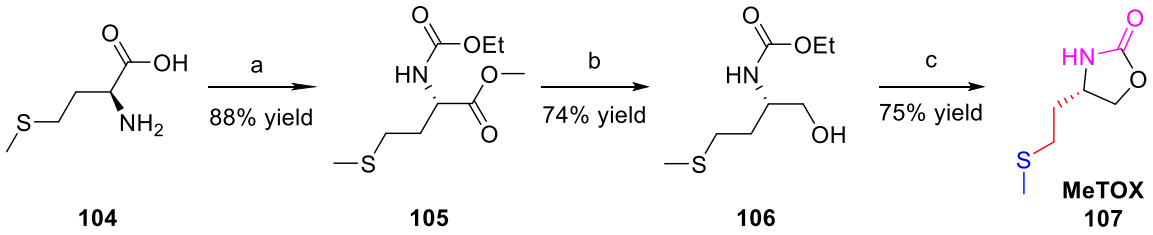

104 **105** **106** **107**

a) i. CH_3COCl, MeOH, reflux ii. $ClCO_2Et$, $NaHCO_3$, H_2O, rt b) $NaBH_4$, $CaCl_2$, THF/EtOH, rt
c) K_2CO_3, toluene, reflux

Scheme 2.1 Synthetic pathway for the synthesis of the MeTOX ligand highlighting the carbons comprising the tether (red), thioether donor (blue), and donating atoms (pink).

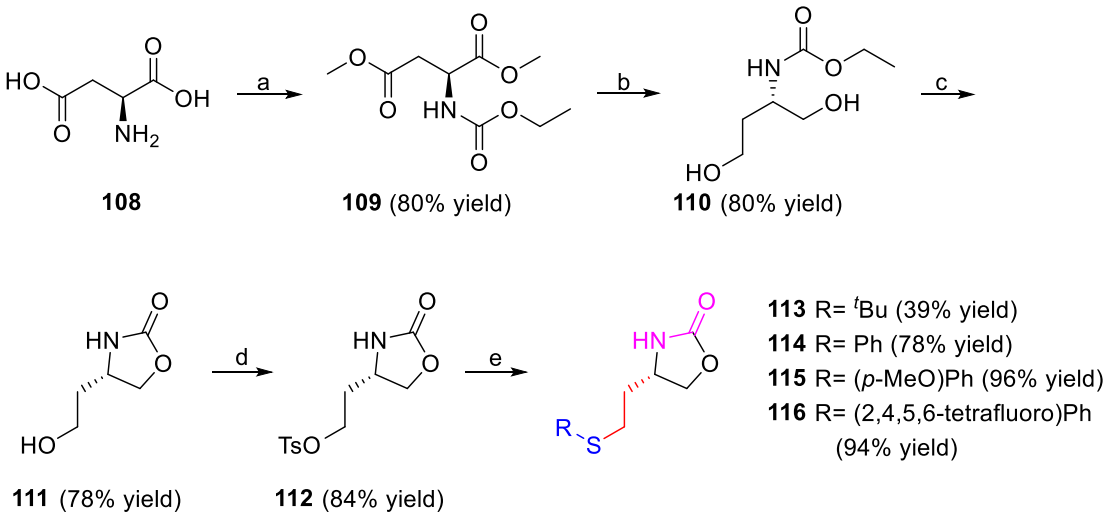

108 **109** (80% yield) **110** (80% yield)

111 (78% yield) **112** (84% yield)

a) i. CH_3COCl, MeOH, reflux ii. $ClCO_2Et$, H_2O, rt b) $NaBH_4$, MeOH, rt c) NaH, THF, reflux d) TsCl, TEA, rt e) RSH, K_2CO_3, acetone, reflux

Scheme 2.2 Synthetic pathway for the synthesis of oxazolidinone ligands from L-aspartic acid highlighting the carbons comprising the tether (red), thioether donor (blue), and donating atoms (pink).

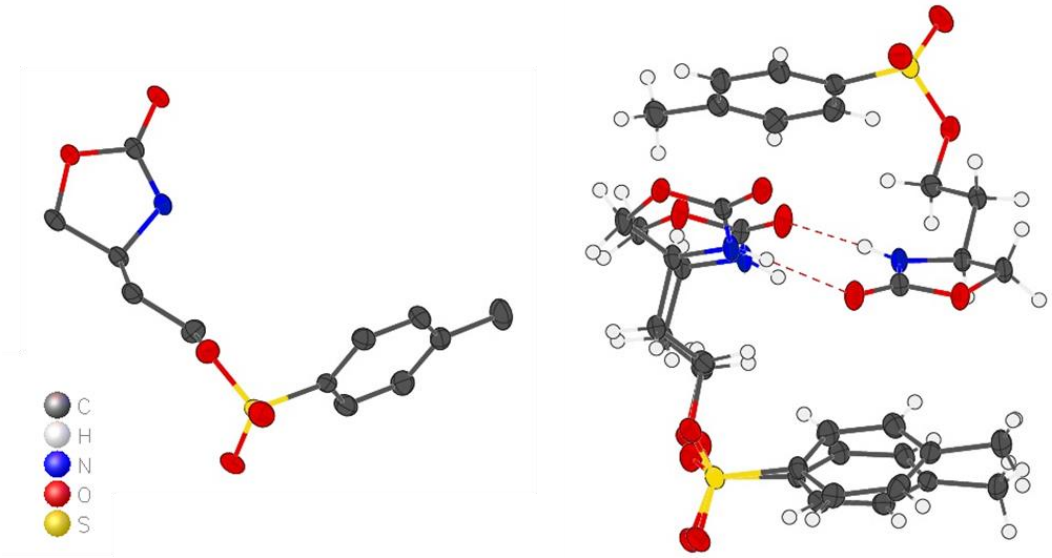

Figure 2.8 Crystal structure compound **112** (left) with protons omitted for clarity and the asymmetric unit (right) showing H-Bonding (dashed red lines). Thermal ellipsoids are shown at the 50% probability level.

Table 2.1 Near stoichiometric thioetherfication

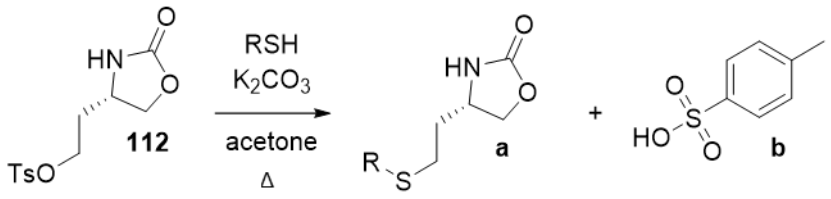

Entry	R	Equivalents RSH	Yield **a** %
1	Ph	10	78
2	Ph	1.5	74
3	(*p*-MeO)Ph	10	72
4	(*p*-MeO)Ph	1.5	96

observed (Table 2.1, entries 3-4). Based on the success of the two test reactions, this modification was then applied to the following thioetherfication reactions, resulting in moderate to high yields (Scheme 2.2).

A similar synthetic sequence was utilized to afford an oxazolidinone ligand with a tether length of one methylene unit (Scheme 2.3).[190] Following the established procedures, compound **117** was generated. The tosylate then underwent nucleophilic substitution to afford the desired thioethers **118** and **119**.

2.5 Oxazolidinate Complex Synthesis

2.5.1 Soxhlet Method

As it is the most common method, the oxazolidinone ligand **107** was implemented in ligand exchange with $Rh_2(OAc)_4$ utilizing the Soxhlet extractor (Scheme 2.4), following methods employed for the synthesis of other carboxamidate Rh^{II} complexes.[76] With the high temperatures required to promote equatorial exchange it was expected that *bis*, *tris*, and *tetra*-substituted products would also be observed. For this reason, only one equivalent of oxazolidinone ligand was added to the reaction mixture. After addition of the oxazolidinone ligand, the initially green solution turned purple, indicating axial coordination of the ligand. This was a good indication of the ligand binding to the axial site through the sulfur.[191] As the reaction was heated, the solution reverted to green before changing to deep purple over time. This suggested that heating facilitated dissociation of the ligand from the axial site before ligand exchange is observed. The reaction was monitored by HPLC. No increase in the formation of the *mono*-substituted product **120a** was observed after 4 hours. Longer reaction times led to increased formation of *bis*-substituted products **120b/c**. Isolation of the products afforded **120a** and **120b/c** in 45% and 13% yield respectively, in addition to unreacted $Rh_2(OAc)_4$. Interestingly, the *tris* and *tetra*-substituted products were not observed even after a reaction time of 18 hours. It was hypothesized that once the *bis*-substituted product was produced there was no longer an open axial site for another oxazolidinone ligand to bind, preventing further equatorial ligand exchange.

Qualitative support for *bis*-substitution comes from the observation that the color of **120b/c** does not change upon dissolving in a coordinating solvent such as acetonitrile

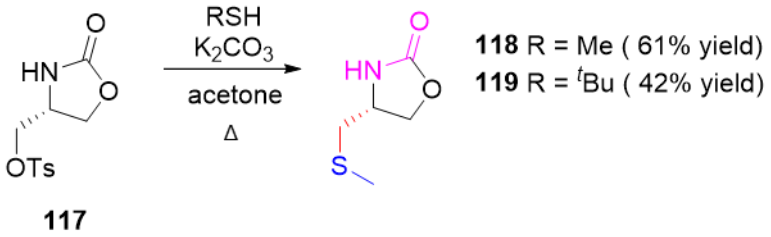

117

Scheme 2.3 Synthesis of ligands with a tether length of one methylene unit

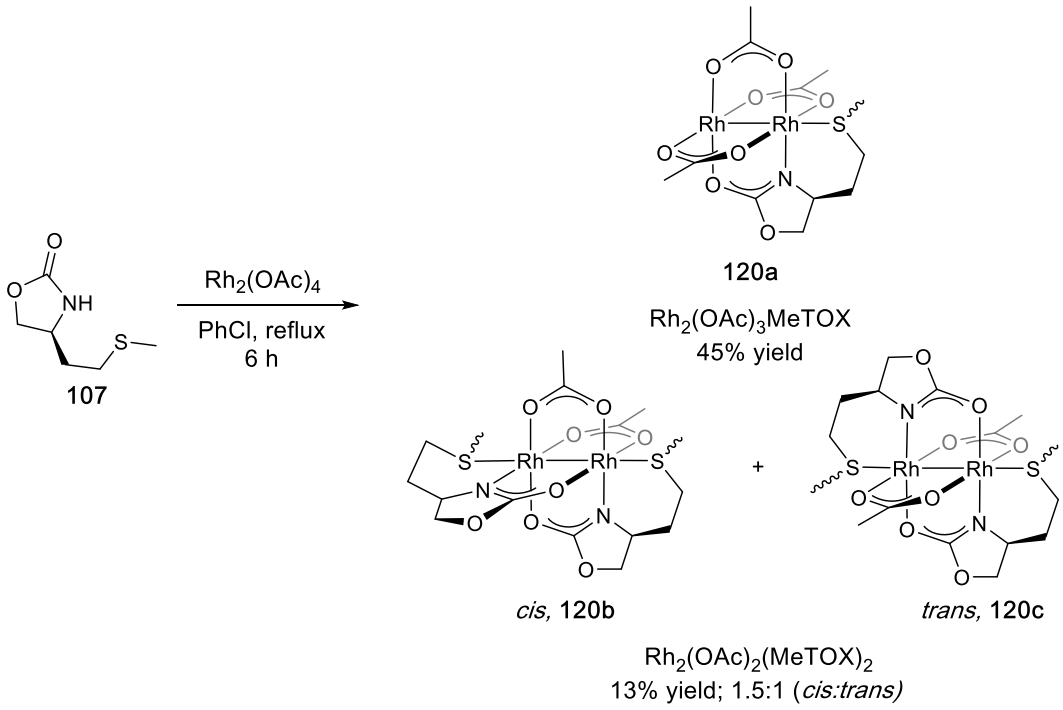

Scheme 2.4 Synthetic scheme for heteroleptic Rh^{II} complexes from compound **107**

(MeCN). Separation of **120b** and **120c** was possible via column chromatography with the most nonpolar, top spot, complex being isolated. The *bis*-substituted products could be distinguished by two groups of signals in the ^{1}H NMR. The most prominent difference is the presence of a multiplet at 3.07 ppm of the more nonpolar isomer. This same signal appears to separate into two signals (2.98 and 3.22 ppm) for the more polar isomer and was used for the calculation of the *cis*:*trans* ratio.

Comparison of the ^{13}C NMR of the more nonpolar isomer and a mixture the two isomers, where the more polar isomer predominated, allowed for assignment of the *cis* and *trans* isomers. The carbonyl carbon of the acetate groups was identified (189.73 ppm) as a single signal, which was expected for both the *cis* and *trans* isomer. A shift of this signal was predicted to occur based on the *trans* influence. When an oxazolidinate ligand is located *trans* to the acetate, then the lability of the acetate is increased due to increased electron density from the nitrogen of the oxazolidinate. An increase in electron density would then result in shielding of the carbonyl carbon of the acetate and an upfield shift of the signal. When an acetate is *trans* to the original acetate the *trans* effect is no longer present, due to the ligands being equivalent. This would result in a more deshielded acetate carbonyl carbon, causing the signal to shift downfield. The examination of the ^{13}C NMR of the isolated top spot showed a downfield shift of the carbonyl carbon of the acetate. This downfield shift is consistent with the two acetates being *trans* to one another, identifying it as the *trans* isomer. Qualitative analysis using TLC further supported this assignment. It appeared that the bottom spot was present in higher concentration than the top spot. It has been established that the *cis* product is the thermodynamically favored species and would be expected to predominate under the high temperatures applied in the reaction.[171]

Initial attempts to synthesize the *mono*-substituted product using ligands **113** and **114** were conducted using a Soxhlet apparatus. This method afforded the desired *mono*-substituted and *bis*-substituted products, in addition to several other colored compounds less polar than the *bis* complexes, based on TLC analysis. The additional colored compounds were believed to be the *tris* and *tetra*-substituted complexes, and their isomers. The formation of *tris* and *tetra*-substituted complexes suggested that ligands **113** and **114** do not coordinate as strongly as the methyl thioether of **120a.** Weaker coordination could enable axial coordination by another ligand molecule, which could lead to further substitution.

Two possible pathways seem probable. First is the displacement of the thioether by another ligand molecule (Figure 2.9, **a**). Alternatively, an equilibrium may be present between the coordinated and uncoordinated species (Figure 2.9, **b**). This process results in an axial site open for coordination by another ligand molecule (Figure 2.9, **c**). Either of these pathways can result in another ligand molecule being axially coordinated. Due to the interest in the *mono*-substituted complex and low yields of the byproducts, complete isolation of the suspected *tris* and *tetra*-substituted complexes was not pursued. It was clear that the Soxhlet method was beneficial for driving the reaction to the thermodynamically favored product, which limits the amount of *mono*-substituted product obtained.

2.5.2 Microwave Method

Due to the complex product mixtures generated when conducting ligand exchanges with **113** and **114**, an alternative method was sought. Microwave reactors had been applied in the synthesis of Rh^{II} complexes, but not extensively. They facilitated ligand exchange reactions to generate a Rh^{II} complex for total synthesis.[192] Additionally, a microwave method was developed for the synthesis of $Rh_2(OAc)_4$ from $RhCl_3 \cdot 3H_2O$.[193] A more prevalent product often observed when using microwave reactors was *bis*-adducts with the formula $Rh_2(OAc)_4 \cdot 2L$. Here, L is solvent or another LB bound to the axial site.[194] Many different adducts of this nature have been realized. Oligomeric chains of these adducts are possible, especially when more than one LB functionality was incorporated into the ligand.

A major advantage of microwave reactors is their ability to heat the reaction evenly and very rapidly. Additionally, many solvents can be heated above their boiling points without loss of solvent in a pressurized tube. Conventional heating relies on contact between the heat source and the surface of the reaction vessel. The solvent contacting the glass is heated before being mixed with the bulk solution. This leads to a temperature gradient where the solvent at the glass surface is hotter than the middle of the flask.[195] In contrast, heating via microwave relies on the dual nature of electromagnetic radiation. The particle nature of the photon (γ) repels electron rich moieties of solvent molecules which results in rotation of the solvent molecule. Because radiation is also a wave, the solvent is constantly rotating as the photon moves closer or further away (Figure 2.10).[196]

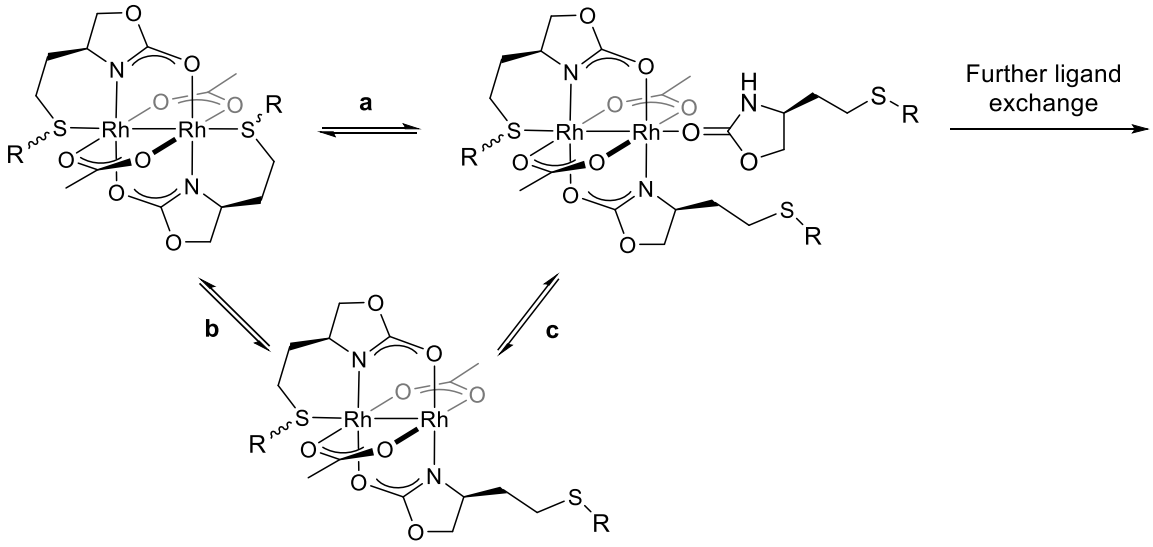

Figure 2.9 Possible equilibria dictating further ligand exchange

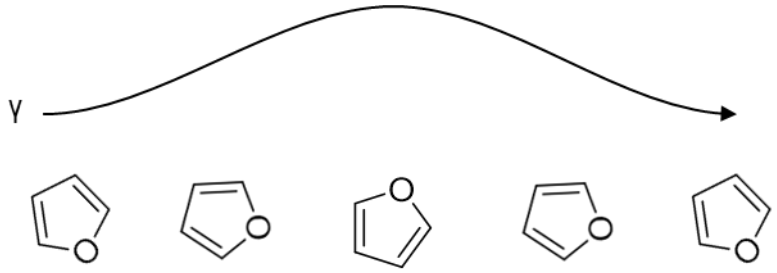

Figure 2.10 Rocking motion of solvent molecules due to microwave radiation

This continual motion generates heat due to the friction between solvent molecules. The microwave radiation can penetrate the solution and results in more uniform heating. Different solvents transform the microwave radiation into thermal energy more effectively than others, with polar solvents often being more efficient.

The rapid uniform heating and lack of hot spots made microwave reactors a promising method for the ligand exchange reaction. We developed a method for synthesizing heteroleptic Rh^{II} complexes using microwave radiation, with the synthesis of **120a** as a model complex. This process was expedited by analyzing each of the reactions by HPLC. A procedure developed by our group enabled the separation of each component for quantification. All microwave experiments were conducted using a Biotage Initiator^{+} microwave. Further experimental parameters are located in chapter 4. This would mark, to the best of our knowledge, the first application of microwave reactors towards the synthesis of heteroleptic Rh^{II} complexes.

Although non-coordinating solvents have been known to give the highest yields of Rh^{II} complexes, there are examples where coordinating solvents were preferred.[170] As such, solvent screening reactions were conducted to determine a suitable solvent for the microwave conditions. Solvent screening reactions were conducted at 180 °C due to pressure limitations of the microwave reactor and the variable pressure buildup of each solvent. As observed with the Soxhlet, noncoordinating solvents performed the best (Table 2.2, entry 1 and 2). Each of the coordinating solvents afforded lower yields of the *mono*-substituted product (Table 2.2, entries 3-6). Ethanol gave the highest percent conversion (Table 2.2, entry 4) but did not result in the desired Rh^{II} complexes. It is believed that ethanol facilitated the reduction of the Rh(II) to Rh(0) metal, as a metallic grey solid was observed on the reaction vessel.[197]

One microwave methodology involves using a biphasic mixture as a means of preventing further reactivity of the product by removing it into a different phase. This technique was investigated by pairing water and chloroform in a 1:1 ratio. It was observed that solid Rh(0) was again deposited on the reaction vial. Interestingly, this was only observed for the area occupied by the water layer. Due to the degradation of the paddlewheel structure, the biphasic conditions were not investigated further. Dichloroethane (DCE) and PhCl afforded similar amounts of *mono*-substituted product, but DCE was deemed a more suitable solvent as it facilitated a more expedient workup.

Temperature screening began at 80 °C. The temperature was then increased by

Table 2.2 Solvent screening for microwave synthesis of heteroleptic oxazolidinate Rh^{II} complex

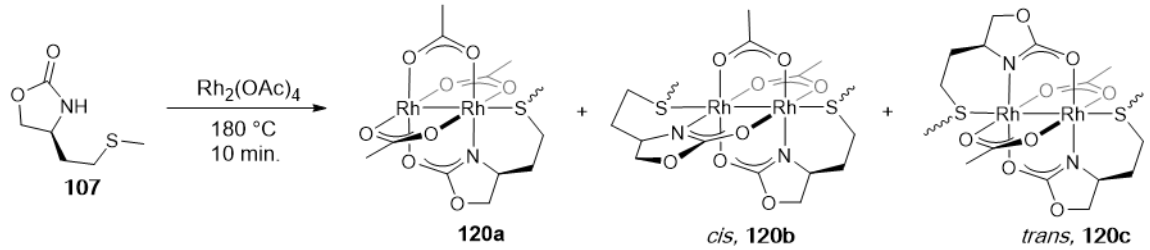

Entry	Solvent	Yield a[a] (%)	Yield b/c[a] (%)	Conversion (%)
1	PhCl	21	5	27
2	**DCE**	**22**	**7**	**46**
3	THF	4	2	9
4	EtOH	14	7	79
5	MeCN	18	5	29
6	H_20	5	4	52

[a]Yield determined by HPLC

20 °C increments, with no product formation observed until trace amounts of the *mono*-substituted product at 140 °C were observed (Table 2.3, entries 1 and 2). Upon increasing the temperature to 160 °C products **120b** and **120c** were observed in conjunction with **120a** (Table 2.3, entry 3). The reaction was then conducted for an extended time at this lower temperature (160 °C), due to the favorable ratio of **120a** to **120b/c**. Extending the reaction time led to a decrease in the ratio between **120a** and **120b/c** (Table 2.3, entries 3-5). Further increasing the temperature facilitated higher yields of each **120a** and **120b/c** before reaching an apparent cap at 200 °C. It was determined that the optimal conditions were 190 °C for ten minutes in DCE.

The optimized conditions found for **120a** were then applied to the other oxazolidinone ligands for the synthesis of the desired *mono*-substitution product. In conjunction with the synthesis of the desired product, this method allows for a comparison of the thioether tether's influence on the ligand exchange process. Ligands **113** and **114** underwent exchange, with **114** yielding more of the desired *mono*-substituted product (Figure 2.11). Not only was more *mono*-substituted product generated, but the ratio of *mono*:*bis* complexes was greater for alkyl thioethers. Again, this is believed to arise from the donating strength of the thioether groups. The stronger alkyl donors do not dissociate as readily, or become displaced, which prevents axial coordination for further substitution. Additionally, stronger donating groups will have a more prominent *trans* effect, which could inhibit axial coordination at the open axial site. Shortening the tether to one methylene linker generated higher yields than complexes with two methylene linkers (Figure 2.11). This microwave method was also applied by Will Sheffield to synthesize the *mono*-substituted oxazolidinate Rh^{II} complex **126a**, but 10 equivalents of ligand were required.[198] This suggests that the incorporation of the tethered LB promotes carboxamidate ligand exchange.

2.6 Characterization

2.6.1 Crystal Structure

Of the novel Rh^{II} complexes synthesized, single crystals of x-ray quality were obtained for complexes **120a** and **125a**. No crystal structures of *bis*-substituted complexes were isolated. It was believed that the presence of the many isomers of the

Table 2.3 Temperature and time screening of heteroleptic oxazolidinate Rh^{II} complex

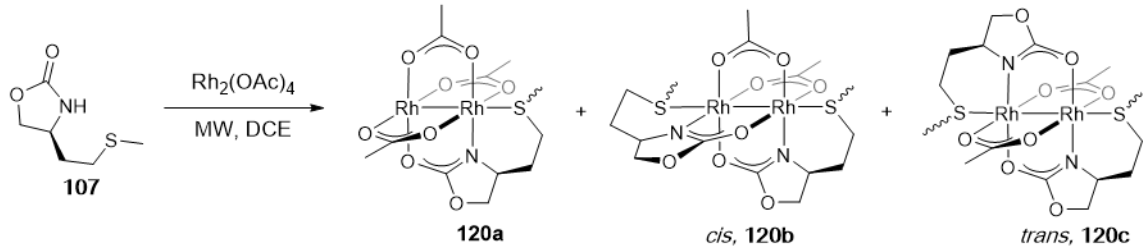

Entry	Hold Time(min)	Temp. (°C)	Yield a[a] (%)	Yield b/c[a] (%)	Conversion (%)
1	10	80	0	0	0
2	10	140	1	0	3
3	10	160	6	1	7
4	20	160	13	3	18
5	30	160	17	5	23
6	10	180	22	7	46
7	**10**	**190**	**33**	**16**	**52**
8	10	200	33	17	53

[a]Yield determined by HPLC

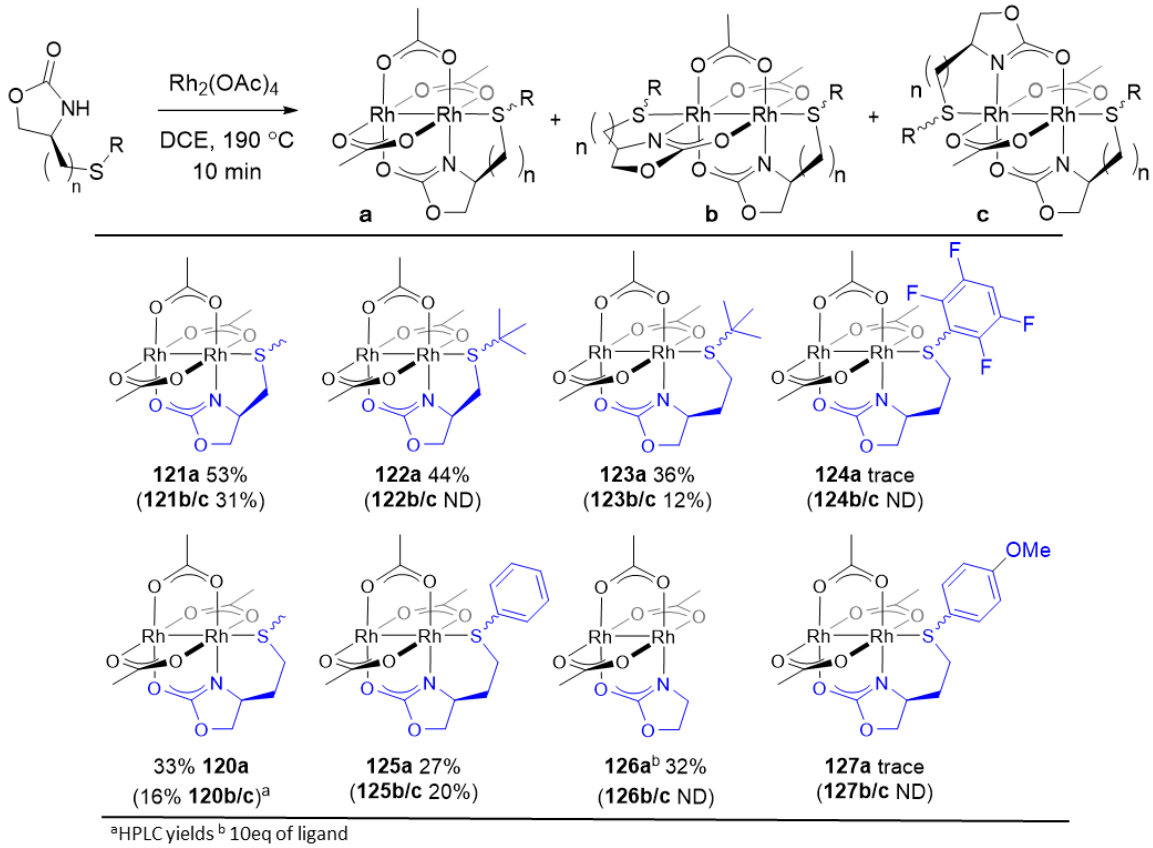

Figure 2.11 Microwave assisted synthesis of heteroleptic Rh^{II} oxazolidinate complexes with various thioether donor groups.

bis-substituted complexes makes formation of single crystals difficult. The crystal structure of **120a** was solved by Dr. Glenn Yap. In the solid-state, complex **120a** formed a series of oligomeric structures wherein the tethered sulfur was bound to two paddlewheel units (Figure 2.12, a). Formation of oligomeric species of paddlewheel complexes has been observed previously with LBs occupying the axial site.[199-201] It can be seen that two diastereomers of the Rh^{II} complex are present due to the formation of a new chiral center when sulfur binds to Rh. These can be defined as the (S_C,R_S) isomer and (S_C,S_S) isomer where the letters indicate the chiral center orientation and the subscript refers to the atom of the chiral center (Figure 2.12, b and c). These two diastereomers are responsible for the apparent shifting of the methyl group from one side of the oligomer to the other. The Rh1–S–Rh2 bond is asymmetrical with the intramolecular Rh2–S (2.484 Å) distance being shorter compared to the intermolecular distance (2.556 Å). The intramolecular Rh–S distance is believed to be shorter due to the chelate effect ensuring proximity of sulfur to the axial site. The shorter intramolecular distance is similar to the distances observed with less sterically demanding thioethers (2.41-2.45 Å) [84] The intermolecular distance is more reminiscent of bulkier thioethers (~2.5 Å). This indicates that axial coordination is present in the solid phase. The Rh–Rh bond distance of complex **120a** (2.427 Å) is longer than the homoleptic parent ligand $Rh_2(OAc)_4$ (2.38 Å).[202] A homoleptic oxazolidinate complex, Rh_2(*S*-MEOX)$_4$, has a Rh–Rh distance of 2.47 Å.[85] It is possible elongation is a result of both axial coordination and the heteroleptic nature of complex **120a**. Upon looking down the Rh–Rh bond it can be observed that the Rh–Rh–S bond angle is near-linear (178°).

Rather than forming an oligomer, complex **125a** crystallized with an asymmetric unit containing four distinct paddlewheels. Each paddlewheel unit has MeCN bound at the second axial site (Figure 2.13, a). Like **120a**, the asymmetric unit contains two different isomers that have crystallized together. The chiral center on the oxazolidinone ligand maintains the *S* configuration while the chiral center that is generated by the sulfur binding to the axial site changes from *R* to *S* (Figure 2.13, b and c). Each paddlewheel unit has a Rh–Rh bond of 2.42 Å, which is the same as observed for **120a**. This suggests that the oxazolidinate ligand is responsible for the increased Rh–Rh bond length, compared to $Rh_2(OAc)_4$, rather than electron donation at the axial site. Upon inspection of the Rh–S bond, each paddlewheel unit has a different length ranging from 2.47-2.52 Å while the Rh–N distance for each paddlewheel unit was unvaried (2.23 Å). The difference in the

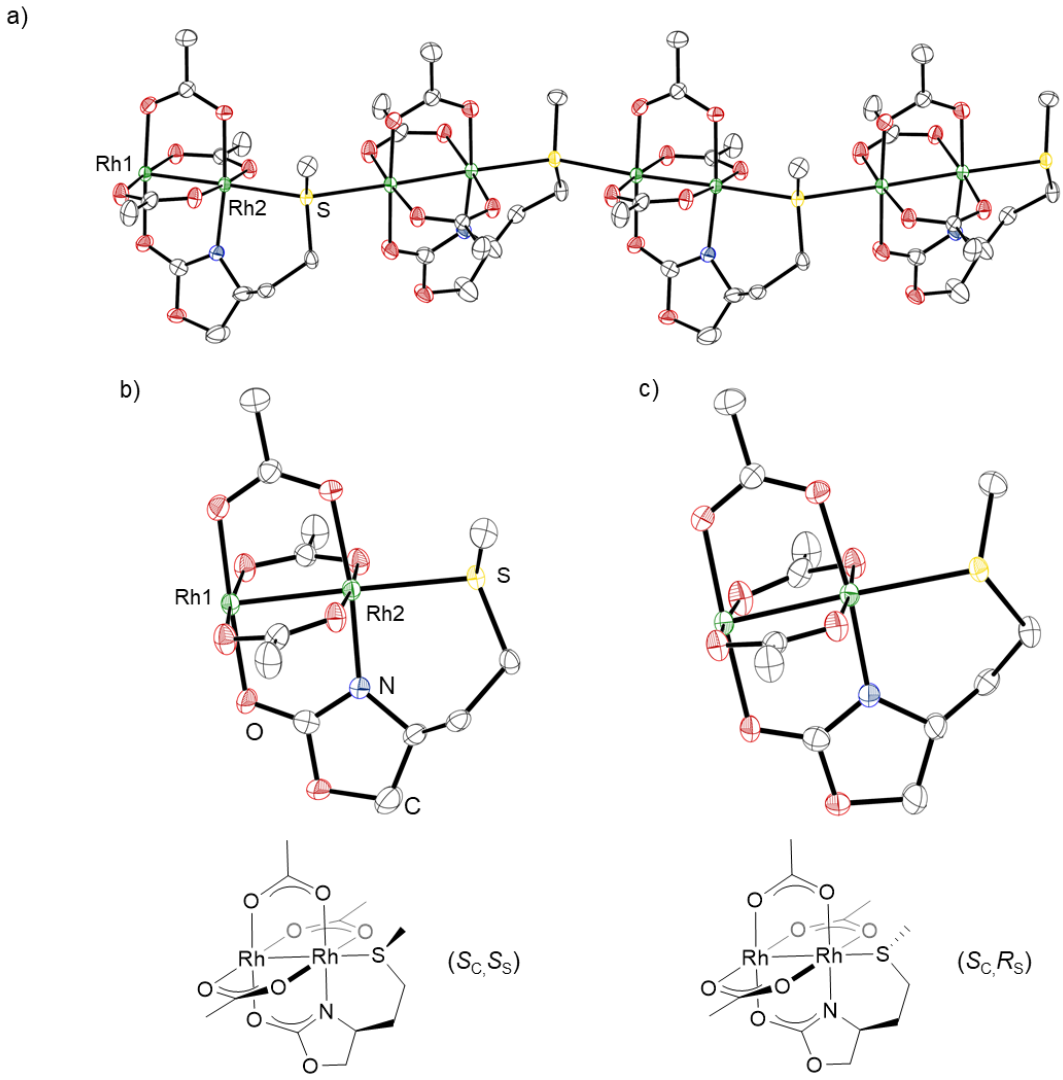

Figure 2.12 The crystal structure of **120a** showing a) the oligomeric chain and b) the (S_C,R_S) diastereomer and c) the (S_C,S_S) diastereomer. Thermal ellipsoids are shown at the 50% probability. H atoms removed for clarity

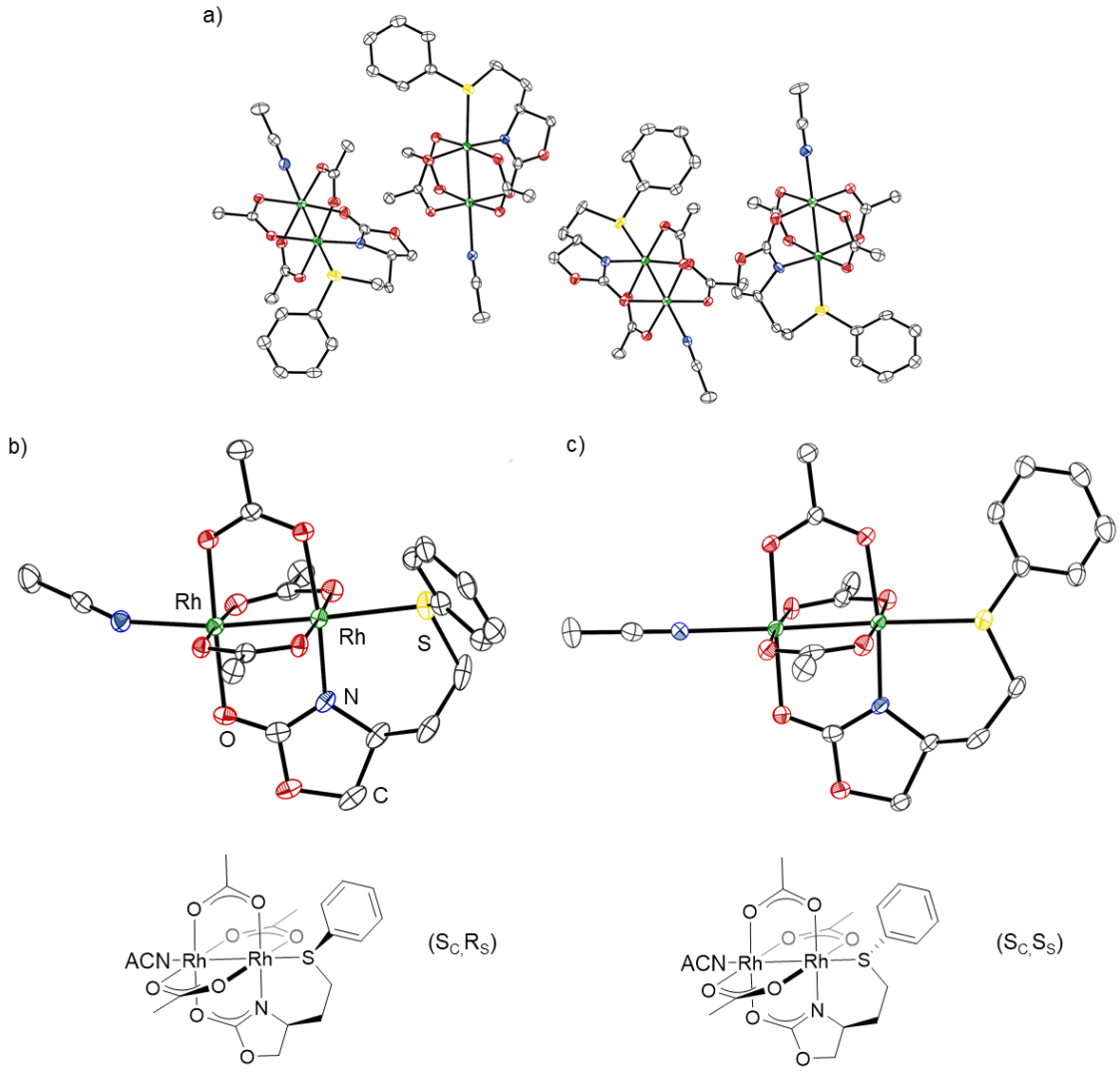

Figure 2.13 The crystal structure of **125a** showing a) the asymmetric unit comprised of individual paddlewheel units b) the (S_C,R_S) isomer and c) the (S_C,S_S) isomer with thermal ellipsoids at the 50% probability level. H atoms removed for clarity

Rh–S bond length between each paddlewheel unit could be a result of the *trans* effect due to the coordinated MeCN. These differences in bond lengths indicate that the thioether may be in a fluxional state. Both complex **120a** and **125a** indicate the two-methylene linker leads to complex with low angle strain, indicated by Rh–Rh–S angles of 178° and 175° for **120a** and **125a**, respectively.

A single crystal was obtained of ligand **114** coordinated to the axial sites of two different molecules of $Rh_2(OAc)_4$ without displacement of the bridging ligands (Figure 2.14, **128**). This structure is similar to solvent adducts where axial coordination is present without displacement of the bridging ligands.[84, 200] The ligand was coordinated to one paddlewheel unit via the carbonyl of the oxazolidinone while coordinating to the second paddlewheel unit via the thioether (Figure 2.14, a and b). This coordination leads to the formation of a sigmoidal oligomeric structure (Figure 2.14, c). A similar linear coordination pattern has been observed with sulfoxides wherein both the sulfur and oxygen act as axial coordinators.[203] Looking down a cross-section of the crystal structure a channel filled with solvent is observed (Figure 2.14, d), similar to metal-organic frameworks.[201, 204] Despite the similarity, it appears that the channel is a result of packing and would collapse if the solvent were removed. The Rh–Rh bond distance (2.39 Å) is similar to that observed in $Rh_2(OAc)_4$ (2.38 Å), further indicating that the axial coordination does not result in a large elongation of the Rh–Rh bond. The Rh–S distance (2.49 Å) is between that observed for complexes **120a** and **125a**. Seeing that both the thioether and carbonyl coordinate to the axial site gives precedent to both binding modes occurring during ligand exchange.

Complex **122a** was isolated as a single crystal, but the structure was unable to be completely solved (Figure 2.15, a). Nevertheless, the model obtained still provides insight into the structure of complexes with serine derived ligands (**121a** and **122a**). The oligomeric structure, as observed in complex **120a**, is again observed with complex 1**22a** (Figure 2.15, a). This may indicate that the absence of the oligomeric structure in complex 1**25a** arises from the donating strength of the thioether rather than the steric bulk of the aryl ring. The Rh–Rh distance (2.42 Å) is the same observed for **120a** and **125a**, which further suggests that the oxazolidinate bridging ligand is primarily responsible for the elongation compared to $Rh_2(OAc)_4$ (2.38 Å). The Rh–S distance appears to be asymmetric with the intramolecular Rh–S distance (2.53 Å) shorter than the intermolecular distance (2.57 Å). The Rh–Rh–S (174°) bond angle deviates more from linearity than that observed in **120a** and **125a**. These distances and angles should not be taken as

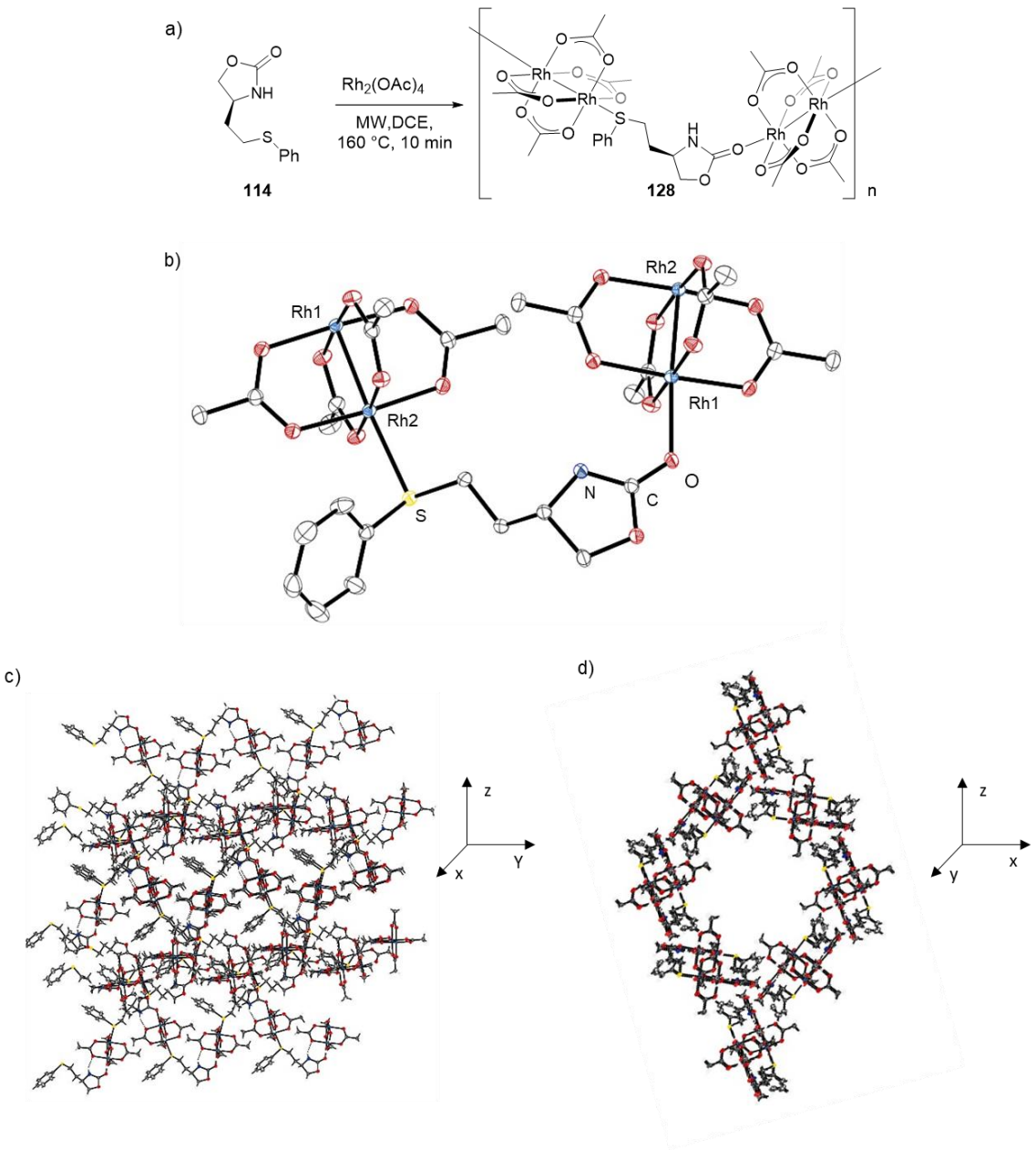

Figure 2.14 Crystal structure of complex **128** showing axial ligand coordination without equatorial displacement b) a cross section of the channel and c) the sigmoidal oligomer forming channels

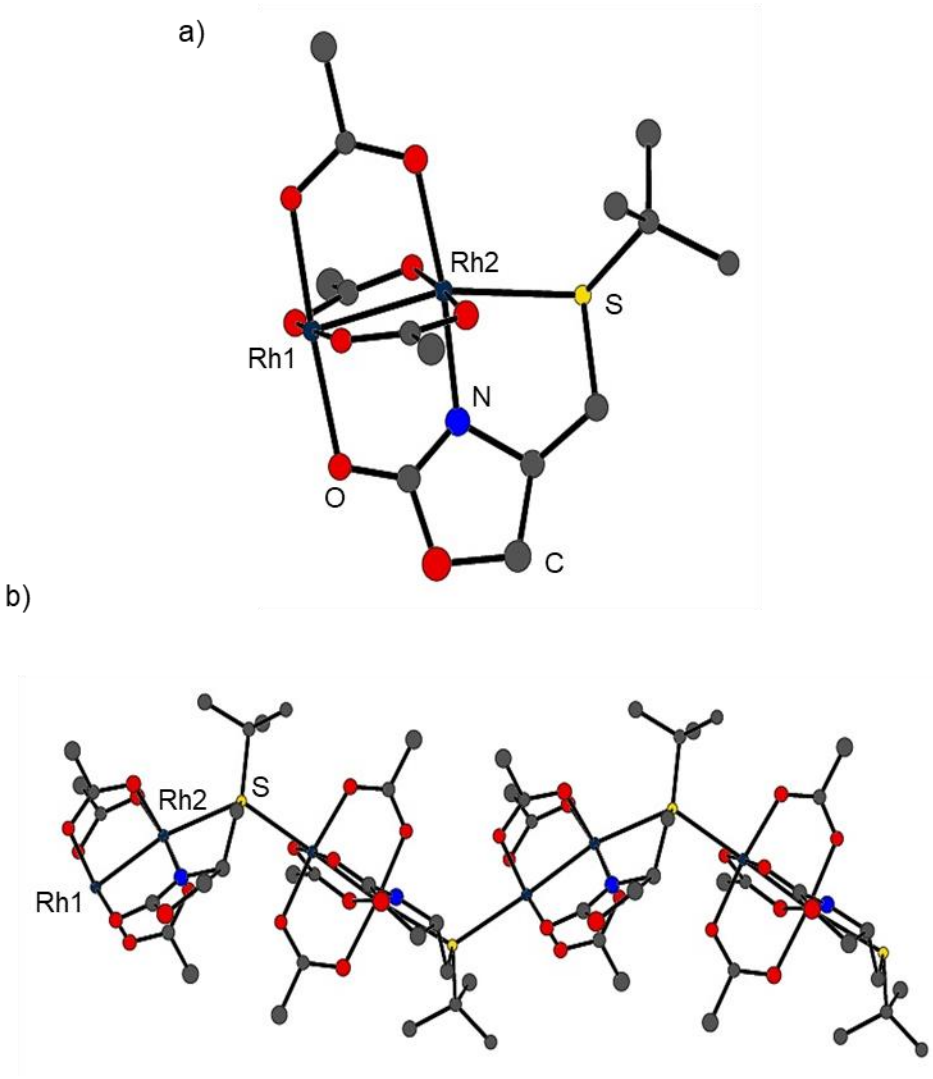

Figure 2.15 The not completely solved crystal structure of **122a** showing a) the asymmetric unit and b) the oligomer structure with thermal ellipsoids at the 50% probability. H atoms removed for clarity

definitive values as the model does not meet current standards. However, it provides insight into the structure of complexes derived from serine (complexes **121a** and **122a**).

Several key observations come from the analysis of these crystal structures. First and foremost is the presence of two diastereomers for each *mono*-substituted species. The differentiating chiral center is formed when the sulfur of the thioether binds to the axial site and appears racemic based on the crystal structure. The length of the Rh–Rh bond appears consistent across each carboxamidate. This suggests that elongation of the Rh–Rh bond is more dependent on the carboxamidate bridging ligand, rather than axial coordination. This would suggest that these complexes will have a reactivity more akin to carboxamidates than carboxylates. Finally, the two-carbon tether appears to allow for stronger coordination of the S to the axial site. This is evidenced by the near-linear Rh–Rh–S bond angle of complexes **120a** and **125a**, compared to the larger deviation from linearity in complex **122a**.

2.6.2 Solution State

Analysis of the novel Rh^{II} complexes by ^{1}H NMR provided insights into the complex's behavior in solution (See Appendix A). Perhaps the most striking feature is the change in the signal corresponding to the different coordinated thioether donors as compared to the free ligand. In the case of **120a**, a distinct downfield shift of the methyl protons (2.55 ppm) is observed when compared to the free ligand **107** (2.11 ppm). A similar change is observed for the ^{t}Bu group of complex **123a** and the methyl group of **121a**. Complex **125a** resulted in the splitting of the aryl protons of the thioether donor, which is contrasted by the unresolved multiplet observed in the spectrum of the free ligand **114**. Each of these observations indicates axial coordination is present when the complex is in solution.

Another prominent feature is the presence of three singlets in the range from 1.7-2.0 ppm, which have been assigned as the methyl groups of the acetate ligands. One of these signals is shifted further downfield while the other two signals are grouped further upfield. This splitting pattern is observed for each of the *mono*-substituted complexes derived from aspartic acid and methionine. It is hypothesized that the differences arise from inequivalent environments generated in part by the chiral center of the tether. A similar pattern is observed in each of the ^{13}C NMR spectra where three distinct signals are

observed for each carbonyl carbon and methyl carbon of the acetate groups. These unique environments are observed to a lesser extent in the ^{1}H NMR of complexes derived from serine (**121a** and **122a**) where the two upfield acetate singlets are closer in chemical shift.

Both the x-ray structures and the ^{1}H NMR data suggest that axial coordination is present. However, the possibility remains that the thioether may be in a fluxional state, as indicated in the x-ray structure. This has been observed in other complexes with multidentate ligands and has been given the term hemilabile.[205] This can be demonstrated using the novel Rh^{II} complexes as an example (Figure 2.16). The novel ligand is bound in a κ^3 fashion, with three atoms binding to the Rh core. However, it is known that the axially bound ligands are more kinetically labile than the bridging ligands. This means that an equilibrium may exist between κ^3 coordination and κ^2 coordination. It was believed that κ^2 coordination could be favored by heating the complex and observed by seeing the thioether signal shift upfield, as in the free oxazolidinone ligand. Observation of this shift in the signal would indicate that the thioether is coordinated at room temperature.

A series of variable temperature ^{1}H NMR (VT ^{1}H NMR) experiments were conducted. Initially, complexes **123a** (Figure 2.17) and **125a** (See Appendix A, **S26**) were examined as they were predicted to not bind as strongly as **120a**. It was expected that the ^{t}Bu signal of **123a** would shift upfield like the free ligand. Reaction temperatures of 80 °C were not reached due to solubility and solvent limitations. The singlet of the ^{t}Bu group did not shift significantly upon heating from room temperature to 70 °C. Instead, a separate peak shifted from 1.70 ppm to 1.54 ppm. This peak, and its shifting upon heating, was also observed when examining 1**25a**. It was hypothesized that this could be water inside the NMR solvent, as water has a chemical shift of 1.56 ppm in deuterated chloroform.[206] This was verified by preparing a sample of **123a** in a glove box under strictly anhydrous conditions. This ensured no water was present, resulting in the disappearance of the signal (See Appendix A, **S27**). Though this was an impurity, it demonstrated that axially coordinated solvents could be displaced by heating and that the axial tether remained proximal to the axial site up to 70 °C. The same observation was made for complexes **120a** and **125a** suggesting the thioether does not completely dissociate.

A similar experiment was conducted with a sample of **120c** as it was expected that the thioether would be easier to displace due to the *trans* effect (Figure 2.18). A sample of **120c** was prepared in deuterated benzene, enabling reaction temperatures, 80 °C, to

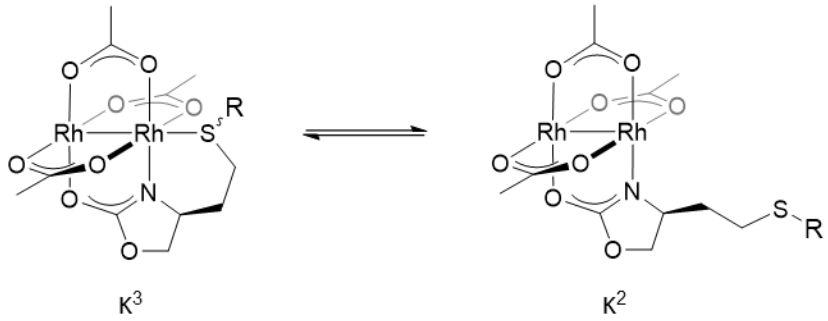

Figure 2.16 Possible equilibrium between the κ^3 and κ^2 binding modes

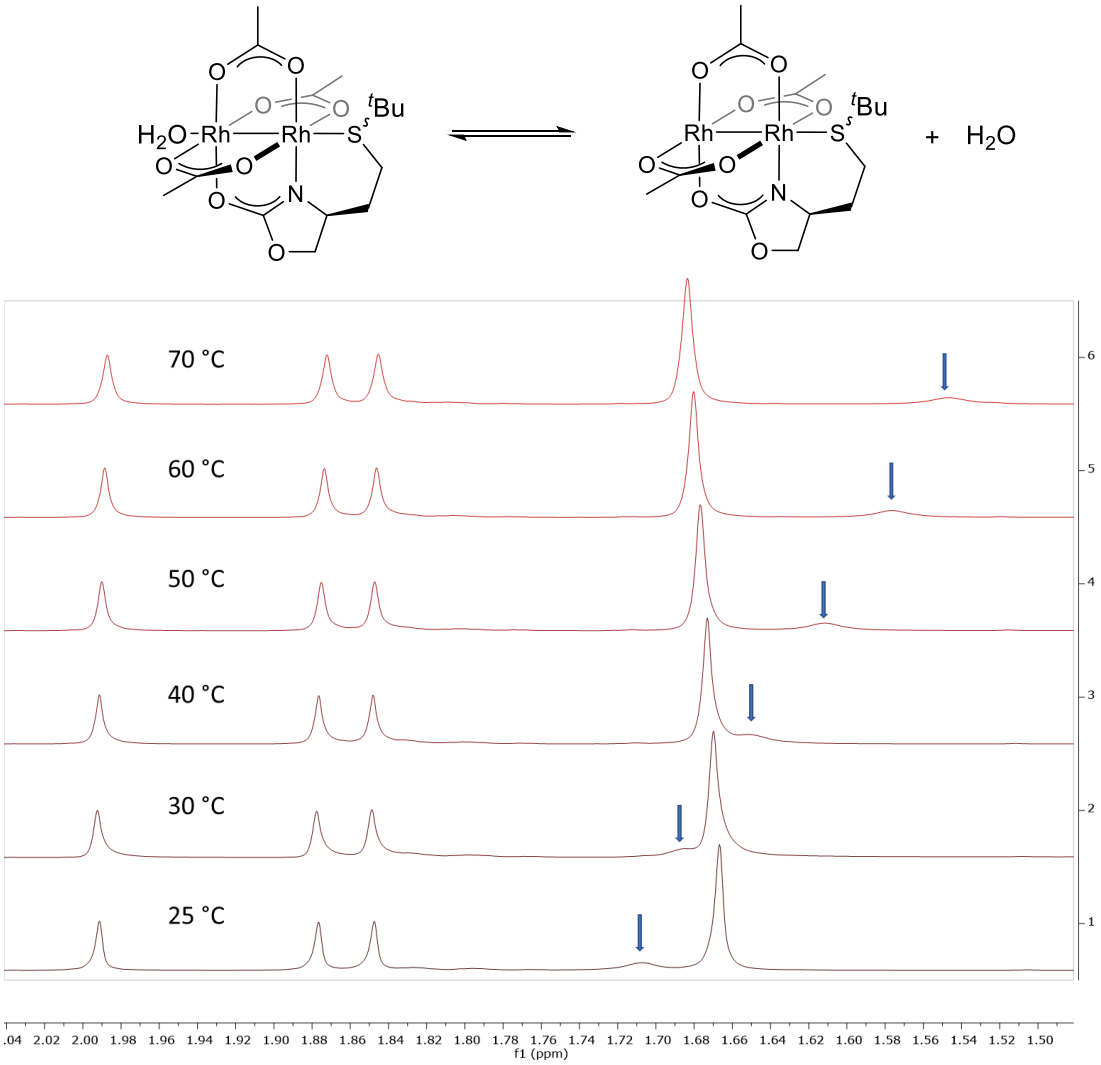

Figure 2.17 VT ^{1}H NMR spectrum of compound **123a** showing no change in thioether group signals with blue arrow indicating shifting water signal

be reached. Again, no change was observed in either the signal of the methyl thioether or the acetate peaks, indicating no hemilability at these temperatures. It is plausible the equilibrium between κ^2 and κ^3 coordination was not observed because higher temperatures are needed to favor κ^2 coordination. It is of note that no degradation is observed upon heating and cooling the complexes, indicating good catalyst stability at reaction temperatures.

Even though the thioether methyl signal of complex **120c** did not change, a shift was observed in the signal that corresponded to the methylene protons of the tether adjacent to the sulfur atom (Figure 2.18, blue arrow). When solving the crystal structure of **120a**, it was found the tether was disordered between two conformations (Figure 2.19). It reasons that the same six-membered ring would be present in the *bis*-substituted complex **120c**. The conformation where the lone pair of the sulfur and the methylene proton are *anti* (Figure 2.19, a) is expected to be more stable and predominate at room temperature. Here, the lone pair of the sulfur can donate into the C–H antibonding orbital and this anomeric effect results in the shielding of the proton.[207] The application of heat enables the eclipsed conformation to be present in higher quantity (Figure 2.19, b). In this conformation the proton signal then shifts downfield because the lone pair is no longer able to donate into the C–H antibonding orbital. This change in conformation could explain the downfield shift of the methylene protons on the tether.

2.7 Electronic and Electrochemical Analysis

The donating ability of each of the thioether donors was investigated in hopes that it could be correlated to reactivity. Axial coordination has traditionally been studied by UV-Vis analysis and was investigated first. It is established that the HOMO-LUMO gap is between the π* and σ* of the Rh–Rh metal bond. The σ* orbital comprises of the antibonding d_{z^2} orbitals between the Rh metals.[81] Axially coordinated molecules, such as solvent, bind to this orbital resulting in an increase in the HOMO-LUMO gap due to destabilization of the LUMO (Figure 2.20). Increased electron density from axial coordination at both axial sites results in a blue shift of the HOMO-LUMO gap as compared to the coordination of a single axial site. These shifts can be monitored by UV-Vis and coordination of both axial ligands can be observed.[208] It was expected that the donation strength of the different thioether donor groups could be observed. Stronger donors were

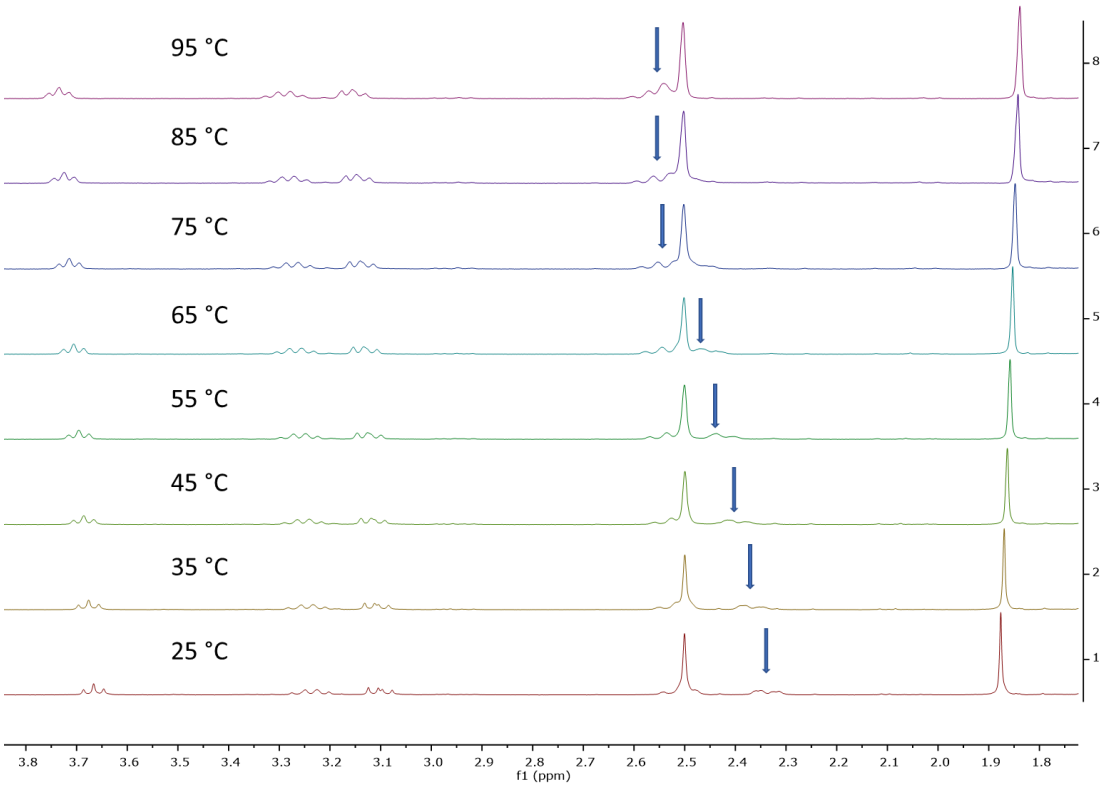

Figure 2.18 VT ^{1}H NMR spectra of compound **120c** with indicating change in tether conformation

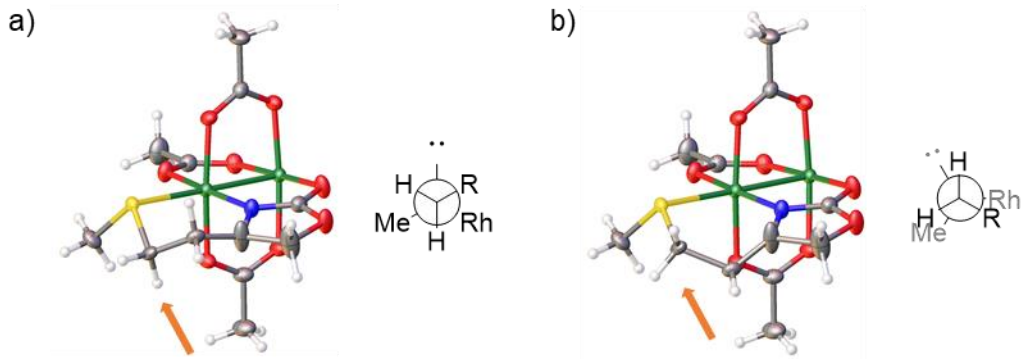

Figure 2.19 Possible conformation of the tether and Newman projection going down the C–S bond

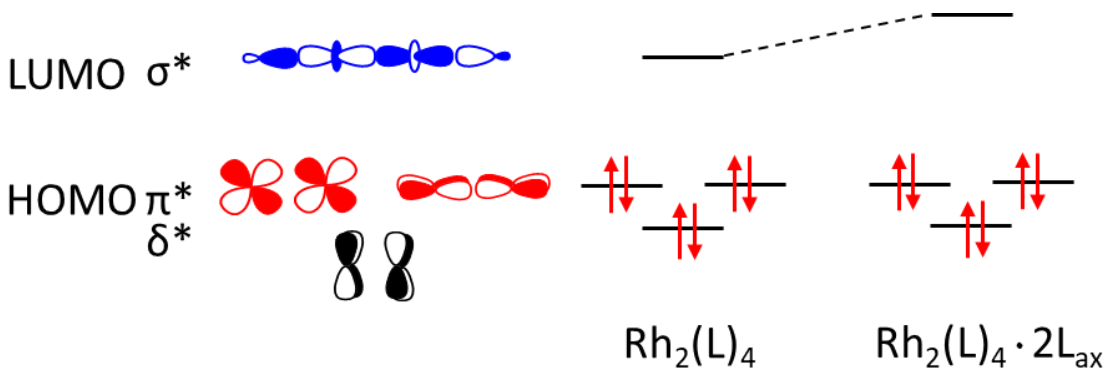

Figure 2.20 Frontier molecular orbitals of Rh^{II} complexes and effect of axial coordination

expected to donate more electron density and thereby cause greater destabilization of the LUMO. This would result in the observation of a larger HOMO-LUMO gap.

For purposes of solubility, dirhodium tetrakispivalate ($Rh_2(OPiv)_4$) was used in place of $Rh_2(OAc)_4$ to represent any changes from the parent carboxylate complex. The control complex **126a**, with a single oxazolidinate ligand and no tether, resulted in a slight blue shift compared to $Rh_2(OPiv)_4$ (637 nm vs 650 nm, respectively). The introduction of the bridging ligand with a tether increased the HOMO-LUMO gap, resulting in another blue shift (Figure 2.21). Upon varying the σ donating strength no significant difference was observed, with the λ_{max} of the π* to σ* transition falling within 10 nm for each complex. This suggested that the donating ability of each thioether was more similar than anticipated. However, the addition of the second ligand resulted in another easily observed blue shift compared to the *mono*-substituted complexes.

As minimal differences were observed by UV-Vis, another method was sought to examine the donating ability of the different thioether donors. Cyclic voltammetry (CV) has been employed as an alternative method for determining the electrophilicity of a Rh^{II} complex.[209] Each complex examined demonstrated a reversible or quasi-reversible oxidation event that was assigned as the $Rh_2^{4+/5+}$ oxidation couple. It is also possible that the thioether could be oxidized, but literature indicates that thioether oxidation occurs at higher potentials.[210] Furthermore, the intermediate generated by electrochemical oxidation of thioethers are known to be very reactive, resulting in irreversible oxidation events.[211] Experiments conducted in DCM exhibited a trend where stronger σ donors resulted in higher oxidation potentials when compared to the control complex **126a** (Figure 2.22). This trend was unexpected as increased electron density on the Rh metals typically results in decreased oxidation potentials, but is not without precedent.[212] In our group, Dr. Brad Anderson synthesized a similar *mono*-substituted Rh^{II} carboxylate complex with an axially coordinated thioether. The oxidation potential of this complex was higher than the oxidation potential of a *mono*-substituted Rh^{II} control catalyst without axial coordination.[213] In the case of formamidate ligands it was calculated that tethered axial coordination resulted in a destabilization of the HOMO.[214] Destabilization of the HOMO by the axially coordinated thioether would increase the oxidation potential. Stronger thioether donorswould destabilize the HOMO more than weaker donors, giving rise to the highest oxidation potentials. It is seen by the redox potentials that the Rh core is being

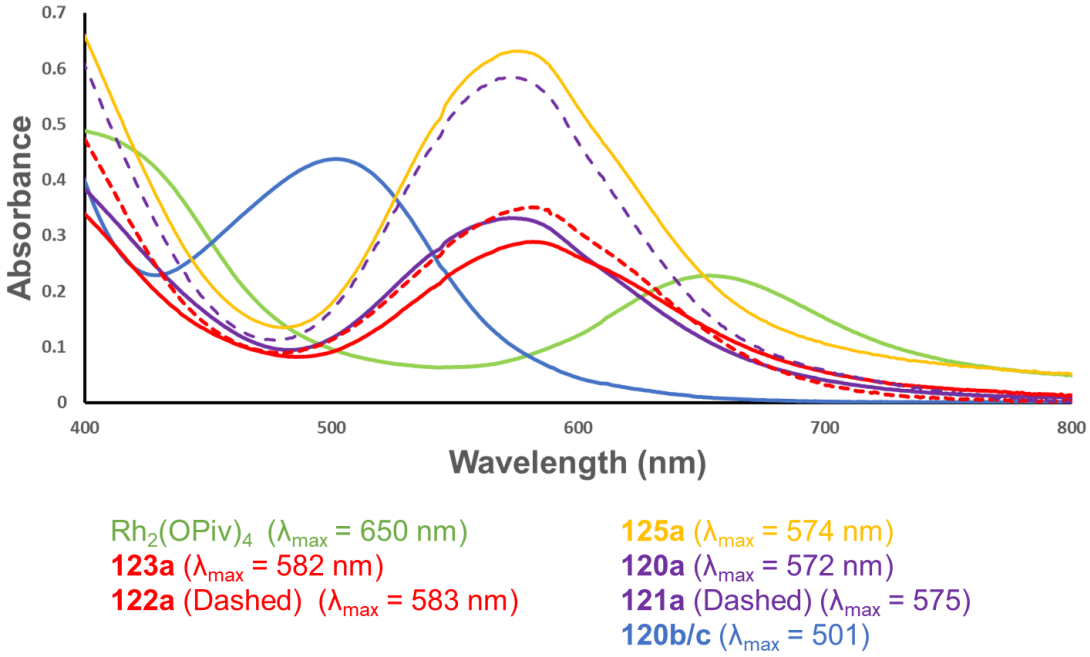

Figure 2.21 UV-Vis spectra of novel Rh^{II} complexes

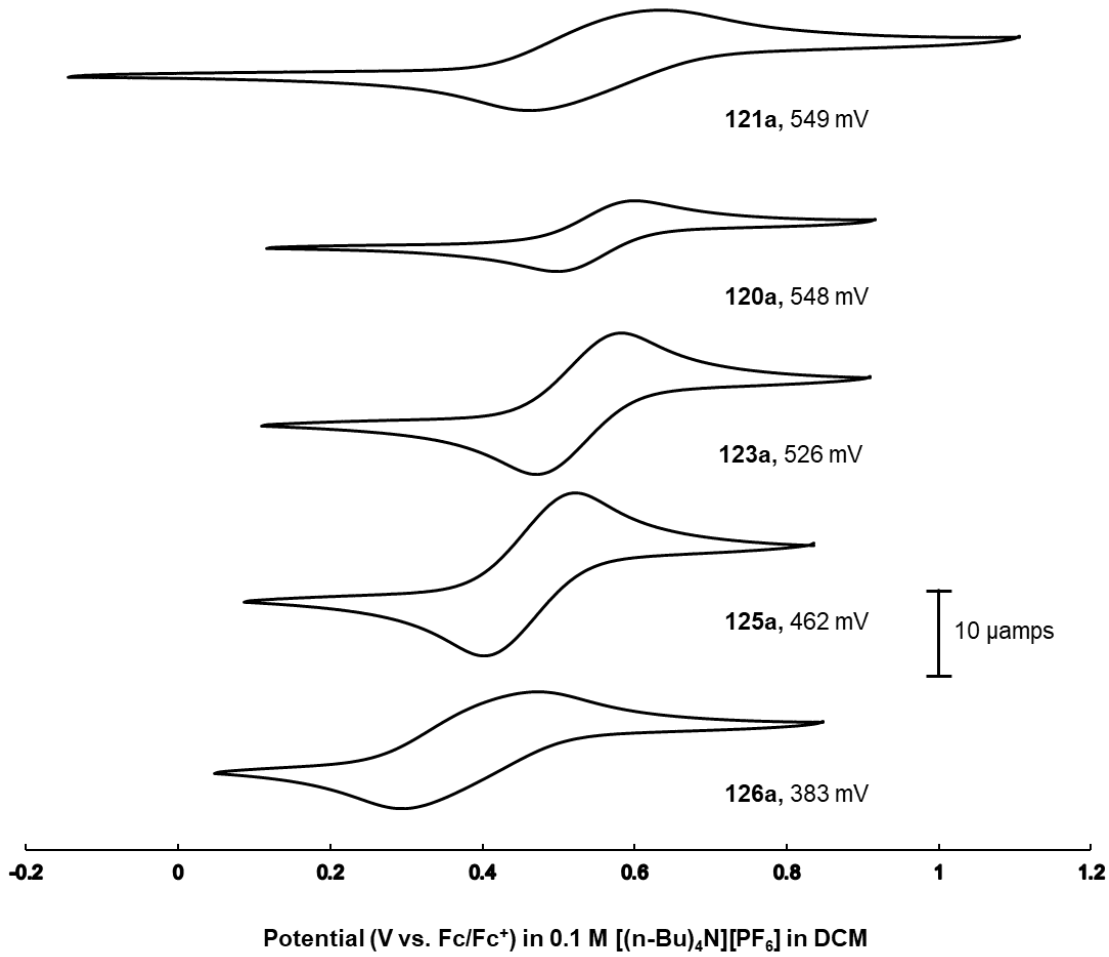

Figure 2.22 Cyclic voltammograms of the catalysts in an electrolyte solution of 0.1 M $[(n\text{-}Bu)_4N][PF_6]$ in DCM and referenced to the Fc/Fc^+ potential

incrementally modulated based on the coordinating thioether.

Examination of the literature demonstrated that solvent influenced the oxidation potentials of Rh^{II} complexes. The established trend indicated axial coordination of different solvents generally results in decreased oxidation potentials.[209, 212] To investigate this influence, further CV experiments were conducted in MeCN (Figure 2.23). Again, each of the complexes demonstrated a reversible or quasi-reversible oxidation event assigned to the $Rh_2^{4+/5+}$ oxidation couple. Complex **123a** demonstrated a loss of reversibility with further scans at lower scan rates (100 mV/s) (Figure 2.24). The loss of reversibility was not observed at higher scan rates (500 mV/s). The oxidation potential and the reversibility at higher scan rates indicate that this oxidation event is centered on the Rh. No clear oxidation or reduction events indicated the degradation of complex **123a**.

Differentiation between thioether donors was possible even though the oxidation potentials of most *mono*-substituted complexes fell within a 100 mV window. Axial coordination of the thioether generally resulted in lower oxidation potentials when compared to the control complex **126a**. The one exception to this was complex **125a**. It was expected that the weak Ph thioether donor would result in the highest oxidation potential of the novel complexes. Rather, the oxidation potential of **125a** was ~300 mV lower than the other complexes and more closely resembled the *bis*-substituted complexes **120b/c**. Despite the observable differences, no correlation between oxidation potentials and the donating abilities of the different thioether donors could be established with MeCN as the solvent.

Another observation was the presence of further oxidation events for complex **125a**; stronger donors do not exhibit these events. One explanation could be that these oxidation events are centered on the ligand and not the metal center. The oxidation of thioethers has been observed to occur at similar oxidation potentials.[210] Additionally, the presence of two oxidation events could indicate the formation of the sulfone, followed by the sulfoxide. The weaker coordination of the phenyl thioether of **125a** could lead to displacement by MeCN, enabling oxidation of the sulfur atom.

A similar oxidation event is observed for complexes **120b/c**. In the case of the *bis*-substituted complex **120b/c**, the *trans* effect could result in weaker coordination of the second axially bound thioether. This could result in the displacement of the thioether by MeCN, and result in oxidation of the ligand. Comparison of a mixture of **120b/c** and **120a** showed that additional bridging ligands results in a lower oxidation potential. The same

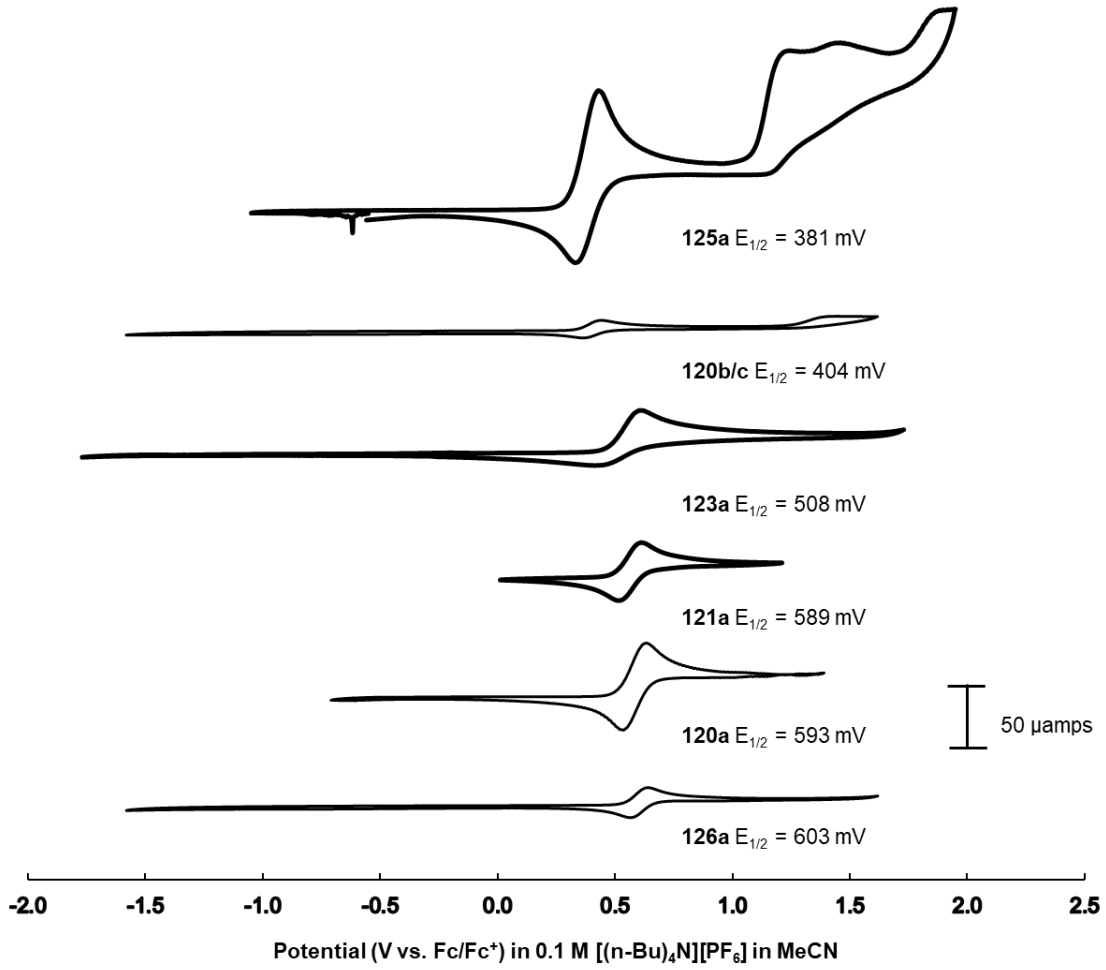

Figure 2.23 Cyclic voltammograms of the catalysts in an electrolyte solution of 0.1 M $[(n\text{-}Bu)_4N][PF_6]$ in MeCN and referenced to the Fc/Fc^+ potential

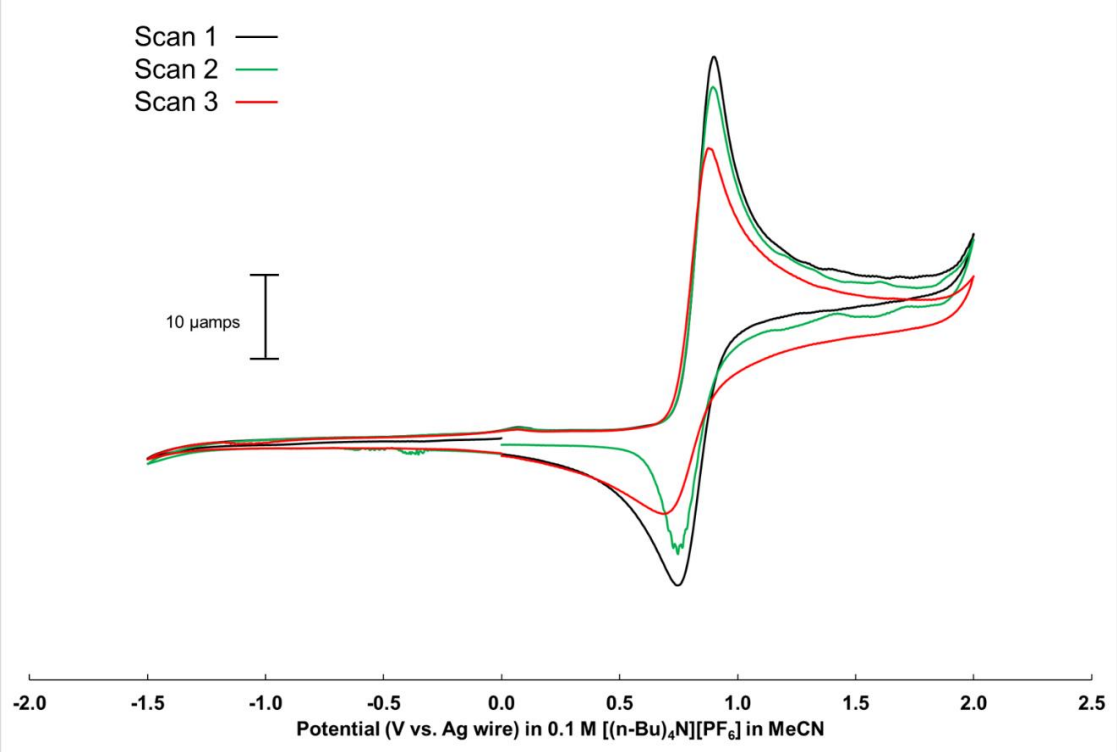

Figure 2.24 CV of complex **123a** showing loss of reversibility of the $Rh_2^{4+/5+}$ oxidation potential after multiple scans

trend was observed with the sequential addition of acetamide ligands.[215]

2.8 Alternative Syntheses of Rh^{II} Complexes

2.7.1 Ligand Salt Method

Heteroleptic carbamate complexes were previously synthesized by Corey via deprotonating the ligand before addition to $Rh_2(OAc)_4$.[170] As this method avoids heating, it was expected that the kinetic *mono*-substituted product would be favored. Investigations into this pathway began with the synthesis of **120a** as the ligand **107** was more readily available. Additionally, authentic samples were already available for comparison (Table 2.4). Based on literature precedence, sodium hexamethyldisilazane (NaHMDS) was selected as the strong base for deprotonating the oxazolidinone ligand.[170] The sodium salt of **107** was dissolved in tetrahydrofuran (THF) before being added to a solution of $Rh_2(OAc)_4$.

Analysis by TLC indicated the formation of the *mono*-substituted product after only an hour and the solution changed from green to yellow-green. TLC analysis also showed Rh starting material remained. Because the starting material remained, the reaction was allowed to continue, and no changes were observed by TLC analysis even after 24 hours. It was then hypothesized that the newly formed product was degrading as the reaction continued. The reaction was repeated and worked up after only an hour affording the similar results. Finally, the reaction was cooled as a means of further facilitating the kinetic product. The same yellow-green solution was generated along with a small amount of the desired *mono*-substituted product. It is believed that the yellow-green color is indicative of Rh(III) species which could be generated upon degradation of the paddlewheel motif.

2.7.2 Pressure Tube Method

Milder conditions were sought as the harsh conditions of the Soxhlet and salt method resulted in complex or ligand degradation. Towards this end, conducting the ligand exchange under pressure was explored (Table 2.5). It was believed the pressure build-up would enable lower reaction temperatures, preventing degradation. The reactions were monitored via TLC for the first sign of the formation of the *bis*-substituted product. Upon observing the *bis*-substituted product by TLC, the reaction was stopped,

Table 2.4 Synthesis of Rh^{II} complexes via ligand salts

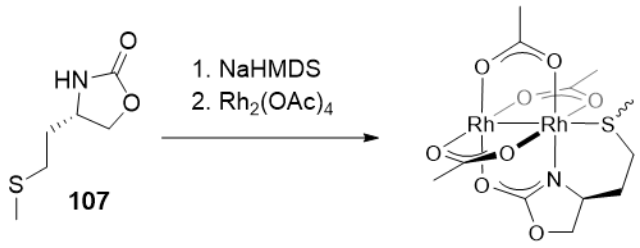

107 **120a**

Entry	Temp. (°C)	Time (hr)	Yield (%)
1	66	24 hr	<10
2	66	1 hr	11
3	0	3 hr	<10

Table 2.5 Synthesis of Rh^{II} complexes via pressure tube

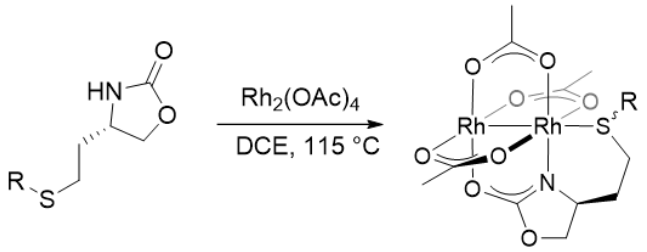

Entry	Product	R	Cycle 1 Yield (%)	Cycle 2 Yield (%)	Cycle 3 Yield (%)	Total Time	Total Yield (%)
1	**123a**	^{t}Bu	34	12	12	13 days	58
2	**125a**	Ph	12	22	10	12 days	44
3	**127a**	p-OMe	9	-	-	6 hours	9

and the *mono*-substituted product was isolated via column chromatography. The remaining fractions were then combined, concentrated, and placed back into the pressure tube with fresh DCE. This process was repeated two more times and led to an increase in the overall yield of the reaction. Yields for each iteration were inconsistent and could be a result of stopping the reaction at different points during the equilibrium process.

It was observed that this method did not result in degradation of the ligand, as was observed in the Soxhlet method. This was attributed to the lower temperature required to drive the reaction forward. Although this route provides an increase in yield, the overall reaction time spanned weeks.

The synthesis of the *p*-methoxyphenyl thioether was limited to one cycle due to the formation of a dark solid on the side of the flask. Unlike previous heteroleptic complexes, the substance was not soluble in coordinating solvents such as MeCN or MeOH. The solubility was then tested using dimethyl sulfoxide (DMSO) which led to a red solution. The ^{1}H NMR showed that equatorial coordination had not occurred, as only a single acetate peak was observed in conjunction with the free ligand (See Appendix A, **S28** and **S29**).

2.7.3 Microwave Method using Ionic Liquids

The microwave method previously described was conducted on a small-scale (15 mg $Rh_2(OAc)_4$). Attempts were made at a larger scale but the desired temperature of 190 °C was unable to be reached. This was believed to stem from the additional solvent, about 5 times more, that required heating. One means of circumventing this issue would be mixed solvent systems of DCE and more polar solvents. However, these solvents are also capable of coordinating to the axial site and result in diminished yields (see section 2.5.2). Instead, ionic liquid (ILs) additives were considered due to their outstanding ability to transform radiation into thermal energy.[196]

One of the most common IL is based on NMI, which is readily alkylated with haloalkanes. Both the methyl substituent and alkylation minimize the coordinating ability of the imidazole. Two sets of ILs were synthesized using NMI and *n*-bromobutane or *n*-bromodecane, which were then metathesized to generate the final ILs (Table 2.6). The two cations were chosen to facilitate solubility in DCE. It was believed the bromide anion may bind to the axial site and result in oxidation of the Rh^{II} complex, as was observed with

Table 2.6 Set of ionic liquids tested for facilitating heating of large-scale microwave reactions

Cations

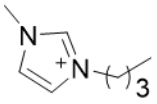

BMIM

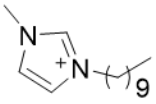

$C_{10}MIM$

Anions

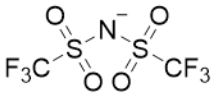

Tf_2N

PF_6

IL	Cation	Anion
IL-1	$C_{10}MIM$	PF_6
IL-2	$C_{10}MIM$	Tf_2N
IL-3	BMIM	PF_6
IL-4	BMIM	Tf_2N

the chloride anion.[216, 217] For this reason, Tf_2N and PF_6 were chosen as anions rather than the more readily accessed bromide. The electron withdrawing groups, in conjunction with low concentration, were predicted to prevent strong binding to the Rh^{II} axial site.

Investigation of the IL additive to facilitate heating was conducted with DCE, as it had been deemed the optimal solvent. Each of the ILs tested, except **IL-3,** reached the target temperature in less than 5 minutes. Testing **IL-2** in a ligand exchange reaction resulted in the desired temperature being reached and the production of the desired Rh^{II} complexes. Analysis by TLC indicated that the products could be purified using column chromatography as before. However, upon analyzing the fractions containing the *mono*-substituted product by ^1H NMR it was determined that IL was present and would require a different purification process. The IL solvents were abandoned in favor of multiple small-scale reactions that could be run in tandem, combined, and purified to supply the desired catalysts.

2.9 Conclusion

A series of novel heteroleptic Rh^{II} complexes with mixed acetate and oxazolidinate ligands was realized. The oxazolidinone ligands contained a tethered thioether that was capable of binding to the axial site of the paddlewheel structure. Of the different methods implemented to synthesize new heteroleptic Rh^{II} complexes, it was determined that microwave radiation provided the most direct path with acceptable yields. Additionally, ligand degradation is reduced when compared to the Soxhlet method; this is believed to occur due to the shortened reaction times and elimination of hot spots through heating with microwave radiation.[196] The tethered thioether appeared to limit the number of ligand substitutions due to *bis*-substitution blocking both axial sites, which inhibited further ligand exchange. It was also clear that the presence of the tethered thioether promoted ligand exchange, although the details are not known. This provided further support for the mechanism requiring axial coordination for ligand displacement.[171] Both solid-state and liquid-state analyses suggested that axial coordination is present, but in a very rapid equilibrium that cannot be detected on the NMR time scale. The donor strength of the thioether donors could not be determined based on UV-Vis spectroscopy but was made possible by CV analysis. This demonstrated that the electronic nature of the Rh^{II} complexes could be modulated by the tethered thioether.

Chapter 3 -

Investigation of the Role of Axial Coordination of Tethered Thioethers in the Cyclopropanation of Olefins by Rh^{II} Carbenoids Generated from α-Diazoesters.

Portions of this chapter were adapted from the publication by Brad Anderson, Derek Cressy, Jay Patel, Caleb Harris, Glen Yapp, John Berry, and Ampofo Darko in the peered reviewed article:

Anderson, B. G.; Cressy, D.; Patel, J. J.; Harris, C. F.; Yap, G. P. A.; Berry, J. F.; Darko, A., Synthesis and Catalytic Properties of Dirhodium Paddlewheel Complexes with Tethered, Axially Coordinating Thioether Ligands. *Inorganic Chemistry* **2019,** *58* (3), 1728-1732

Dr. Brad Anderson, assisted by Jay Patel, was responsible for synthesis, characterization, catalytic screening of the carboxylate derived catalyst, and writing the manuscript. Derek Cressy was responsible for the synthesis, characterization, catalytic screening involving the oxazolidinone derived catalyst, and UV-Vis, along with aiding in manuscript preparation. Dr. Glenn Yapp was responsible for solving the crystal structure for the oxazolidinone derived complex. Dr. Caleb Harris was responsible for CV analysis. Prof. John Berry and Prof. Ampofo Darko both advised the work.

Portions of this chapter were also adapted from a manuscript by Derek Cressy, Cris Zavala, Anthony Abshire, Will Sheffield and Ampofo Darko, which is currently published as a preprint:

Cressy, D.; Zavala, C.; Abshire, A.; Sheffield, W.; Darko, A., Tuning Rh(II)-Catalyzed Cyclopropanation with Tethered Thioether Ligands. *Dalton Trans*. **2020**. DOI 10.1039/D0DT03019H

Derek Cressy was responsible for the synthesis, characterization, x-ray structure elucidation, catalyst screening, UV-Vis, electrochemical analysis, and manuscript preparation. Cris Zavala was responsible for catalytic testing and aided in manuscript preparation. Anthony Abshire was responsible for all calculations, while Will Sheffield aided in characterization and manuscript preparation. Prof. Ampofo Darko advised the work.

3.1 Abstract

Exogenous LBs have been applied in cyclopropanation reactions mediated by Rh^{II} carbenoids. However, the results from these reports are often contradictory. For every reported improvement in yield or enantioselectivity, there appears to be a report where only diminished yields were observed. To investigate this dichotomy, novel Rh^{II} complexes containing tethered thioethers were applied as catalysts in cyclopropanation reactions. It was found that the novel complexes facilitated reactions with EDA more readily than with methyl (4-nitro)phenyldiazoacetate. With EDA as the diazo reagent, each novel catalyst afforded higher yields than a heteroleptic Rh^{II} control catalyst. They also provided higher yields compared to the benchmark Rh^{II} catalyst $Rh_2(OAc)_4$. Computational analysis was conducted to aid in understanding the observed reactivity.

3.2 Introduction

It was demonstrated that the primary method of controlling catalytic activity of Rh^{II} complexes relies on the modification of the bridging ligands. Investigation of the axial site indicated that LBs, such as solvent, readily coordinated. The most obvious effect of axial coordination was catalyst inhibition, due to the catalytically active site being blocked. The work by Pirrung and co-workers, who analyzed Rh^{II} catalysis under Michaelis-Menten kinetics, supports inhibition by axial coordination.[77] Interestingly, they also demonstrated only a single axial site participates in carbenoid formation during one turnover of the catalyst. An open axial site suggests that axial coordination at one axial site could be exploited as a means of controlling the electrophilicity of the distal Rh via electronic communication through the Rh–Rh bond. This manner of controlling Rh^{II} catalyst reactivity has not been investigated as thoroughly as the bridging ligands but is not unknown.

Axial coordination is most easily achieved by the introduction of exogenous LBs. This method was employed by the Davies group for the cyclopropanation of styrene and methyl phenyldiazoacetate with a Rh^{II} prolinate catalyst (Figure 3.1).[218] It was found that the addition of a weakly coordinating LB, such as methyl benzoate, led to a distinct increase in the ee. The same study also demonstrated an increase in ee when select phosphine oxide and urea additives were employed. However, a decrease in yield was also observed, again showing the inhibitory effects of axial coordination. An amine additive resulted in almost complete inhibition of catalytic activity (5% yield) and no results

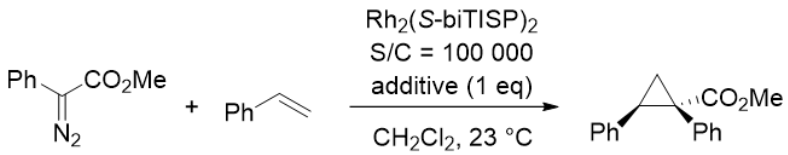

Additive	*Yield (%)*	ee (%)
None	82	65
$PhCO_2Me$	85	83
$(Me_2N)_2C{=}O$	48	74
$OP(Oct)_3$	36	78
$(^iPr)_2NEt$	5	ND

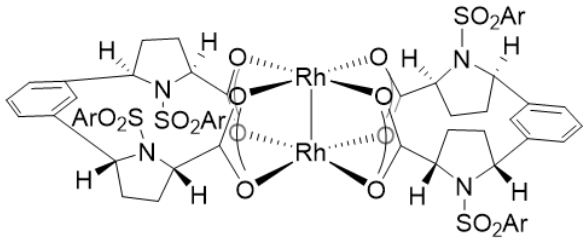

Rh_2(*S*-biTISP)$_2$
Ar = 2,4,6-tri-^{i}PrC$_6$H$_2$

Figure 3.1 Cyclopropanation of styrene and methyl phenyldiazoacetate with Rh_2(*S*-biTISP)$_2$ demonstrating increased enanatioselectivity in the presence of additives.

on ee were given. It should be noted that additives were only effective at low catalyst loadings, while no increase in ee was observed at higher catalyst loading. The difference in selectivity was not further investigated but axial coordination was cited as a possible cause.

Wynne and co-workers also examined cyclopropanation of olefins and methyl phenyldiazoacetate with a Rh^{II} prolinate catalyst, similar to the catalyst used by Davies (Figure 3.2).[181] Yields were not reported, but the addition of exogenous phosphine oxides and phosphines did not result in increased enantioselectivity. Rather, the exogenous LBs resulted in a decrease in ee, contradicting the finding of the Davies group. It was believed less sterically hindered LBs were better suited to coordinate to the axial sites, thereby decreasing enantioselectivity. Conversely, steric interactions between bulky phosphines and the catalyst was believed to prevent axial coordination. The lack of axial coordination then resulted in similar enantioselectivity as when no additives were present. The coordination strength of the phosphines was corroborated by UV-Vis experiments, where the HOMO-LUMO energy gap was larger for strongly donating alkyl phosphines, as compared to the weaker phosphine oxides.

Even with evidence for increased enantioselectivity, the benefits of axial coordination are uncertain and hard to predict. The dichotomy of axial coordination was even observed in the same group when Charette and co-workers examined the cyclopropanation of olefins and acceptor/acceptor diazo reagents (Figure 3.3).[180, 219] For the cyclopropanation of styrene and an amido diazo reagent with Rh_2(*S*-NTTL)$_4$ the LB additive did not result in increased enantioselectivity, rather only a decrease in yield (Figure 3.3, a). Conversely, the cyclopropanation of styrene and an α-ketodiazo reagent by Rh_2(*S*-TCPTTL)$_4$ in the presence of LBs led to an increase in enantioselectivity (Figure 3.3, b). The increase in enantioselectivity was accompanied by a decrease in yield and diastereomeric ratio. When these reactions were conducted at higher temperatures, there was also a decrease in the diastereomeric and enantiomeric ratios. It was postulated that lower temperatures resulted in the complexation of the LB additive, resulting in higher overall stereoselectivity.

Although the addition of exogenous ligands is the easiest way to introduce axial coordination, the active catalyst remains ambiguous. Two distinct active catalysts can be generated depending upon the number of axially coordinated compounds (Scheme 3.1). When no LBs are axially coordinated, the active catalyst will be the same as if no LB was

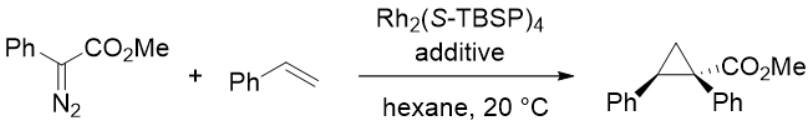

Additive (%)	ee (%)
None	90
$OP(Oct)_3$	90
$P(mes)_3$	90
PPh_3	46
PEt_3	21

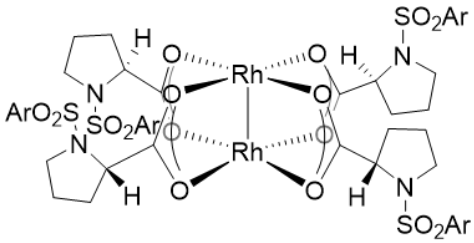

Rh_2(*S*-TBSP)$_4$
Ar = *p*-^{t}BuC_6H_4

Figure 3.2 Cyclopropanation of styrene and methyl phenyldiazoacetate where additives did not result in increased enantioselectivity

a)

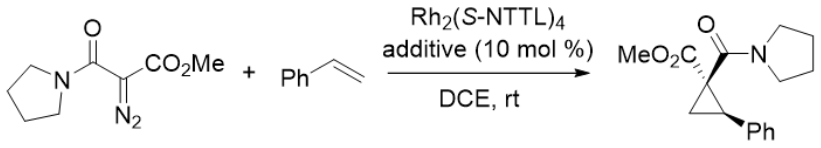

Additive	*Yield (%)*	er
None	79	49:1
DMAP	NR	NR
Pyridine[a]	14	ND
MeCN	67	49:1
DMF	62	59:1

[a] 1 mol % additive

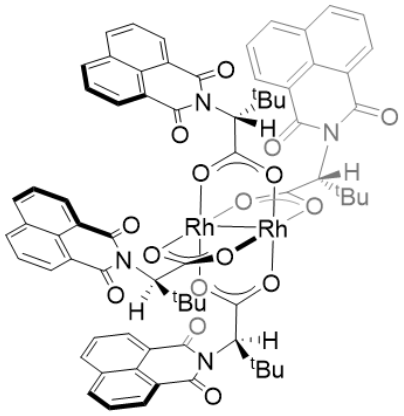

b)

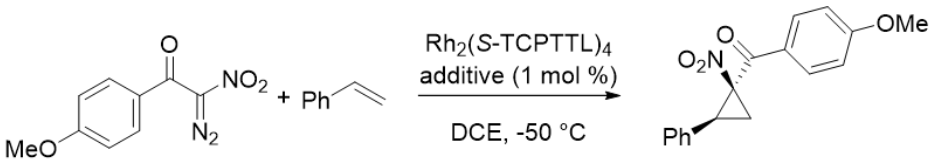

Additive (mol %)	*Yield (%)*	dr	er
None	80	49:1	27:1
DMAP (1)	78	32:1	39:1
Pyridine (1)	70	32:1	32:1
None[a]	68	16:1	14:1
DMAP (1)[a]	70	16:1	14:1

[a] Run at 0 °C

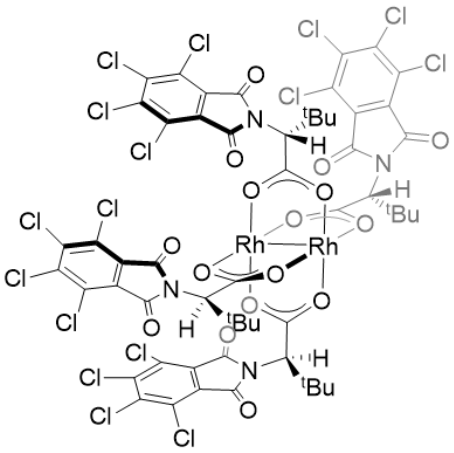

Figure 3.3 Examples of a) LB additives having no effect and b) LB additives increasing enantioselectivity from the same research group

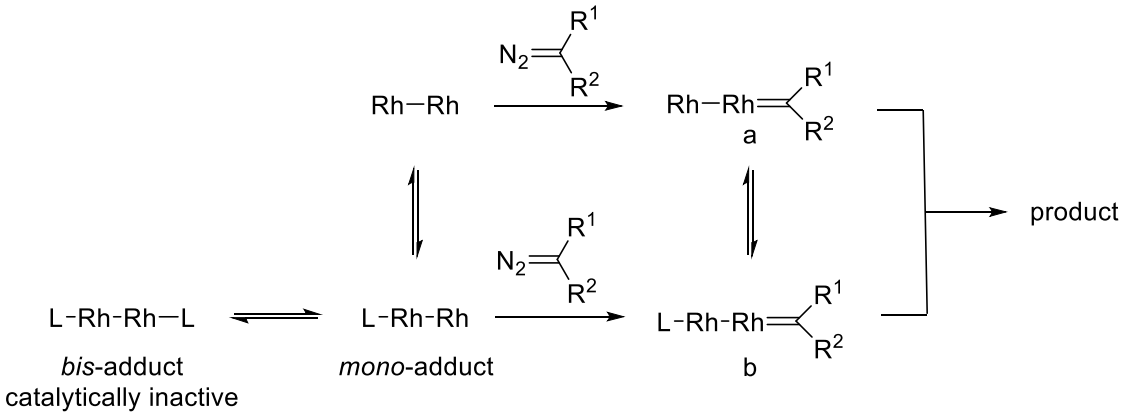

Scheme 3.1 Equilibrium process of axial coordination of Rh^{II} complexes resulting in different catalytically active species

added (Scheme 3.1, **a**). Coordination of a LB to one axial site results in the formation of the *mono*-adduct, which has an open axial site for catalysis, results in the second catalytically active complex (Scheme 3.1, **b**). Axial coordination of a second LB molecule generates the *bis*-adduct which is not catalytically active. Two different methods have been employed to ensure that the *mono*-adduct is prevalent in solution. One method is to introduce strongly coordinating LBs which allows near equimolar amounts of the Rh^{II} species to be added.[220] This helps facilitate the formation of the *mono*-adduct, but hinders tunability, as weaker donors will likely dissociate. To facilitate the investigation of weak donors, an excess of the LB is added to promote the formation of the *mono*-adduct. However, it remains possible that catalysis is being accomplished, at least in part, by the Rh^{II} without any axial coordination (Scheme 3.1, **a**).

In early investigations, Ball and co-workers found the addition of exogenous phosphites resulted in an increase in enantioselectivity during Rh^{II} carbenoid mediated reactions.[221] Due to the complications outlined above, they sought to verify that axial coordination was indeed responsible. To this end, they synthesized metallopeptide Rh^{II} complexes bound to resin beads. These complexes were equipped with a histidine residue capable of axial coordination (Figure 3.4).[222] Several of these metallopeptide Rh^{II} complexes facilitated the asymmetric cyclopropanation of styrene with a donor/acceptor diazo reagent in high ee. An analogous Rh^{II} metallopeptide complex was synthesized where the axially coordinated histidine residue was replaced with isosteric phenylalanine. This substitution resulted in a decrease in ee upon removal of the axially coordinating histidine, further suggesting that axial coordination results in improved stereoselectivity. It was proposed that axial coordination of the histidine results in a change in the folding of the peptide chain. This change in folding then resulted in a modification of the environment around the catalytically active axial site.

Different theories have been proposed as to why axial coordination results in higher enantioselectivity. One explanation, based primarily on steric arguments, states axial coordination results in modification of the chiral pocket around the axial site, as was put forward by Ball for Rh^{II} metallopeptide complexes. This theory agrees with the research by Doyle and co-workers which demonstrated that conformational changes around the axial site affected enantioselectivity. Conformational changes were effected by choosing between two diastereomers of the bridging ligands, rather than axial

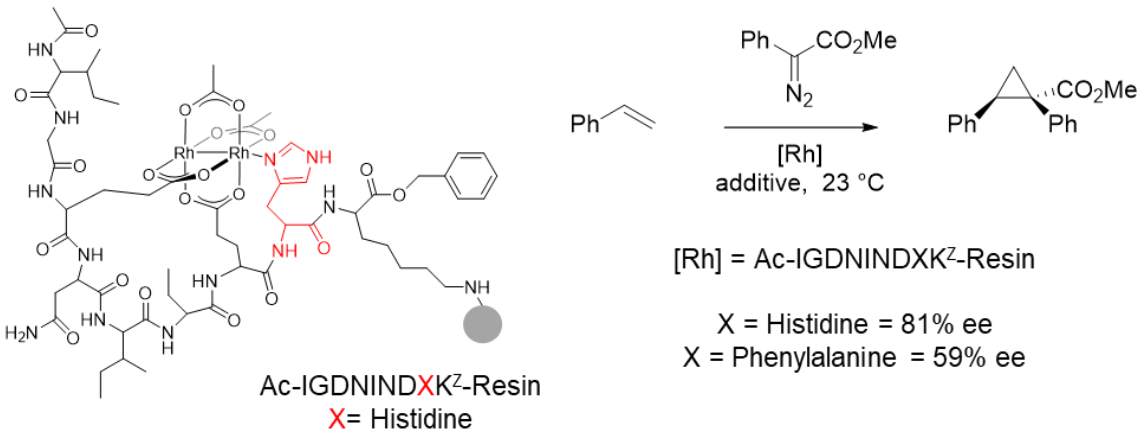

Figure 3.4 Coordination of metallopeptide Rh^{II} complex results in higher enantioselectivity. Z= benzyloxycarbonyl, Grey sphere= resin

coordination, and resulted in a “matched/mismatched” system.[89] One diastereomer generated the Rh^{II} complex where the chiral groups protruded over the axial site in a clockwise fashion (Figure 3.5, b). Conversely, the second diastereomer led to a less symmetric chiral pocket (Figure 3.5, c). When both of these were applied to intramolecular cyclopropanation, complex B afforded higher yields and ee than complex C. It was stated that the chiral environment of B matched the substrate and diazo reagent, which afforded better results. However, predicting which Rh^{II} isomer will match a select substrate and diazo reagent is not straight forward.

Another theory states that increased electron density from axial coordination results in a late transition state. Electron density from axial coordination is believed to stabilize the carbenoid intermediate, requiring the olefin substrate to be closer to the carbenoid before reacting.[94] This results in increased interaction between the substrate and the chiral environment which leads to a later transition state, which more closely resembles the asymmetric product. This theory focuses primarily on the electronic nature of the complex. Both explanations outlined above are based on two extremes, disregarding the interplay between electronic and steric factors. It is more likely that the true influence of axial coordination involves both aspects to a certain degree.

Even after examination of axial coordination by several groups, the role of axial coordination remains ambiguous. The direct comparison of these examples is not possible as different catalysts and diazo reagents were applied in each experiment. Without a direct comparison, it is not possible to determine what causes axial coordination to be beneficial and what causes it to be detrimental. To begin delineating which factors are beneficial, the novel Rh^{II} complexes synthesized in chapter 2 were applied as catalysts in the cyclopropanation of olefins and diazo esters. By systematically varying the tether length and thioether donor, a direct comparison can be made between different axially coordinating groups.

3.3 Cyclopropanation of Olefins with EDA

Carboxamidates have proven to be efficient catalysts when paired with acceptor diazo compounds. Therefore, catalytic testing with the standard cyclopropanation of styrene and EDA in DCM was investigated (Table 3.1). The addition of the diazo reagent to the solution of $Rh_2(OAc)_4$ and styrene resulted in the visible formation of bubbles,

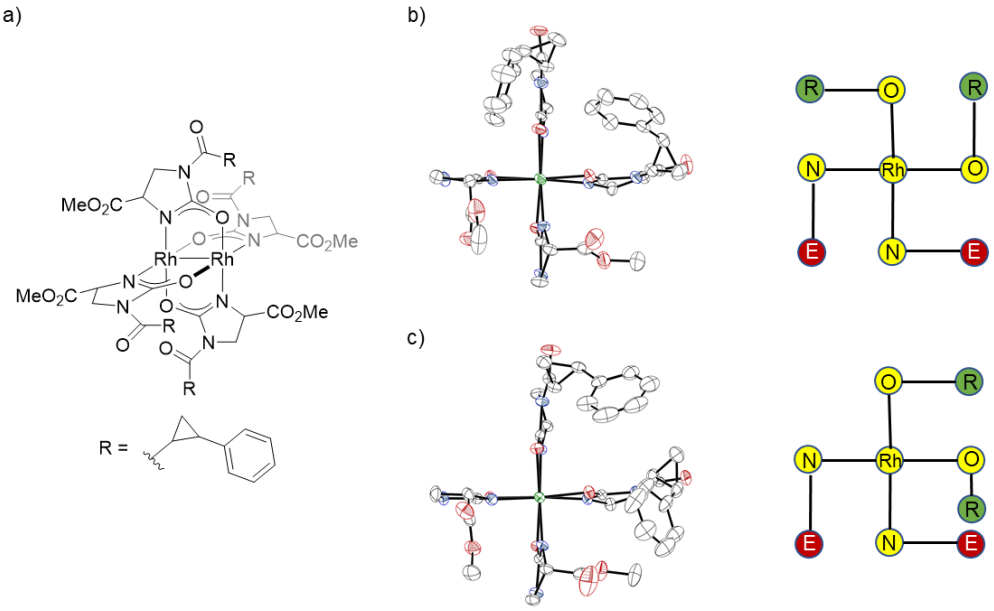

Figure 3.5 Example of the "match/mismatch" conformation with diastereomers of a) $Rh_2(MCPIM)_4$ with the b) matched diastereomer (4*S*,2'*S*,3'*S*) and c) mismatched diastereomer (4*S*,2'*R*,3'*R*)

indicating extrusion of dinitrogen. Visible formation of dinitrogen was not observed with the novel Rh^{II} complexes **120a** or **120b/c**. However, TLC analysis showed the complete decomposition of the diazo reagent in the case of catalyst **120a**, while indicating EDA remained for **120b/c**. After reactions workup it was observed that even the *bis*-substituted complex was capable of catalysis, but the dual axial coordination inhibited reactivity much more than the *mono*-substituted complex (Table 3.1, entries 1 and 2). Despite having the lowest yield, the highest diastereoselectivity was observed with the *bis*-substituted **120b/c**.

Comparison of **120a** and $Rh_2(OAc)_4$ indicates similar reactivity, with comparable yields and diastereoselectivity (Table 3.1, entries 2 and 3). Concomitant to this investigation, a member of our group, William Sheffield, demonstrated that complex **120a** performed better in Si-H insertion reactions at elevated temperatures.[198] The noncoordinating solvent DCE was employed to allow for these elevated temperatures as well as catalyst solubility. Elevating the temperature resulted in **120a** affording a quantitative yield while the yield with $Rh_2(OAc)_4$ did not change greatly (Table 3.1, entries 4 and 5). Although excess olefin is a common practice to prevent diazo dimer formation, the use of stoichiometric amounts of olefin is desirable. Towards this end, Cris Zavala further tested catalytic ability by reducing the amount of olefin substrate (Table 3.1, entries 6-8). Good to high yields were observed as low as 1 equivalent of olefin substrate with minimal changes in diastereoselectivity. The minimal changes in diastereoselectivity were not unexpected as EDA does not afford great diastereoselectivity and no chiral ligands protrude over the axial site. Enantioselectivity was not determined for the same reason. These results indicated that the Rh^{II} complexes were catalytically active with the presence of the axially coordinated tether. The focus was then directed towards *mono*-substituted complexes because higher yields and complete consumption of diazo reagent were observed.

Each novel catalyst containing the tethered thioether group resulted in higher yields when compared to a control catalyst **126a** (Figure 3.6). The improved yields of catalysts **120a**-**125a** suggested that the thioether tether is responsible for the increased yield. Furthermore, catalysts **120a**-**125a** each provided the cyclopropane product in higher yields than the benchmark catalyst $Rh_2(OAc)_4$. Comparison of the different thioether donors showed that the weakest donor (see Section 2.3 for discussion of thioether donor strength) 1**25a** resulted in the highest yield of the desired cyclopropane. This trend was not observed with **120a** and **123a**. The similarity between the two could

Table 3.1 Catalytic activity of heteroleptic Rh^{II} complexes

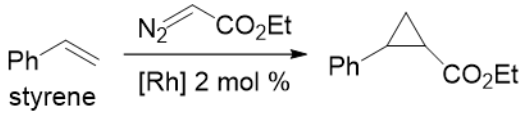

Entry	[Rh]	Solvent	eq. styrene	Temp. (°C)	Yield [a](%)	*trans*/*cis*[b]
1	**120b/c**	DCM	10	rt	49	2:1
2	**120a**	DCM	10	rt	75	1.4:1
3	$Rh_2(OAc)_4$	DCM	10	rt	76	1.2:1
4	$Rh_2(OAc)_4$	DCE	10	80	78[c]	1.4:1
5	**120a**	DCE	10	80	99[c]	1.5:1
6	**120a**	**DCE**	**5**	**80**	**99**[c]	**1.6:1**
7	**120a**	DCE	2	80	78[c]	1.3:1
8	**120a**	DCE	1	80	63[c]	1.5:1

[a]Determined by ^1H NMR using mesitylene as a standard [b]Ratios determined by ^1H NMR [c]Determined by GC

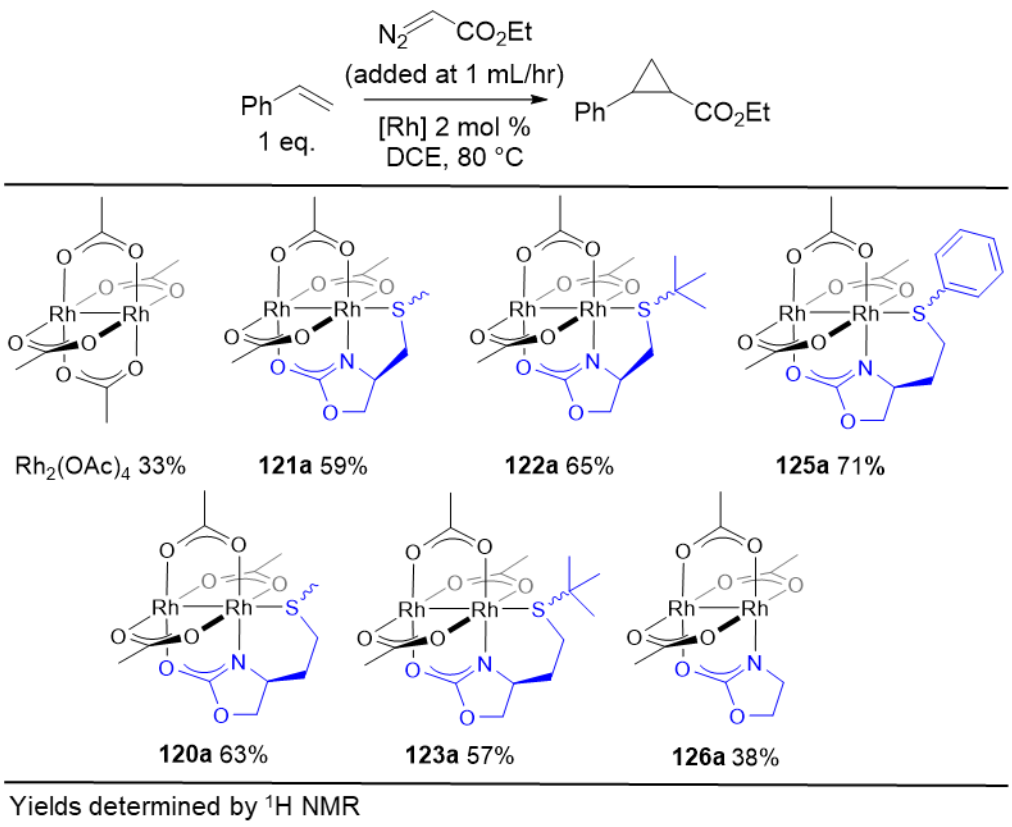

Figure 3.6 Screening of the novel Rh^{II} complexes with tethered thioethers

be a result of their donor strength being similar. The ^{t}Bu group is a stronger electronic donor, but coordination could be diminished due to the steric bulk of the ^{t}Bu group, thereby making it more like the methyl thioether.

The tether length influenced catalytic activity but does not follow a trend. The longer tether length resulted in higher yields with methyl thioethers while the converse is true for the ^{t}Bu thioethers. It is possible this arises from the poorer donation of the sulfur lone pair when the tether is only one methylene unit compared to two. This was observed in the x-ray structure where the Rh–Rh–S angle of **122a** (174°) was smaller than **120a** (178°). However, each of the thioether donors is different in these complexes and would require crystallization of **121a** or **123a** for further evidence.

A substrate scope was then conducted by Cris Zavala at 5 equivalents of olefin and 2 mol% of the lead catalyst 1**25a** (Figure 3.7). The 5 equivalents of olefin were used for a better comparison to the conventional use of 10 equivalents. Styrene derivatives maintained excellent yields with the reaction of 4-*t*-butylstyrene generating the product in 99% yield. The lower yield of 4-chlorostyrene is consistent with the inductive withdrawing effects of the Cl, which results in a less nucleophilic olefin. This is in contrast to the electron rich olefin, ethyl vinyl ether, which afforded quantitative amounts of the cyclopropane product. The introduction of steric hindrance via disubstituted olefins was well tolerated and also resulted in excellent yields. Again, the more electron rich diphenyl olefin resulted in a slight increase in yield compared to the methyl/phenyl substituted olefin. The more synthetically challenging substrate norbornene afforded the corresponding cyclopropane in 55% yield. Although a preference for the *trans* product is seen for select substrates, it is not by a large margin nor markedly different than that observed in the literature.[223] This was anticipated as bulky ester groups and bulky bridging ligands are the primary sources of diastereoselectivity and neither were present in these reactions.

3.4 Cyclopropanation of Olefins with Donor/Acceptor Diazo Compounds

The capability of the novel Rh^{II} catalysts were further tested with the donor/acceptor diazo reagent methyl (4-nitro)phenyldiazoacetate. This diazo reagent historically resulted in low yields and formation of the homocoupled dimer product.[21] The

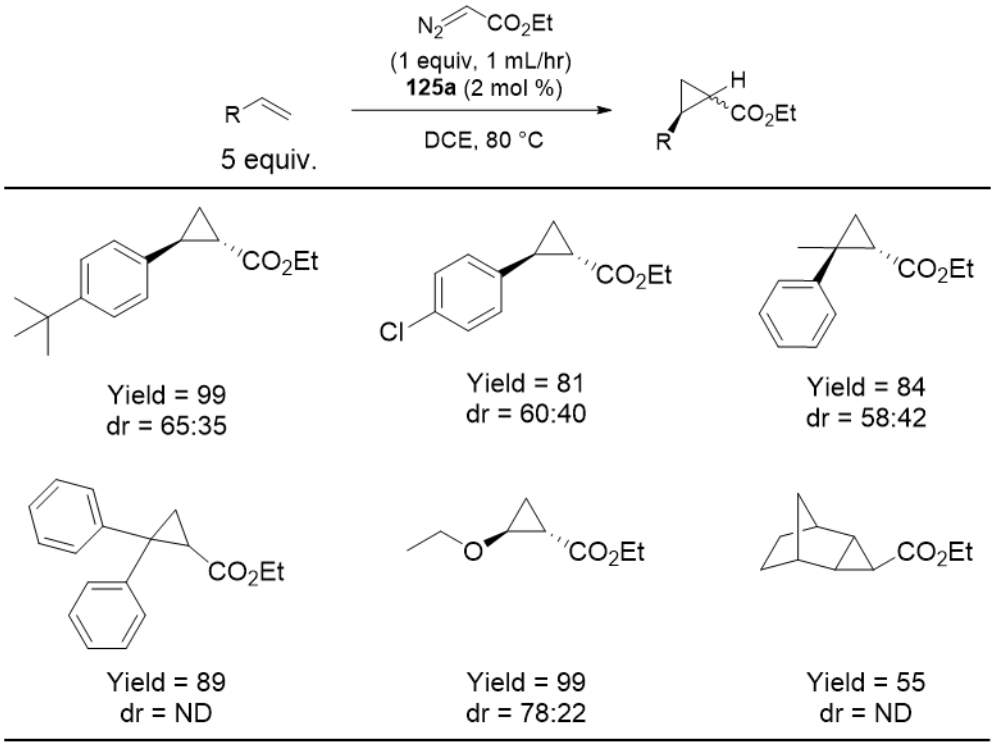

Yields and dr determined by ^{1}H NMR

Figure 3.7 Select substrate scope with lead catalyst **125a**

yield with carboxamidate **120a** was lower than that obtained with $Rh_2(OAc)_4$ (Table 3.2, entries 1 and 2). A control reaction was conducted by combining $Rh_2(OAc)_4$ and one equivalent of ligand **107**. It was expected that axial coordination of the exogenous ligand during catalysis would be evidenced by a yield similar to 120a. Rather, similar results to that obtained by $Rh_2(OAc)_4$ were observed (Table 3.2, entry 3). This supports that incorporating the ligand onto the Rh^{II} complex is necessary for modifying its reactivity. In an attempt to increase the yield, the reaction with120a was examined reflux (Table 3.2, entry 4). This resulted in the yield doubling, although it was still low. It was noted that a higher preference for the cyclopropane product was observed at elevated temperatures. As a means of increasing the yield even more, higher temperatures were examined (Table 3.2, entries 5 and 6). Switching to DCE enabled higher temperatures to be achieved, while still employing a chlorinated solvent. The elevated temperature achieved with DCE gave the highest yield, along with the highest ratio of cyclopropane product to diazo dimer for both **120a** and $Rh_2(OAc)_4$. As was observed with EDA, the *bis*-substituted complexes **120b/c** gave the desired cyclopropane in low yield but showed a comparable preference for the formation of cyclopropane over the diazo dimer product (Table 3.2, entry 7). These results indicate that the novel Rh^{II} complexes are not highly effective for reactions with donor/acceptor diazo reagents. Rather, they are better suited as catalysts for the cyclopropanation of olefins and acceptor diazo reagents.

3.5 Computational Analysis

To gain further insight into the influence of the tethered thioether with regards to reactivity, calculations were conducted by Anthony Abshire. All calculations were conducted at the MO6-2X/def2-TZVPP level of theory and allowed determination of the ground state energies of $Rh_2(OAc)_4$, **126a**, **120a**, and **125a**.[224] The coordinates obtained from the crystal structures served as starting points in the calculations for **120a** and **125a**. From the models of the complexes in the ground state, the energy levels of the HOMO and LUMO were determined (Figure 3.8). The HOMO energy rises in the order **126a**<**125a**<**120a**, which was also observed experimentally by CV analysis. In conjunction with the destabilization of the HOMO, an even larger destabilization of the LUMO was observed. The donating ability of the thioether groups could be seen with more destabilization by the stronger donor (methyl thioether of **120a**) compared to the

Table 3.2 Cyclopropanation of styrene and methyl (4-nitro)phenyldiazoacetate

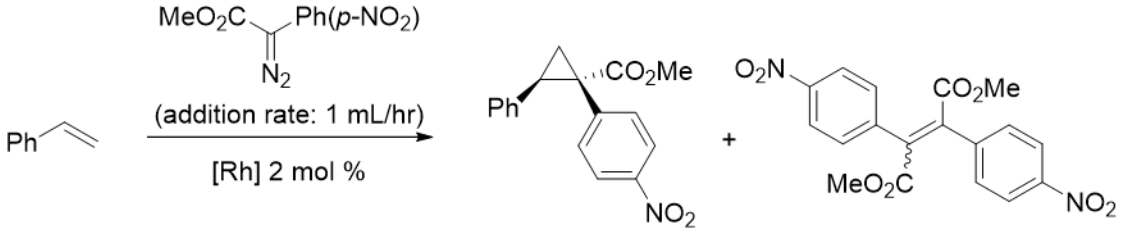

Entry	[Rh]	Solvent	Temp.	Yield[a] (%)	Product:Dimer[b]
1	**120a**	DCM	rt	10	1:1
2[c]	$Rh_2(OAc)_4$	DCM	rt	16	1.7:1
3	$Rh_2(OAc)_4$ + **107**	DCM	rt	19	1.6:1
4[c]	**120a**	DCM	reflux	28	2.6:1
5	**120a**	DCE	reflux	46	5:1
6	$Rh_2(OAc)_4$	DCE	reflux	48	5.5:1
7	**120b/c**	DCE	reflux	18	4:1

[a]Yields are an average over two runs. Determined by ^{1}H NMR using mesitylene as a standard. [b]Ratios determined by ^{1}H NMR. [c] Results of one run

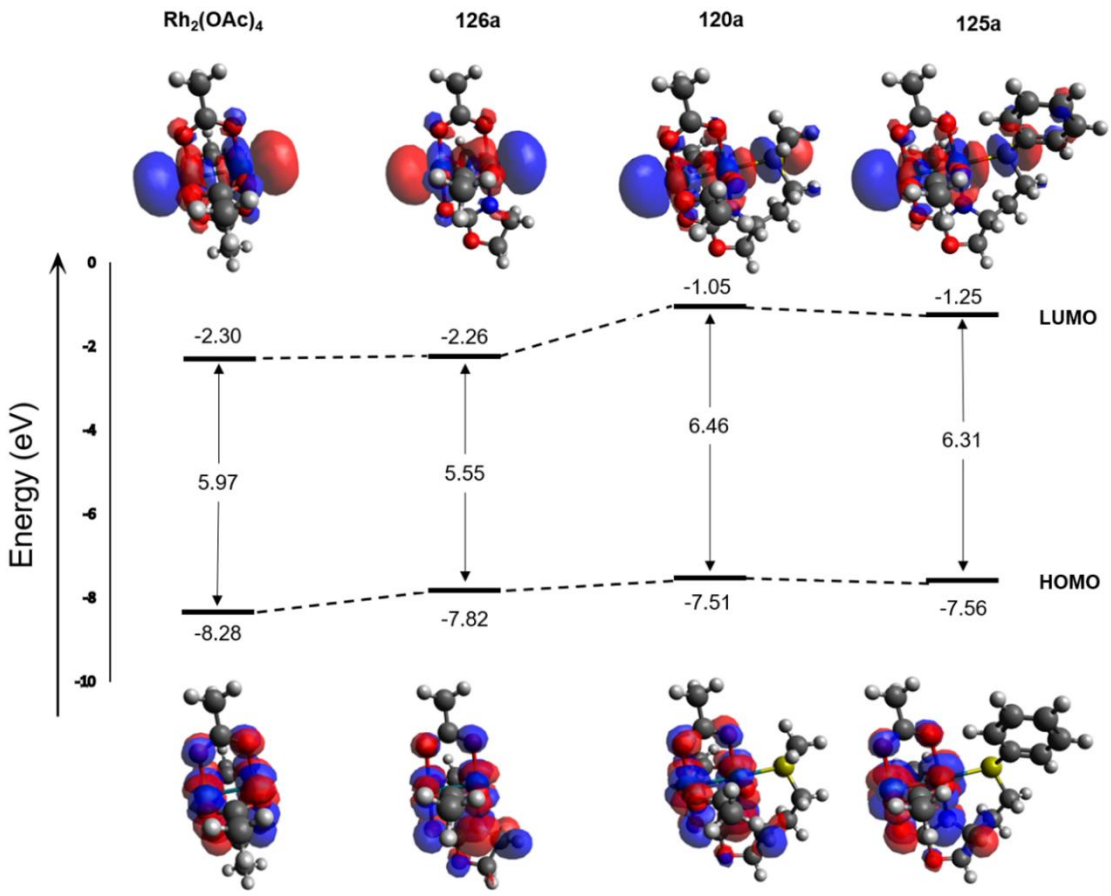

Figure 3.8 Calculations of the HOMO and LUMO energies of select Rh^{II} complexes with and without axial coordination.

weaker donor (aryl thioether of **125a**). The combined destabilization of the HOMO and LUMO results in an overall increase in the HOMO-LUMO gap, which agrees with experimental UV-Vis data (See Figure 2.21).

Although calculations on Rh^{II} catalysts have been conducted, very few examine axial coordination.[13, 83] One example, by Davies and co-workers, compared the reaction pathways of $Rh_2(OAc)_4$ and the *mono*-adduct $Rh_2(OAc)_4 \cdot OC(CH_3)_2$ in the cyclopropanation of styrene and a donor/acceptor diazo reagent.[225] This study showed that axial coordination resulted in a higher energy intermediate upon coordination of the diazo compound compared to intermediate generated from $Rh_2(OAc)_4$. Furthermore, the energy barrier for the extrusion of N_2 by $Rh_2(OAc)_4 \cdot OC(CH_3)_2$ was higher than the uncoordinated $Rh_2(OAc)_4$. It is believed that the axial coordination of the tethered thioether acts in a similar manner to $Rh_2(OAc)_4 \cdot OC(CH_3)_2$. This provides a reasonable explanation why the novel Rh^{II} catalysts proceeded more readily at elevated temperatures.

Further calculations were then conducted for the carbenoid species formed between EDA and $Rh_2(OAc)_4$, **126a**, **120a**, and **125a** (Figure 3.9). The LUMO of the carbenoid is primarily considered during the catalytic cycle because it undergoes nucleophilic attack by the olefin. Complexes **126a(EDA)** and **$Rh_2(OAc)_4$(EDA)** show the common 3c/4e π system which can stabilize the carbenoid. Alternatively, **120a(EDA)** and **125a(EDA)** indicate a disruption of the 3c/4e system. This is evidenced by a mixed electronic environment at the Rh core, with interactions of both π symmetry (Rh–C) and σ symmetry (Rh–S). It is possible this electronic mixing is the cause of the destabilization of the LUMO for complexes **120(EDA)** and **125(EDDA)**. Electronic mixing has been shown to result in the destabilization of the LUMO of other complexes with metal-metal bonds.[226] Both **120a(EDA)** and **125a(EDA)** do not show a dramatic increase in the LUMO energy compared to **126a(EDA)** (8.76 and 7.29 kcal/mol, respectively). However, this further supports that axial coordination can modulate the carbenoid LUMO energy.

A more notable difference is observed between the HOMOs of the Rh^{II} complexes. It is evident that the HOMO of **126a** comprises different orbitals than the HOMOs of **120a** and **125a**. The HOMOs of Rh^{II} carbenoids without axial coordination, **126a(EDA)** and **$Rh_2(OAc)_4$(EDA)**, do not have any electron density on the carbenoid carbon. Conversely, the HOMOs of carbenoids with axial coordination, **120a(EDA)** and **125a(EDA)**, show electron density localized on the carbon of the carbene. The examination of lower energy

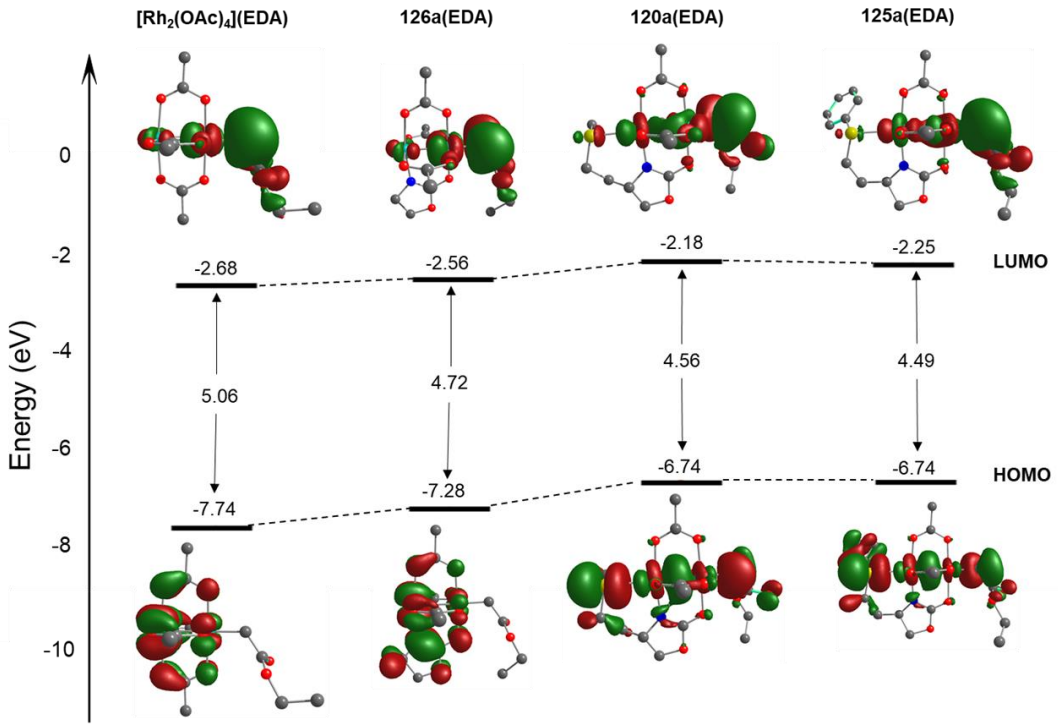

Figure 3.9 Calculated HOMO and LUMO energies of Rh^{II} carbenoids with and without axial coordination

orbitals of **126a(EDA)** shows that orbital with electron density on the carbene carbon is present as the HOMO -1 (Figure 3.10, a). This suggests that axial coordination results in destabilization of this orbital, which results in it then becoming the new HOMO. This is further supported by the HOMO -1 of **125a(EDA)** having the same orbital topology as the HOMO of **126a(EDA)** (Figure 3.10, b).

Based on the similar topologies of the LUMOs of each carbenoid species, it stands to reason that each will initially undergo this process. The nucleophilic olefin should readily attack the electrophilic carbene carbon. However, higher yields are clearly observed with the novel Rh^{II} catalysts compared to the control catalyst **126a**. Davies and co-workers calculated similar qualitative orbital topologies for carbenoids generated by Rh–Bi paddlewheel complexes and diazo methane.[227] It was stated that the localization of electron density on the carbene carbon should result in a more nucleophilic carbenoid. This theory provides a plausible explanation as to why axially coordinated complexes are more reactive than complexes without axial coordination. It is generally accepted for cyclopropanation to proceed via a concerted yet asynchronous process. This process is initiated by nucleophilic attack of the carbene by the olefin substrate. Based on the similar topologies of the LUMOs of each carbenoid species, it stands to reason that each will initially undergo this process. The formation of the cyclopropane ring could be more readily facilitated by complexes with axial coordination because the HOMO lies partially on the carbene carbon.

3.6 Conclusion

In conclusion, heteroleptic Rh^{II} complexes containing tethered thioether groups were applied as catalysts for the cyclopropanation of olefins. Both the acceptor diazo reagent EDA and the donor/acceptor diazo reagent methyl (4-nitro)phenyldiazo acetate underwent cyclopropanation with olefin substrates using the novel Rh^{II} catalysts. The novel catalysts demonstrated higher yields with acceptor diazo reagents than donor/acceptor diazo reagents, outcompeting the control catalysts. It was demonstrated that the length of the tether, in conjunction with donating strength, influences reactivity in both catalyst synthesis and catalytic reactions. It was demonstrated that the tethered thioether facilitated high yields as catalysts in the cyclopropanation of equimolar amounts of styrene with EDA. The observed reactivity did not correlate with the predicted donating

a)

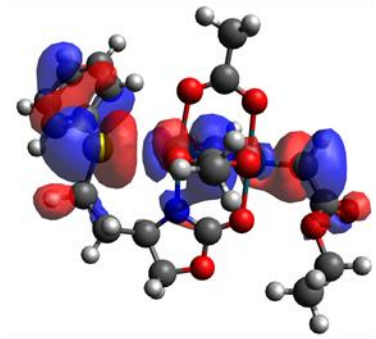

125a(EDA)
HOMO (-6.739 eV)

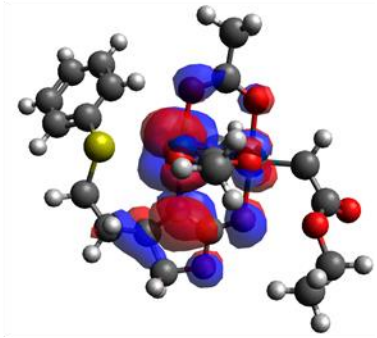

125a(EDA)
HOMO -1 (-7.429 eV)

b)

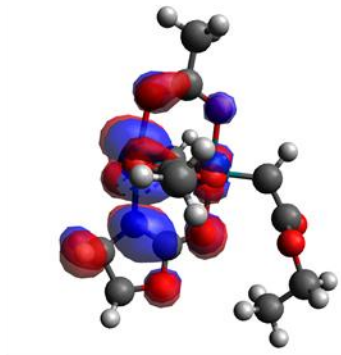

126a(EDA)
HOMO (-7.285 eV)

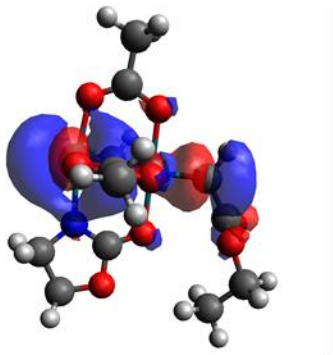

126a(EDA)
HOMO -1 (-7.429 eV)

Figure 3.10 Comparison of the HOMO and HOMO -1 between 1**25a** and **126a** carbenoids

strength of the thioether. Computational methods were then employed and indicate that the different HOMO orbitals of the tethered complexes may facilitate the formation of the cyclopropane ring, as a result of having a more electron rich carbene carbon.

Chapter 4 - Experimental Procedures

4.1 General Considerations

Unless otherwise noted, all reagents were used as received from the manufacturer without further purification. (S)-4-(2-(methylthio)ethyl)-2-oxazolidinone (**107**) and (R)-4-((methylthio)methyl)oxazolidin-2-one) (**118**) were both synthesized via procedures established in the literature.[188, 190] Methyl 2-diazo-2(4-nitrophenyl)acetate was prepared from 2-(4-nitrophenyl)acetic acid according to literature procedures.[228, 229] All products that had been previously synthesized were verified, using ^{1}H NMR, against that established in the literature. All reactions were carried out under a nitrogen atmosphere using Schlenk techniques unless otherwise specified. Hexanes, THF, diethyl ether, DCM, and MeCN were dried with columns packed with alumina using an Inert® PureSolv Micro Solvent Purification System and stored over molecular sieves. Reactions were monitored using TLC on Sorbent Technologies Silica XG TLC Plates. Column chromatography was performed using 60 Å, 40-63 µm silica from Sorbent Technologies. ^{1}H and ^{13}C NMR spectra were recorded on a Varian Mercury Vx 300 MHz, Bruker 400 MHz, Varian VNMRS 500 MHz, or Varian VNMRS 600 MHz spectrometers. All NMR chemical shifts are reported in ppm on the δ (ppm) scale. Signals were referenced by residual solvent signal for ^{1}H NMR ($CHCl_3$ = 7.26 ppm, acetone = 2.05 ppm, MeCN = 1.94 ppm, DMSO = 2.50 ppm) and ^{13}C NMR ($CHCl_3$ = 77.16 ppm, acetone = 206.26 ppm, MeCN = 1.32 ppm, DMSO = 39.52 ppm). Cyclic voltammetry experiments were performed inside an N_2-filled electrochemical cell in MeCN with 0.1 M [TBA][PF_6] as the supporting electrolyte. Anhydrous MeCN and electrochemical grade [TBA][PF_6] were purchased from SigmaAldrich and used as received. The voltammograms were recorded with a BASi Epsilon potentiostat, using a 2.5 mm (o.d.) 1.0 mm (i.d.) Pt-disk working electrode, Ag-wire quasi-reference electrode, and a Pt wire auxiliary electrode. Reported potentials are referenced to the Fc/Fc^{+} redox couple, added as an internal standard at the conclusion of each experiment. The mass spectra for compounds **113**-**116** were obtained using an AccuTOF Mass spectrometer equipped with a DART ionization apparatus. The mass spectra for **120a** and **120b/c** were obtained using an Exactive Plus OrbitrapTM Mass Spectrometer (Thermo Scientific, San Jose, CA, USA) via direct injection. Finally, the mass spectra for complexes **121a**, **123a**, and **125a** were obtained using a Water SYNAPT

G2-*Si* MALDI-TOF Mass Spectrometer. The matrix consisted of 2,5-dihydroxybenzoic acid with 1% trifluoroacetic acid as a cationization agent. Samples consisted of an analyte:matrix ratio of 1:1. The sample spot size was 1 µL of this mixture and was analyzed under the positive ionization mode. Each sample was scanned 100 times over the course of 100 seconds. X-ray diffraction experiments were conducted using a Bruker APEX-II CCD diffractometer and solved with OLEX2.[230] UV-Visible data was obtained in a 10mm quartz cell using a Cary 5000 spectrophotometer. Elemental analysis was conducted by Atlanta Microlabs.

4.2 Ligand Synthesis

(R)-4-((tert-butylthio)methyl)oxazolidin-2-one (113)

To a flame dried 5 mL flask, equipped with a stir bar, was added compound **112** (0.16 g, .60 mmol) and ^{t}Bu thiol (.13 mL, 1.1 mmol). The reagents were then dissolved in 6 mL acetone and heated to 45 °C for 24 hours. The reaction was then filtered, and the filtrate was concentrated *in vacuo*. This mixture was then purified by column chromatography (25% EtOAc/Hexanes to 50% EtOAc/Hexanes) to afford **119** as a pale-yellow oil (47 mg, 0.25 mmol, 42% yield). ^{1}H NMR (300 MHz, Chloroform-*d*) δ 5.33 (s, 1H), 4.58 – 4.47 (m, 1H), 4.15 (dd, *J* = 8.9, 5.1 Hz, 1H), 4.01 – 3.88 (m, 1H), 2.76 – 2.62 (m, 2H), 1.33 (s, 9H). Calculated *m/z*: $[M+H]^+$ = 204.1014, found m/z: $[M+H]^+$ = 204.1069

(*S*)-4-(2-(phenylthiol)oxazolidin-2-one (114)

To a flame dried 5 mL flask, equipped with a stir bar, was added compound **112** (0.10 g, 0.36 mmol), followed by thiophenol (1.5 mL, .54 mmol). The reagents were then dissolved in 1 mL acetone and set to reflux for four hours. Having concentrated the reaction *in vacuo*, the resultant mixture was dissolved in 2 mL DI water and extracted twice with 2 mL DCM. The organic was washed with brine (1 X 1 mL) and saturated sodium bicarbonate solution (1 X 1 mL). The organic layer was then dried over anhydrous sodium sulfate and concentrated. This mixture was then purified by column chromatography (2.5% MeOH/DCM) to afford **114** as a yellow oil (68 mg, 0.29 mmol, 84% yield). ^{1}H NMR (500 MHz, Chloroform-*d*) δ 7.38 – 7.21 (m, 4H), 5.73 – 5.65 (m, 1H), 4.55 – 4.47 (m, 1H), 4.09 – 3.99 (m, 2H), 2.97 (td, *J* = 7.0, 2.5 Hz, 2H), 1.99 – 1.83 (m, 2H). ^{13}C NMR (126 MHz, Chloroform-*d*) δ 159.18, 134.88, 129.88, 129.20, 126.79, 51.63, 34.33, 30.21. Calculated

m/z: $[M+H]^+$ = 224.0701, found m/z: $[M+H]^+$ = 224.0691

(S)-4-(2-((4-methoxyphenyl)thio)ethyl)oxazolidin-2-one (115)

Compound **112** (0.43 g, 1.5 mmol) was added to a flame dried, 5 mL, flask equipped with a stir bar. 4-methoxybenzenethiol (1.5 mL, 13 mmol) was then added before dissolving the reagents in 6 mL acetone. The reaction was then heated to 45 °C for 24 hours before being concentrated *in vacuo*. The resultant mixture was dissolved in 10 mL DI water and extracted DCM (2 X 5 mL). The organic was washed with brine solution (1 X5 mL) and saturated sodium bicarbonate solution (1 X 5 mL) before being dried with anhydrous sodium sulfate. Having removed the solvent, the mixture was further purified by column chromatography (25% EtOAc/Hexanes to 50% EtOAc/Hexanes) to afford **115** as a pale-yellow oil (0.1181 g, 0.58 mmol, 39% yield). ^{1}H NMR (500 MHz, Chloroform-*d*) δ 7.37 – 7.33 (m, 2H), 6.88 – 6.84 (m, 2H), 5.43 (s, 1H), 4.51 – 4.46 (m, 1H), 4.06 – 3.97 (m, 2H), 3.81 (s, 3H), 2.86 (t, *J* = 7.0 Hz, 2H), 1.90 – 1.79 (m, 2H). ^{13}C NMR (126 MHz, Chloroform-*d*) δ 159.43, 133.76, 124.86, 114.88, 69.95, 55.36, 51.65, 34.41, 32.30.

(S)-4-(2-((2,3,5,6-tetrafluorophenyl)thio)ethyl)oxazolidin-2-one (116)

To a flame dried 5 mL flask, equipped with a stir bar, was added compound **112** (0.43 g, 1.5 mmol) followed by 2,3,5,6-tetrafluorobenzenethiol (1.5 mL, 13 mmol). The reagents were then dissolved in 6 mL acetone and heated to 45 °C for 24 hours. The reaction was then concentrated *in vacuo*. The resultant mixture was dissolved in 10 mL DI water and extracted twice with 5 mL DCM. The organic was washed with 5 mL brine solution and 5 mL saturated sodium bicarbonate solution. The organic was then dried with anhydrous sodium sulfate and concentrated. This mixture was then purified by column chromatography (25% EtOAc/Hexanes to 50% EtOAc/Hexanes) to afford **116** as a pale-yellow oil (0.1181 g, 0.58 mmol, 39% yield). ^{1}H NMR (500 MHz, Chloroform-*d*) δ 7.07 (tt, *J* = 9.5, 7.3 Hz, 1H), 6.71 (s, 1H), 4.52 (t, *J* = 8.2 Hz, 1H), 4.11 – 4.00 (m, 2H), 3.06 – 2.90 (m, 2H), 1.93 – 1.73 (m, 2H). ^{13}C NMR (126 MHz, Chloroform-*d*) δ 148.11 – 147.87 (m), 147.12 (ddd, *J* = 15.0, 10.4, 4.2 Hz), 146.13 – 145.89 (m), 145.12 (ddd, *J* = 15.2, 10.4, 4.3 Hz), 114.26 (t, *J* = 20.0 Hz), 106.62 (t, *J* = 22.8 Hz). ^{19}F NMR (470 MHz, Chloroform-*d*) δ -133.63 – -133.83 (m), -137.51 – -137.72 (m). Calculated *m/z*: $[M+H]^+$ = 296.0290, found m/z: $[M+H]^+$= 296.0627.

4.3 Complex Synthesis

General Soxhlet Procedure. The following reaction was modified from past methods developed by Doyle.[76] To a three-neck round bottom flask, fitted with a Soxhlet apparatus with a thimble containing an oven-dried 5% sand/sodium carbonate mixture, was added to the desired ligand (1 eq) and $Rh_2(OAc)_4$ (48 mg, 0.30 mmol). Dry PhCl (25 mL) was added via a syringe to dissolve the reagents. The reaction was refluxed for six hours, allowed to cool, and concentrated in vacuo. The mixture was then dissolved in methanol and any insoluble material was filtered. The filtrate afforded a mixture of substitution products which were concentrated in vacuo and separated by column chromatography (1:1 MeCN/toluene).

General Solvothermal Procedure. To a flame dried 25 mL Youngs tube charged with $Rh_2(OAc)_4$ (48 mg, 0.30 mmol) was added the ligand (1 eq) and DCE (13 mL). The reaction was then heated in an oil bath set to 115 °C until a back pressure was observed, and the tube was sealed with a Teflon tap. The reaction was monitored by TLC and upon the formation of the *bis*-substituted product, the reaction was allowed to cool. The reaction was transferred to a flask and concentrated in vacuo. The *mono*-substituted product was removed by column chromatography (1:1 MeCN/toluene). The remaining fractions were combined, concentrated, and transferred back to the Youngs tube with THF. The sample was concentrated and fresh DCE (13 mL) was added to the flask. This constituted one cycle and was repeated for future cycles.

General Microwave Procedure. All microwave reactions were conducted using a Biotage Initiator+ microwave reactor. Variable power was applied, up to 400W, to maintain the set temperature which was measured using an IR sensor. Hold time indicates the amount of time the reaction was maintained at the set temperature and does not include the time required to reach the set temperature. A 2-5 mL microwave vial, equipped with a magnetic stir bar, was charged with $Rh_2(OAc)_4$ (15 mg, 34 mmol) and the desired ligand (34 mmol). The edges of the flask were rinsed with 4 mL of solvent. The vial was then capped and run under the conditions outlined in Table 3.2 under normal absorbance. The product distribution for the optimization of the ligand exchange reaction with ligand **107** was quantified via HPLC using 75% 1:1 MeCN:MeOH with 0.1% TFA/25% water with

0.1%TFA on a C_{18} column. Compounds **120b** and **120c** eluted together. Calibration curves were generated for **120a**, **120b/c**, and $Rh_2(OAc)_4$. The yields for complexes **121**-**125** and **126a** were determined after isolation of the material by column chromatography ((1:1 MeCN/toluene).

$Rh_2(OAc)_3$MeTOX·MeCN (120a)

^{1}H NMR (500 MHz, $CDCl_3$/CD_3CN) δ 4.31 (s, 1H), 3.62 (s, 2H), 3.04 (s, 2H), 2.55 (s, 3H), 1.96 (ddd, *J* = 4.9, 2.4, 0.8 Hz, 1H), 1.94 (s, 3H), 1.86 (m, *J* = 9.7, 5.1 Hz, 1H), 1.83 (s, 3H), 1.81 (s, 3H). ^{13}C NMR (126 MHz, $CDCl_3$/CD_3CN) δ 191.91, 191.36, 190.90, 168.37, 69.73, 59.30, 35.64, 30.30, 23.82, 23.76, 23.28, 17.90 ppm. Calculated *m/z*: $[M+H]^+$ = 543.9019, found *m/z*: $[M+H]^+$ = 543.9011. Anal. Calcd for $C_{14}H_{22}N_2O_8$ Rh_2S: C, 28.78; H, 3.80; N, 4.80; S, 5.49. Found: C, 28.62; H, 3.71; N, 4.30; S, 5.39.

$Rh_2(OAc)_2(MeTOX)_2$ (120b/c)

Compounds **120b** and **120c** were isolated together as a red solid (8.5 mg, 12 % yield) ^{1}H NMR (400 MHz, CDCl3) δ 4.33 – 4.23 (m, 1H), 3.76 – 3.53 (m, 2H), 3.23 (dd, J = 13.3, 5.5, 2.1 Hz, 1H), 3.11 – 3.04 (m, 1H), 2.98 (td, J = 13.2, 12.5, 2.6 Hz, 1H), 2.62 (s, J = 8.6 Hz, 3H), 2.09 – 1.70 (m, 6H). ^{13}C NMR (101 MHz, Chloroform-d) δ 192.09, 191.77, 140.34, 135.25, 132.44, 131.66, 129.49, 128.98, 128.67, 128.52, 126.17, 54.57, 48.65, 28.36, 23.99. Calculated m/z: [M+H]+ = 644.9319, found m/z: [M+H]+ = 644.9269. Anal. Calcd for $C_{16}H_{26}N_2O_8Rh_2S_2$: C, 29.83; H, 4.08; N, 4.35; S, 9.96. Found: C, 29.20; H, 3.94; N, 4.18; S, 9.47.

***trans*-$Rh_2(OAc)_2(MeTOX)_2$ (120c)**

^{1}H NMR (500 MHz, Chloroform-*d*) δ 4.30 (t, *J* = 7.7 Hz, 1H), 3.66 (dd, *J* = 11.1, 7.6 Hz, 1H), 3.59 (m, *J* = 11.2, 9.7, 7.8, 1.6 Hz, 1H), 3.13 – 3.02 (m, 2H), 2.61 (s, 3H), 2.02 – 1.84 (m, 2H), 1.90 (s, 3H). ^{13}C NMR (126 MHz, Chloroform-*d*) δ 190.27, 167.77, 69.58, 59.69, 35.64, 30.75, 29.85, 23.68, 17.73, 1.16.

$Rh_2(OAc)_3$SerMeTOX (121a)

^{1}H NMR (500 MHz, Chloroform-*d*) δ 4.69 (t, *J* = 8.0 Hz, 1H), 4.11 (m, *J* = 11.4, 10.2, 7.8, 3.5 Hz, 1H), 3.98 (dd, *J* = 10.4, 8.2 Hz, 1H), 2.86 (dd, *J* = 12.2, 3.5 Hz, 1H), 2.55 (s, 3H),

2.26 (t, *J* = 12.0 Hz, 1H), 2.03 (s, 3H), 1.84 (d, *J* = 5.4 Hz, 6H).^{13}C NMR (126 MHz, Chloroform-*d*) δ 192.49, 192.22, 191.04, 168.35, 72.96, 59.70, 41.16, 24.27, 24.18, 23.77, 16.27. Calculated *m/z*: $[M+H]^+$ = 529.8863, found m/z: $[M+H]^+$= 529.3375. Anal. Calcd for $C_{11}H_{17}NO_8Rh_2S$: C, 24.97; H, 3.25; N,2.65; S, 6.06. Found: C, 29.71; H, 4.26; N, 2.74.

$Rh_2(OAc)_3$(^{t}BuTOX) (123a)

^{1}H NMR (500 MHz, Chloroform-*d*) δ 4.45 – 4.39 (m, 1H), 3.76 – 3.65 (m, 1H), 3.11 (ddd, *J* = 12.7, 5.4, 2.7 Hz, 1H), 2.97 (td, *J* = 12.4, 3.0 Hz, 1H), 2.11 (dddd, *J* = 14.7, 5.4, 3.0, 1.3 Hz, 1H), 1.99 (s, 3H), 1.87 (s, 3H), 1.84 (s, 3H), 1.84 – 1.76 (m, 1H), 1.66 (s, 10H). ^{13}C NMR (126 MHz, Chloroform-*d*) δ 190.82, 190.79, 189.00, 167.23, 70.04, 58.95, 49.59, 31.96, 29.15, 29.03, 24.07, 23.90, 23.34. Calculated *m/z*: $[M+H]^+$ = 585.9489 , found m/z: $[M+H]^+$ 585.9444. Anal. Calcd for $C_{15}H_{25}NO_8Rh_2S$: C, 30.79; H, 4.31; N, 2.39; S, 5.48. Found: C, 32.80; H, 4.79; N, 2.42; S, 5.18.

$Rh_2(OAc)_3$(PhTOX) (125a)

^{1}H NMR (500 MHz, Chloroform-*d*) δ 7.93 – 7.89 (m, 2H), 7.44 – 7.40 (m, 3H), 4.45 – 4.38 (m, 1H), 3.83 – 3.73 (m, 2H), 3.55 (ddd, *J* = 13.1, 5.8, 2.3 Hz, 1H), 3.37 (ddd, *J* = 13.1, 11.8, 2.5 Hz, 1H), 2.18 (dddd, *J* = 14.8, 6.0, 2.6, 1.4 Hz, 1H), 2.02 (dddd, *J* = 14.6, 12.1, 9.9, 2.4 Hz, 1H), 1.96 (s, 3H), 1.88 (s, 3H), 1.81 (s, 3H). ^{13}C NMR (126 MHz, Chloroform-*d*) δ 191.27, 190.97, 189.55, 167.73, 133.00, 131.05, 129.04, 128.54, 69.89, 59.09, 37.26, 31.16, 23.94, 23.91, 23.35. Calculated *m/z*: $[M+H]^+$ = 605.9176 , found m/z: $[M+H]^+$ 605.9180. Anal. Calcd for $C_{17}H_{21}NO_8Rh_2S$: C, 33.74; H, 3.50; N,2.32; S, 5.30. Found: C, 37.79; H, 4.40; N, 2.51.

4.4 Catalytic Reactions

General Procedure for the Cyclopropanation of 1 Equivalent of Styrene. Under an atmosphere of N_2, a 25 mL Schlenk flask equipped with a magnetic stir bar was flame dried and charged with styrene (0.19 mL, 1.7 mmol, 1.0 equiv.), catalyst (2 mol%), and DCE (0.5 mL). The solution was then brought to the desired temperature, followed by slow addition of ethyl diazoacetate (1.7 mL, 0.17 mmol, 1.0 equiv.) by a syringe pump (1 mL/hr). Once the addition was complete, 16.54 μL of mesitylene standard was added to the

reaction mixture and stirred. The solution was then eluted through a Nylon66 0.2 μm syringe filter into a 2 mL glass GC vial. Yields and diastereoselectivity were determined by gas chromatography using a multiple point internal standard of the cyclopropyl product and mesitylene as the internal standard.[231]

General Procedure for the Cyclopropanation of 5 Equivalents of Olefin Substrates. Under an atmosphere of N_2, a 25 mL Schlenk flask equipped with a magnetic stir bar was flame dried and charged with an olefin (8.5 mmol, 5.0 equiv.), **125a** (2 mol%), and DCE (0.5 mL). The solution was then brought to the desired temperature, followed by slow addition of ethyl diazoacetate (1.7 mL, 0.17 mmol, 1.0 equiv.) by a syringe pump (1 mL/hr). After the addition was complete, the reaction solution was filtered through a 1.5-inch silica plug and eluted with 4 mL of DCM. The eluent was then concentrated *in vacuo* with a rotary evaporator. 10 μL of mesitylene was then added as an internal standard for ^{1}H NMR determination of cyclopropane product yield and diastereoselectivity.

Cyclopropanation of Olefin Substrates at 5 Equivalents: ^{1}H NMR Yield Calculations. Yields and diastereoselectivities for each cyclopropanation were calculated using ^{1}H NMR and mesitylene as an internal standard. Normalized integration of the methyl protons of mesitylene (2.26 ppm) was compared to the integration of the diastereotopic protons of the methylene unit of the cyclopropane for the *cis* (2.06 ppm) and *trans* (1.90 ppm) isomers to give the total yield of the cyclopropyl product.

List of References

1. Gagnon, A.; Duplessis, M.; Fader, L., Arylcyclopropanes: properties, synthesis and use in medicinal chemistry. *Org. Prep. Proced. Int.* **2010,** *42* (1), 1-69.
2. Brackmann, F.; de Meijere, A., Natural occurrence, syntheses, and applications of cyclopropyl-group-containing α-amino acids. 1. 1-aminocyclopropanecarboxylic acid and other 2,3-methanoamino acids. *Chem. Rev.* **2007,** *107* (11), 4493-4537.
3. Časar, Z., Synthetic approaches to contemporary drugs that contain the cyclopropyl moiety. *Synthesis* **2020,** *52* (9), 1315-1345.
4. Salaün, J., Cyclopropane derivatives and their diverse biological activities. In *Small Ring Compounds in Organic Synthesis VI*, de Meijere, A., Ed. Springer Berlin Heidelberg: Berlin, Heidelberg, 2000; pp 1-67.
5. Bartoli, G.; Bencivenni, G.; Dalpozzo, R., Asymmetric cyclopropanation reactions. *Synthesis* **2014,** *46* (8), 979-1029.
6. Pellissier, H., Recent developments in asymmetric cyclopropanation. *Tetrahedron* **2008,** *64* (30-31), 7041-7095.
7. Lebel, H.; Marcoux, J.-F.; Molinaro, C.; Charette, A. B., Stereoselective cyclopropanation reactions. *Chem. Rev.* **2003,** *103* (4), 977-1050.
8. Chen, D. Y. K.; Pouwer, R. H.; Richard, J.-A., Recent advances in the total synthesis of cyclopropane-containing natural products. *Chem. Soc. Rev.* **2012,** *41* (13), 4631-4642.
9. Donaldson, W. A., Synthesis of cyclopropane containing natural products. *Tetrahedron* **2001,** *57* (41), 8589-8627.
10. Ebner, C.; Carreira, E. M., Cyclopropanation strategies in recent total syntheses. *Chem. Rev.* **2017,** *117* (18), 11651-11679.
11. von E. Doering, W.; Buttery, R. G.; Laughlin, R. G.; Chaudhuri, N., Indiscriminate reaction of methylene with the carbon-hydrogen bond. *J. Am. Chem. Soc.* **1956,** *78* (13), 3224-3224.
12. Wei, Y.; Tinoco, A.; Steck, V.; Fasan, R.; Zhang, Y., Cyclopropanations via heme carbenes: basic mechanism and effects of carbene substituent, protein axial ligand, and porphyrin substitution. *J. Am. Chem. Soc.* **2018,** *140* (5), 1649-1662.
13. Nowlan, D. T.; Gregg, T. M.; Davies, H. M. L.; Singleton, D. A., Isotope effects and the nature of selectivity in rhodium-catalyzed cyclopropanations. *J. Am. Chem. Soc.* **2003,** *125* (51), 15902-15911.
14. Straub, B. F.; Gruber, I.; Rominger, F.; Hofmann, P., Mechanism of copper(I)-catalyzed cyclopropanation: a DFT study calibrated with copper(I) alkene complexes. *J. Organomet. Chem.* **2003,** *684* (1), 124-143.
15. Straub, B. F., Pd(0) mechanism of palladium-catalyzed cyclopropanation of alkenes by CH_2N_2: a DFT Study. *J. Am. Chem. Soc.* **2002,** *124* (47), 14195-14201.
16. Doyle, M. P., Exceptional selectivity in cyclopropanation reactions catalyzed by chiral cobalt(II)–porphyrin catalysts. *Angew. Chem., Int. Ed.* **2009,** *48* (5), 850-852.

17. Doyle, M. P., Catalytic methods for metal carbene transformations. *Chem. Rev.* **1986,** *86* (5), 919-939.
18. Gillingham, D.; Fei, N., Catalytic X–H insertion reactions based on carbenoids. *Chem. Soc. Rev.* **2013,** *42* (12), 4918-4931.
19. Davies, H. M. L., Finding opportunities from surprises and failures. Development of rhodium-stabilized donor/acceptor carbenes and their application to catalyst-controlled C–H functionalization. *J. Org. Chem.* **2019,** *84* (20), 12722-12745.
20. Hansen, J.; Autschbach, J.; Davies, H. M. L., Computational study on the selectivity of donor/acceptor-substituted rhodium carbenoids. *J. Org. Chem.* **2009,** *74* (17), 6555-6563.
21. Chen, P.-A.; Setthakarn, K.; May, J. A., A binaphthyl-based scaffold for a chiral dirhodium(II) biscarboxylate ligand with α-quaternary carbon centers. *ACS Catal.* **2017,** *7* (9), 6155-6161.
22. Ford, A.; Miel, H.; Ring, A.; Slattery, C. N.; Maguire, A. R.; McKervey, M. A., Modern organic synthesis with α-diazocarbonyl compounds. *Chem. Rev.* **2015,** *115* (18), 9981-10080.
23. Doyle, M. P.; Forbes, D. C., Recent advances in asymmetric catalytic metal carbene transformations. *Chem. Rev.* **1998,** *98* (2), 911-935.
24. Caballero, A.; Prieto, A.; Diaz-Requejo, M. M.; Perez, P. J., Metal-catalyzed olefin cyclopropanation with ethyl diazoacetate: control of the diastereoselectivity. *Eur. J. Inorg. Chem.* **2009,** (9), 1137-1144.
25. Gurmessa, G.; Singh, G., Recent progress in insertion and cyclopropanation reactions of metal carbenoids from α-diazocarbonyl compounds. *Res. Chem. Intermed.* **2017,** *43* (11), 6447-6504.
26. Wu, W.; Lin, Z.; Jiang, H., Recent advances in the synthesis of cyclopropanes. *Org. Biomol. Chem.* **2018,** *16* (40), 7315-7329.
27. Herndon, J. W., The chemistry of the carbon-transition metal double and triple bond: annual survey covering the year 2018. *Coord. Chem. Rev.* **2019,** *401*, 213051.
28. Herndon, J. W., The chemistry of the carbon-transition metal double and triple bond: annual survey covering the year 2017. *Coord. Chem. Rev.* **2018,** *377*, 86-190.
29. Herndon, J. W., The chemistry of the carbon-transition metal double and triple bond: annual survey covering the year 2016. *Coord. Chem. Rev.* **2018,** *356*, 1-114.
30. Doyle, M. P.; Dorow, R. L.; Buhro, W. E.; Griffin, J. H.; Tamblyn, W. H.; Trudell, M. L., Stereoselectivity of catalytic cyclopropanation reactions - catalyst dependence in reactions of ethyl diazoacetate with alkenes. *Organometallics* **1984,** *3* (1), 44-52.
31. Alexakis, A.; Krause, N.; Woodward, S., *Copper-Catalyzed Asymmetric Synthesis*. John Wiley & Sons, Incorporated: Weinheim, Germany, 2014.

32. Nozaki, H.; Moriuti, S.; Takaya, H.; Noyori, R., Asymmetric induction in carbenoid reaction by means of a dissymmetric copper chelate. *Tetrahedron Lett.* **1966,** *7* (43), 5239-5244.
33. Aratani, T.; Yoneyoshi, Y.; Nagase, T., Asymmetric synthesis of chrysanthemic acid. An application of copper carbenoid reaction. *Tetrahedron Lett.* **1977,** *18* (30), 2599-2602.
34. Aratani, T., Catalytic asymmetric synthesis of cyclopropanecarboxylic acids: an application of chiral copper carbenoid reaction. *Pure Appl. Chem.* **1985,** *57* (12), 1839-1844.
35. Kahan, F. M.; Kropp, H.; Sundelof, J. G.; Birnbaum, J., Thienamycin: development of imipenem-cilastatin. *J. Antimicrob. Chemother.* **1983,** *12* (suppl_D), 1-35.
36. Fritschi, H.; Leutenegger, U.; Pfaltz, A., Semicorrin metal complexes as enantioselective catalysts. Part 2. Enantioselective cyclopropane formation from olefins with diazo compounds catalyzed by chiral (semicorrinato)copper complexes. *Helv. Chim. Acta* **1988,** *71* (6), 1553-1565.
37. Hargaden, G. C.; Guiry, P. J., Recent applications of oxazoline-containing ligands in asymmetric catalysis. *Chem. Rev.* **2009,** *109* (6), 2505-2550.
38. Desimoni, G.; Faita, G.; Jørgensen, K. A., C_2-Symmetric chiral bis(oxazoline) ligands in asymmetric catalysis. *Chem. Rev.* **2006,** *106* (9), 3561-3651.
39. Lowenthal, R. E.; Abiko, A.; Masamune, S., Asymmetric catalytic cyclopropanation of olefins: bis-oxazoline copper complexes. *Tetrahedron Lett.* **1990,** *31* (42), 6005-6008.
40. Leutenegger, U.; Umbricht, G.; Fahrni, C.; von Matt, P.; Pfaltz, A., 5-Aza-semicorrins: a new class of bidentate nitrogen ligands for enantioselective catalysis. *Tetrahedron* **1992,** *48* (11), 2143-2156.
41. Lattanzi, A.; Dalpozzo, R.; Pellissier, H., *Asymmetric Synthesis of Three-Membered Rings*. John Wiley & Sons, Incorporated: Newark, Germany, 2017.
42. Roy, A.; Goswami, S. P.; Sarkar, A., Transition metal catalyzed asymmetric cyclopropanation via diazo decomposition: ligand architecture defining stereoselectivity. *Synth. Commun.* **2018,** *48* (16), 2003-2036.
43. Aguado-Ullate, S.; Urbano-Cuadrado, M.; Villalba, I.; Pires, E.; García, J. I.; Bo, C.; Carbó, J. J., Predicting the enantioselectivity of the copper-catalysed cyclopropanation of alkenes by using quantitative quadrant-diagram representations of the catalysts. *Chem. Eur. J.* **2012,** *18* (44), 14026-14036.
44. Bellemin-Laponnaz, S.; Gade, L. H., A modular approach to C_1 and C_3 chiral N-tripodal ligands for asymmetric catalysis. *Angew. Chem., Int. Ed.* **2002,** *41* (18), 3473-3475.
45. Xu, Z.-H.; Zhu, S.-N.; Sun, X.-L.; Tang, Y.; Dai, L.-X., Sidearm effects in the enantioselective cyclopropanation of alkenes with aryldiazoacetates catalyzed by trisoxazoline/Cu(I). *Chem. Commun.* **2007,** (19), 1960-1962.

46. Lee, W.-S.; Yeung, C.-T.; Sham, K.-C.; Wong, W.-T.; Kwong, H.-L., Chiral copper–bipyridine complexes: synthesis, characterization and mechanistic studies on asymmetric cyclopropanation. *Polyhedron* **2011,** *30* (1), 178-186.
47. Ito, K.; Katsuki, T., Catalytic asymmetric cyclopropanation using copper complex of optically active bipyridine as a catalyst. *Tetrahedron Lett.* **1993,** *34* (16), 2661-2664.
48. Chelucci, G.; Loriga, G.; Murineddu, G.; Pinna, G. A., Design of a new class of chiral C_2-symmetric dipyridylmethane ligands and their application in asymmetric catalysis. *Tetrahedron Lett.* **2002,** *43* (47), 8599-8602.
49. Ito, K.; Tabuchi, S.; Katsuki, T., Synthesis of new chiral bipyridine ligands and their application to asymmetric cyclopropanation. *Synlett* **1992,** *1992* (7), 575-576.
50. Li, J.; Liao, S.-H.; Xiong, H.; Zhou, Y.-Y.; Sun, X.-L.; Zhang, Y.; Zhou, X.-G.; Tang, Y., Highly diastereo- and enantioselective cyclopropanation of 1,2-disubstituted alkenes. *Angew. Chem., Int. Ed.* **2012,** *51* (35), 8838-8841.
51. Deng, C.; Liu, H.-K.; Zheng, Z.-B.; Wang, L.; Yu, X.; Zhang, W.; Tang, Y., Copper-catalyzed enantioselective cyclopropanation of internal olefins with diazomalonates. *Org. Lett.* **2017,** *19* (21), 5717-5719.
52. Li, J.; Zheng, L.; Chen, H.; Wang, L.; Sun, X.-L.; Zhu, J.; Tang, Y., Highly enantioselective cyclopropanation of trisubstituted olefins. *Sci. China: Chem.* **2018,** *61* (5), 526-530.
53. Feng, L.-W.; Wang, P.; Wang, L.; Tang, Y., Copper(I)/SaBOX catalyzed highly diastereo- and enantio-selective cyclopropanation of *cis*-1,2-disubstituted olefins with α-nitrodiazoacetates. *Sci. Bull.* **2015,** *60* (2), 210-215.
54. Carreras, J.; Caballero, A.; Pérez, P. J., Enantio- and diastereoselective cyclopropanation of 1-alkenylboronates: synthesis of 1-boryl-2,3-disubstituted cyclopropanes. *Angew. Chem., Int. Ed.* **2018,** *57* (9), 2334-2338.
55. Talele, T. T., The “cyclopropyl fragment” is a versatile player that frequently appears in preclinical/clinical drug molecules. *J. Med. Chem.* **2016,** *59* (19), 8712-8756.
56. Konishi, S.; Mitani, Y.; Mori, N.; Takikawa, H.; Watanabe, H., First enantioselective synthesis of exiguamide, a nitrogen-containing spirocyclic sesquiterpene isolated from the marine sponge geodia exigua. *Tetrahedron* **2019,** *75* (5), 652-657.
57. Hosokawa, S.; Nakanishi, K.; Udagawa, Y.; Maeda, M.; Sato, S.; Nakano, K.; Masuda, T.; Ichikawa, Y., Total synthesis of exigurin: the Ugi reaction in a hypothetical biosynthesis of natural products. *Org. Biomol. Chem.* **2020,** *18* (4), 687-693.
58. Aoyagi, Y.; Yamazaki, A.; Nakatsugawa, C.; Fukaya, H.; Takeya, K.; Kawauchi, S.; Izumi, H., Salvileucalin B, a novel diterpenoid with an unprecedented rearranged neoclerodane skeleton from *salvia leucantha* cav. *Org. Lett.* **2008,** *10* (20), 4429-4432.
59. Levin, S.; Nani, R. R.; Reisman, S. E., Enantioselective total synthesis of (+)-salvileucalin B. *J. Am. Chem. Soc.* **2011,** *133* (4), 774-776.

60. Zhu, G.; Zhou, C.; Chen, S.; Fu, S.; Liu, B., Construction of BCDEF core of andilesin C. *Org. Lett.* **2019,** *21* (19), 7809-7812.
61. Zhang, D.; Song, H.; Qin, Y., Total synthesis of indoline alkaloids: a cyclopropanation strategy. *Acc. Chem. Res.* **2011,** *44* (6), 447-457.
62. Özüduru, G.; Schubach, T.; Boysen, M. M. K., Enantioselective cyclopropanation of indoles: construction of all-carbon quaternary stereocenters. *Org. Lett.* **2012,** *14* (19), 4990-4993.
63. Minuth, T.; Boysen, M. M. K., Carbohydrate-derived bis(oxazoline) ligand in the total synthesis of grenadamide. *Synthesis* **2010,** *2010* (16), 2799-2803.
64. Chen, S.; Rong, C.; Feng, P.; Li, S.; Shi, Y., Stereoselective construction of the tetracyclic core of cryptotrione. *Org. Biomol. Chem.* **2012,** *10* (29), 5518-5520.
65. Arora, R.; Kashyap, K.; Mittal, A.; Kakkar, R., Synthesis and reactions of diazoketones. *Org. Prep. Proced. Int.* **2019,** *51* (2), 103-146.
66. Rasika Dias, H. V.; Polach, S. A., An isolable, oxygen-coordinated silver(I) complex of dimethyl diazomalonate: synthesis and characterization of [HB(3,5-$(CF_3)_2Pz)_3$]Ag[$OC(OCH_3)]_2CN_2$ (where Pz = pyrazolyl). *Inorg. Chem.* **2000,** *39* (21), 4676-4677.
67. Urbano, J.; Belderraín, T. R.; Nicasio, M. C.; Trofimenko, S.; Díaz-Requejo, M. M.; Pérez, P. J., Functionalization of primary carbon−hydrogen bonds of alkanes by carbene insertion with a silver-based catalyst. *Organometallics* **2005,** *24* (7), 1528-1532.
68. Thompson, J. L.; Davies, H. M. L., Enhancement of cyclopropanation chemistry in the silver-catalyzed reactions of aryldiazoacetates. *J. Am. Chem. Soc.* **2007,** *129* (19), 6090-6091.
69. Wang, Z.; Xu, G.; Tang, S.; Shao, Y.; Sun, J., Catalyst-controlled selective alkylation/cyclopropanation of indoles with vinyl diazoesters. *Org. Lett.* **2019,** *21* (20), 8488-8491.
70. Fructos, M. R.; Belderrain, T. R.; de Frémont, P.; Scott, N. M.; Nolan, S. P.; Díaz-Requejo, M. M.; Pérez, P. J., A gold catalyst for carbene-transfer reactions from ethyl diazoacetate. *Angew. Chem., Int. Ed.* **2005,** *44* (33), 5284-5288.
71. Prieto, A.; Fructos, M. R.; Mar Díaz-Requejo, M.; Pérez, P. J.; Pérez-Galán, P.; Delpont, N.; Echavarren, A. M., Gold-catalyzed olefin cyclopropanation. *Tetrahedron* **2009,** *65* (9), 1790-1793.
72. Cao, Z.-Y.; Wang, X.; Tan, C.; Zhao, X.-L.; Zhou, J.; Ding, K., Highly stereoselective olefin cyclopropanation of diazooxindoles catalyzed by a C_2-symmetric spiroketal bisphosphine/Au(I) complex. *J. Am. Chem. Soc.* **2013,** *135* (22), 8197-8200.
73. Cao, Z.-Y.; Wang, W.; Liao, K.; Wang, X.; Zhou, J.; Ma, J., Catalytic enantioselective synthesis of cyclopropanes featuring vicinal all-carbon quaternary stereocenters with a CH_2F group; study of the influence of C–F···H–N interactions on reactivity. *Org. Chem. Front.* **2018,** *5* (20), 2960-2968.

74. Chu, Z.; Tang, Z.; Zhang, K.; Wang, L.; Li, W.; Wu, H.-H.; Zhang, J., Gold(I)-catalyzed enantioselective cyclopropanation of α-aryl diazoacetates with enamides. *Organometallics* **2019,** *38* (20), 4036-4042.
75. Rull, S. G.; Olmos, A.; Pérez, P. J., Gold-catalyzed ethylene cyclopropanation. *Beilstein J. Org. Chem.* **2019,** *15*, 67-71.
76. Doyle, M. P.; McKervey, M. A.; Ye, T., *Modern Catalytic Methods for Organic Synthesis with Diazo Compounds: from Cyclopropanes to Ylides*. Wiley: New York, 1998; p xvii, 652 p.
77. Pirrung, M. C.; Liu, H.; Morehead, A. T., Rhodium chemzymes: Michaelis−Menten kinetics in dirhodium(II) carboxylate-catalyzed carbenoid reactions. *J. Am. Chem. Soc.* **2002,** *124* (6), 1014-1023.
78. Anciaux, A. J.; Hubert, A. J.; Noels, A. F.; Petiniot, N.; Teyssie, P., Transition-metal-catalyzed reactions of diazo compounds .1. Cyclopropanation of double-bonds. *J. Org. Chem.* **1980,** *45* (4), 695-702.
79. Padwa, A.; Austin, D. J.; Price, A. T.; Semones, M. A.; Doyle, M. P.; Protopopova, M. N.; Winchester, W. R.; Tran, A., Ligand effects on dirhodium(II) carbene reactivities - highly effective switching between competitive carbenoid transformations. *J. Am. Chem. Soc.* **1993,** *115* (19), 8669-8680.
80. Doyle, M. P.; Loh, K.-L.; DeVries, K. M.; Chinn, M. S., Enhancement of stereoselectivity in catalytic cyclopropanation reactions. *Tetrahedron Lett.* **1987,** *28* (8), 833-836.
81. Berry, J. F., The role of three-center/four-electron bonds in superelectrophilic dirhodium carbene and nitrene catalytic intermediates. *Dalton Trans.* **2012,** *41* (3), 700-713.
82. Kornecki, K. P.; Briones, J. F.; Boyarskikh, V.; Fullilove, F.; Autschbach, J.; Schrote, K. E.; Lancaster, K. M.; Davies, H. M.; Berry, J. F., Direct Spectroscopic characterization of a transitory dirhodium donor-acceptor carbene complex. *Science* **2013,** *342* (6156), 351-354.
83. Nakamura, E.; Yoshikai, N.; Yamanaka, M., Mechanism of C–H bond activation/C–C bond formation reaction between diazo compound and alkane catalyzed by dirhodium tetracarboxylate. *J. Am. Chem. Soc.* **2002,** *124* (24), 7181-7192.
84. Cotton, F. A.; Murillo, C. A.; Walton, R. A., *Multiple Bonds Between Metal Atoms*. 3rd ed.; Springer Science and Business Media: New York, NY, 2005.
85. Doyle, M. P.; Dyatkin, A. B.; Protopopova, M. N.; Yang, C. I.; Miertschin, C. S.; Winchester, W. R.; Simonsen, S. H.; Lynch, V.; Ghosh, R., Enhanced enantiocontrol in catalytic metal carbene transformations with dirhodium(II) tetrakis[methyl 2-oxooxazolidin-4(*S*)-carboxylate], Rh_2(4*S*-MEOX)$_4$. *Recl. Trav. Chim. Pays-Bas* **1995,** *114* (4-5), 163-170.
86. Doyle, M. P.; Zhou, Q. L.; Simonsen, S. H.; Lynch, V., Dirhodium(II) tetrakis[alkyl 2-oxaazetidine-4(*S*)-carboxylates]. A new set of effective chiral catalysts for asymmetric intermolecular cyclopropanation reactions with diazoacetates. *Synlett* **1996,** (7), 697-698.

87. Müller, P.; Baud, C.; Ené, D.; Motallebi, S.; Doyle, M. P.; Brandes, B. D.; Dyatkin, A. B.; See, M. M., Enantioselectivity and *cis*/*trans*-selectivity in dirhodium(II)-catalyzed addition of diazoacetates to olefins. *Helv. Chim. Acta* **1995,** *78* (2), 459-470.
88. P. Doyle, M.; S. Peterson, C.; Zhou, Q.-L.; Nishiyama, H., Comparative evaluation of enantiocontrol for intramolecular cyclopropanation of diazoacetates with chiral Cu^{I}, Rh^{II} and Ru^{II} catalysts. *Chem. Commun.* **1997,** (2), 211-212.
89. Doyle, M. P.; Morgan, J. P.; Fettinger, J. C.; Zavalij, P. Y.; Colyer, J. T.; Timmons, D. J.; Carducci, M. D., "Matched/mismatched" diastereomeric dirhodium(II) carboxamidate catalyst pairs. Structure−selectivity correlations in diazo decomposition and hetero-Diels−Alder reactions. *J. Org. Chem.* **2005,** *70* (13), 5291-5301.
90. Doyle, M. P.; Winchester, W. R.; Hoorn, J. A. A.; Lynch, V.; Simonsen, S. H.; Ghosh, R., Dirhodium(II) tetrakis(carboxamidates) with chiral ligands. structure and selectivity in catalytic metal-carbene transformations. *J. Am. Chem. Soc.* **1993,** *115* (22), 9968-9978.
91. Doyle, M. P.; Winchester, W. R.; Simonsen, S. H.; Ghosh, R., Dirhodium(II) tetrakis[N,N-dimethyl-2-pyrrolidone-5(*S*)-carboxamide]. Structural effects on enantioselection in metal carbene transformations. *Inorg. Chim. Acta* **1994,** *220* (1-2), 193-199.
92. McKervey, M. A.; Ye, T., Asymmetric synthesis of substituted chromanones via C–H insertion reactions of α-diazoketones catalysed by homochiral rhodium(II) carboxylates. *J. Chem. Soc., Chem. Commun.* **1992,** (11), 823-824.
93. Davies, H. M. L.; Panaro, S. A., Effect of rhodium carbenoid structure on cyclopropanation chemoselectivity. *Tetrahedron* **2000,** *56* (28), 4871-4880.
94. Davies, H. M. L.; Bruzinski, P. R.; Lake, D. H.; Kong, N.; Fall, M. J., Asymmetric cyclopropanations by rhodium(II) N-(arylsulfonyl)prolinate catalyzed decomposition of vinyldiazomethanes in the presence of alkenes. Practical enantioselective synthesis of the four stereoisomers of 2-phenylcyclopropan-1-amino acid. *J. Am. Chem. Soc.* **1996,** *118* (29), 6897-6907.
95. Davies, H. M. L.; Rusiniak, L., Effect of catalyst on the diastereoselectivity of methyl phenyldiazoacetate cyclopropanations. *Tetrahedron Lett.* **1998,** *39* (48), 8811-8812.
96. Adly, F. G., On the structure of chiral dirhodium(II) carboxylate catalysts: stereoselectivity relevance and insights. *Catalysts* **2017,** *7* (11), 347.
97. Davies, H. M. L.; Morton, D., Guiding principles for site selective and stereoselective intermolecular C–H functionalization by donor/acceptor rhodium carbenes. *Chem. Soc. Rev.* **2011,** *40* (4), 1857-1869.
98. L. Davies, H. M., Dirhodium tetra(N-arylsulfonylprolinates) as chiral catalysts for asymmetric transformations of vinyl- and aryldiazoacetates. *Eur. J. Org. Chem.* **1999,** (10), 2459-2469.
99. Hashimoto, S.; Watanabe, N.; Ikegami, S., Dirhodium(II) tetra(triphenylacetate): a highly efficient catalyst for the site-selective

intramolecular C–H insertion reactions of alpha-diazo beta-keto esters. *Tetrahedron Lett.* **1992,** *33* (19), 2709-2712.
100. Briones, J. F.; Davies, H. M. L., Rh_2(S-PTAD)$_4$-catalyzed asymmetric cyclopropenation of aryl alkynes. *Tetrahedron* **2011,** *67* (24), 4313-4317.
101. Hashimoto, S.; Watanabe, N.; Ikegami, S., Enantioselective intramolecular C–H insertion reactions of alpha-diazo beta-keto-esters catalyzed by dirhodium(II) tetrakis[N-phthaloyl-(*S*)-phenylalaninate] - the effect of the substituent at the insertion site on enantioselectivity. *Synlett* **1994,** (5), 353-355.
102. Chepiga, K. M.; Qin, C. M.; Alford, J. S.; Chennamadhavuni, S.; Gregg, T. M.; Olson, J. P.; Davies, H. M. L., Guide to enantioselective dirhodium(II)-catalyzed cyclopropanation with aryldiazoacetates. *Tetrahedron* **2013,** *69* (27-28), 5765-5771.
103. Denton, J. R.; Cheng, K.; L. Davies, H. M., Stereoselective construction of nitrile-substituted cyclopropanes. *Chem. Commun.* **2008,** (10), 1238-1240.
104. Reddy, R. P.; Lee, G. H.; Davies, H. M. L., Dirhodium tetracarboxylate derived from adamantylglycine as a chiral catalyst for carbenoid reactions. *Org. Lett.* **2006,** *8* (16), 3437-3440.
105. Denton, J. R.; Sukumaran, D.; Davies, H. M. L., Enantioselective synthesis of trifluoromethyl-substituted cyclopropanes. *Org. Lett.* **2007,** *9* (14), 2625-2628.
106. Denton, J. R.; Davies, H. M. L., Enantioselective reactions of donor/acceptor carbenoids derived from α-aryl-α-diazoketones. *Org. Lett.* **2009,** *11* (4), 787-790.
107. Lindsay, V. N. G.; Lin, W.; Charette, A. B., Experimental evidence for the all-up reactive conformation of chiral rhodium(II) carboxylate catalysts: enantioselective synthesis of *cis*-cyclopropane α-amino acids. *J. Am. Chem. Soc.* **2009,** *131* (45), 16383-16385.
108. DeAngelis, A.; Boruta, D. T.; Lubin, J.-B.; Plampin, I. I. I. J. N.; Yap, G. P. A.; Fox, J. M., The chiral crown conformation in paddlewheel complexes. *Chem. Commun.* **2010,** *46* (25), 4541-4543.
109. Boruta, D. T.; Dmitrenko, O.; Yap, G. P. A.; Fox, J. M., Rh_2(S-PTTL)$_3$TPA-a mixed-ligand dirhodium(II) catalyst for enantioselective reactions of α-alkyl-α-diazoesters. *Chem. Sci.* **2012,** *3* (5), 1589-1593.
110. Lindsay, V. N. G.; Fiset, D.; Gritsch, P. J.; Azzi, S.; Charette, A. B., Stereoselective Rh_2(S-IBAZ)$_4$-catalyzed cyclopropanation of alkenes, alkynes, and allenes: asymmetric synthesis of diacceptor cyclopropylphosphonates and alkylidenecyclopropanes. *J. Am. Chem. Soc.* **2013,** *135* (4), 1463-1470.
111. Qin, C.; Boyarskikh, V.; Hansen, J. H.; Hardcastle, K. I.; Musaev, D. G.; Davies, H. M. L., D_2-symmetric dirhodium catalyst derived from a 1,2,2-triarylcyclopropanecarboxylate ligand: design, synthesis and application. *J. Am. Chem. Soc.* **2011,** *133* (47), 19198-19204.
112. Wei, B.; Sharland, J. C.; Lin, P.; Wilkerson-Hill, S. M.; Fullilove, F. A.; McKinnon, S.; Blackmond, D. G.; Davies, H. M. L., In situ kinetic studies of

Rh(II)-catalyzed asymmetric cyclopropanation with low catalyst loadings. *ACS Catal.* **2020,** *10* (2), 1161-1170.
113. Fu, J.; Wurzer, N.; Lehner, V.; Reiser, O.; Davies, H. M. L., Rh(II)-catalyzed monocyclopropanation of pyrroles and its application to the synthesis pharmaceutically relevant compounds. *Org. Lett.* **2019,** *21* (15), 6102-6106.
114. Lehner, V.; Davies, H. M. L.; Reiser, O., Rh(II)-catalyzed cyclopropanation of furans and its application to the total synthesis of natural product derivatives. *Org. Lett.* **2017,** *19* (18), 4722-4725.
115. Wang, H. B.; Guptill, D. M.; Varela-Alvarez, A.; Musaev, D. G.; Davies, H. M. L., Rhodium-catalyzed enantioselective cyclopropanation of electron-deficient alkenes. *Chem. Sci.* **2013,** *4* (7), 2844-2850.
116. Gladow, D.; Reissig, H.-U., Synthesis of perfluoroalkyl-substituted γ-lactones and 4,5-dihydropyridazin-3(2H)-ones via donor-acceptor cyclopropanes. *Helv. Chim. Acta* **2012,** *95* (10), 1818-1830.
117. Huang, W.-S.; Schlinquer, C.; Poisson, T.; Pannecoucke, X.; Charette, A. B.; Jubault, P., General catalytic enantioselective access to monohalomethyl and trifluoromethyl cyclopropanes. *Chem. Eur. J.* **2018,** *24* (41), 10339-10343.
118. Schlinquer, C.; Huang, W.-S.; Chen, L.; Poisson, T.; Pannecoucke, X.; Charette, A. B.; Jubault, P., Rhodium catalysed enantioselective synthesis of mono-(halo)-methyl-cyclopropanes. *Org. Biomol. Chem.* **2019,** *17* (3), 472-476.
119. Pons, A.; Beucher, H.; Ivashkin, P.; Lemonnier, G.; Poisson, T.; Charette, A. B.; Jubault, P.; Pannecoucke, X., Rhodium-catalyzed cyclopropanation of fluorinated olefins: a straightforward route to highly functionalized fluorocyclopropanes. *Org. Lett.* **2015,** *17* (7), 1790-1793.
120. Pons, A.; Tognetti, V.; Joubert, L.; Poisson, T.; Pannecoucke, X.; Charette, A. B.; Jubault, P., Catalytic enantioselective cyclopropanation of α-fluoroacrylates: an experimental and theoretical study. *ACS Catal.* **2019,** *9* (3), 2594-2598.
121. McCabe, S. R.; Wipf, P., Eight-step enantioselective total synthesis of (−)-cycloclavine. *Angew. Chem., Int. Ed.* **2017,** *56* (1), 324-327.
122. Deng, L.; Chen, M.; Dong, G., Concise synthesis of (−)-cycloclavine and (−)-5-epi-cycloclavine via asymmetric C–C activation. *J. Am. Chem. Soc.* **2018,** *140* (30), 9652-9658.
123. Sim, J.; Park, H.; Lim, J.; Yoon, I.; Lim, C.; An, H.; Yun, H.; Choi, H. J.; Suh, Y.-G., Stereoselective synthesis of 1,4,5-tri-*cis*-guaiane sesquiterpene: first total synthesis of (−)-dendroside C aglycon. *Org. Lett.* **2018,** *20* (3), 586-589.
124. Panish, R. A.; Chintala, S. R.; Fox, J. M., A mixed-ligand chiral rhodium(II) catalyst enables the enantioselective total synthesis of piperarborenine B. *Angew. Chem., Int. Ed.* **2016,** *55* (16), 4983-4987.
125. Xu, G.; Chen, L.; Sun, J., Rhodium-catalyzed asymmetric dearomative [4 + 3]-cycloaddition of vinylindoles with vinyldiazoacetates: access to cyclohepta[b]indoles. *Org. Lett.* **2018,** *20* (11), 3408-3412.
126. Davies, H. M. L.; Smith, H. D.; Korkor, O., Tandem cyclopropanation/Cope rearrangement sequence. Stereospecific [3 + 4]

cycloaddition reaction of vinylcarbenoids with cyclopentadiene. *Tetrahedron Lett.* **1987,** *28* (17), 1853-1856.
127. Krüger, S.; Gaich, T., Recent applications of the divinylcyclopropane–cycloheptadiene rearrangement in organic synthesis. *Beilstein J. Org. Chem.* **2014,** *10*, 163-193.
128. Xu, J.; Caro-Diaz, E. J. E.; Theodorakis, E. A., Enantioselective formal synthesis of (−)-englerin A via a Rh-catalyzed [4 + 3] cycloaddition reaction. *Org. Lett.* **2010,** *12* (16), 3708-3711.
129. Lian, Y.; Miller, L. C.; Born, S.; Sarpong, R.; Davies, H. M. L., Catalyst-controlled formal [4 + 3] cycloaddition applied to the total synthesis of (+)-barekoxide and (−)-barekol. *J. Am. Chem. Soc.* **2010,** *132* (35), 12422-12425.
130. Spangler, J. E.; Lian, Y.; Raikar, S. N.; Davies, H. M. L., Synthesis of complex hexacyclic compounds via a tandem Rh(II)-catalyzed double-cyclopropanation/Cope rearrangement/Diels–Alder reaction. *Org. Lett.* **2014,** *16* (18), 4794-4797.
131. Nakamura, A.; Konishi, A.; Tatsuno, Y.; Otsuka, S., A highly enantioselective synthesis of cyclopropane derivatives through chiral cobalt(II) complex catalyzed carbenoid reaction. General scope and factors determining the enantioselectivity. *J. Am. Chem. Soc.* **1978,** *100* (11), 3443-3448.
132. Tohru, Y.; Taketo, I.; Hiroyuki, S.; Mitsuo, S., Optically active aldiminato cobalt(II) complexes as efficient catalysts for enantioselective cyclopropanation of styrenes with diazoacetates. *Chem. Lett.* **1999,** *28* (8), 719-720.
133. Taketo, I.; Mitsuo, S.; Tohru, Y., Highly enantioselective cyclopropanation of styrenes with diazoacetates catalyzed by optically active β-ketoiminato cobalt(II) complexes. *Chem. Lett.* **1999,** *28* (12), 1345-1346.
134. Niimi, T.; Uchida, T.; Irie, R.; Katsuki, T., Co(II)–salen-catalyzed highly *cis*- and enantioselective cyclopropanation. *Tetrahedron Lett.* **2000,** *41* (19), 3647-3651.
135. Shitama, H.; Katsuki, T., Synthesis of metal–(pentadentate-salen) complexes: asymmetric epoxidation with aqueous hydrogen peroxide and asymmetric cyclopropanation (salenH_2: N,N′-bis(salicylidene)ethylene-1,2-diamine). *Chem. Eur. J.* **2007,** *13* (17), 4849-4858.
136. Uchida, T.; Katsuki, T., α-Diazoacetates as carbene precursors: metallosalen-catalyzed asymmetric cyclopropanation. *Synthesis* **2006,** *2006* (10), 1715-1723.
137. Kräutler, B., Vitamin B_{12}: chemistry and biochemistry. *Biochem. Soc. Trans.* **2005,** *33* (4), 806-810.
138. Chen, Y.; Zhang, X. P., Vitamin B_{12} derivatives as natural asymmetric catalysts: enantioselective cyclopropanation of alkenes. *J. Org. Chem.* **2004,** *69* (7), 2431-2435.
139. Huang, L.; Chen, Y.; Gao, G.-Y.; Zhang, X. P., Diastereoselective and enantioselective cyclopropanation of alkenes catalyzed by cobalt porphyrins. *J. Org. Chem.* **2003,** *68* (21), 8179-8184.

140. Chen, Y.; Fields, K. B.; Zhang, X. P., Bromoporphyrins as versatile synthons for modular construction of chiral porphyrins: cobalt-catalyzed highly enantioselective and diastereoselective cyclopropanation. *J. Am. Chem. Soc.* **2004,** *126* (45), 14718-14719.
141. Chen, Y.; Zhang, X. P., *Trans* effect on cobalt porphyrin catalyzed asymmetric cyclopropanation. *Synthesis* **2006,** (10), 1697-1700.
142. Zhu, S.; Perman, J. A.; Zhang, X. P., Acceptor/acceptor-substituted diazo reagents for carbene transfers: cobalt-catalyzed asymmetric Z-cyclopropanation of alkenes with α-nitrodiazoacetates. *Angew. Chem., Int. Ed.* **2008,** *47* (44), 8460-8463.
143. Zhu, S.; Ruppel, J. V.; Lu, H.; Wojtas, L.; Zhang, X. P., Cobalt-catalyzed asymmetric cyclopropanation with diazosulfones: rigidification and polarization of ligand chiral environment via hydrogen bonding and cyclization. *J. Am. Chem. Soc.* **2008,** *130* (15), 5042-5043.
144. Fantauzzi, S.; Gallo, E.; Rose, E.; Raoul, N.; Caselli, A.; Issa, S.; Ragaini, F.; Cenini, S., Asymmetric cyclopropanation of olefins catalyzed by chiral cobalt(II)-binaphthyl porphyrins. *Organometallics* **2008,** *27* (23), 6143-6151.
145. Ikeno, T.; Iwakura, I.; Yamada, T., Cobalt−carbene complex with single-bond character: intermediate for the cobalt complex-catalyzed cyclopropanation. *J. Am. Chem. Soc.* **2002,** *124* (51), 15152-15153.
146. Carminati, D. M.; Intrieri, D.; Le Gac, S.; Roisnel, T.; Boitrel, B.; Toma, L.; Legnani, L.; Gallo, E., Synthesis, characterisation and catalytic use of iron porphyrin amino ester conjugates. *New J. Chem.* **2017,** *41* (13), 5950-5959.
147. Zhu, S.; Cui, X.; Zhang, X. P., Ligand effect on cobalt(II)-catalyzed asymmetric cyclopropanation with diazosulfones – approaching high stereoselectivity through modular design of D_2-symmetric chiral porphyrins. *Eur. J. Inorg. Chem.* **2012,** *2012* (3), 430-434.
148. White, J. D.; Shaw, S., A new cobalt–salen catalyst for asymmetric cyclopropanation. Synthesis of the serotonin–norepinephrine repuptake inhibitor (+)-synosutine. *Org. Lett.* **2014,** *16* (15), 3880-3883.
149. Joshi-Pangu, A.; Cohen, R. D.; Tudge, M. T.; Chen, Y., Dearomatization of electron-deficient nitrogen heterocycles via cobalt-catalyzed asymmetric cyclopropanation. *J. Org. Chem.* **2016,** *81* (8), 3070-3075.
150. Xu, X.; Zhu, S.; Cui, X.; Wojtas, L.; Zhang, X. P., Cobalt(II)-catalyzed asymmetric olefin cyclopropanation with α-ketodiazoacetates. *Angew. Chem., Int. Ed.* **2013,** *52* (45), 11857-11861.
151. Zhu, S.; Xu, X.; Perman, J. A.; Zhang, X. P., A general and efficient cobalt(II)-based catalytic system for highly stereoselective cyclopropanation of alkenes with α-cyanodiazoacetates. *J. Am. Chem. Soc.* **2010,** *132* (37), 12796-12799.
152. Xu, X.; Wang, Y.; Cui, X.; Wojtas, L.; Zhang, X. P., Metalloradical activation of α-formyldiazoacetates for the catalytic asymmetric radical cyclopropanation of alkenes. *Chem. Sci.* **2017,** *8* (6), 4347-4351.

153. Xu, X.; Lu, H.; Ruppel, J. V.; Cui, X.; Lopez de Mesa, S.; Wojtas, L.; Zhang, X. P., Highly asymmetric intramolecular cyclopropanation of acceptor-substituted diazoacetates by Co(II)-based metalloradical catalysis: iterative approach for development of new-generation catalysts. *J. Am. Chem. Soc.* **2011,** *133* (39), 15292-15295.
154. Hu, Y.; Lang, K.; Tao, J.; Marshall, M. K.; Cheng, Q.; Cui, X.; Wojtas, L.; Zhang, X. P., Next-generation D_2-symmetric chiral porphyrins for Cobalt(II)-based metalloradical catalysis: catalyst engineering by distal bridging. *Angew. Chem., Int. Ed.* **2019,** *58* (9), 2670-2674.
155. Jin, C.; Decker, A. M.; Huang, X.-P.; Gilmour, B. P.; Blough, B. E.; Roth, B. L.; Hu, Y.; Gill, J. B.; Zhang, X. P., Synthesis, pharmacological characterization, and structure–activity relationship studies of small molecular agonists for the orphan GPR88 receptor. *ACS Chem. Neurosci.* **2014,** *5* (7), 576-587.
156. Schafer, A. G.; Blakey, S. B., Ir-catalyzed enantioselective group transfer reactions. *Chem. Soc. Rev.* **2015,** *44* (17), 5969-5980.
157. Weldy, N. M.; Schafer, A. G.; Owens, C. P.; Herting, C. J.; Varela-Alvarez, A.; Chen, S.; Niemeyer, Z.; Musaev, D. G.; Sigman, M. S.; Davies, H. M. L.; Blakey, S. B., Iridium(III)-bis(imidazolinyl)phenyl catalysts for enantioselective C-H functionalization with ethyl diazoacetate. *Chem. Sci.* **2016,** *7* (5), 3142-3146.
158. Kanchiku, S.; Suematsu, H.; Matsumoto, K.; Uchida, T.; Katsuki, T., Construction of an aryliridium–salen complex for highly *cis*- and enantioselective cyclopropanations. *Angew. Chem., Int. Ed.* **2007,** *46* (21), 3889-3891.
159. Suematsu, H.; Kanchiku, S.; Uchida, T.; Katsuki, T., Construction of aryliridium−salen complexes: enantio- and c*is*-selective cyclopropanation of conjugated and nonconjugated olefins. *J. Am. Chem. Soc.* **2008,** *130* (31), 10327-10337.
160. Inuki, S.; Fujimoto, Y., Total synthesis of naturally occurring chiral cyclopropane fatty acids and related compounds. *Tetrahedron Lett.* **2019,** *60* (16), 1083-1090.
161. Anding, B. J.; Ellern, A.; Woo, L. K., Olefin cyclopropanation catalyzed by iridium(III) porphyrin complexes. *Organometallics* **2012,** *31* (9), 3628-3635.
162. Chen, K.; Arnold, F. H., Engineering new catalytic activities in enzymes. *Nat. Catal.* **2020,** *3* (3), 203-213.
163. Key, H. M.; Dydio, P.; Liu, Z.; Rha, J. Y. E.; Nazarenko, A.; Seyedkazemi, V.; Clark, D. S.; Hartwig, J. F., Beyond iron: iridium-containing P450 enzymes for selective cyclopropanations of structurally diverse alkenes. *ACS Cent. Sci.* **2017,** *3* (4), 302-308.
164. Doyle, M. P.; Griffin, J. H.; Bagheri, V.; Dorow, R. L., Correlations between catalytic reactions of diazo compounds and stoichiometric reactions of transition-metal carbenes with alkenes. Mechanism of the cyclopropanation reaction. *Organometallics* **1984,** *3* (1), 53-61.

165. Rackl, D.; Yoo, C.-J.; Jones, C. W.; Davies, H. M. L., Synthesis of donor/acceptor-substituted diazo compounds in flow and their application in enantioselective dirhodium-catalyzed cyclopropanation and C–H functionalization. *Org. Lett.* **2017,** *19* (12), 3055-3058.
166. Rempel, G. A.; Legzdins, P.; Smith, H.; Wilkinson, G.; Ucko, D. A., Tetrakis(acetato)dirhodium(II) and similar carboxylato compounds. In *Inorganic Syntheses*, John Wiley & Sons, Inc.: 2007; pp 90-91.
167. Li, Z. Y.; Chifotides, H. T.; Dunbar, K. R., Unprecedented partial paddlewheel dirhodium methyl isocyanide compounds with unusual structural and electronic properties: a comprehensive experimental and theoretical study. *Chem. Sci.* **2013,** *4* (12), 4470-4485.
168. Millet, A.; Xue, C.; Song, E.; Turro, C.; Dunbar, K. R., Synthetic strategies for trapping the elusive *trans*-dirhodium(II,II) formamidinate isomer: effects of *cis* versus *trans* geometry on the photophysical properties. *Inorg. Chem.* **2020,** *59* (4), 2255-2265.
169. Ahsan, M. Q.; Bernal, I.; Bear, J. L., Reaction of $Rh_2(OOCCH_3)_4$ with acetamide-crystal and molecular-structure of $[Rh_2(HNOCCH_3)_4 \cdot 2H_2O] \cdot 3H_2O$. *Inorg. Chem.* **1986,** *25* (3), 260-265.
170. Lou, Y.; Remarchuk, T. P.; Corey, E. J., Catalysis of enantioselective [2+1]-cycloaddition reactions of ethyl diazoacetate and terminal acetylenes using mixed-ligand complexes of the series $Rh_2(RCO_2)_n$ (L^*_{4-n}). Stereochemical heuristics for ligand exchange and catalyst synthesis. *J. Am. Chem. Soc.* **2005,** *127* (41), 14223-14230.
171. Doyle, M. P.; Raab, C. E.; Roos, G. H. P.; Lynch, V.; Simonsen, S. H., (4,0)-Dirhodium(II) tetrakis[methyl 1-acetyl-2-oxoimidazolidine-4(*S*)-carboxylate]. Implications for the mechanism of ligand exchange reactions. *Inorg. Chim. Acta* **1997,** *266* (1), 13-18.
172. Drago, R. S.; Long, J. R.; Cosmano, R., Metal synergism in the coordination chemistry of a metal-metal bonded system: $Rh_2(C_3H_7COO)_4$. *Inorg. Chem.* **1981,** *20* (9), 2920-2927.
173. Lahuerta, P.; Ubeda, M. A.; Paya, J.; Garciagranda, S.; Gomezbeltran, F.; Anillo, A., Reactions of rhodium trifluoroacetate with triphenylphosphine and pyridine - molecular-structure of $Rh_2(O_2CCF_3)_4(Py)_4$. *Inorg. Chim. Acta* **1993,** *205* (1), 91-97.
174. Crawford, C. A.; Matonic, J. H.; Streib, W. E.; Huffman, J. C.; Dunbar, K. R.; Christou, G., Reaction of 2,2'-bipyridine (bpy) with dirhodium carboxylates: mono-bpy products with variable chelate binding modes and insights into the reaction mechanism. *Inorg. Chem.* **1993,** *32* (14), 3125-3133.
175. Angeles-Boza, A. M.; Chifotides, H. T.; Aguirre, J. D.; Chouai, A.; Fu, P. K. L.; Dunbar, K. R.; Turro, C., Dirhodium(II,II) complexes: molecular characteristics that affect in vitro activity. *J. Med. Chem.* **2006,** *49* (23), 6841-6847.
176. Tu, Q.; Wang, T. B.; Welch, C. J.; Wang, P.; Jia, X. J.; Raab, C.; Bu, X. D.; Bykowski, D.; Hohenstaufen, B.; Doyle, M. P., Identification and

characterization of isomeric intermediates in a catalyst formation reaction by means of speciation analysis using HPLC-ICPMS and HPLC-ESI-MS. *Anal. Chem.* **2006,** *78* (4), 1282-1289.
177. Lindsay, V. N. G.; Charette, A. B., Design and synthesis of chiral heteroleptic rhodium(II) carboxylate catalysts: experimental investigation of halogen bond rigidification effects in asymmetric cyclopropanation. *ACS Catal.* **2012,** *2* (6), 1221-1225.
178. Sarkar, M.; Daw, P.; Ghatak, T.; Bera, J. K., Amide-functionalized naphthyridines on a Rh^{II}–Rh^{II} platform: effect of steric crowding, hemilability, and hydrogen-bonding interactions on the structural diversity and catalytic activity of dirhodium(II) complexes. *Chem. Eur. J.* **2014,** *20* (50), 16537-16549.
179. Sambasivan, R.; Ball, Z. T., Metallopeptides for asymmetric dirhodium catalysis. *J. Am. Chem. Soc.* **2010,** *132* (27), 9289-9291.
180. Marcoux, D.; Lindsay, V. N. G.; Charette, A. B., Use of achiral additives to increase the stereoselectivity in Rh(II)-catalyzed cyclopropanations. *Chem. Commun.* **2010,** *46* (6), 910-912.
181. Wynne, D. C.; Olmstead, M. M.; Jessop, P. G., Supercritical and liquid solvent effects on the enantioselectivity of asymmetric cyclopropanation with tetrakis[1-[(4-tert-butylphenyl)-sulfonyl]-(2*S*)-pyrrolidinecarboxylate]dirhodium(II). *J. Am. Chem. Soc.* **2000,** *122* (32), 7638-7647.
182. Davies, H. M. L.; Venkataramani, C., Dirhodium tetraprolinate-catalyzed asymmetric cycloproplanations with high turnover numbers. *Organic Letters* **2003,** *5* (9), 1403-1406.
183. Bilgrien, C.; Drago, R. S.; Vogel, G. C.; Stahlbush, J., *Trans* influence across a Rh–Rh bond. Effect of a series of Lewis bases on the stretching frequency of coordinated CO. *Inorg. Chem.* **1986,** *25* (16), 2864-2866.
184. Wong, D. L.; Zhang, A.; Faponle, A. S.; de Visser, S. P.; Stillman, M. J., Glutathione binding to dirhodium tetraacetate: a spectroscopic, mass spectral and computational study of an anti-tumour compound. *Metallomics* **2017,** *9* (5), 501-516.
185. Tracey, A. A.; Eriks, K.; Prock, A.; Giering, W. P., Electrochemical investigation of the substitution reactions of the solvent-coordinated acyl complexes *η*-Cp(acetone)(CO)$FeCOMe^{0,+}$ involving thioethers. Applications of the quantitative analysis of ligand effects. *Organometallics* **1990,** *9* (5), 1399-1405.
186. Gatard, S.; Guo, C.; Foxman, B. M.; Ozerov, O. V., Thioether, dinitrogen, and olefin complexes of (PNP)Rh: kinetics and thermodynamics of exchange and oxidative addition reactions. *Organometallics* **2007,** *26* (25), 6066-6075.
187. Shi, T.; Elding, L. I., Structure−reactivity correlations for complex formation reactions between square-planar metal centers and thioethers. *Inorg. Chem.* **1996,** *35* (20), 5941-5947.
188. Lewis, N.; Mckillop, A.; Taylor, R. J. K.; Watson, R. J., A simple and efficient procedure for the preparation of chiral 2-oxazolidinones from α-amino acids. *Synth. Commun.* **1995,** *25* (4), 561-568.

189. Hou, D. R.; Reibenspies, J. H.; Burgess, K., New, optically active phosphine oxazoline (JM-Phos) ligands: syntheses and applications in allylation reactions. *J. Org. Chem.* **2001,** *66* (1), 206-215.
190. Sibi, M. P.; Rutherford, D.; Renhowe, P. A.; Li, B., Investigations of a nucleophilic alaninol synthon derived from serine. *J. Am. Chem. Soc.* **1999,** *121* (33), 7509-7516.
191. Warzecha, E.; Berto, T. C.; Wilkinson, C. C.; Berry, J. F., Rhodium rainbow: a colorful laboratory experiment highlighting ligand field effects of dirhodium tetraacetate. *J. Chem. Educ.* **2019**.
192. Keaney, G. F.; Wood, J. L., Rhodium perfluorobutyramide ($Rh_2(pfm)_4$): a synthetically useful catalyst for olefin aziridinations. *Tetrahedron Lett.* **2005,** *46* (23), 4031-4034.
193. Ezerskaya, N. A.; Toropchenova, E. S.; Kubrakova, I. V.; Krasheninnikova, S. V.; Kudinova, T. F.; Fomina, T. A.; Kiseleva, I. N., Preparation of binuclear rhodium(II) tetraacetate (initial compound for the coulometric determination of rhodium) under the action of microwave radiation. *J. Anal. Chem.* **2000,** *55* (12), 1132-1135.
194. Gonzalez-Belman, O. F.; Varela, Y.; Flores-lamo, M.; Wrobel, K.; Gutierrez-Granados, S.; Peralta-Hernndez, J. M.; Jimnez-Halla, J. O. C.; Serrano, O., Microwave-assisted synthesis and characterization of $[Rh_2(OAc)_4(L)_2]$ paddlewheel complexes: a joint experimental and computational study. *Int. J. Inorg. Chem.* **2017**, 1-12.
195. Schanche, J.-S., Microwave synthesis solutions from personal chemistry. *Mol. Diversity* **2003,** *7* (2), 291-298.
196. Kappe, C. O.; Dallinger, D.; Murphree, S. S., *Practical Microwave Synthesis for Organic Chemists: Strategies, Instruments, and Protocols*. Wiley-VCH: Weinheim, 2009; p x, 299 p.
197. Johnson, S. A.; Hunt, H. R.; Neumann, H. M., Preparation and properties of anhydrous rhodium(II) acetate and some adducts thereof. *Inorg. Chem.* **1963,** *2* (5), 960-962.
198. Sheffield, W.; Abshire, A.; Darko, A., Effect of tethered, axial thioether coordination on rhodium(II)-catalyzed silyl-hydrogen insertion. *Eur. J. Org. Chem.* **2019,** (37), 6347-6351.
199. Cruz, P.; Fernandez-Bartolome, E.; Cortijo, M.; Delgado-Martínez, P.; González-Prieto, R.; Priego, J. L.; Torres, M. R.; Jiménez-Aparicio, R., Synthesis and structural characterization of a series of one-dimensional heteronuclear dirhodium-silver coordination polymers. *Polymers* **2019,** *11* (1), 111.
200. Cotton, F. A.; Dikarev, E. V.; Stiriba, S.-E., Studies of dirhodium tetra(trifluoroacetate). 3. Solid state isomers of the compound $Rh_2(O_2CCF_3)_4(THF)$ prepared by sublimation. *Inorg. Chem.* **1999,** *38* (21), 4877-4881.
201. Kataoka, Y.; Kataoka, K. S.; Murata, H.; Handa, M.; Mori, W.; Kawamoto, T., Synthesis and characterizations of a paddlewheel-type dirhodium-

based photoactive porous metal-organic framework. *Inorg. Chem. Commun.* **2016,** *68*, 37-41.
202. Cotton, F. A.; DeBoer, B. G.; LaPrade, M. D.; Pipal, J. R.; Ucko, D. A., The crystal and molecular structures of dichromium tetraacetate dihydrate and dirhodium tetraacetate dihydrate. *Acta Crystallogr., Sect. B: Struct. Sci., Cryst. Eng. Mater.* **1971,** *27* (8), 1664-1671.
203. Cotton, F. A.; Dikarev, E. V.; Petrukhina, M. A.; Stiriba, S.-E., Studies of dirhodium(II) tetra(trifluoroacetate). 5. Remarkable examples of the ambidentate character of dimethyl sulfoxide. *Inorg. Chem.* **2000,** *39* (8), 1748-1754.
204. Alzahrani, K. A. H.; Deeth, R. J., Molecular modeling of zinc paddlewheel molecular complexes and the pores of a flexible metal organic framework. *J. Mol. Model.* **2016,** *22* (4), 1-13.
205. Braunstein, P.; Naud, F., Hemilability of hybrid ligands and the coordination chemistry of oxazoline-based systems. *Angew. Chem., Int. Ed.* **2001,** *40* (4), 680-699.
206. Gottlieb, H. E.; Kotlyar, V.; Nudelman, A., NMR chemical shifts of common laboratory solvents as trace impurities. *J. Org. Chem.* **1997,** *62* (21), 7512-7515.
207. Atkins, T. J., Tricyclic trisaminomethanes. *J. Am. Chem. Soc.* **1980,** *102* (20), 6364-6365.
208. L. Bear, J.; Howard, R. A.; E. Korn, J., The thermodynamic and kinetic stabilities of some tetra-μ-carboxylatodirhodium(II) adducts. *Inorg. Chim. Acta* **1979,** *32*, 123-126.
209. Das, K.; Kadish, K. M.; Bear, J. L., Substituent and solvent effects on the electrochemical properties of tetra-μ-carboxylato-dirhodium(II). *Inorg. Chem.* **1978,** *17* (4), 930-934.
210. Taras-Goslinska, K.; Jonsson, M., Solvent effects on the redox properties of thioethers. *J. Phys. Chem. A* **2006,** *110* (30), 9513-9517.
211. Liu, S.; Chen, B.; Yang, Y.; Yang, Y.; Chen, Q.; Zeng, X.; Xu, B., Electrochemical oxidations of thioethers: modulation of oxidation potential using a hydrogen bonding network. *Electrochem. Commun.* **2019,** *109*, 106583.
212. Chavan, M. Y.; Zhu, T. P.; Lin, X. Q.; Ahsan, M. Q.; Bear, J. L.; Kadish, K. M., Axial-ligand-dependent electrochemical and spectral properties of a series of acetate- and acetamidate-bridged dirhodium complexes. *Inorg. Chem.* **1984,** *23* (26), 4538-4545.
213. Anderson, B. G.; Cressy, D.; Patel, J. J.; Harris, C. F.; Yap, G. P. A.; Berry, J. F.; Darko, A., Synthesis and catalytic properties of dirhodium paddlewheel complexes with tethered, axially coordinating thioether ligands. *Inorg. Chem.* **2019,** *58* (3), 1728-1732.
214. Aguirre, J. D.; Lutterman, D. A.; Angeles-Boza, A. M.; Dunbar, K. R.; Turro, C., Effect of axial coordination on the electronic structure and biological activity of dirhodium(II,II) complexes. *Inorg. Chem.* **2007,** *46* (18), 7494-7502.

215. Zhu, T. P.; Ahsan, M. Q.; Malinski, T.; Kadish, K. M.; Bear, J. L., Electrochemical studies of a series of dirhodium(II) complexes with acetate and acetamidate bridging ligands. *Inorg. Chem.* **1984,** *23* (1), 2-3.
216. Kornecki, K. P.; Berry, J. F., Introducing a mixed-valent dirhodium(II,III) catalyst with increased stability in C–H amination. *Chem. Commun.* **2012,** *48* (99), 12097-12099.
217. Cannon, R. D.; Powell, D. B.; Sarawek, K.; Stillman, J. S., A novel mixed valence rhodium dimer, $[Rh_2(OAc)_4]^+$. *J. Chem. Soc., Chem. Commun.* **1976,** (1), 31-32.
218. Davies, H. M. L.; Venkataramani, C., Dirhodium tetraprolinate-catalyzed asymmetric cyclopropanations with high turnover numbers. *Org. Lett.* **2003,** *5* (9), 1403-1406.
219. Marcoux, D.; Charette, A. B., *Trans*-directing ability of amide groups in cyclopropanation: application to the asymmetric cyclopropanation of alkenes with diazo reagents bearing two carboxy groups. *Angew. Chem., Int. Ed.* **2008,** *47* (52), 10155-10158.
220. Gomes, L. F. R.; Trindade, A. F.; Candeias, N. R.; Gois, P. M. P.; Afonso, C. A. M., Intramolecular C–H insertion using NHC-di-rhodium(II) complexes: the influence of axial coordination. *Tetrahedron Lett.* **2008,** *49* (52), 7372-7375.
221. Zaykov, A. N.; Ball, Z. T., Kinetic and stereoselectivity effects of phosphite ligands in dirhodium catalysis. *Tetrahedron* **2011,** *67* (24), 4397-4401.
222. Sambasivan, R.; Zheng, W.; Burya, S. J.; Popp, B. V.; Turro, C.; Clementi, C.; Ball, Z. T., A tripodal peptide ligand for asymmetric Rh(II) catalysis highlights unique features of on-bead catalyst development. *Chem. Sci.* **2014,** *5* (4), 1401-1407.
223. Davies, H. M. L., Intermolecular metal-catalyzed carbenoid cyclopropanations. In *Organic Reactions*, Larry R. Overman, Ed. John Wiley & Sons: 2001; Vol. 57.
224. Cressy, D.; Zavala, C.; Abshire, A.; Sheffield, W.; Darko, A., Tuning Rh(II)-catalysed cyclopropanation with tethered thioether ligands. *Dalton Trans.* **2020**.
225. Hansen, J.; Li, B.; Dikarev, E.; Autschbach, J.; Davies, H. M. L., Combined experimental and computational studies of heterobimetallic Bi-Rh paddlewheel carboxylates as catalysts for metal carbenoid transformations. *J. Org. Chem.* **2009,** *74* (17), 6564-6571.
226. Mohan, P. J.; Georgiev, V. P.; McGrady, J. E., Periodic trends in electron transport through extended metal atom chains: comparison of $Ru_3(dpa)_4(NCS)_2$ with its first-row analogues. *Chem. Sci.* **2012,** *3* (4), 1319-1329.
227. Ren, Z.; Sunderland, T. L.; Tortoreto, C.; Yang, T.; Berry, J. F.; Musaev, D. G.; Davies, H. M. L., Comparison of reactivity and enantioselectivity between chiral bimetallic catalysts: bismuth rhodium- and dirhodium-catalyzed carbene chemistry. *ACS Catal.* **2018,** *8* (11), 10676-10682.

228. Muthusamy, S.; Sivaguru, M., Atom-economical access to highly substituted indenes and furan-2-ones via tandem reaction of diazo compounds and propargyl alcohols. *Org. Lett.* **2014,** *16* (16), 4248-51.
229. Miyazaki, T.; Kasai, S.; Ogiwara, Y.; Sakai, N., Indium-catalyzed reductive sulfidation of esters by using thiols: an approach to the diverse synthesis of sulfides. *Eur. J. Org. Chem.* **2016,** (5), 1043-1049.
230. Dolomanov, O. V.; Bourhis, L. J.; Gildea, R. J.; Howard, J. A. K.; Puschmann, H., OLEX2: a complete structure solution, refinement and analysis program. *J. Appl. Crystallogr.* **2009,** *42* (2), 339-341.
231. Cachet, T.; Anal, I. W. G. M., Guidelines for the quantitative gas chromatography of volatile flavouring substances, from the Working Group on Methods of Analysis of the International Organization of the Flavor Industry (IOFI). *Flavour Fragrance J.* **2011,** *26* (5), 297-299.

Appendix A - NMR Spectra

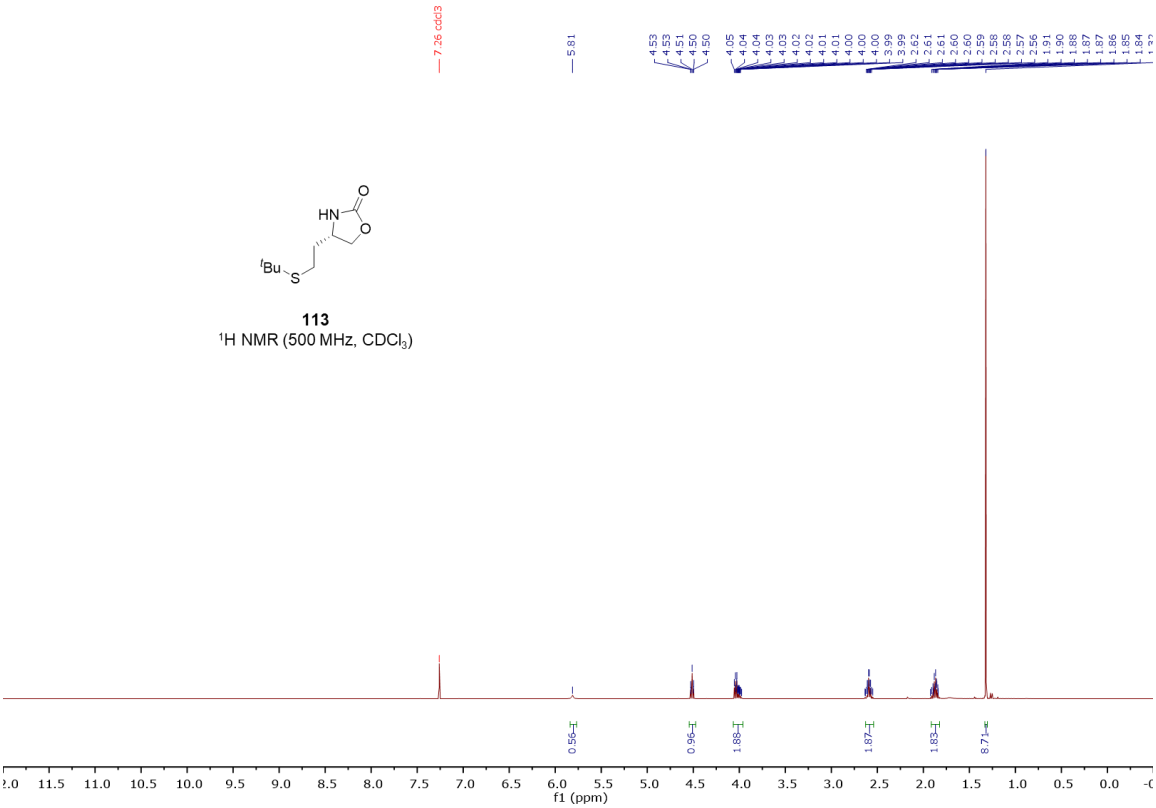

S 1 ^{1}H NMR spectrum of compound **113**

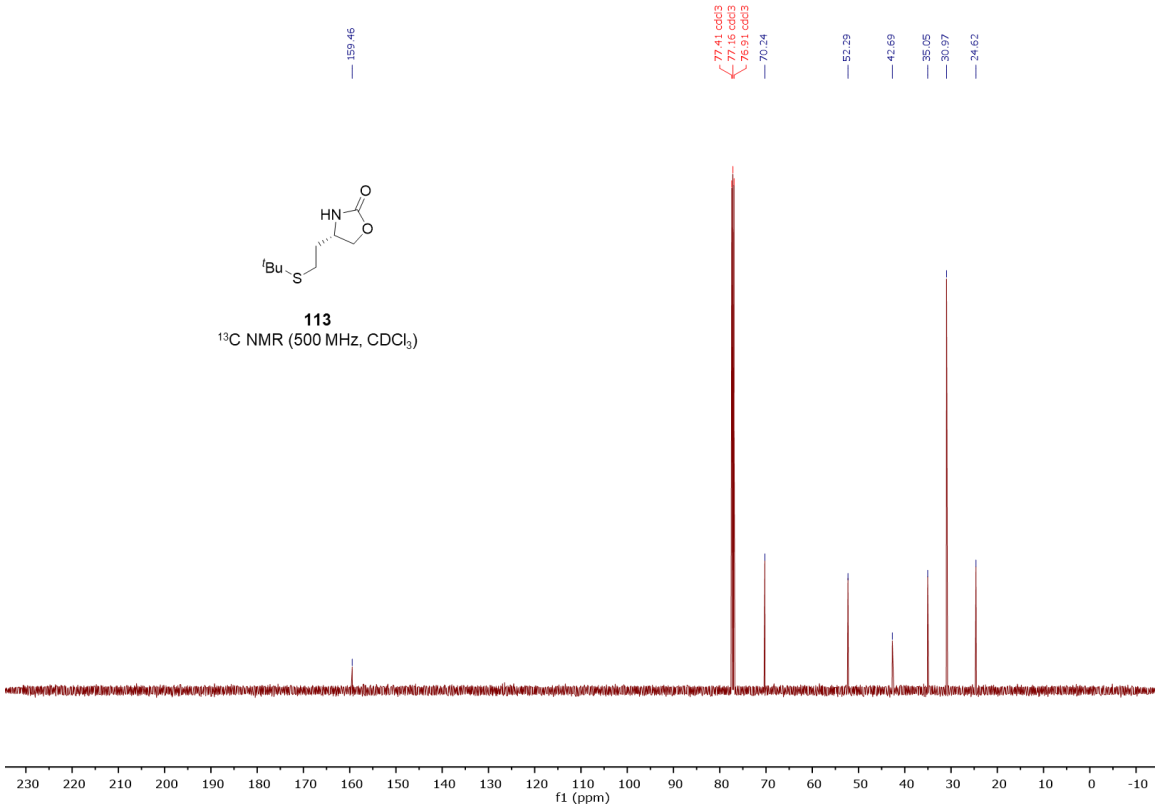

S 2 ^{13}C NMR spectrum of compound **113**

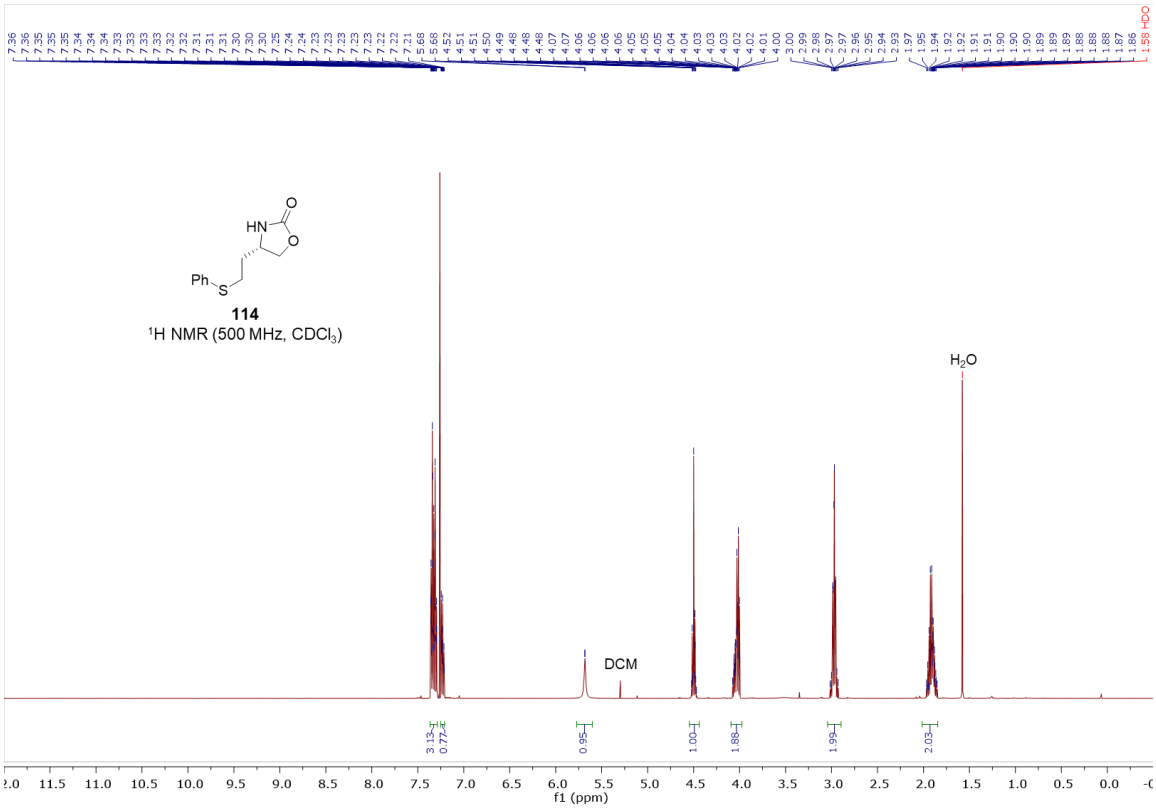

S 3 ^{1}H NMR spectrum of compound **114**

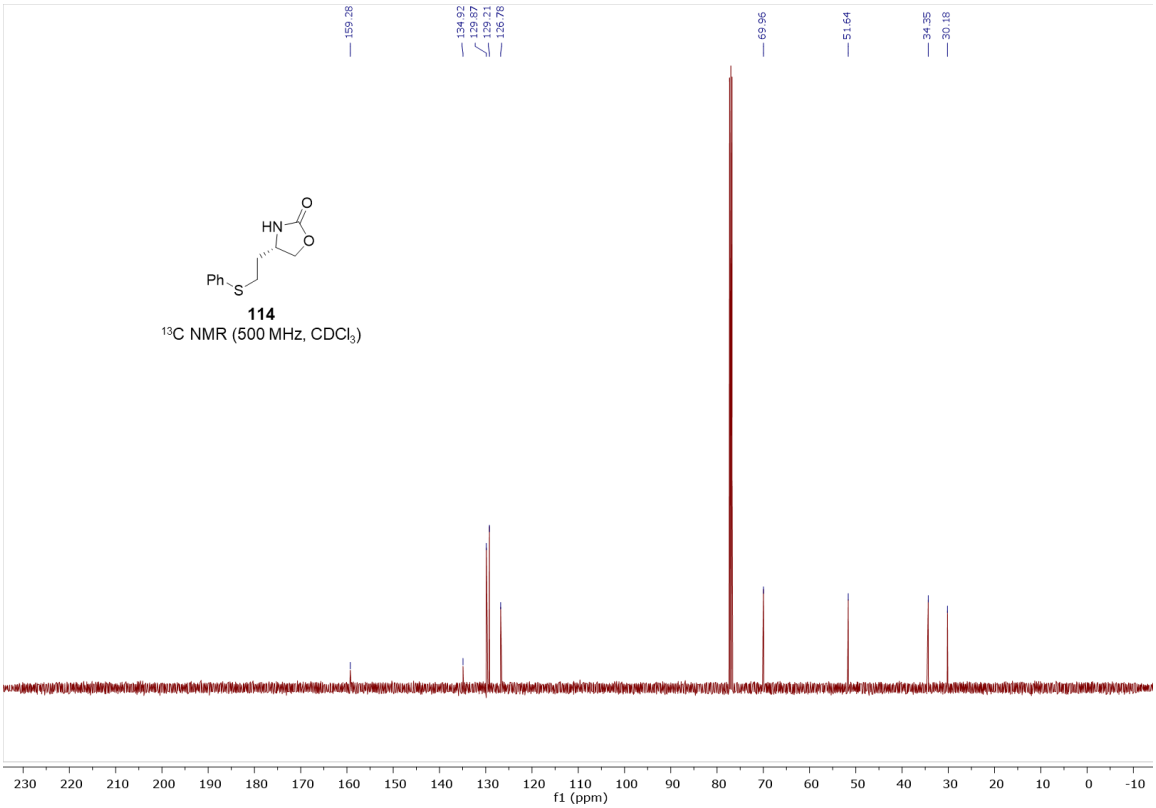

S 4 ^{13}C NMR spectrum of compound **114**

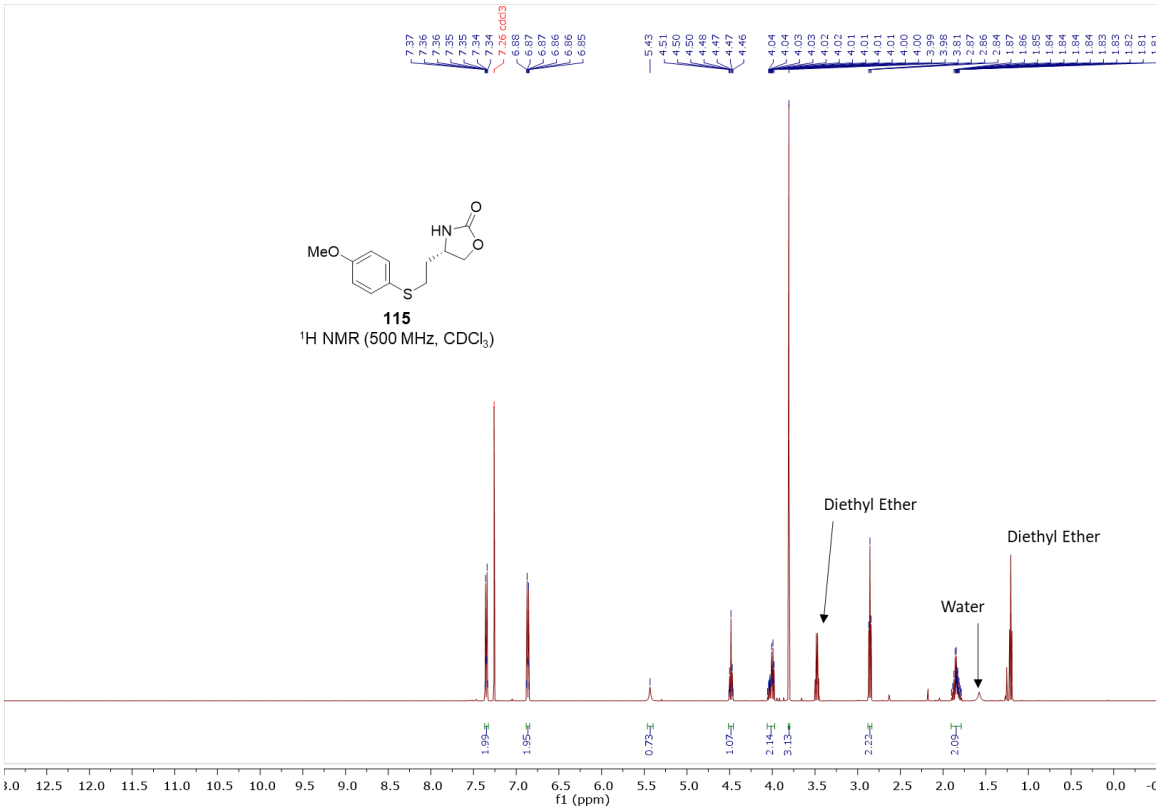

S 5 ^{1}H NMR spectrum of compound **115**

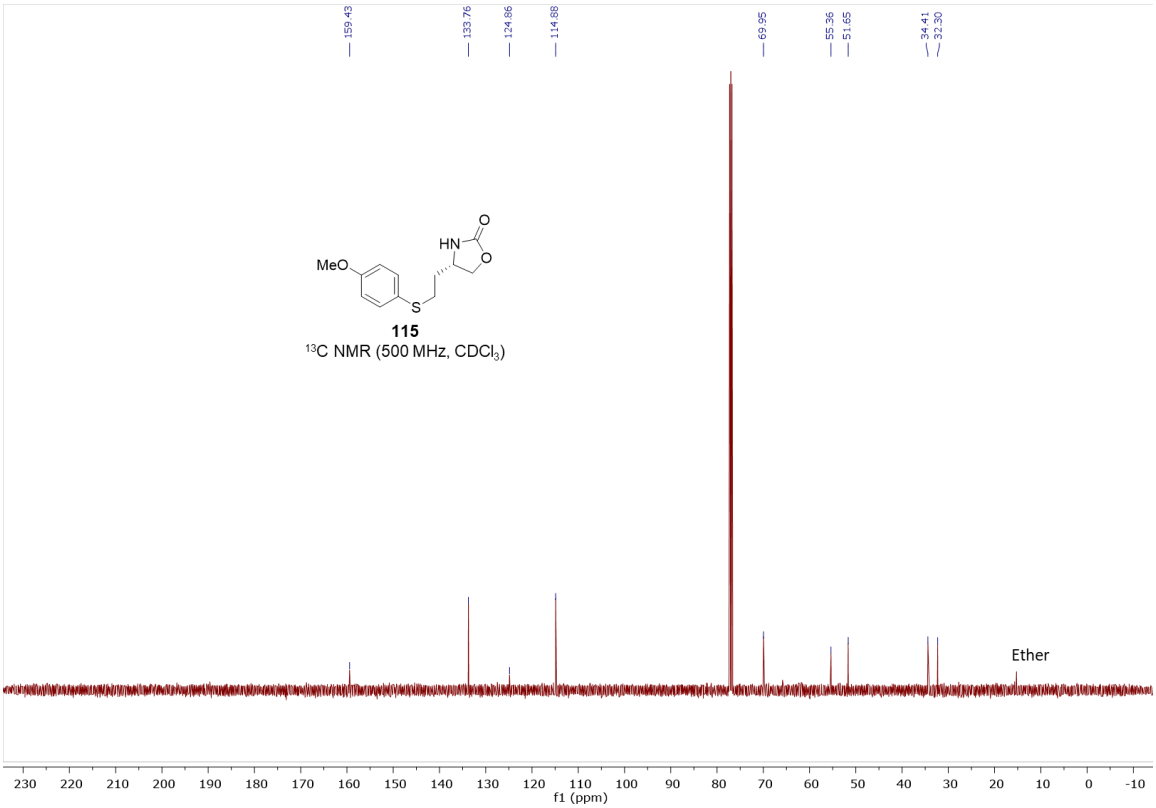

S 6 ^{13}C NMR spectrum of compound **115**

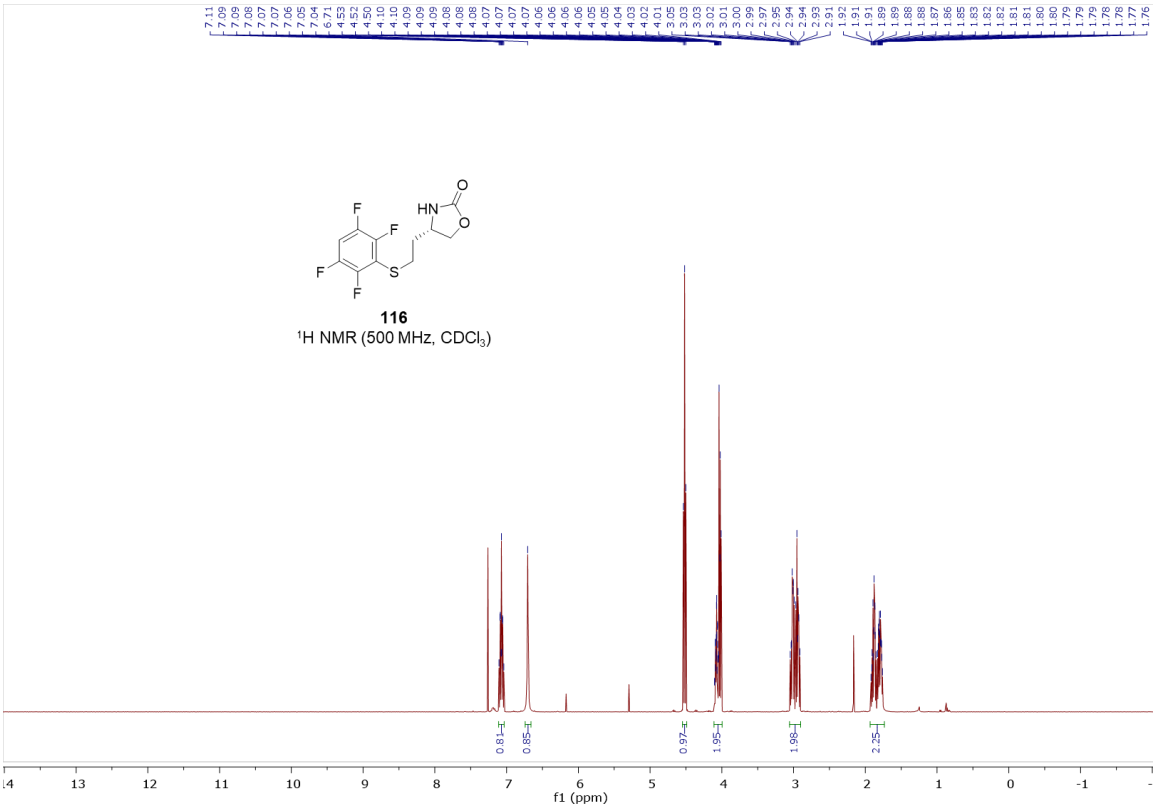

S 7 ^{1}H NMR spectrum of compound **116**

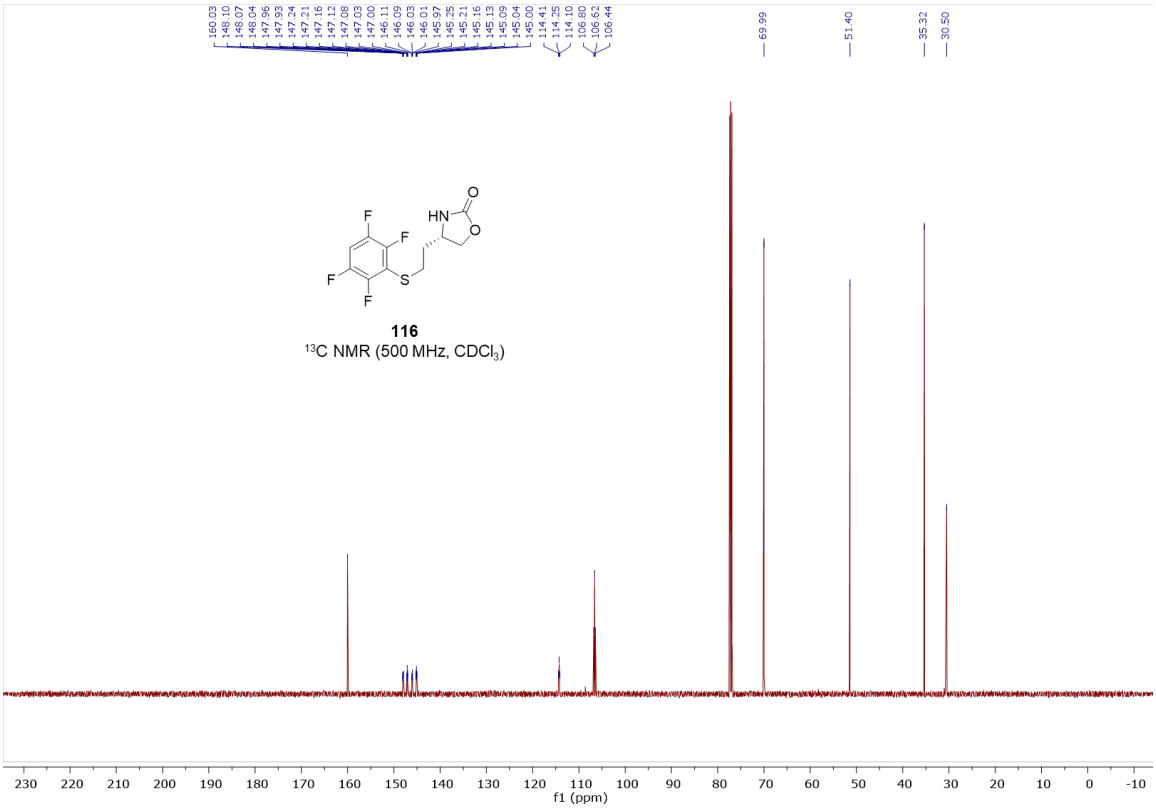

S 8 ^{13}C NMR spectrum of compound **116**

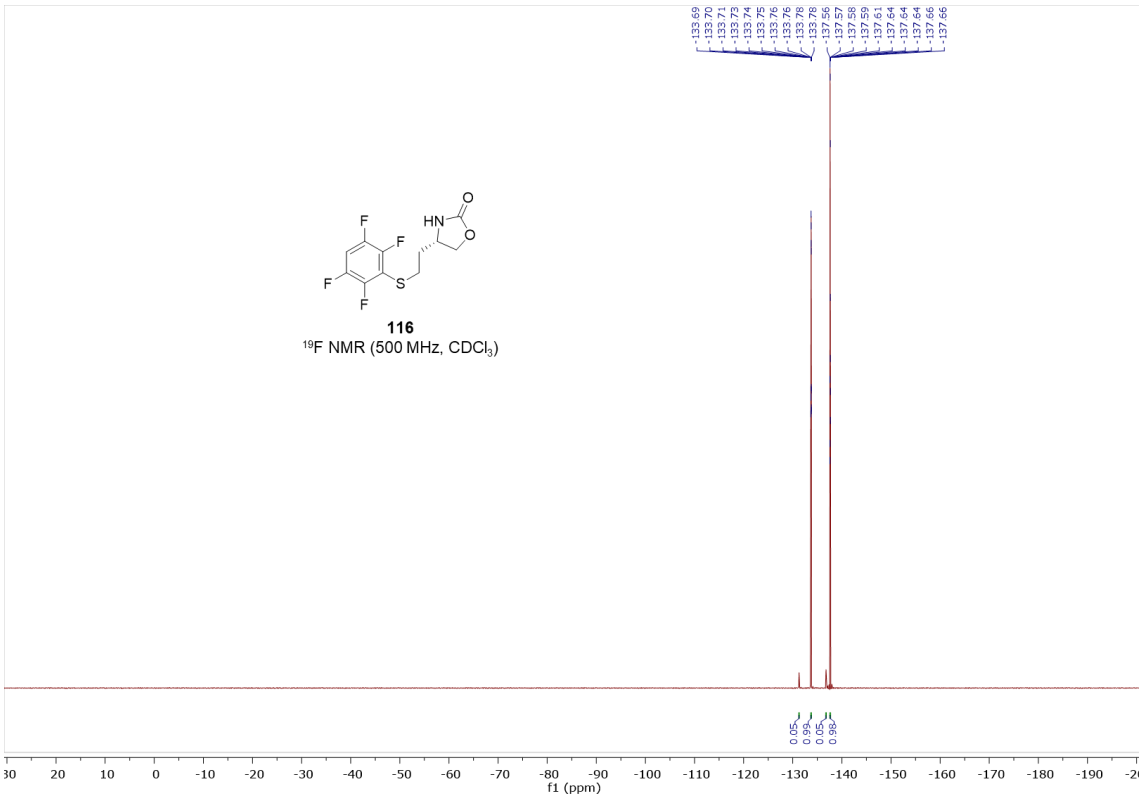

S 9 ^{19}F NMR spectrum of compound **116**

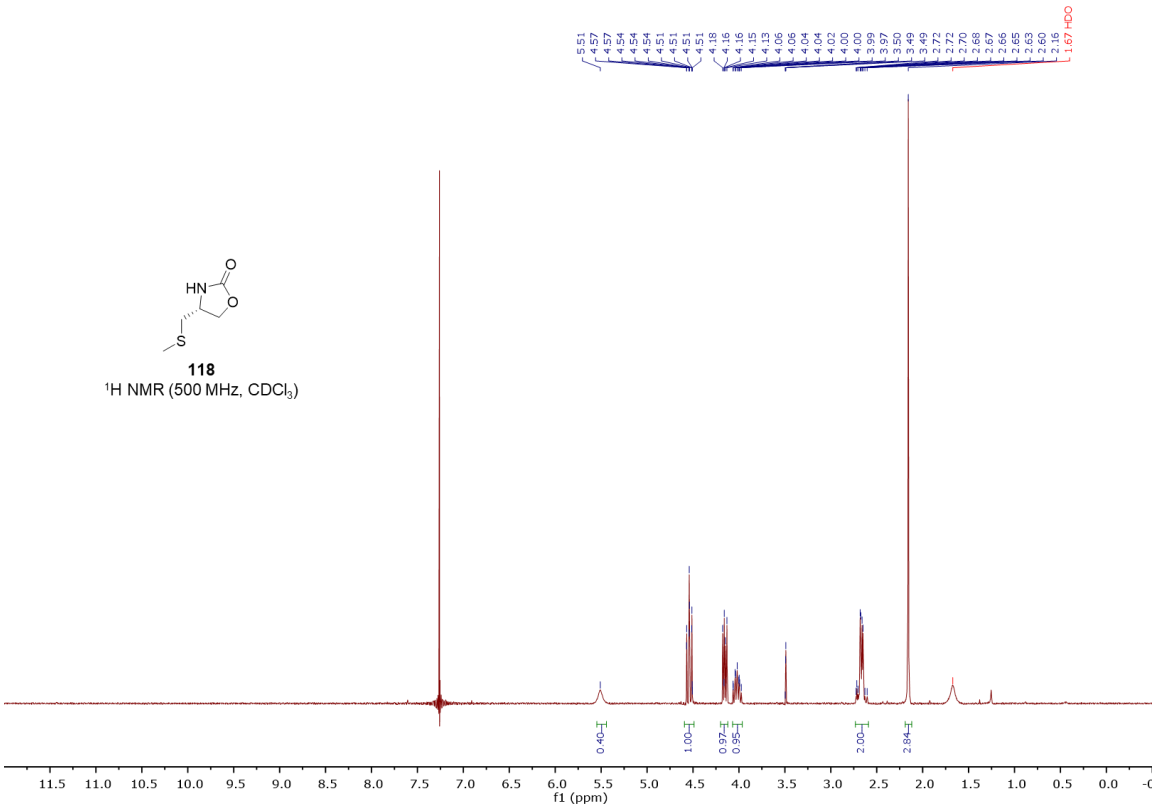

S 10 ^{1}H NMR spectrum of compound **118**

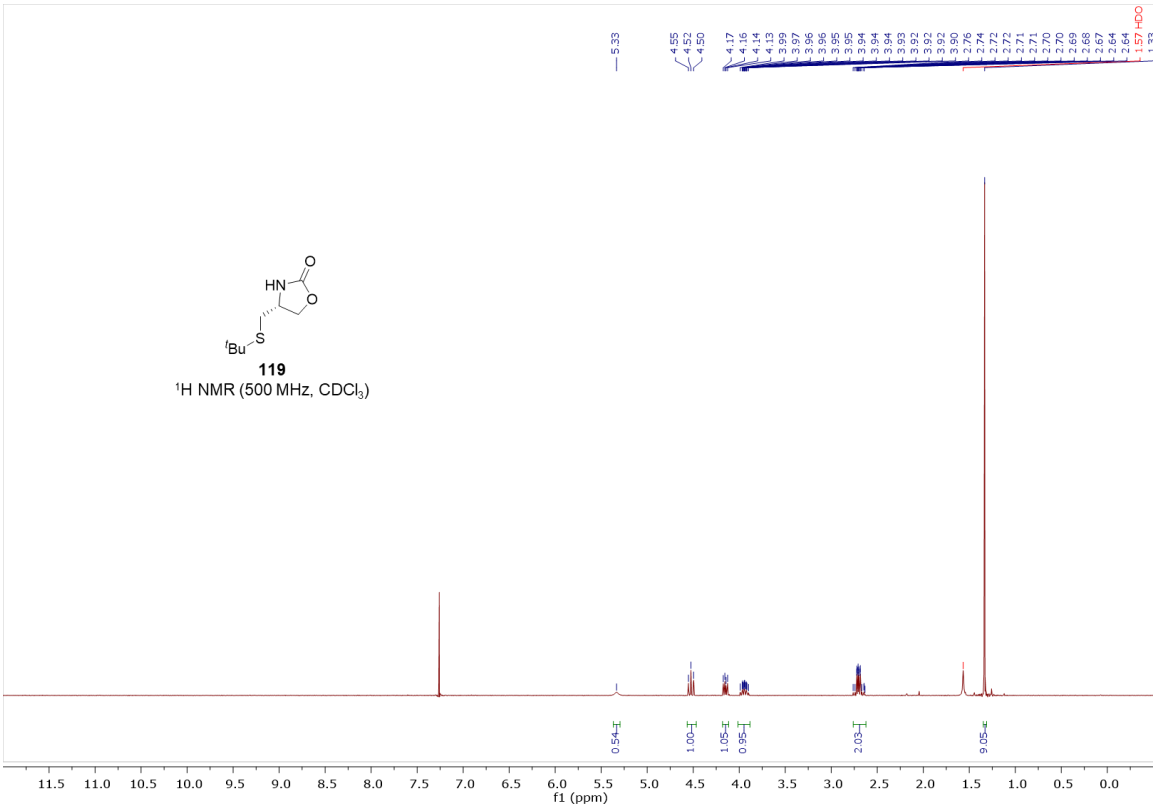

S 11 ^{1}H NMR spectrum of compound **119**

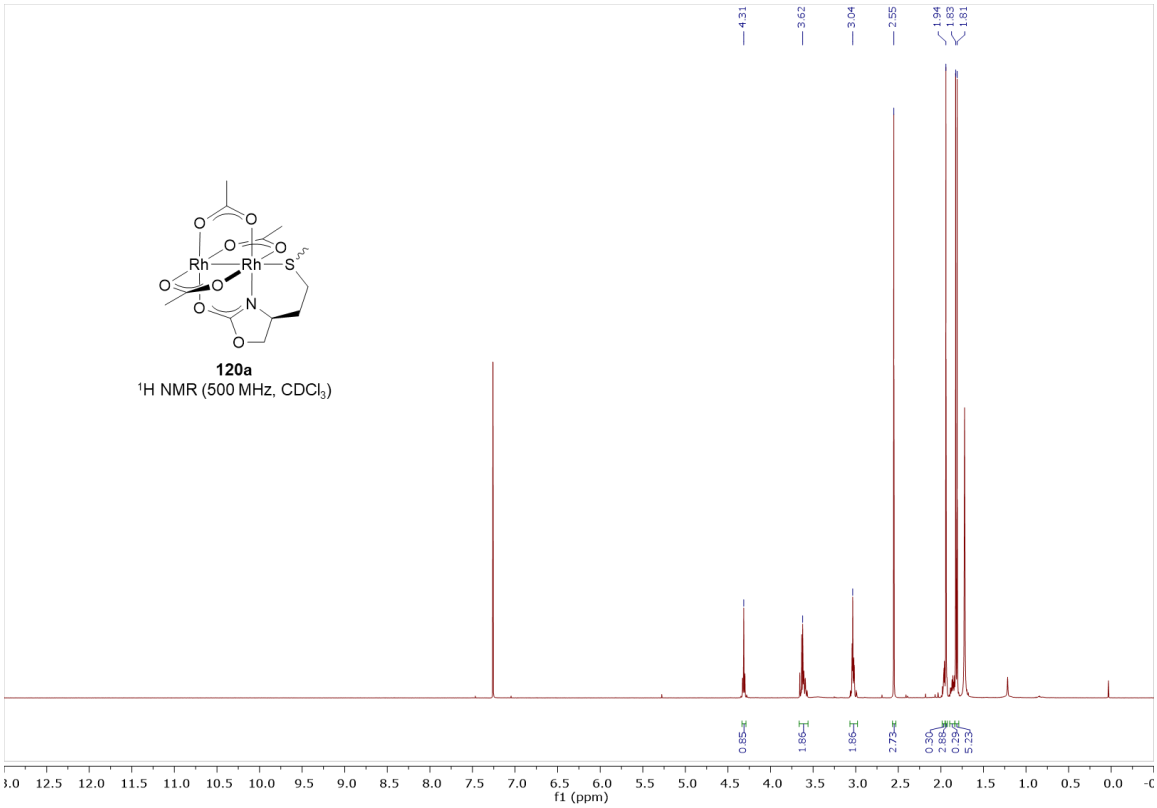

S 12 ^{1}H NMR spectrum of compound **120a**

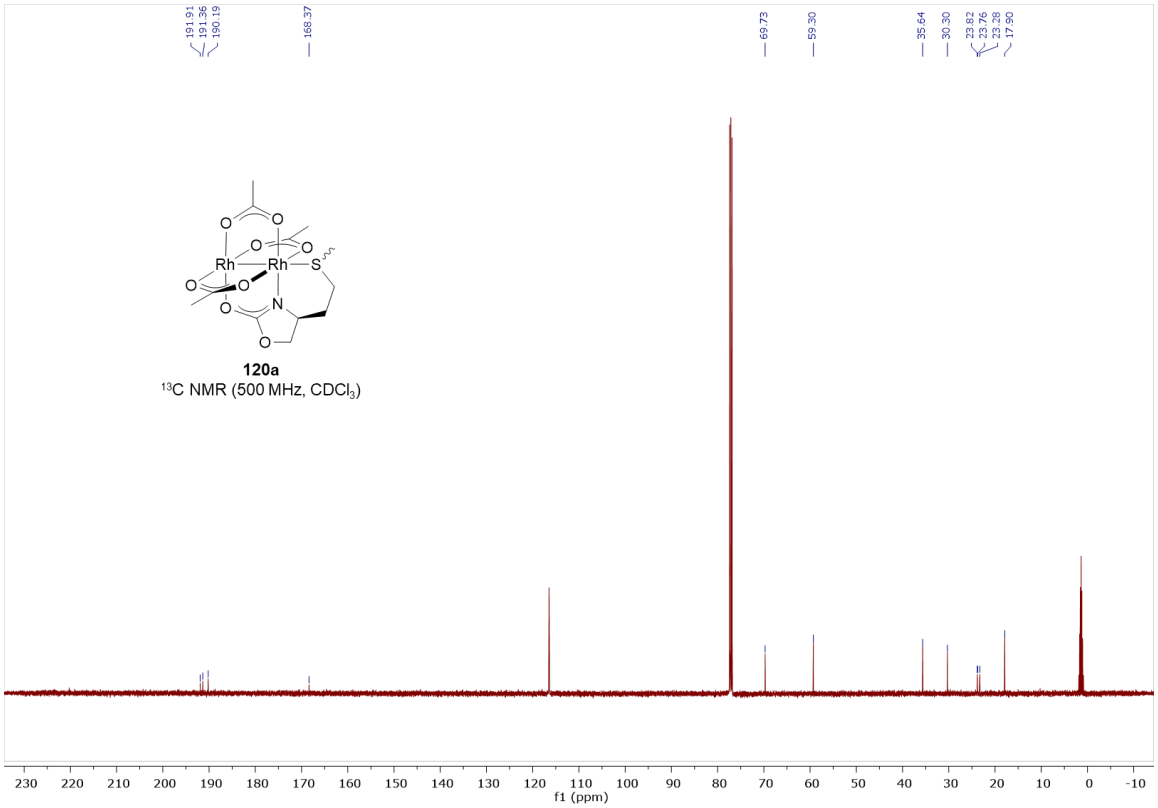

S 13 ^{13}C NMR spectrum of compound **120a**

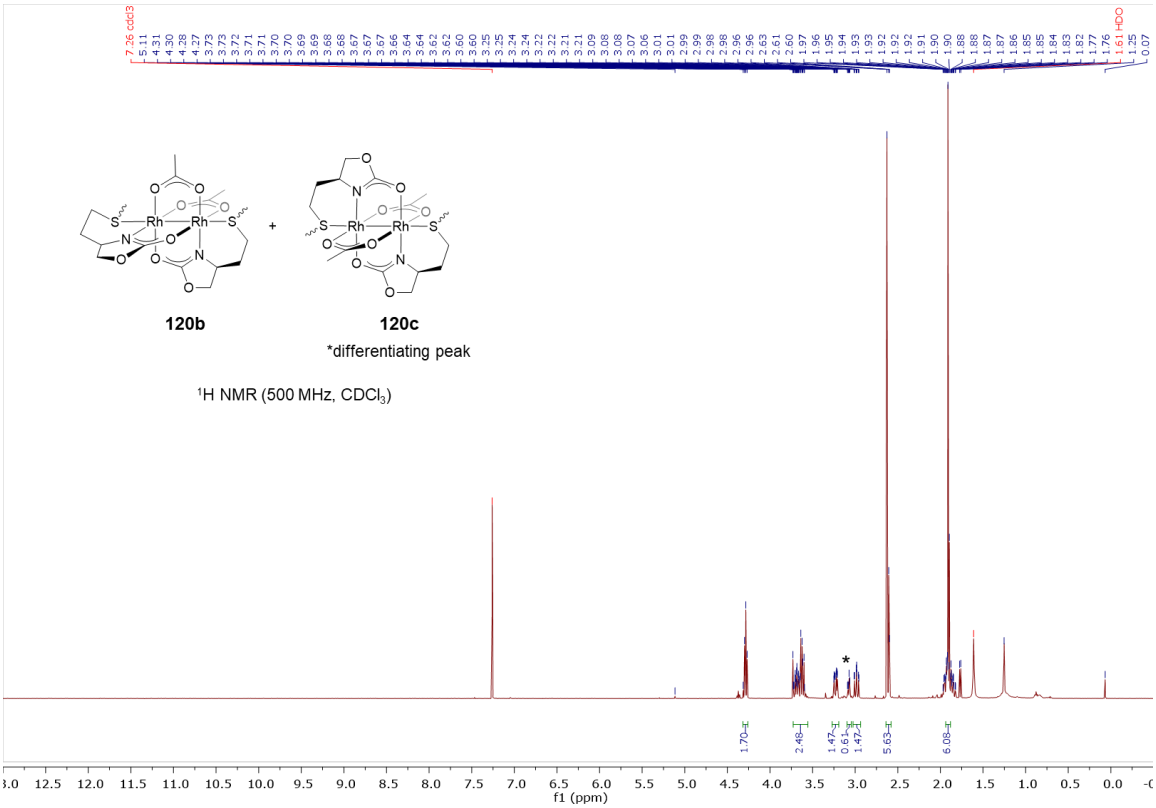

S 14 ^{1}H NMR spectrum of compound **120b/c**

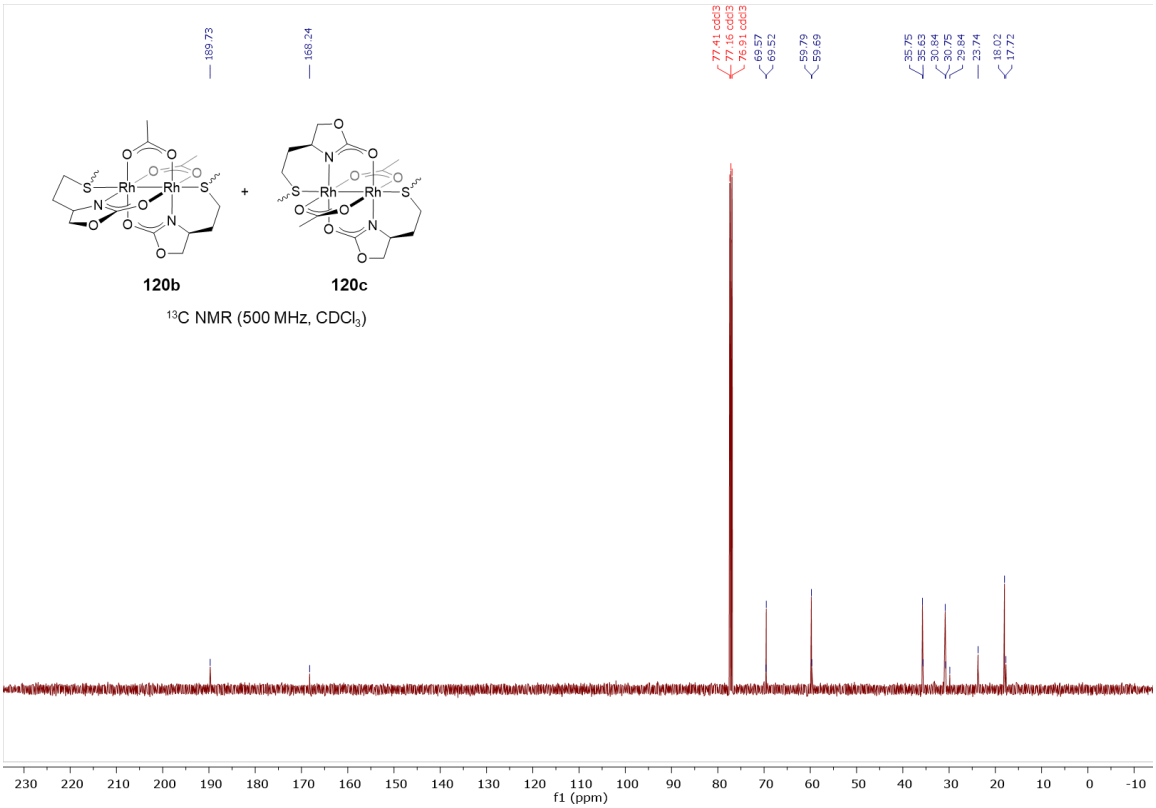

S 15 ^{13}C NMR spectrum of compound **120b/c**

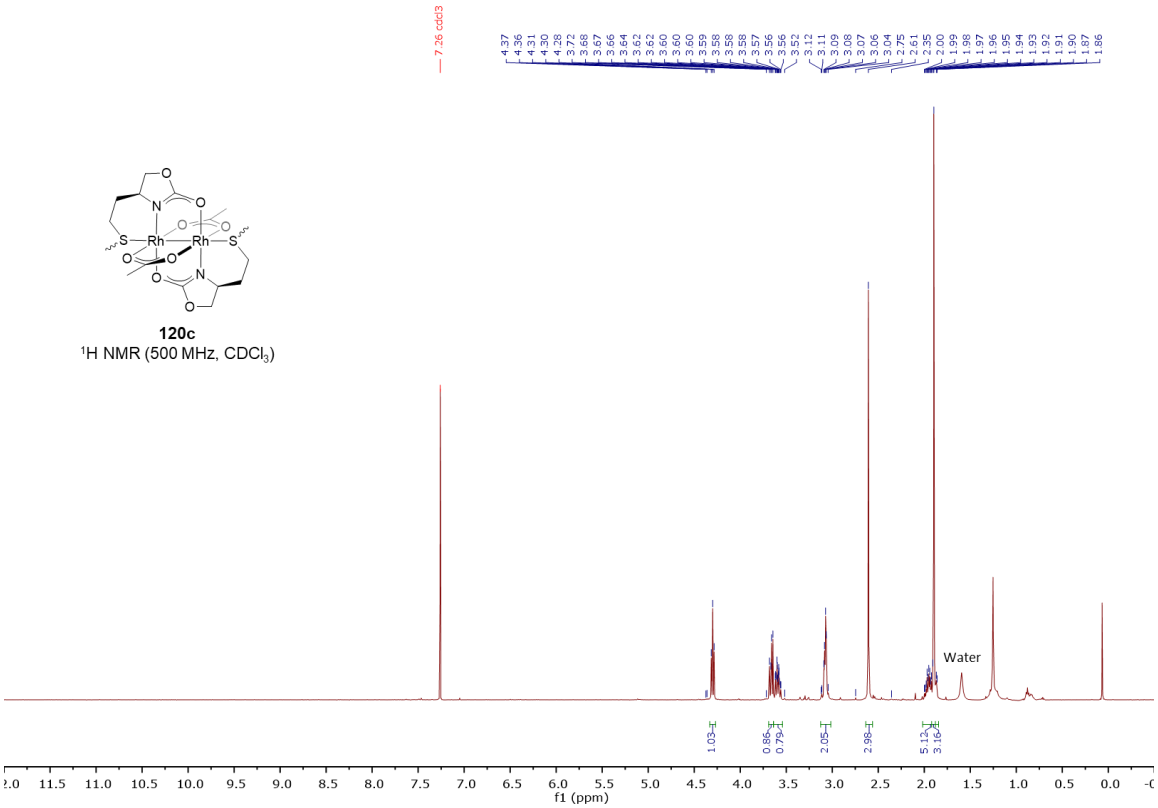

S 16 ^{1}H NMR spectrum of compound **120c**

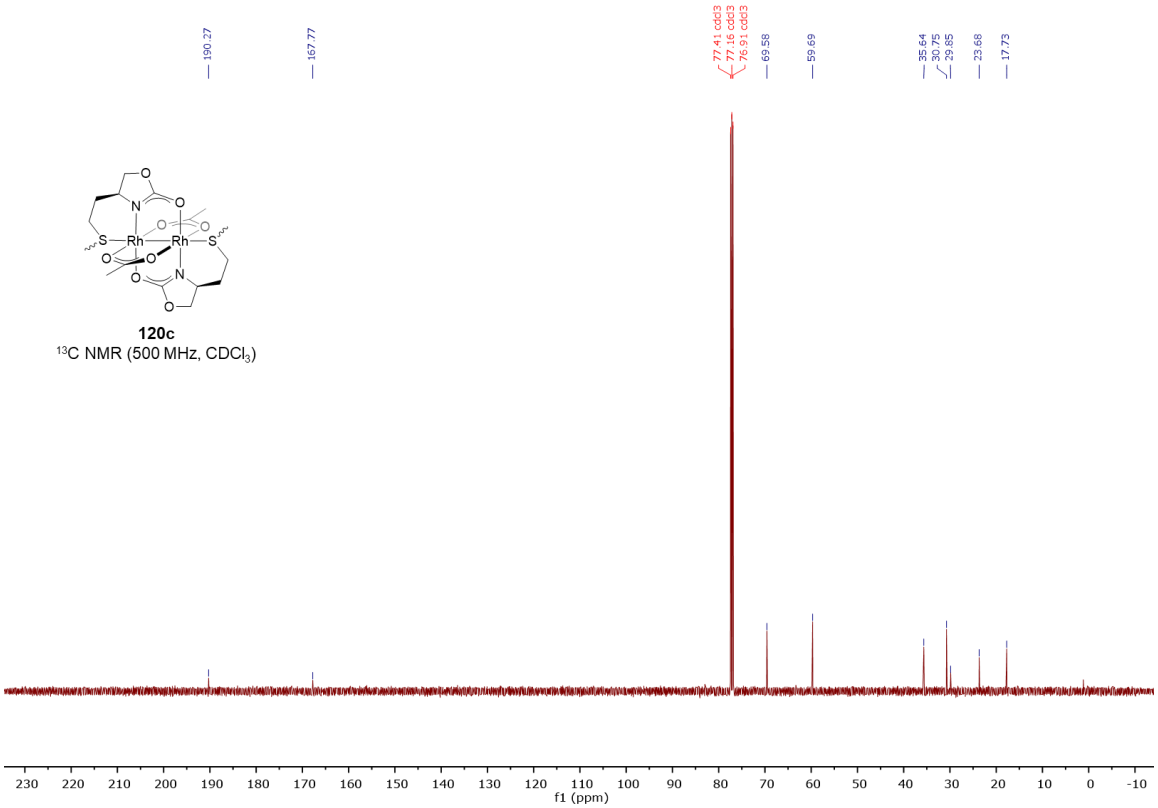

S 17 ^{13}C NMR spectrum of compound **120c**

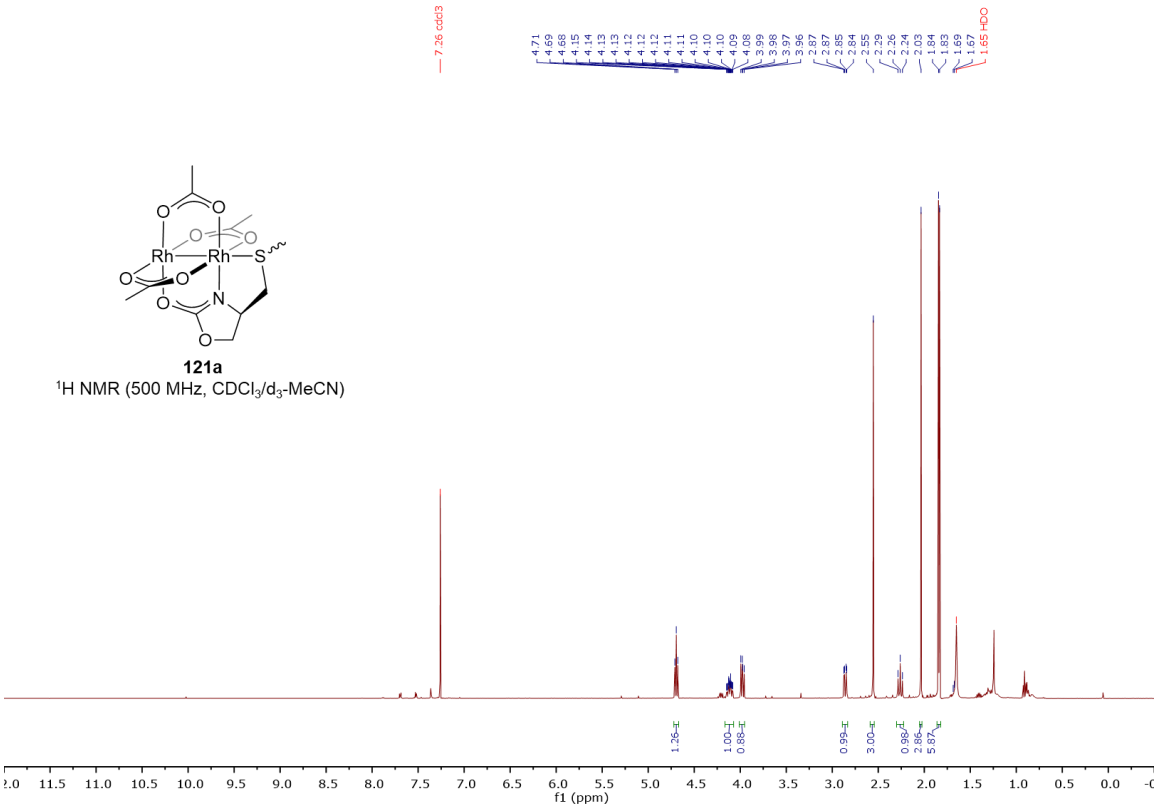

121a

^{1}H NMR (500 MHz, $CDCl_3/d_3$-MeCN)

S 18 ^{1}H NMR spectrum of compound **121a**

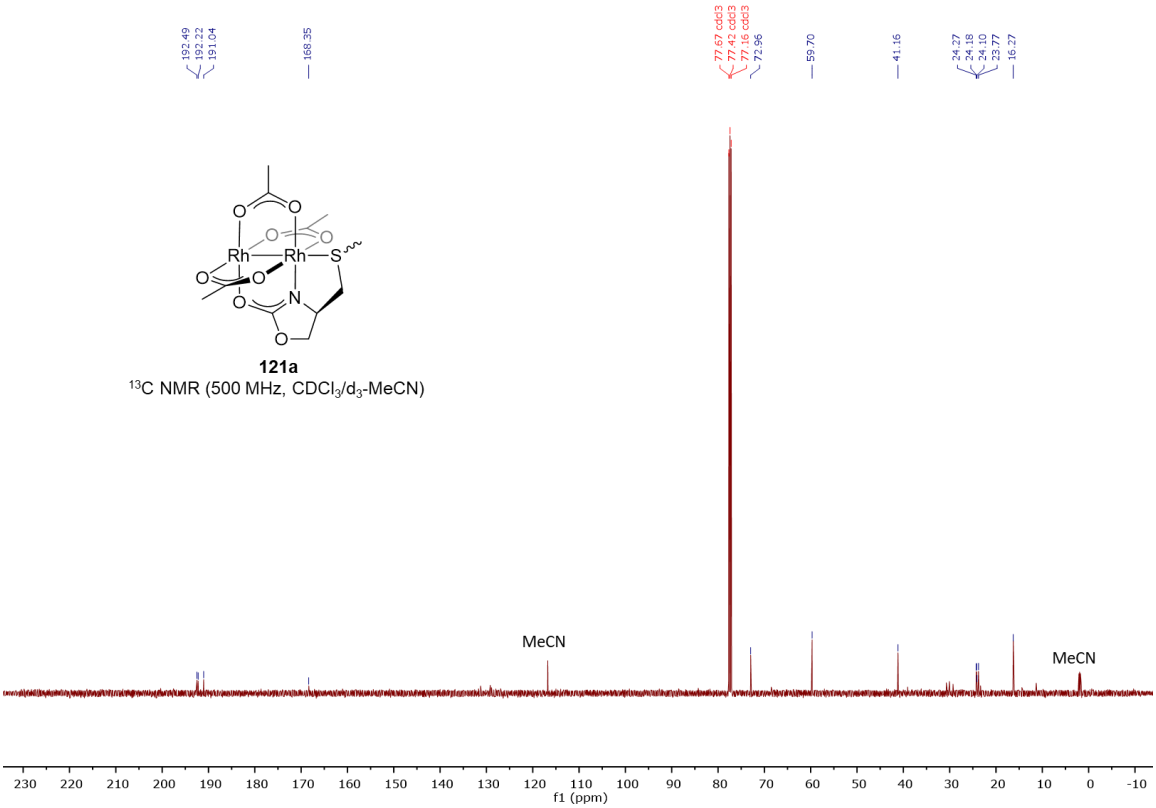

S 19 ^{13}C NMR spectrum of compound **121a**

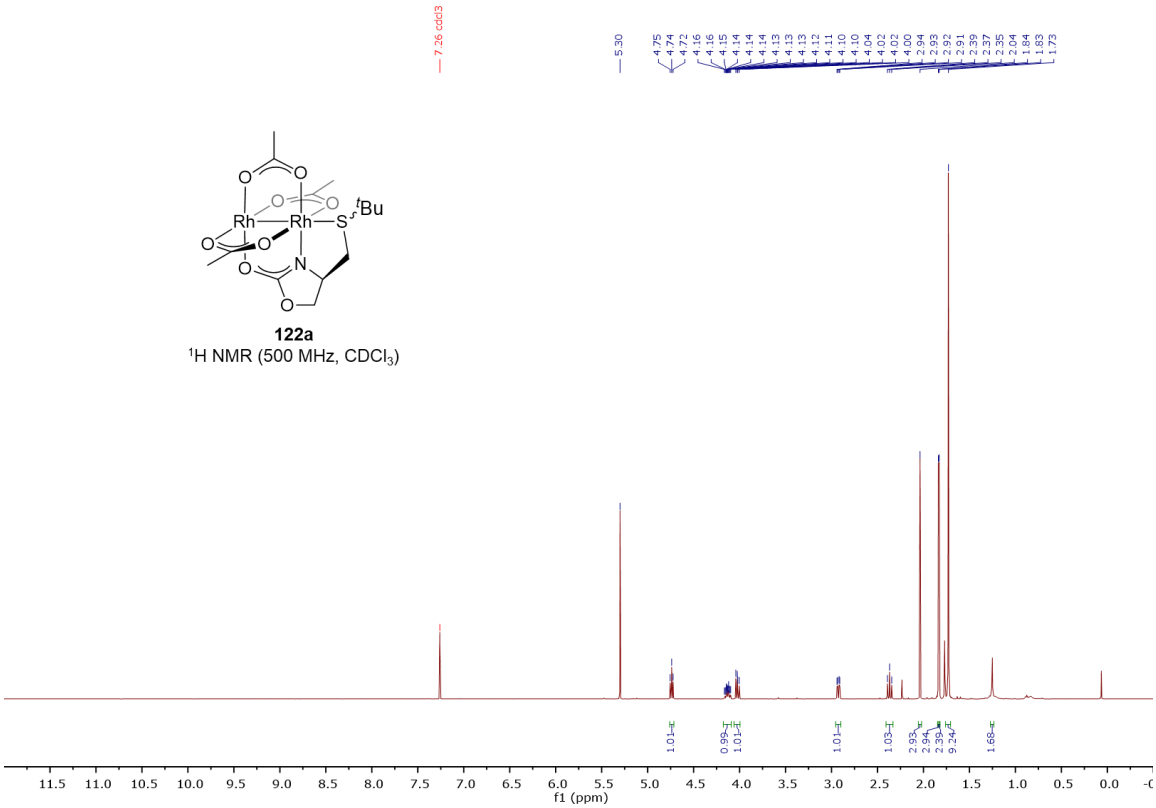

S 20 ^{1}H NMR spectrum of compound **122a**

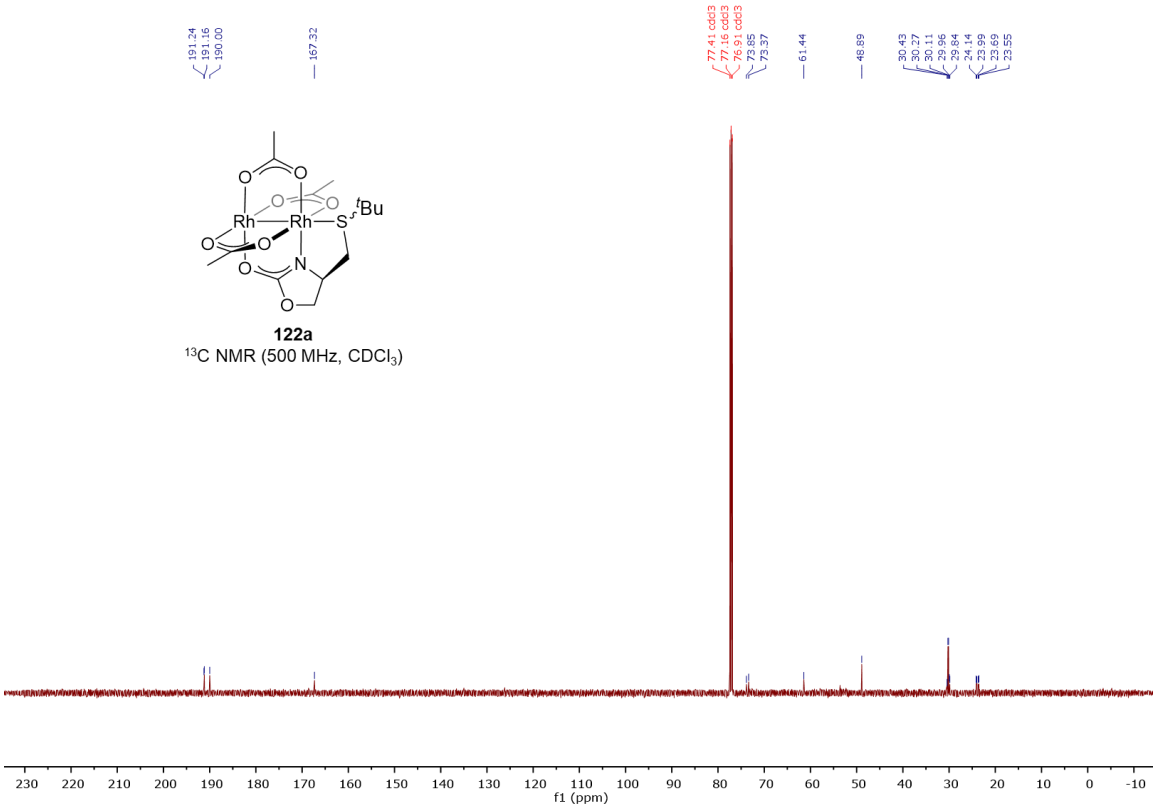

S 21 ^{13}C NMR spectrum of compound **122a**

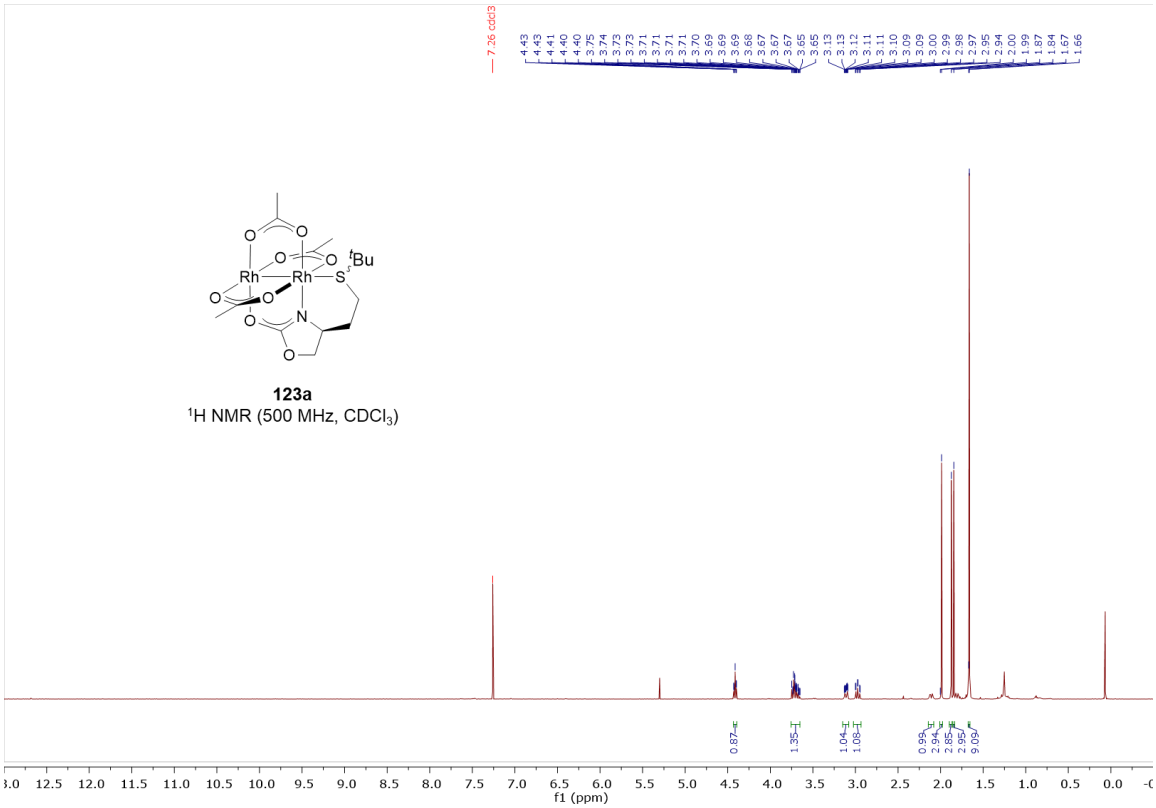

S 22 ^{1}H NMR spectrum of compound **123a**

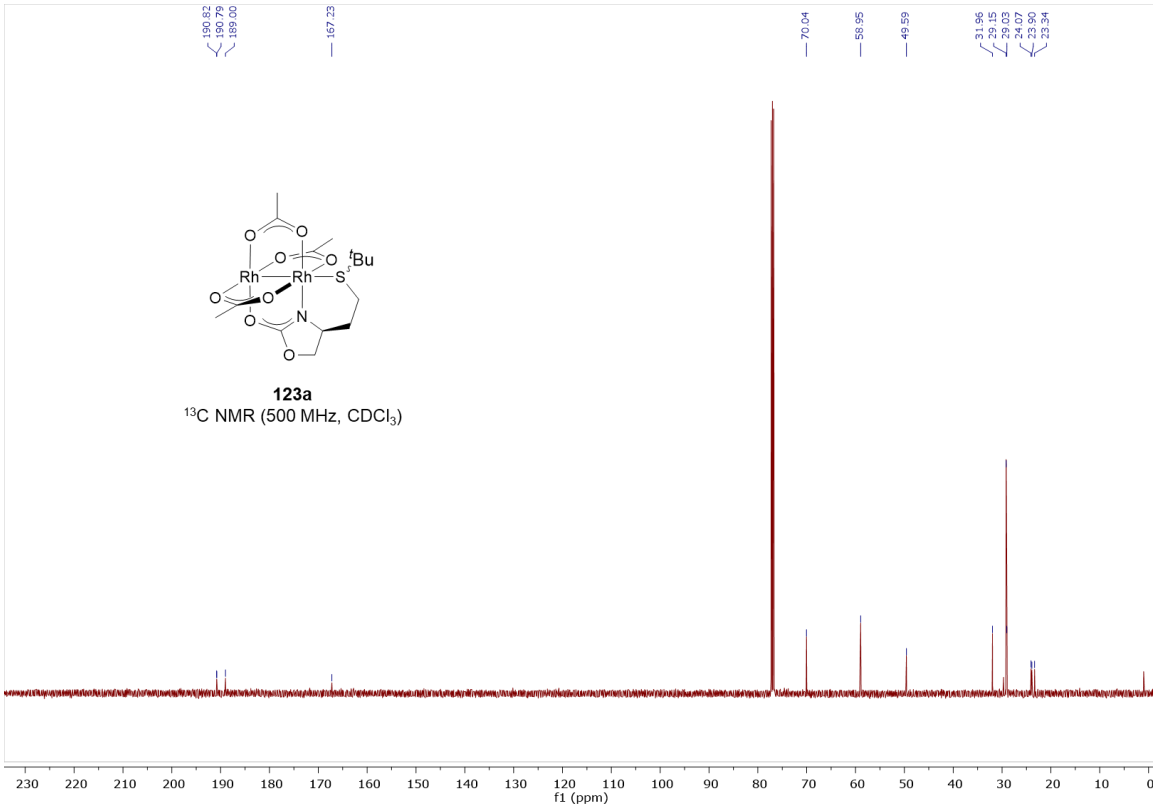

S 23 ^{13}C NMR spectrum of compound **123a**

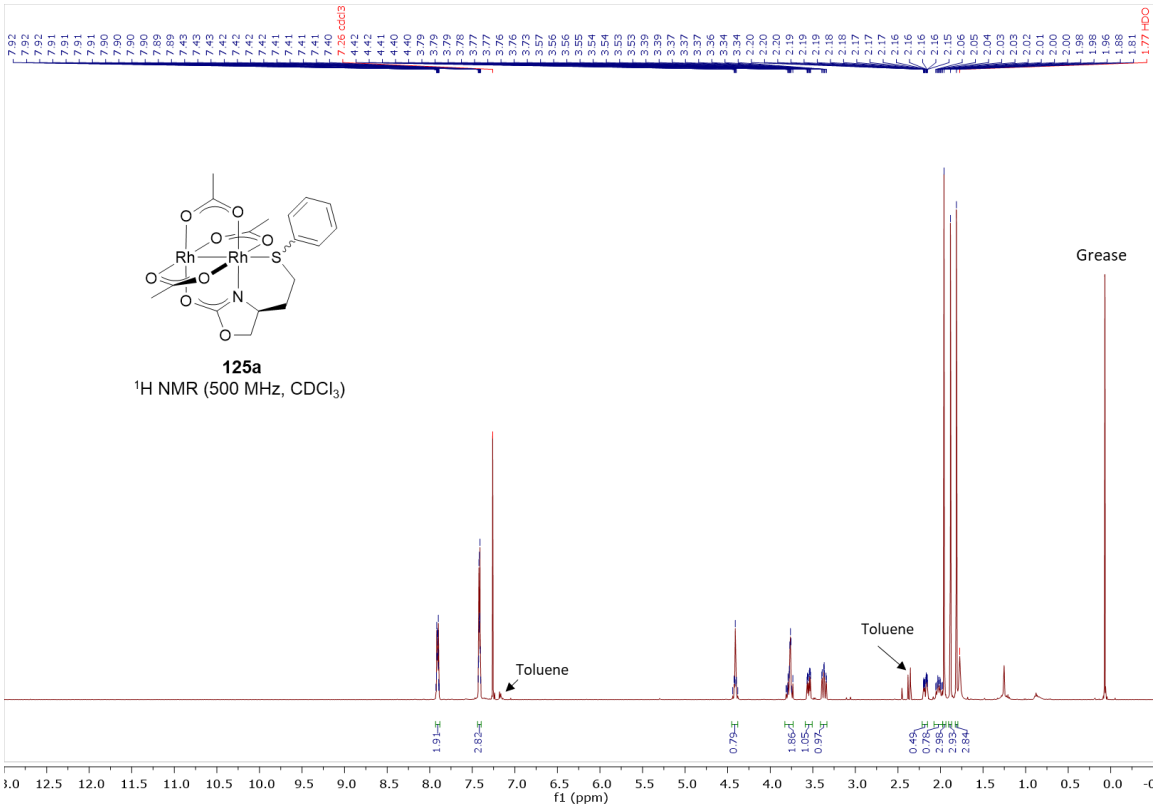

S 24 ^{1}H NMR spectrum of compound **125a**

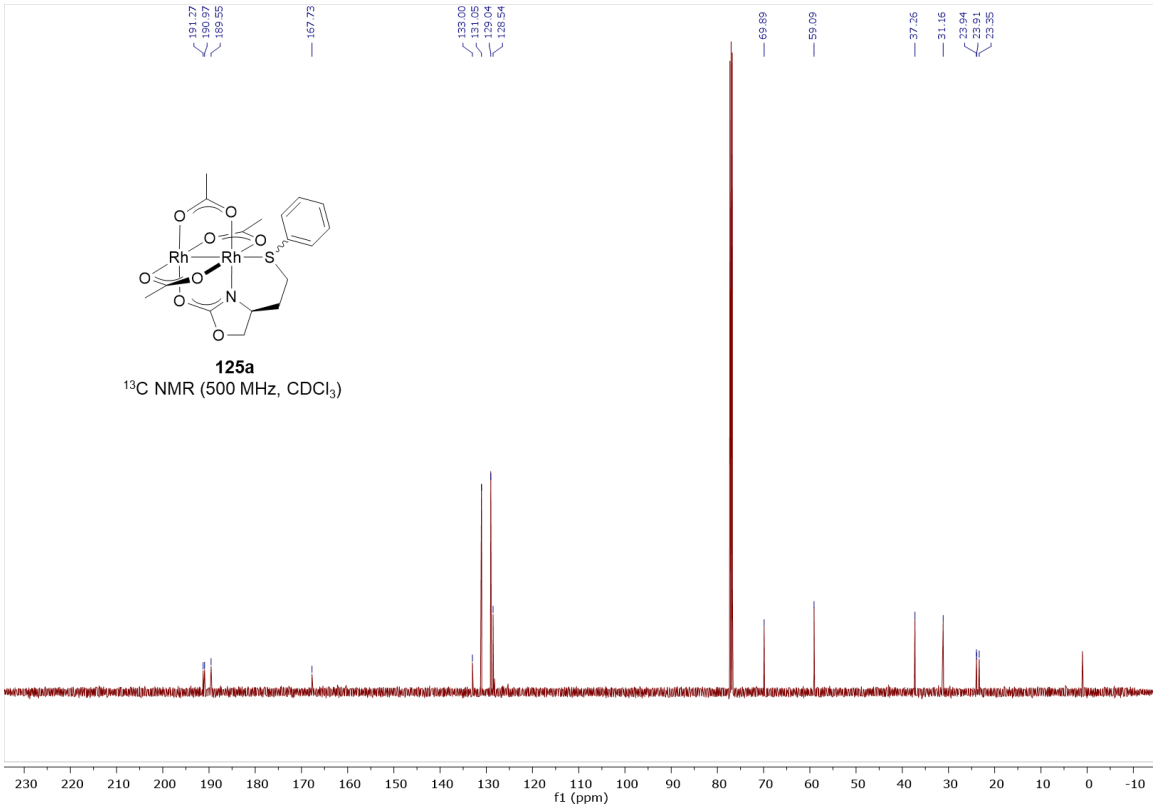

S 25 ^{13}C NMR spectrum of compound **125a**

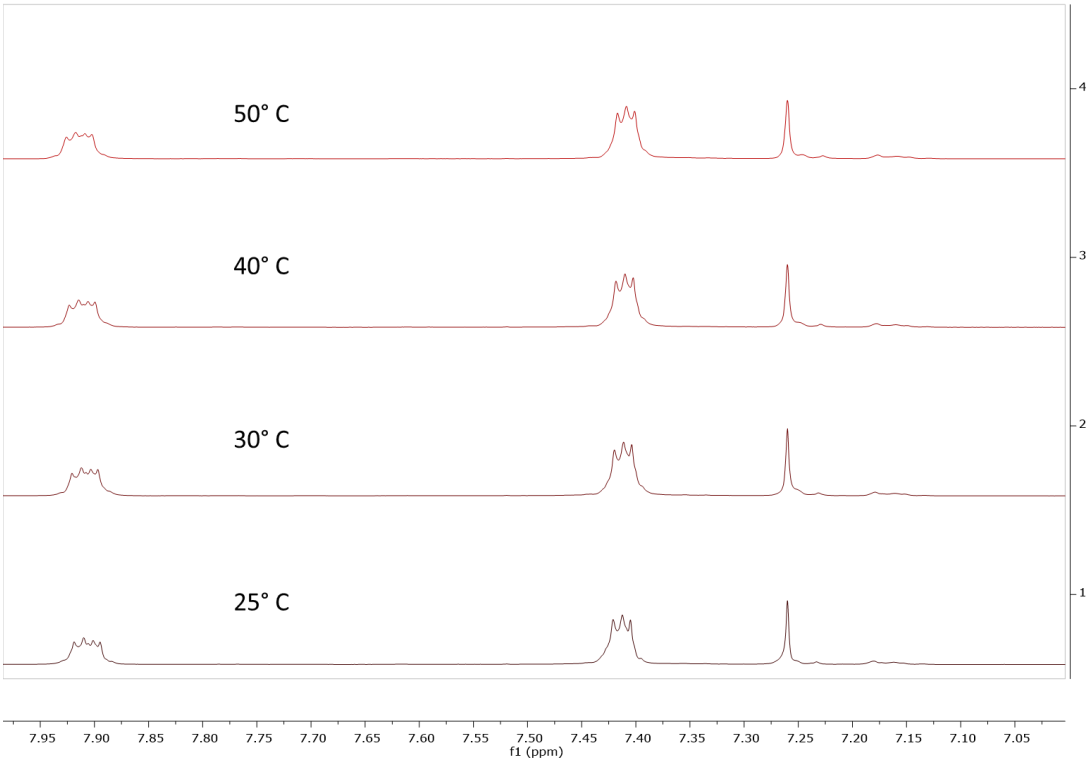

S 26 VT ^{1}H NMR of compound **125a** showing no change in thioether ligand signals

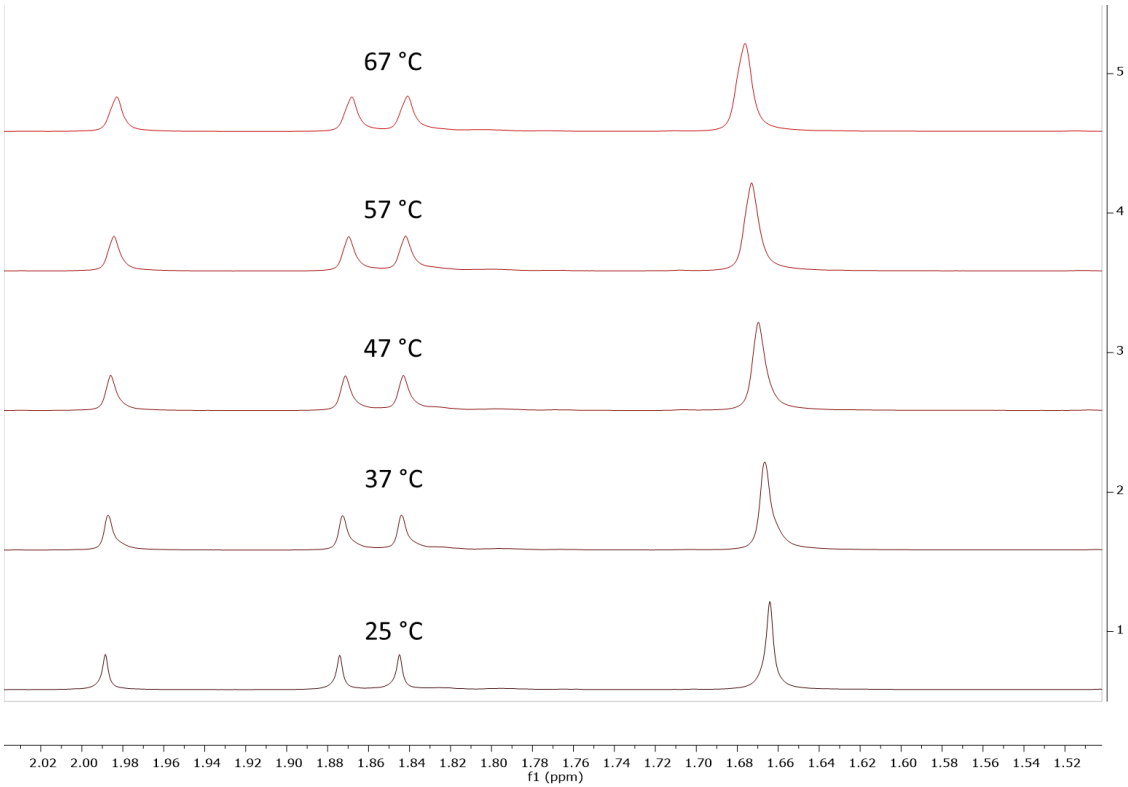

S 27 VT ^{1}H NMR spectra of compound **123a** prepared under dry conditions indicating that the water being dissociated from the axial site

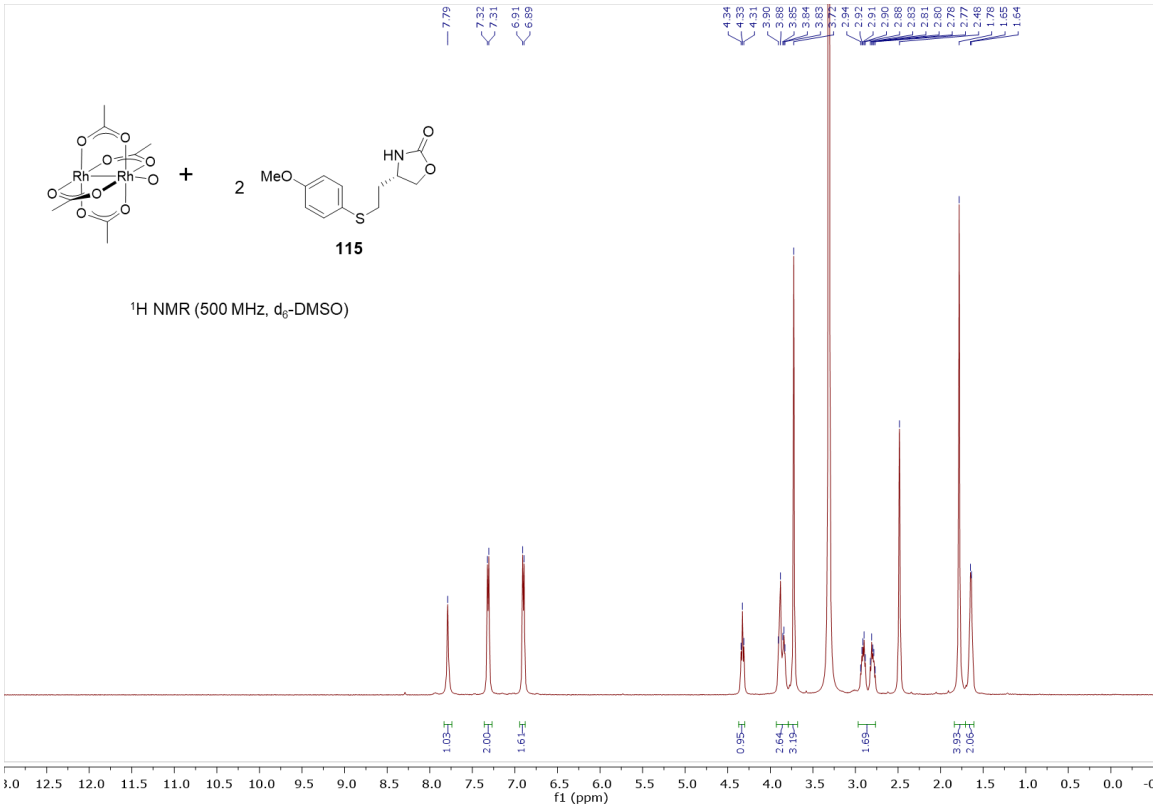

S 28 ^{1}H NMR spectrum of ligand **115** with $Rh_2(OAc)_4$ which precipitated from pressure tube synthesis

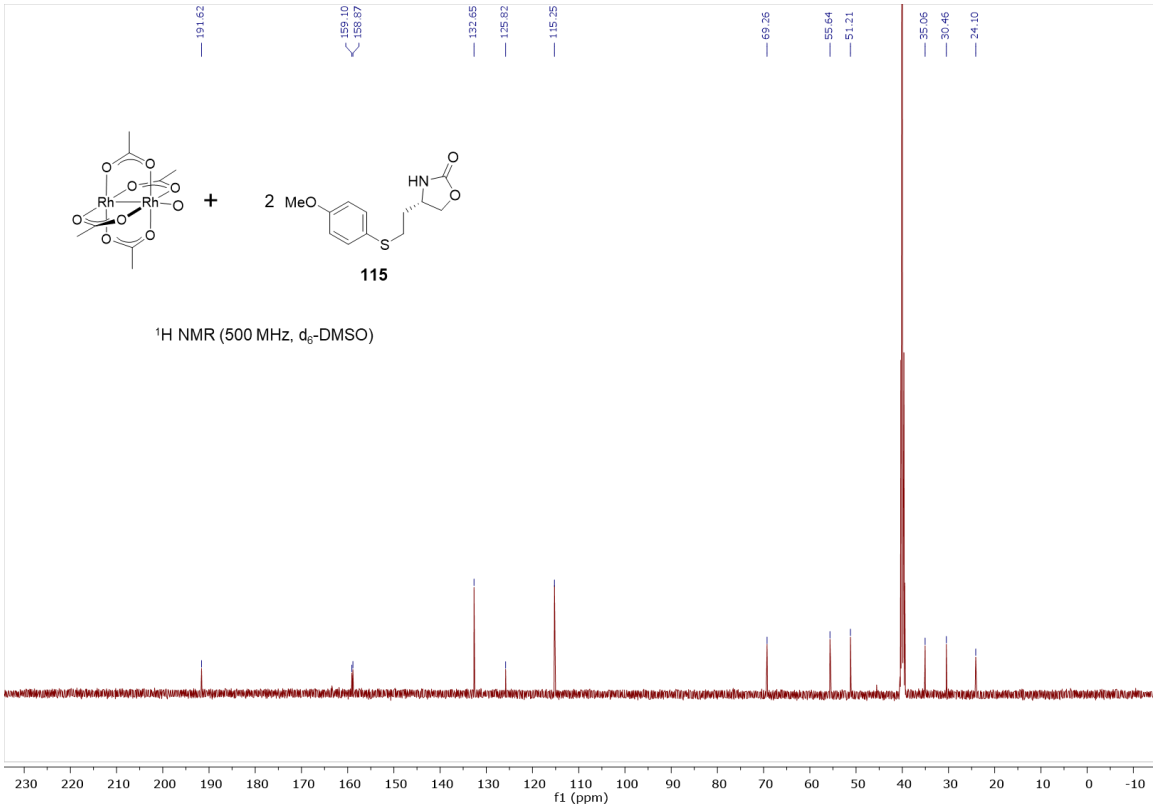

S 29 ^{13}C NMR spectrum of ligand **115** with $Rh_2(OAc)_4$ which precipitated from pressure tube synthesis

Appendix B - Crystallographic Data

The complete crystallographic data sets for **120a** (CCDC Deposition # 2021387) and **125a** (CCDC Deposition # 1861874) are available free of charge from the Cambridge Crystallographic Data Center.

Compound 112

Table 1 Crystal data and structure refinement for DAC_253_L_0m_a.

Identification code	DAC_253_L_0m_a
Empirical formula	$C_{12}H_{15}NO_5S$
Formula weight	285.31
Temperature/K	99.99
Crystal system	orthorhombic
Space group	$P2_12_12_1$
a/Å	11.9443(6)
b/Å	17.2365(8)
c/Å	18.9212(9)
α/°	90
β/°	90
γ/°	90
Volume/Å^3	3895.5(3)
Z	12
ρ_{calc}g/cm^3	1.459
μ/mm^{-1}	2.388
F(000)	1800.0
Crystal size/mm^3	? × ? × ?
Radiation	CuKα (λ = 1.54178)
2Θ range for data collection/°	6.936 to 144.358
Index ranges	-14 ≤ h ≤ 14, -15 ≤ k ≤ 21, -23 ≤ l ≤ 23
Reflections collected	31269
Independent reflections	7643 [R_{int} = 0.0413, R_{sigma} = 0.0398]
Data/restraints/parameters	7643/0/525
Goodness-of-fit on F^2	1.074
Final R indexes [I>=2σ (I)]	R_1 = 0.0323, wR_2 = 0.0892
Final R indexes [all data]	R_1 = 0.0334, wR_2 = 0.0904
Largest diff. peak/hole / e Å^{-3}	0.52/-0.58
Flack parameter	0.019(4)

Table 2 Fractional Atomic Coordinates (×10^4) and Equivalent Isotropic Displacement Parameters (Å^2×10^3) for DAC_253_L_0m_a. U_{eq} is defined as 1/3 of of the trace of the orthogonalised U_{IJ} tensor.

Atom	*x*	*y*	*z*	U(eq)
S001	7740.4(6)	473.6(3)	4316.3(3)	18.00(14)
S002	1642.6(6)	2531.6(3)	1163.9(3)	20.46(15)
S003	8346.7(6)	3866.4(3)	3997.7(3)	21.17(15)
O004	3647.1(17)	6542.5(9)	3763.4(10)	21.0(4)
O005	6205.1(18)	4810.1(10)	861.0(10)	25.2(4)
O006	3568(2)	3428.5(10)	3886.8(10)	27.5(5)
O007	4044.0(18)	6806.9(11)	2629.2(10)	25.2(4)
O008	4078(2)	3580.1(11)	2758.4(11)	32.2(5)
O009	5890(2)	5155.7(12)	1986.8(11)	32.1(5)
O00A	2813.8(17)	2253.4(10)	867.4(10)	23.1(4)
O00B	7031.1(18)	-175.9(10)	4455.9(10)	24.7(4)
O00C	7076.5(16)	1243.2(9)	4475.1(9)	19.3(4)
O00D	1581.6(18)	3358.4(10)	1165.1(10)	26.1(4)
O00E	8765.4(17)	555.2(10)	4702.5(10)	24.6(4)
O00F	7796(2)	3197.7(11)	4280.8(10)	29.2(5)
O10	7571.4(17)	4600.6(10)	4103.0(10)	24.6(4)
N00H	4741(2)	5723.4(13)	3186.3(12)	22.6(5)
O00I	9401.1(19)	4104.5(11)	4282.2(11)	29.9(5)
O00J	853.8(19)	2099.1(12)	757.7(11)	31.5(5)
N00K	5236(2)	4004.6(12)	1530.4(12)	22.8(5)
N00L	4396(2)	2442.0(14)	3363.3(12)	26.1(5)
C00M	4149(2)	6374.8(14)	3135.2(13)	18.5(5)
C00N	5773(3)	4682.1(16)	1512.6(14)	23.8(6)
C00O	1938(2)	1430.5(15)	2176.7(15)	23.9(6)
C00P	4039(2)	3168.7(15)	3281.3(14)	21.3(5)
C00Q	8565(2)	616.0(15)	1979.2(14)	22.8(5)
C00R	7841(3)	3191.6(15)	2730.9(15)	24.4(6)
C00S	1646(2)	2198.1(13)	2043.1(14)	19.7(5)
C00T	7653(2)	-48.1(14)	2949.4(14)	21.4(5)
C00U	5792(3)	4211.2(15)	388.4(14)	22.8(5)
C00V	5361(2)	3564.9(14)	879.1(14)	20.7(5)
C00W	8450(2)	3764.0(13)	3077.6(14)	20.0(5)
C00X	9206(3)	4198.6(16)	1977.5(16)	28.6(6)
C00Y	8609(3)	3631.8(16)	1613.0(15)	25.9(6)
C00Z	1223(3)	2391.0(15)	3268.7(14)	25.0(6)
C010	9134(3)	4271.4(15)	2702.6(15)	24.7(6)
C011	8909(2)	1196.9(15)	2452.4(15)	23.4(5)
C012	3623(3)	2829.9(14)	4420.0(14)	23.5(6)
C013	4268(2)	3199.7(14)	622.5(13)	20.2(5)
C014	1300(3)	2683.8(14)	2582.8(15)	23.8(6)

Table 2 continued

C015	1501(3)	1623.9(15)	3415.5(15)	24.0(5)
C016	7928(3)	3127.9(15)	2002.3(16)	26.8(6)
C017	1881(3)	1153.4(15)	2862.2(16)	25.9(6)
C018	7935(3)	2.7(15)	2237.5(15)	24.7(6)
C019	8643(2)	1157.7(14)	3160.9(14)	21.5(5)
C01A	8910(3)	666.5(18)	1216.9(16)	31.7(7)
C01B	8021(2)	529.6(13)	3408.7(13)	18.3(5)
C01C	4637(2)	5346.3(14)	3873.8(13)	21.3(5)
C01D	4290(2)	2161.3(13)	4085.1(14)	19.8(5)
C01E	1390(3)	1288.3(17)	4145.7(16)	31.7(6)
C01F	3964(3)	5965.1(15)	4281.9(14)	27.4(6)
C01G	8684(3)	3564(2)	823.7(16)	38.4(8)
C01H	5965(2)	1297.8(13)	4155.9(14)	21.1(5)
C01I	5419(2)	2024.3(13)	4442.8(13)	19.3(5)
C01J	5778(2)	5191.0(14)	4210.0(14)	21.4(5)
C01K	6425(2)	4567.7(15)	3827.5(15)	24.6(6)
C01L	3811(2)	2630.6(15)	1154.6(14)	23.7(5)

Table 3 Anisotropic Displacement Parameters ($Å^2×10^3$) for DAC_253_L_0m_a. The Anisotropic displacement factor exponent takes the form: $-2π^2[h^2a^{*2}U_{11}+2hka^*b^*U_{12}+…]$.

Atom	U_{11}	U_{22}	U_{33}	U_{23}	U_{13}	U_{12}
S001	24.1(3)	17.0(3)	12.9(3)	1.20(19)	-1.2(2)	1.3(2)
S002	24.7(3)	20.9(3)	15.8(3)	-0.2(2)	-1.8(3)	-2.4(2)
S003	25.3(3)	22.5(3)	15.8(3)	3.2(2)	-1.5(3)	2.7(2)
O004	25.8(10)	21.2(8)	15.9(8)	2.5(6)	4.3(8)	2.1(7)
O005	32.0(11)	27.1(8)	16.5(9)	-3.0(7)	4.4(8)	-6.6(8)
O006	47.9(13)	18.5(7)	16.2(9)	2.8(7)	11.5(9)	6.0(8)
O007	30.8(12)	27.0(9)	17.8(9)	7.2(7)	4.7(8)	0.3(8)
O008	50.2(14)	29.2(9)	17.2(10)	5.5(8)	10.2(10)	3.5(9)
O009	36.6(12)	38.7(10)	20.9(10)	-11.6(8)	5.0(9)	-6.7(9)
O00A	27.9(11)	23.3(8)	18.1(9)	-3.0(7)	2.8(8)	-1.2(7)
O00B	36.3(12)	19.7(8)	18.3(9)	3.2(7)	2.9(8)	0.5(8)
O00C	21.9(10)	19.2(8)	16.9(8)	-3.0(6)	-3.3(7)	0.4(7)
O00D	31.7(11)	21.4(8)	25.1(10)	3.9(7)	-0.2(9)	1.7(7)
O00E	28.6(11)	28.3(9)	16.8(9)	1.3(7)	-4.4(8)	3.7(8)
O00F	37.7(12)	28.3(9)	21.5(10)	9.6(7)	3.2(9)	2.6(8)
O10	28.8(11)	24.2(8)	20.8(9)	-3.3(7)	-4.3(8)	1.2(7)
N00H	32.5(14)	24.4(10)	10.8(11)	0.5(8)	1.9(10)	5.1(9)
O00I	31.3(12)	35.8(10)	22.5(10)	0.9(8)	-7.3(9)	2.1(8)
O00J	34.9(12)	36.7(10)	23.0(10)	-1.3(8)	-7.7(9)	-9.9(9)

Table 3 Continued

N00K	27.1(13)	29.2(11)	12.0(10)	-0.8(8)	2.5(9)	-4.1(9)
N00L	37.6(15)	30.1(11)	10.7(10)	-0.6(9)	2.5(10)	13.3(10)
C00M	20.2(13)	21.3(11)	14.1(11)	0.0(9)	0.0(10)	-4.6(9)
C00N	24.8(15)	30.7(12)	15.8(12)	-2.2(10)	0.1(11)	2.8(10)
C00O	26.1(15)	22.1(11)	23.4(14)	-1.6(10)	3.7(11)	1.6(10)
C00P	26.9(15)	21.8(11)	15.1(12)	-1.9(9)	3.9(10)	-0.6(10)
C00Q	21.6(14)	29.9(12)	17.1(13)	2.2(10)	-0.8(11)	8.7(10)
C00R	29.7(16)	21.7(11)	21.8(13)	2.7(9)	1.0(12)	-3.1(11)
C00S	19.3(13)	21.1(10)	18.6(12)	0.8(9)	-0.3(11)	-3.5(9)
C00T	25.9(14)	18.7(11)	19.7(13)	1.3(9)	-1.0(11)	0.2(9)
C00U	27.6(15)	26.8(11)	13.9(12)	-2.8(10)	1.8(11)	-6.4(11)
C00V	24.9(14)	23.1(11)	14.3(12)	0.0(9)	1.3(11)	2.6(10)
C00W	25.8(14)	18.6(10)	15.5(11)	1.7(8)	0.2(11)	4.1(10)
C00X	30.2(16)	28.9(12)	26.7(15)	7.9(11)	9.3(13)	1.1(11)
C00Y	25.2(15)	32.8(13)	19.7(13)	3.5(10)	1.6(11)	11.5(11)
C00Z	29.0(15)	27.4(12)	18.5(13)	-4.9(10)	0.0(11)	-0.6(11)
C010	27.2(15)	21.8(11)	24.9(14)	1.6(10)	1.4(12)	-1.6(11)
C011	21.6(14)	26.4(12)	22.1(13)	6.0(10)	-0.2(11)	-1.0(10)
C012	35.1(17)	21.3(10)	14.0(12)	3.0(9)	5.5(11)	6.5(10)
C013	25.4(14)	21.5(10)	13.6(12)	-0.7(9)	-0.5(10)	0.5(10)
C014	30.4(16)	20.9(11)	20.0(13)	-1.5(9)	-3.2(11)	0.8(10)
C015	22.9(14)	29.7(12)	19.3(13)	2.4(10)	-2.3(11)	-5.0(10)
C016	30.2(16)	27.2(12)	22.9(14)	-2.7(10)	-2.7(12)	0.9(11)
C017	29.1(15)	21.0(11)	27.8(14)	5.1(10)	2.3(12)	0.0(10)
C018	31.8(16)	24.2(12)	18.0(13)	-3.5(9)	-3.9(12)	4.4(11)
C019	22.5(14)	21.7(11)	20.2(12)	-0.1(9)	-2.5(11)	-1.4(10)
C01A	33.3(17)	43.7(15)	18.1(13)	4.6(12)	3.9(13)	9.9(13)
C01B	23.0(14)	18.4(10)	13.7(12)	1.7(9)	-0.3(10)	2.7(9)
C01C	27.9(15)	22.1(11)	14.0(12)	2.7(9)	1.3(11)	0.6(9)
C01D	25.6(14)	20.0(10)	13.7(12)	-0.1(9)	2.2(10)	1.7(10)
C01E	33.8(17)	38.8(14)	22.4(14)	6.5(11)	-1.7(13)	-4.1(12)
C01F	38.3(18)	31.7(13)	12.4(12)	6.5(10)	2.1(12)	8.1(12)
C01G	38.5(19)	58.1(19)	18.5(15)	0.6(13)	0.7(13)	11.7(15)
C01H	22.4(14)	21.1(11)	19.7(13)	-3.3(9)	-3.7(11)	2.8(10)
C01I	25.3(14)	18.4(10)	14.1(12)	-1.6(9)	1.8(10)	-0.5(9)
C01J	27.2(14)	22.3(11)	14.6(12)	1.9(9)	-0.2(11)	0.0(10)
C01K	26.1(15)	24.3(11)	23.4(13)	-2.2(10)	-4.6(12)	3.0(10)
C01L	23.2(14)	29.1(12)	18.8(13)	5.0(10)	-0.7(11)	-0.2(10)

Table 4 Bond Lengths for DAC_253_L_0m_a.

Atom	Atom	Length/Å	Atom	Atom	Length/Å
S001	O00B	1.429(2)	C00O	C00S	1.392(3)
S001	O00C	1.5744(18)	C00O	C017	1.384(4)

Table 4 Continued

S001	O00E	1.433(2)	C00Q	C011	1.405(4)
S001	C01B	1.752(3)	C00Q	C018	1.386(4)
S002	O00A	1.582(2)	C00Q	C01A	1.502(4)
S002	O00D	1.4270(18)	C00R	C00W	1.390(4)
S002	O00J	1.426(2)	C00R	C016	1.387(4)
S002	C00S	1.760(3)	C00S	C014	1.384(4)
S003	O00F	1.431(2)	C00T	C018	1.391(4)
S003	O10	1.5808(19)	C00T	C01B	1.393(4)
S003	O00I	1.430(2)	C00U	C00V	1.539(3)
S003	C00W	1.754(3)	C00V	C013	1.529(4)
O004	C00M	1.362(3)	C00W	C010	1.391(4)
O004	C01F	1.448(3)	C00X	C00Y	1.392(4)
O005	C00N	1.355(3)	C00X	C010	1.380(4)
O005	C00U	1.452(3)	C00Y	C016	1.399(4)
O006	C00P	1.353(3)	C00Y	C01G	1.501(4)
O006	C012	1.445(3)	C00Z	C014	1.396(4)
O007	C00M	1.220(3)	C00Z	C015	1.391(4)
O008	C00P	1.218(3)	C011	C019	1.379(4)
O009	C00N	1.221(3)	C012	C01D	1.538(3)
O00A	C01L	1.461(3)	C013	C01L	1.508(3)
O00C	C01H	1.461(3)	C015	C017	1.400(4)
O10	C01K	1.466(3)	C015	C01E	1.504(4)
N00H	C00M	1.330(3)	C019	C01B	1.394(4)
N00H	C01C	1.460(3)	C01C	C01F	1.543(4)
N00K	C00N	1.333(4)	C01C	C01J	1.528(4)
N00K	C00V	1.455(3)	C01D	C01I	1.527(4)
N00L	C00P	1.332(3)	C01H	C01I	1.513(3)
N00L	C01D	1.455(3)	C01J	C01K	1.508(4)

Table 5 Bond Angles for DAC_253_L_0m_a.

Atom	Atom	Atom	Angle/˚	Atom	Atom	Atom	Angle/˚
O00B	S001	O00C	109.04(11)	C014	C00S	S002	119.95(19)
O00B	S001	O00E	119.30(12)	C014	C00S	C00O	121.1(2)
O00B	S001	C01B	109.76(12)	C018	C00T	C01B	118.8(2)
O00C	S001	C01B	103.72(11)	O005	C00U	C00V	104.9(2)
O00E	S001	O00C	104.49(10)	N00K	C00V	C00U	99.70(19)
O00E	S001	C01B	109.31(13)	N00K	C00V	C013	113.3(2)
O00A	S002	C00S	103.54(12)	C013	C00V	C00U	113.1(2)
O00D	S002	O00A	110.40(11)	C00R	C00W	S003	120.2(2)
O00D	S002	C00S	108.95(12)	C00R	C00W	C010	120.8(3)
O00J	S002	O00A	103.57(12)	C010	C00W	S003	119.0(2)

Table 5 Continued

O00J	S002	O00D	119.28(13)	C010	C00X	C00Y	121.6(3)
O00J	S002	C00S	109.89(12)	C00X	C00Y	C016	118.2(3)
O00F	S003	O10	109.17(12)	C00X	C00Y	C01G	121.1(3)
O00F	S003	C00W	108.83(12)	C016	C00Y	C01G	120.7(3)
O10	S003	C00W	104.28(11)	C015	C00Z	C014	120.9(2)
O00I	S003	O00F	119.68(13)	C00X	C010	C00W	119.1(3)
O00I	S003	O10	103.81(11)	C019	C011	C00Q	121.1(2)
O00I	S003	C00W	109.91(13)	O006	C012	C01D	105.7(2)
C00M	O004	C01F	109.3(2)	C01L	C013	C00V	111.4(2)
C00N	O005	C00U	108.4(2)	C00S	C014	C00Z	119.2(2)
C00P	O006	C012	109.63(19)	C00Z	C015	C017	118.6(3)
C01L	O00A	S002	116.99(16)	C00Z	C015	C01E	121.9(3)
C01H	O00C	S001	115.65(14)	C017	C015	C01E	119.5(2)
C01K	O10	S003	118.12(15)	C00R	C016	C00Y	121.2(3)
C00M	N00H	C01C	113.3(2)	C00O	C017	C015	121.1(2)
C00N	N00K	C00V	112.7(2)	C00Q	C018	C00T	121.4(2)
C00P	N00L	C01D	113.2(2)	C011	C019	C01B	119.2(2)
O007	C00M	O004	120.7(2)	C00T	C01B	S001	120.8(2)
O007	C00M	N00H	128.8(3)	C00T	C01B	C019	120.9(2)
N00H	C00M	O004	110.5(2)	C019	C01B	S001	118.3(2)
O009	C00N	O005	121.1(3)	N00H	C01C	C01F	100.5(2)
O009	C00N	N00K	128.5(3)	N00H	C01C	C01J	111.9(2)
N00K	C00N	O005	110.4(2)	C01J	C01C	C01F	112.2(2)
C017	C00O	C00S	119.1(3)	N00L	C01D	C012	100.5(2)
O008	C00P	O006	120.7(2)	N00L	C01D	C01I	113.0(2)
O008	C00P	N00L	129.0(3)	C01I	C01D	C012	113.0(2)
N00L	C00P	O006	110.2(2)	O004	C01F	C01C	105.8(2)
C011	C00Q	C01A	119.4(3)	O00C	C01H	C01I	107.3(2)
C018	C00Q	C011	118.5(3)	C01H	C01I	C01D	110.5(2)
C018	C00Q	C01A	122.1(3)	C01K	C01J	C01C	112.5(2)
C016	C00R	C00W	119.1(3)	O10	C01K	C01J	106.3(2)
C00O	C00S	S002	118.9(2)	O00A	C01L	C013	109.7(2)

Table 6 Hydrogen Atom Coordinates (Å×10⁴) and Isotropic Displacement Parameters (Å²×10³) for DAC_253_L_0m_a.

Atom	*x*	*y*	*z*	U(eq)
H00K	4847	3841	1896	27
H00O	2174	1101	1803	29
H00R	7372	2849	2989	29
H00T	7216	-469	3119	26
H00A	6400	4016	80	27

Table 6 Continued

H00B	5180	4413	88	27
H00V	5948	3156	939	25
H00X	9674	4544	1721	34
H00Z	978	2720	3641	30
H010	9546	4663	2942	30
H011	9332	1624	2282	28
H01A	2862	2655	4552	28
H01B	4006	3024	4849	28
H01K	3709	3613	538	24
H01L	4402	2929	169	24
H014	1117	3210	2488	29
H016	7519	2735	1763	32
H017	2103	635	2959	31
H018	7691	-391	1922	30
H019	8880	1554	3476	26
H01C	8605	1142	1008	48
H01D	8621	215	960	48
H01E	9729	675	1185	48
H01R	4198	4854	3832	26
H01F	3836	1674	4094	24
H01M	1423	1707	4495	47
H01N	2002	922	4231	47
H01O	671	1017	4187	47
H01S	3291	5732	4501	33
H01T	4429	6201	4658	33
H01U	8403	4041	606	58
H01V	8231	3123	665	58
H01W	9466	3483	686	58
H01G	5513	836	4279	25
H01H	6028	1328	3635	25
H01I	5914	2475	4358	23
H01J	5309	1971	4959	23
H01X	6221	5677	4209	26
H01Y	5669	5032	4708	26
H01Z	6090	4052	3918	30
H	6420	4664	3312	30
H01P	4386	2235	1265	28
H01Q	3617	2906	1597	28
H00L	4800(30)	2250(20)	3050(20)	33(10)
H00H	5030(30)	5525(19)	2839(19)	23(8)

Experimental

Single crystals of $C_{12}H_{15}NO_5S$ [DAC_253_L_0m_a] were grown by slow evaporation of DCM. A suitable crystal was selected and mounted on a Bruker D8 Venture diffractometer. The crystal was kept at 99.99 K during data collection. Using Olex2, the structure was solved with the ShelXS structure solution program using the Patterson method and refined with the ShelXL refinement package using least squares minimization.

Complex 128

Table 7 Crystal data and structure refinement for abs2_a.

Identification code	abs2_a
Empirical formula	$C_{16.97}H_{21.47}Cl_{8.16}N_{0.75}O_{7.5}Rh_{1.5}S_{0.75}$
Formula weight	823.49
Temperature/K	104.26
Crystal system	hexagonal
Space group	$P6_1$
a/Å	22.3637(9)
b/Å	22.3637(9)
c/Å	15.1267(6)
α/°	90
β/°	90
γ/°	120
Volume/Å^3	6551.8(6)
Z	7.99998
ρ_{calc}g/cm^3	1.670
μ/mm^{-1}	1.512
F(000)	3254.0
Crystal size/mm^3	0.5 × 0.39 × 0.18
Radiation	MoKα (λ = 0.71073)
2Θ range for data collection/°	4.53 to 63.1
Index ranges	-30 ≤ h ≤ 32, -32 ≤ k ≤ 32, -22 ≤ l ≤ 22
Reflections collected	98745
Independent reflections	14574 [R_{int} = 0.0213, R_{sigma} = 0.0140]
Data/restraints/parameters	14574/19/447
Goodness-of-fit on F^2	1.093
Final R indexes [I>=2σ (I)]	R_1 = 0.0250, wR_2 = 0.0728
Final R indexes [all data]	R_1 = 0.0252, wR_2 = 0.0729
Largest diff. peak/hole / e Å^{-3}	2.91/-0.77
Flack parameter	0.009(4)

Table 8 Fractional Atomic Coordinates (×10^4) and Equivalent Isotropic Displacement Parameters (Å^2×10^3) for abs2_a. U_{eq} is defined as 1/3 of of the trace of the orthogonalised U_{IJ} tensor.

Atom	*x*	*y*	*z*	U(eq)
Rh01	4080.4(2)	8964.7(2)	6734.8(2)	13.35(5)
Rh02	4255.0(2)	10085.5(2)	7083.0(2)	12.64(5)
S003	5604.8(4)	8785.4(4)	2563.2(5)	15.01(12)
Cl04	3580.4(6)	10607.4(5)	9818.7(7)	34.1(2)
Cl05	2588.5(6)	9176.6(5)	9451.4(8)	37.7(2)
Cl06	5571.0(6)	8116.0(7)	6278.5(8)	40.4(2)
Cl07	4843.6(7)	7160.1(6)	7684.7(7)	38.6(2)
Cl08	2264.8(6)	10245.2(6)	9020.9(10)	41.6(2)
Cl09	2327.7(8)	9654.9(7)	5201.7(9)	46.7(3)
Cl0A	2490.5(8)	10622.4(8)	6588.2(10)	51.3(3)
Cl0B	3027.5(12)	11113.2(9)	4850.4(11)	68.2(5)
Cl0C	5899.7(9)	8539.2(8)	8110.5(12)	61.1(4)
O00D	4287.6(12)	9865.4(12)	8378.2(16)	17.7(4)
O00E	3212.6(12)	9649.0(11)	7179.0(16)	17.6(4)
O00F	4099.8(13)	8799.2(12)	8053.5(16)	19.0(4)
O00G	4076.5(12)	9190.4(12)	5424.9(16)	17.9(4)
O00H	4191.1(12)	10229.5(12)	5759.1(16)	16.6(4)
O00I	5294.0(11)	10452.1(11)	6988.4(16)	17.2(4)
O00J	3045.7(12)	8600.1(12)	6808.4(17)	18.8(4)
O00K	5124.1(12)	9386.5(12)	6704.4(17)	19.3(4)
O00L	3880.2(13)	7864.9(12)	6510.3(15)	17.1(4)
O00N	3836.4(15)	6985.6(12)	5752.0(16)	22.0(5)
N00O	4064.4(17)	7924.8(14)	5004.1(19)	21.0(5)
C00Q	4188.4(16)	9273.0(16)	8590(2)	17.5(5)
C00S	6272.9(17)	10312.2(19)	6830(3)	23.4(6)
C00T	4112.4(16)	9760.6(16)	5217(2)	17.0(5)
C00U	5506.4(15)	10028.9(16)	6844(2)	16.4(5)
C00V	4743.6(16)	7811.0(15)	3774(2)	16.9(5)
C00W	2829.2(16)	9002.3(15)	7036(2)	16.9(5)
C00X	4850.7(16)	8446.9(16)	3279(2)	17.3(5)
C00Y	4073.4(17)	7477.7(15)	4305(2)	17.2(5)
C00Z	4047(2)	9888.5(19)	4250(2)	22.6(6)
C010	3927.1(16)	7624.2(15)	5798(2)	15.8(5)
C011	4176(2)	9119(2)	9558(2)	24.4(6)
C012	2066.4(17)	8694.1(18)	7154(3)	25.6(7)
C013	3967(3)	6852.9(18)	4853(2)	29.7(8)
C014	5293.7(16)	8204.3(15)	1649(2)	17.7(5)
C015	4775(2)	8161.0(19)	1103(3)	27.2(7)
C016	2858(2)	10485(2)	5653(3)	34.9(8)
C017	5615(2)	7826(2)	1465(3)	30.7(8)

Table 8 Continued

C018	4912(3)	7373(2)	161(3)	35.0(9)
C019	2927(2)	10038.3(19)	9096(3)	28.1(7)
C01A	4578(3)	7739(2)	362(3)	34.7(9)
C01D	5257(2)	8041(2)	7352(3)	29.2(7)
C01E	5419(3)	7410(3)	704(3)	42.4(11)
C6	1745(4)	11606(5)	3684(6)	42.0(16)
Cl1	2554.9(15)	11995.8(15)	3146(2)	64.1(8)
Cl3	1114(2)	11667(3)	3150(2)	106.2(19)
Cl1A	1945(2)	12030(3)	4757(2)	94.7(15)

Table 9 Anisotropic Displacement Parameters ($Å^2 \times 10^3$) for abs2_a. The Anisotropic displacement factor exponent takes the form: $-2\pi^2[h^2a^{*2}U_{11}+2hka^*b^*U_{12}+\ldots]$.

Atom	U_{11}	U_{22}	U_{33}	U_{23}	U_{13}	U_{12}
Rh01	16.05(9)	10.80(9)	12.90(9)	-0.15(7)	0.93(7)	6.49(7)
Rh02	13.90(9)	10.46(8)	12.85(8)	-0.38(7)	0.05(7)	5.56(7)
S003	16.4(3)	13.1(3)	15.4(3)	1.6(2)	0.8(2)	7.2(2)
Cl04	41.9(5)	23.3(4)	29.2(4)	-2.1(3)	-2.1(4)	10.5(4)
Cl05	43.2(5)	19.9(4)	43.3(6)	3.1(4)	4.0(4)	10.9(4)
Cl06	42.1(5)	49.4(6)	41.9(6)	15.0(5)	15.7(5)	32.0(5)
Cl07	53.6(6)	34.8(5)	26.8(4)	2.3(4)	-0.4(4)	21.6(5)
Cl08	39.6(5)	33.6(5)	52.2(6)	4.3(5)	1.2(5)	18.7(4)
Cl09	51.8(7)	38.5(5)	43.1(6)	-2.8(5)	-7.7(5)	17.6(5)
Cl0A	63.4(8)	52.1(7)	50.4(7)	1.9(6)	16.8(6)	37.9(7)
Cl0B	89.6(13)	46.1(7)	49.2(8)	15.5(6)	8.7(8)	19.1(8)
Cl0C	67.1(9)	44.6(7)	70.2(10)	-21.9(7)	-37.8(8)	26.9(7)
O00D	21.6(10)	15.4(9)	14.4(9)	-0.9(8)	-0.2(8)	7.9(8)
O00E	15.6(9)	13.8(9)	22.1(11)	-2.6(8)	0.7(8)	6.5(8)
O00F	27.8(11)	15.2(9)	14.4(10)	2.1(8)	-0.1(8)	11.0(9)
O00G	24.9(10)	16.1(9)	14.1(9)	0.2(8)	1.5(8)	11.3(8)
O00H	19.4(10)	14.7(9)	15.6(9)	0.3(8)	0.2(8)	8.5(8)
O00I	14.4(9)	13.6(9)	21.3(10)	-0.9(8)	-0.5(8)	5.2(7)
O00J	17.5(9)	13.8(9)	23.4(10)	-2.6(8)	1.6(8)	6.5(8)
O00K	18.3(10)	18.2(10)	23.1(11)	-0.6(9)	1.5(9)	10.3(8)
O00L	23.0(10)	15.4(9)	12.8(9)	-0.9(7)	3.1(7)	9.5(8)
O00N	36.6(13)	13.8(9)	15.7(10)	1.8(8)	7.1(9)	12.8(10)
N00O	35.6(15)	17.0(11)	14.2(11)	1.4(9)	5.5(10)	16.0(11)
C00Q	17.8(12)	18.1(12)	15.3(13)	1.9(10)	-0.3(9)	7.9(10)
C00S	16.0(13)	25.3(15)	28.1(16)	-1.8(12)	0.5(11)	9.7(12)
C00T	17.0(12)	16.9(12)	16.1(13)	0.5(10)	0.2(9)	7.8(10)
C00U	15.6(12)	18.0(12)	15.4(12)	1.4(10)	0.5(9)	8.2(10)

Table 9 Continued

C00V	21.7(13)	14.9(11)	16.1(11)	1.1(10)	3.2(10)	10.7(10)
C00W	16.5(12)	14.0(11)	17.7(12)	-0.2(10)	1.5(10)	5.7(10)
C00X	20.3(13)	16.3(12)	17.8(13)	4.9(10)	5.6(10)	10.9(10)
C00Y	21.9(13)	12.9(11)	15.8(12)	0.4(9)	3.8(10)	7.9(10)
C00Z	30.9(16)	24.9(15)	13.5(13)	2.3(11)	-0.3(12)	15.1(14)
C010	17.2(12)	14.1(11)	15.4(12)	1.0(9)	3.3(10)	7.2(10)
C011	32.7(17)	23.9(15)	14.9(13)	2.8(11)	0.0(12)	12.9(13)
C012	16.6(13)	19.4(14)	34.9(18)	-3.7(13)	2.6(13)	4.6(11)
C013	55(2)	16.4(14)	17.9(14)	3.8(11)	15.7(15)	17.6(15)
C014	21.7(13)	14.6(11)	15.5(12)	0.6(10)	0.4(10)	8.2(10)
C015	30.9(17)	19.4(14)	33.1(18)	-6.3(13)	-13.6(14)	14.1(13)
C016	34(2)	38(2)	39(2)	1.6(17)	1.9(17)	22.6(17)
C017	40(2)	37(2)	26.3(17)	-7.9(15)	-3.7(15)	28.0(18)
C018	53(2)	24.1(16)	19.6(15)	-3.6(13)	1.0(16)	12.7(16)
C019	35.3(19)	18.7(14)	24.6(16)	-0.6(12)	3.9(14)	9.3(14)
C01A	45(2)	21.8(16)	29.5(18)	-5.3(14)	-14.9(17)	10.8(15)
C01D	33.1(18)	30.7(18)	30.4(18)	-6.9(14)	-8.0(15)	20.8(16)
C01E	59(3)	45(3)	34(2)	-14.1(19)	0(2)	35(2)
C6	41(4)	49(4)	41(4)	-6(3)	6(3)	26(3)
Cl1	53.2(13)	57.4(14)	70.8(17)	20.4(12)	15.7(12)	19.3(11)
Cl3	84(2)	219(6)	52.9(16)	-14(2)	-15.6(15)	103(3)
Cl1A	111(3)	158(4)	48.5(15)	-39(2)	-16.3(16)	92(3)

Table 10 Bond Lengths for abs2_a.

Atom	Atom	Length/Å	Atom	Atom	Length/Å
Rh01	Rh02	2.3946(3)	O00G	C00T	1.277(4)
Rh01	O00F	2.033(2)	O00H	C00T	1.273(4)
Rh01	O00G	2.046(2)	O00I	C00U	1.272(4)
Rh01	O00J	2.036(2)	O00J	C00W	1.264(4)
Rh01	O00K	2.034(2)	O00K	C00U	1.269(4)
Rh01	O00L	2.294(2)	O00L	C010	1.233(4)
Rh02	S003[1]	2.4921(7)	O00N	C010	1.340(4)
Rh02	O00D	2.030(2)	O00N	C013	1.452(4)
Rh02	O00E	2.033(2)	N00O	C00Y	1.463(4)
Rh02	O00H	2.045(2)	N00O	C010	1.334(4)
Rh02	O00I	2.046(2)	C00Q	C011	1.502(5)
S003	Rh02[2]	2.4920(7)	C00S	C00U	1.501(4)
S003	C00X	1.820(3)	C00T	C00Z	1.511(4)
S003	C014	1.783(3)	C00V	C00X	1.516(4)
Cl04	C019	1.758(4)	C00V	C00Y	1.526(4)
Cl05	C019	1.766(4)	C00W	C012	1.497(5)

Table 10 Continued

Cl06	C01D	1.743(5)	C00Y	C013	1.537(5)
Cl07	C01D	1.779(4)	C014	C015	1.387(5)
Cl08	C019	1.762(5)	C014	C017	1.385(5)
Cl09	C016	1.767(5)	C015	C01A	1.388(5)
Cl0A	C016	1.738(5)	C017	C01E	1.405(6)
Cl0B	C016	1.749(5)	C018	C01A	1.389(7)
Cl0C	C01D	1.738(4)	C018	C01E	1.369(8)
O00D	C00Q	1.270(4)	C6	Cl1	1.767(8)
O00E	C00W	1.278(4)	C6	Cl3	1.690(9)
O00F	C00Q	1.269(4)	C6	Cl1A	1.820(9)

[1]1-X,2-Y,1/2+Z; [2]1-X,2-Y,-1/2+Z

Table 11 Bond Angles for abs2_a.

Atom	Atom	Atom	Angle/˚	Atom	Atom	Atom	Angle/˚
O00F	Rh01	Rh02	88.14(7)	C010	N00O	C00Y	112.6(3)
O00F	Rh01	O00G	176.59(10)	O00D	C00Q	C011	117.2(3)
O00F	Rh01	O00J	89.82(11)	O00F	C00Q	O00D	125.7(3)
O00F	Rh01	O00K	89.00(11)	O00F	C00Q	C011	117.1(3)
O00F	Rh01	O00L	87.74(9)	O00G	C00T	C00Z	117.7(3)
O00G	Rh01	Rh02	88.48(6)	O00H	C00T	O00G	125.3(3)
O00G	Rh01	O00L	95.65(8)	O00H	C00T	C00Z	117.0(3)
O00J	Rh01	Rh02	88.00(6)	O00I	C00U	C00S	117.4(3)
O00J	Rh01	O00G	90.43(10)	O00K	C00U	O00I	125.4(3)
O00J	Rh01	O00L	90.30(9)	O00K	C00U	C00S	117.1(3)
O00K	Rh01	Rh02	88.33(7)	C00X	C00V	C00Y	112.0(2)
O00K	Rh01	O00G	90.53(10)	O00E	C00W	C012	117.8(3)
O00K	Rh01	O00J	176.18(10)	O00J	C00W	O00E	124.9(3)
O00K	Rh01	O00L	93.29(9)	O00J	C00W	C012	117.3(3)
O00L	Rh01	Rh02	175.55(6)	C00V	C00X	S003	111.3(2)
Rh01	Rh02	S003[1]	175.42(2)	N00O	C00Y	C00V	113.1(3)
O00D	Rh02	Rh01	88.01(7)	N00O	C00Y	C013	100.5(2)
O00D	Rh02	S003[1]	87.87(7)	C00V	C00Y	C013	113.3(3)
O00D	Rh02	O00E	89.21(10)	O00L	C010	O00N	120.6(3)
O00D	Rh02	O00H	175.68(9)	O00L	C010	N00O	128.0(3)
O00D	Rh02	O00I	89.62(10)	N00O	C010	O00N	111.4(3)
O00E	Rh02	Rh01	88.02(6)	O00N	C013	C00Y	106.0(3)
O00E	Rh02	S003[1]	89.93(6)	C015	C014	S003	121.4(3)
O00E	Rh02	O00H	89.54(10)	C017	C014	S003	117.9(3)
O00E	Rh02	O00I	175.72(9)	C017	C014	C015	120.6(3)
O00H	Rh02	Rh01	87.81(6)	C014	C015	C01A	119.9(4)

Table 11 Continued

O00H	Rh02	S003[1]	96.27(7)	Cl0A	C016	Cl09	111.8(3)
O00H	Rh02	O00I	91.33(10)	Cl0A	C016	Cl0B	110.8(3)
O00I	Rh02	Rh01	87.83(6)	Cl0B	C016	Cl09	109.7(3)
O00I	Rh02	S003[1]	94.14(7)	C014	C017	C01E	119.0(4)
C00X	S003	Rh02[2]	102.46(10)	C01E	C018	C01A	120.4(4)
C014	S003	Rh02[2]	108.54(10)	Cl04	C019	Cl05	110.4(2)
C014	S003	C00X	102.43(15)	Cl04	C019	Cl08	110.7(2)
C00Q	O00D	Rh02	119.2(2)	Cl08	C019	Cl05	110.4(2)
C00W	O00E	Rh02	119.4(2)	C015	C01A	C018	119.8(4)
C00Q	O00F	Rh01	118.9(2)	Cl06	C01D	Cl07	109.4(2)
C00T	O00G	Rh01	118.7(2)	Cl0C	C01D	Cl06	112.9(3)
C00T	O00H	Rh02	119.6(2)	Cl0C	C01D	Cl07	109.2(2)
C00U	O00I	Rh02	119.05(19)	C018	C01E	C017	120.4(4)
C00W	O00J	Rh01	119.5(2)	Cl1	C6	Cl1A	103.3(5)
C00U	O00K	Rh01	119.2(2)	Cl3	C6	Cl1	115.5(6)
C010	O00L	Rh01	125.7(2)	Cl3	C6	Cl1A	112.4(5)
C010	O00N	C013	109.1(2)				

[1]1-X,2-Y,1/2+Z; [2]1-X,2-Y,-1/2+Z

Table 12 Hydrogen Atom Coordinates (Å×10⁴) and Isotropic Displacement Parameters (Å²×10³) for abs2_a.

Atom	*x*	*y*	*z*	U(eq)
H00O	4141	8346	4912	25
H00A	6442	10430	6221	35
H00B	6377	9964	7059	35
H00C	6500	10727	7199	35
H00D	5137	7942	4180	20
H00E	4734	7471	3346	20
H00F	4911	8807	3709	21
H00G	4436	8328	2918	21
H00Y	3672	7338	3899	21
H00H	4248	9670	3889	34
H00I	4292	10387	4136	34
H00J	3558	9692	4099	34
H01A	4364	9550	9896	37
H01B	4457	8903	9667	37
H01C	3700	8805	9745	37
H01D	1928	8456	7725	38
H01E	1824	8363	6678	38
H01F	1948	9061	7137	38

Table 12 Continued

H01G	3569	6423	4625	36
H01H	4383	6806	4830	36
H015	4555	8420	1236	33
H016	3307	10524	5830	42
H017	5963	7848	1847	37
H018	4788	7096	-357	42
H019	3133	10086	8495	34
H01I	4217	7700	-6	42
H01K	4907	8194	7354	35
H01J	5640	7153	565	51
H6	1588	11106	3776	50

Table 13 Atomic Occupancy for abs2_a.

Atom	***Occupancy***	**Atom**	***Occupancy***	**Atom**	***Occupancy***
C6	0.625(5)	H6	0.625(5)	Cl1	0.625(5)
Cl3	0.625(5)	Cl1A	0.625(5)		

Table 14 Solvent masks information for abs2_a.

Number	**X**	**Y**	**Z**	**Volume**	**Electron count**	**Content**
1	0.000	0.000	-0.171	509.8	99.7	

Experimental

Single crystals of $C_{16.97}H_{21.47}Cl_{8.16}N_{0.75}O_{7.5}Rh_{1.5}S_{0.75}$ [abs2_a] were grown by [Slow evaporation of $CDCl_3$]. A suitable crystal was selected and mounted on a 'Bruker APEX-II CCD' diffractometer. The crystal was kept at 104.26 K during data collection. Using Olex2 [1], the structure was solved with the ShelXS structure solution program using the structure expansion method and refined with the ShelXL refinement package using least squares minimization.

1. Dolomanov, O.V., Bourhis, L.J., Gildea, R.J, Howard, J.A.K. & Puschmann, H. (2009), J. Appl. Cryst. 42, 339-341.

Complex 122a

Table 15 Crystal data and structure refinement for completeMonoSerMeTOX_a.

Identification code	completeMonoSerMeTOX_a
Empirical formula	$C_{12}H_{17}Cl_2NO_8Rh_2S$

Table 15 Continued

Formula weight	612.04
Temperature/K	100.0
Crystal system	monoclinic
Space group	$P2_1/c$
a/Å	12.8093(7)
b/Å	11.5013(6)
c/Å	13.0035(8)
α/°	90
β/°	96.634(2)
γ/°	90
Volume/Å^3	1902.90(19)
Z	4
ρ_{calc}g/cm^3	2.136
μ/mm^{-1}	2.164
F(000)	1200.0
Crystal size/mm^3	ND
Radiation	MoKα (λ = 0.71073)
2Θ range for data collection/°	4.742 to 55.122
Index ranges	-16 ≤ h ≤ 16, -14 ≤ k ≤ 14, -14 ≤ l ≤ 16
Reflections collected	11340
Independent reflections	4354 [R_{int} = 0.0330, R_{sigma} = 0.0425]
Data/restraints/parameters	4354/0/105
Goodness-of-fit on F^2	1.951
Final R indexes [I>=2σ (I)]	R_1 = 0.1512, wR_2 = 0.3903
Final R indexes [all data]	R_1 = 0.1524, wR_2 = 0.3941
Largest diff. peak/hole / e Å^{-3}	12.92/-11.78

Table 16 Fractional Atomic Coordinates (×10^4) and Equivalent Isotropic Displacement Parameters (Å^2×10^3) for completeMonoSerMeTOX_a. U_{eq} is defined as 1/3 of the trace of the orthogonalised U_{IJ} tensor.

Atom	*x*	*y*	*z*	U(eq)
Rh1	7431.5(4)	7948.4(5)	4638.2(4)	9.8(4)
Rh2	7625.9(4)	6800.4(5)	3107.6(4)	10.4(4)
S3	7337.2(14)	9113.3(15)	6319.5(13)	9.5(5)
O4	7873(5)	9333(5)	3819(4)	16.9(12)
O1	8954(4)	7586(5)	5103(4)	13.7(11)
O2	5845(5)	8234(5)	4109(4)	16.5(12)
O3	9114(5)	6346(5)	3780(4)	18.6(12)
O0AA	8267(5)	8220(5)	2502(4)	14.8(12)
O5	6938(4)	6467(5)	5305(4)	14.1(11)
O6	6984(5)	5432(5)	3830(5)	19.6(12)
O7	4520(5)	7686(6)	2939(5)	26.5(14)

Table 16 Continued

C8	6806(6)	5582(7)	4755(6)	13.5(15)
N10	6162(6)	7317(7)	2633(6)	19.0(15)
C11	9444(6)	6849(6)	4622(6)	12.4(14)
C12	5576(7)	7753(8)	3264(7)	17.4(16)
C13	8205(6)	9187(7)	2938(6)	14.7(15)
C18	10527(7)	6521(8)	5135(7)	20.9(17)
C5	7181(6)	11279(6)	5353(6)	13.7(14)
C0AA	7853(6)	10619(7)	6214(6)	13.5(14)
C1AA	8568(7)	10238(8)	2400(7)	23.9(18)
C6AA	4425(8)	6936(8)	2056(7)	23.1(18)
C9	5540(7)	6914(7)	1663(7)	17.9(16)
C2AA	5924(6)	5699(7)	1387(6)	17.1(16)
C3AA	7895(6)	11213(7)	7261(6)	17.6(16)
C4AA	8971(7)	10432(7)	5933(6)	19.1(16)
C5AA	6339(7)	4508(8)	5258(7)	23.1(18)

Table 17 Bond Lengths for completeMonoSerMeTOX_a.

Atom	Atom	Length/Å	Atom	Atom	Length/Å
Rh1	Rh2	2.4251(7)	O3	C11	1.267(10)
Rh1	S3	2.5788(17)	O0AA	C13	1.255(10)
Rh1	O4	2.033(6)	O5	C8	1.243(10)
Rh1	O1	2.018(6)	O6	C8	1.262(10)
Rh1	O2	2.095(6)	O7	C12	1.372(11)
Rh1	O5	2.045(6)	O7	C6AA	1.430(11)
Rh2	S3[1]	2.5395(18)	C8	C5AA	1.550(12)
Rh2	O3	2.070(6)	N10	C12	1.276(11)
Rh2	O0AA	2.027(6)	N10	C9	1.486(11)
Rh2	O6	2.053(6)	C11	C18	1.516(12)
Rh2	N10	1.995(8)	C13	C1AA	1.497(12)
S3	Rh2[2]	2.5395(18)	C5	C0AA	1.533(11)
S3	C0AA	1.864(8)	C0AA	C3AA	1.519(10)
S3	C2AA[2]	1.835(8)	C0AA	C4AA	1.534(11)
O4	C13	1.278(10)	C6AA	C9	1.573(13)
O1	C11	1.264(10)	C9	C2AA	1.537(11)
O2	C12	1.243(11)	C2AA	S3[1]	1.835(8)

[1]+X,3/2-Y,-1/2+Z; [2]+X,3/2-Y,1/2+Z

Table 18 Bond Angles for completeMonoSerMeTOX_a.

Atom	Atom	Atom	Angle/˚	Atom	Atom	Atom	Angle/˚
Rh2	Rh1	S3	176.33(5)	C2AA[2]	S3	C0AA	104.7(4)
O4	Rh1	Rh2	86.29(17)	C13	O4	Rh1	120.5(5)
O4	Rh1	S3	94.61(17)	C11	O1	Rh1	120.6(5)
O4	Rh1	O2	91.3(2)	C12	O2	Rh1	112.3(6)
O4	Rh1	O5	173.5(2)	C11	O3	Rh2	116.7(5)
O1	Rh1	Rh2	86.92(16)	C13	O0AA	Rh2	119.3(5)
O1	Rh1	S3	89.52(17)	C8	O5	Rh1	117.8(5)
O1	Rh1	O4	90.1(2)	C8	O6	Rh2	117.2(5)
O1	Rh1	O2	176.7(2)	C12	O7	C6AA	105.7(7)
O1	Rh1	O5	92.1(2)	O5	C8	O6	129.2(8)
O2	Rh1	Rh2	90.18(16)	O5	C8	C5AA	116.3(7)
O2	Rh1	S3	93.36(16)	O6	C8	C5AA	114.5(7)
O5	Rh1	Rh2	87.73(15)	C12	N10	Rh2	121.3(6)
O5	Rh1	S3	91.52(16)	C12	N10	C9	111.8(7)
O5	Rh1	O2	86.2(2)	C9	N10	Rh2	124.2(6)
Rh1	Rh2	S3[1]	163.51(5)	O1	C11	O3	126.8(8)
O3	Rh2	Rh1	88.14(17)	O1	C11	C18	115.5(7)
O3	Rh2	S3[1]	108.16(17)	O3	C11	C18	117.7(7)
O0AA	Rh2	Rh1	88.00(16)	O2	C12	O7	117.3(8)
O0AA	Rh2	S3[1]	90.01(16)	O2	C12	N10	128.3(8)
O0AA	Rh2	O3	88.5(2)	N10	C12	O7	114.4(8)
O0AA	Rh2	O6	175.5(2)	O4	C13	C1AA	117.8(8)
O6	Rh2	Rh1	87.55(17)	O0AA	C13	O4	124.5(8)
O6	Rh2	S3[1]	94.48(17)	O0AA	C13	C1AA	117.7(7)
O6	Rh2	O3	90.6(2)	C5	C0AA	S3	109.9(5)
N10	Rh2	Rh1	84.8(2)	C5	C0AA	C4AA	110.9(6)
N10	Rh2	S3[1]	78.9(2)	C3AA	C0AA	S3	109.2(5)
N10	Rh2	O3	172.8(3)	C3AA	C0AA	C5	113.0(6)
N10	Rh2	O0AA	92.8(3)	C3AA	C0AA	C4AA	109.8(6)
N10	Rh2	O6	87.6(3)	C4AA	C0AA	S3	103.7(5)
Rh2[2]	S3	Rh1	123.03(7)	O7	C6AA	C9	105.9(7)
C0AA	S3	Rh1	111.6(2)	N10	C9	C6AA	97.9(7)
C0AA	S3	Rh2[2]	115.9(2)	N10	C9	C2AA	109.1(7)
C2AA[2]	S3	Rh1	104.2(3)	C2AA	C9	C6AA	114.7(7)
C2AA[2]	S3	Rh2[2]	92.6(3)	C9	C2AA	S3[1]	104.4(6)

[1]+X,3/2-Y,-1/2+Z; [2]+X,3/2-Y,1/2+Z

Experimental

Single crystals of $C_{12}H_{17}Cl_2NO_8Rh_2S$ [completemonosermetox_a] were grown by layering DCM and hexane. A suitable crystal was selected and mounted on a 'Bruker APEX-II CCD' diffractometer. The crystal was kept at 100 K during data collection. Using Olex2 [1], the structure was solved with the ShelXS structure solution program using the Patterson method and refined with the ShelXL refinement package using least squares minimization.

1. Dolomanov, O.V., Bourhis, L.J., Gildea, R.J, Howard, J.A.K. & Puschmann, H. (2009), J. Appl. Cryst. 42, 339-341.

Vita

Derek Cressy was born in 1990 to Bill and Yvonne Cressy. He received his B.S. in Chemistry from Harding University in 2013. Upon graduating he was employed as a researcher at the Center for Renewable Carbon at the University of Tennessee. Here he worked in developing carbon fiber using lignin from readily available biological feedstocks. In the Fall of 2014 he was accepted into graduate school at the University of Tennessee and studied under the direction of Dr. Ampofo Darko. It was here that he was introduced to organometallic chemistry through the synthesis of dirhodium paddlewheel complexes for applicatoin in diazo decomposition reactions.